3-13-2017

Control of Ciliogenesis by an Evolutionarily Ancient Peptide Amidating Enzyme

Dhivya Kumar
dhivkmr@gmail.com

Control of Ciliogenesis by an Evolutionarily Ancient Peptide Amidating Enzyme

Dhivya Kumar, PhD

University of Connecticut, 2017

Cilia are highly complex microtubule-based cellular extensions present on most eukaryotic cells that play key roles in sensing the extracellular environment, processing developmental signals and generating propulsive force. Although many details of the ciliary assembly process are well understood, there are numerous aspects of this overall process that remain very unclear. Accumulating evidence points to an ancient connection between peptidergic signaling and cilia. A crucial last step in generating active neuropeptides capable of intercellular signaling involves modification of the C-terminus to a protease-resistant and uncharged amide group in the lumen of the secretory pathway. This modification is mediated by peptidylglycine alpha-amidating monooxygenase (PAM) and is generally essential for neuropeptide bioactivity and indeed in mammals is required for life. Phylogenetics revealed that metazoans lacking nervous systems contain PAM, and that PAM-like genes are present in unicellular green algae. In this thesis, I describe the identification of active PAM enzyme in the green alga *Chlamydomonas reinhardtii*, and demonstrate that it localizes to both Golgi and punctate structures within cilia; PAM is also present in both motile and immotile (primary) cilia in mammals. The presence of this novel enzymatic activity in cilia of organisms across phylogeny suggests these organelles may have a previously unappreciated role in peptide-based signaling that emerged early in the history of eukaryotes. Furthermore, I demonstrate that this enzyme is absolutely required for normal ciliary assembly in *Chlamydomonas*, planaria and mice; in the absence of PAM, these organelles either do not assemble past the transition zone (*Chlamydomonas*), fail during

remodeling (planaria) or are much shorter than controls (mouse). In *Chlamydomonas*, loss of PAM alters Golgi structure and function, and affects levels of specific ciliary assembly proteins. Biochemical analysis reveals that PAM is released in extracellular vesicles (ectosomes) that are shed from the surface of cilia in *Chlamydomonas*, which may have important implications for cell-cell communication. Finally, I also describe connections between PAM and the actin cytoskeleton, and demonstrate that both cilia and actin-based microvilli are lost from the pronephros of PAM-null zebrafish. This raises the possibility that PAM plays a general role in the formation and/or maintenance of membrane-bound cellular extensions.

Control of Ciliogenesis by an Evolutionarily Ancient Peptide Amidating Enzyme

Dhivya Kumar

B.Tech. Indraprastha University, India, 2008

M.S., University of Tennessee, Knoxville, USA 2012

Ph.D., University of Connecticut, USA 2017

A Dissertation

Submitted in Partial Fulfillment of the

Requirements for the Degree of

Doctor of Philosophy

at the

University of Connecticut

2017

APPROVAL PAGE

Doctor of Philosophy Dissertation

Control of Ciliogenesis by an Evolutionarily Ancient Peptide Amidating Enzyme

Presented by

Dhivya Kumar, B.Tech., M.S., Ph.D.

Major Advisor

_____

Betty A. Eipper

Major Co-Advisor

_____

Stephen M. King

Associate Advisor

_____

Richard E. Mains

Associate Advisor

_____

Peter Setlow

Associate Advisor

_____

Bing Hao

University of Connecticut
2017

Acknowledgements

First and foremost, I would like to thank my advisors, Drs. Betty Eipper, Richard Mains and Stephen King for their support and guidance throughout this journey. My PhD journey has been a transformative experience and I feel extremely lucky to have worked with outstanding advisors. I walk away from this experience a more confident and better scientist then I thought was ever possible.

The “We can do it!” poster that hangs outside Betty’s office is very fitting, for she is an incredible role model for women in science. I will forever be in awe of her dedication to science and mentorship to trainees. I appreciate the freedom she gave me to develop and pursue my own ideas and all the sound advice over the years that have kept me sane. Perhaps the most valuable lesson I learnt from Dick and Betty is to not be afraid to learn new things. I thank them for always leaving their doors open for questions, no matter how big or small.

Steve’s enthusiasm and love for science is contagious. I feel very fortunate to have walked- both literally and figuratively- along the “tetsugaku no michi” (path of philosophy) with him. I enjoyed every minute I spent interacting with him over the years- both at work and during our wonderful adventures in Japan and Amsterdam. Thank you for being my constant cheerleader- I am very appreciative and I hope I make you proud.

I have to thank all the present and past members of the Neuropeptide and Molecular Motors laboratories for their support and comradery. It was a pleasure working with such a talented group of people. Dr. K.S. Vishwanatha deserves a special thank you for always patiently answering my innumerable questions over the years. Thanks to Darlene D’Amato, Yanping Wang and Andrew Yanik for outstanding technical assistance. A big thanks to Taylor LaRese for help with the animal experiments and conversations about coffee and life. I would also like to acknowledge Ramila Patel-King for help with the planarian experiments and Maya Yankova for

her expertise with electron microscopy. I enjoyed working with Myah Bartolotta, a very sharp undergraduate from Wheaton College for two consecutive summers and I appreciate her hard work and efforts on generating extracellular vesicles from *Chlamydomonas*.

This work would not have come together without the continued support of many collaborators. I would like to thank Dr. Sabeeha Merchant, Dr. Daniela Strenkert and Dr. Crysten Blaby-Haas for helping us navigate through the tricky world of *Chlamydomonas* biology. The zebrafish experiments presented in this dissertation would not have been possible without the efforts of Dr. Jonathan Gitlin and Dr. Rebecca Thomason at Marine Biological Laboratory.

I would like to thank the entire Molecular Biology and Biophysics department for fostering a fantastic environment for graduate students to learn and grow in. Special thanks to Drs. Peter Setlow and Bing Hao for serving on my thesis committee and their interest, advice and helpful comments over the years. I also thank Drs. Kimberly Dodge-Kafka and Larry Klobutcher for their willingness to serve on my general exam committee. I appreciate the efforts and dedication of Dr. Barbara Kream, Jody Gridley, Anna Sagan, Bridget Clancy-Tenan and Patricia Schultz in the Neuroscience, Molecular Biology and Biomedical Science graduate programs.

Last, but certainly not least, I am indebted to my family and friends for their unconditional love and endless patience throughout these years. I am very grateful to my partner, Arvind for his unwavering support, even during countless late nights spent in the lab. Thanks to my brother, Bharani for helping me see the lighter side of life. These past years would have been very dreary without my friends- Sudershana, Nozomi, Kristen, Swati and Pragya. Finally, I thank my parents for believing in me and instilling in me the value of hard work: I owe all my success to you.

Table of Contents

OUTLINE

Cilia are sensory antennae present on most eukaryotic cells that play key roles in fluid propulsion and signaling. The ciliary compartment houses a distinct set of proteins and lipids; the protein complement of this organelle has not been fully elucidated. Accumulating evidence points to a connection between peptidergic signaling and cilia. A crucial last step in generating active neuropeptides capable of intercellular signaling involves modification of the C-terminus to a protease-resistant and uncharged amide group in the lumen of the secretory pathway. This modification is mediated by peptidylglycine alpha-amidating monooxygenase (PAM) and is generally essential for neuropeptide bioactivity. Extensive work in mammalian systems has revealed the crucial roles played by this enzyme; deficits in endocrine and cardiovascular function disrupt embryonic development in mice lacking this enzyme. **This work is focused on exploring the connection between this bioactive peptide amidating enzyme and the ciliary compartment. I demonstrate that PAM not only localizes to cilia in diverse cell types, but that PAM is an evolutionarily conserved factor required for ciliary assembly.**

Chapter 1 reviews our understanding of ciliary function and biogenesis. I highlight the underappreciated diversity that exists in ciliary forms and outstanding questions in the field of ciliary biology.

In **Chapter 2**, I review the bioactive peptide amidating enzyme, PAM. I discuss the discovery, function and recent advances made towards understanding this multifaceted enzyme.

Chapter 3 shows that peptidylglycine alpha-amidating monooxygenase (PAM) displays an evolutionarily conserved localization in cilia, thus strengthening the link between peptidergic signaling and cilia. The presence of this novel enzymatic activity in cilia in organisms across phylogeny suggests that these organelles have a previously unappreciated role in peptide-based signaling that emerged early in the history of eukaryotes.

In **Chapter 4** examines the function of PAM in ciliated cells. We find that PAM is required for ciliary assembly in *Chlamydomonas*, planaria and mice. In addition, loss of PAM alters Golgi structure and function, and affects levels of specific known ciliary assembly proteins in *Chlamydomonas*.

Chapter 5 demonstrates the release of PAM in extracellular vesicles (ectosomes) that are shed from the surface of cilia in *Chlamydomonas*. I discuss the implications of the release of a peptide amidating enzyme in vesicles for cell-cell communication.

In **Chapter 6** explores a connection between PAM and the actin cytoskeleton based on the observation that PAM null zebrafish display a striking loss of microvilli in the pronephros during development.

Chapter 7 summarizes this study and discusses avenues for future research.

Chapter 1

Cilia: Form, Function and Genesis

ABSTRACT

Cilia are highly conserved, microtubule-based cellular organelles present in nearly all cells in mammals, where they perform diverse roles ranging from fluid propulsion to signaling. Motile cilia, such as those lining the surface of the airways and ventricles of the brain, propel the mucus and cerebrospinal fluid, respectively. Immotile cilia, also called primary cilia and present on most other cell types, serve as important signaling hubs. The cilium is a complex structure with several sub-compartments that serve distinct functions. Currently, about 700 proteins are known to be enriched in this organelle, and this list is rapidly expanding. Key signaling pathways such as Wnt and Hedgehog signaling and a number of receptors are localized in the cilium. In recent years, several heterogeneous, multisystemic disorders known as ciliopathies because they result from defective ciliary function have been described. Here, I review the diversity in ciliary structure and function, steps leading to cilia formation in cells and highlight outstanding questions that currently exist in the field of ciliary biology.

INTRODUCTION

Cilia are membrane-bound, cellular projections comprised of a microtubular backbone arising from a basal body. Owing to their key roles in motility, signaling and sensory perception, nearly all cells in mammals possess at least one cilium. Cells invest more than 5% of all genes in building a cilium; at least 700 proteins and certain lipids are specifically trafficked into the cilium (Davis et al., 2006; Arnaiz et al., 2009; Arnaiz et al., 2014). The repertoire of signaling pathways tied to cilia is rapidly expanding. Well-known cilia-dependent pathways include non-canonical Wnt and hedgehog signaling. The normal functioning and genesis of this organelle is therefore critical to cellular and organismal homeostasis; ciliary dysfunction leads to several multi-systemic disorders, collectively termed ciliopathies.

Cilia were one of the first organelles discovered by Antony van Leeuwenhoek in 1675, when he noted ‘tiny legs’ in ‘animalcules’ or protozoa (Dobell and Leeuwenhoek, 1932). Till the late 1990s, this organelle was considered as only playing a role in motility, and although immotile (primary) cilia had been observed in 1898 by Zimmerman, immotile cilia were dismissed as evolutionary vestiges. The discovery of ciliopathies (diseases linked to ciliary dysfunction), protein trafficking into the cilium and presence of sensory and signaling proteins in this compartment, energized the field of cilia biology. This renaissance has placed cilia in center stage, revealing their critical roles in mammalian physiology and gaps in our understanding of ciliary form and function.

One organelle, many functions

Broadly, cilia can be categorized as being motile (capable of cell and/or fluid propulsion) or immotile (also known as primary cilia) (**Fig 1**). The sperm flagellum is a modified motile cilium, meaning that ciliary motility is critical for one of the most fundamental processes of life – reproduction. Multiple motile cilia present on the surface of ventricular ependymal cells

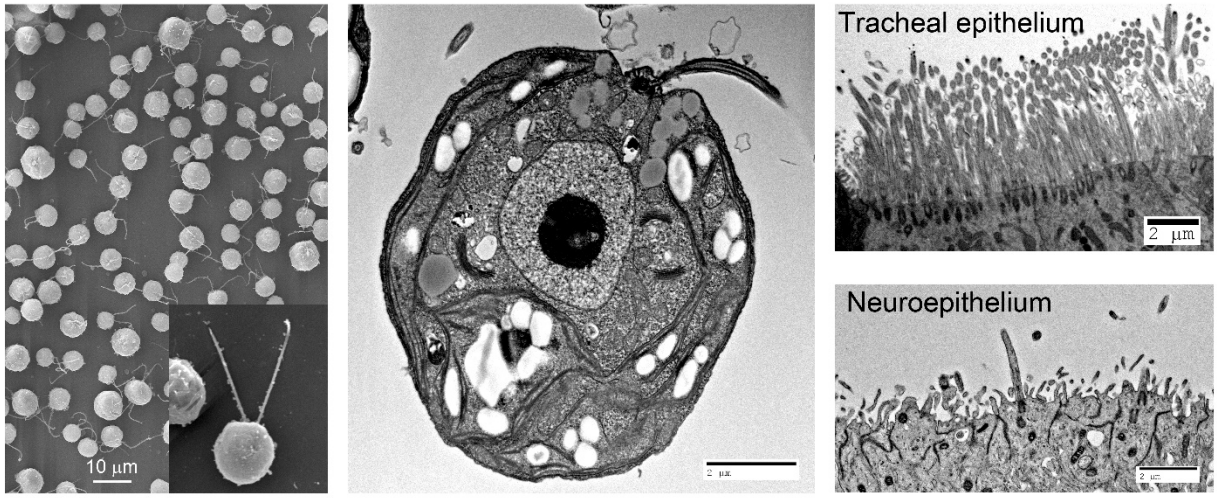

Fig 1. Motile and primary cilia. Cilia are highly conserved microtubule-based organelles. Scanning and transmission electron micrographs of the biciliated unicellular green alga *Chlamydomonas* are shown. Motile cilia of *Chlamydomonas* (left and middle panels) and the tracheal epithelium of mice (upper right panel) share many similarities. The murine neuroepithelium contains cells with a solitary, immotile primary cilium (bottom right panel).

generate the force needed to move cerebrospinal fluid. In the respiratory epithelium, cilia play a role in mucus clearance, which acts as a first line of defense against airborne pathogens (**Fig 1**). Although motile cilia have classically been considered non-sensory, a plethora of evidence now indicates that this is incorrect (Bloodgood, 2010). For example, ciliated tracheal epithelial cells are mechanosensitive, modulating ciliary beat frequency to match the viscosity of the mucus they encounter (Johnson et al., 1991). These cilia also possess chemoreceptors of the bitter taste family that can sense and respond to noxious compounds, conferring chemosensory properties to them (Shah et al., 2009). In addition, the initial steps of the cAMP-mediated signaling pathway initiated in response to cell-cell contact during sexual reproduction in *Chlamydomonas* are confined to its motile cilia (**Fig 1**) (Pan and Snell, 2000).

Most other cells in the human body (except those of lymphoid and myeloid origins) possess a solitary, immotile cilium. These primary cilia are cellular sensory antennae, surveying the extracellular milieu and initiating appropriate signaling cascades. Growth factor, morphogen and peptide-based signaling is compartmentalized in the cilium; the smaller volume of the cilium compared to the remainder of the cell potentially increases the concentration of receptors and signaling molecules, thereby making the cell more sensitive to these cues (Nachury, 2014). Perhaps the most well studied signaling pathway linked intricately to the cilium is Hedgehog (Hh) signaling, which plays a role in early development and tissue patterning in vertebrates (**Fig 2**). This is a clear example of how compartmentalization of pathway components in the cilium can influence signal transduction. In the absence of the secreted polypeptide Sonic Hedgehog (Shh), the transmembrane Shh receptor (Patched) is localized in the ciliary membrane, while seven-pass protein-protein coupled receptor Smoothened is excluded. In this ‘off’ state, the Gli transcription factors (Gli 2, Gli 3) bound to Sufu (Suppressor of fused), enter the cilium and are processed into a form (GliR) that represses transcription of Hh target genes. In the presence of Shh ligand, Patched is trafficked out of the cilium, while Smoothened now localizes to the ciliary

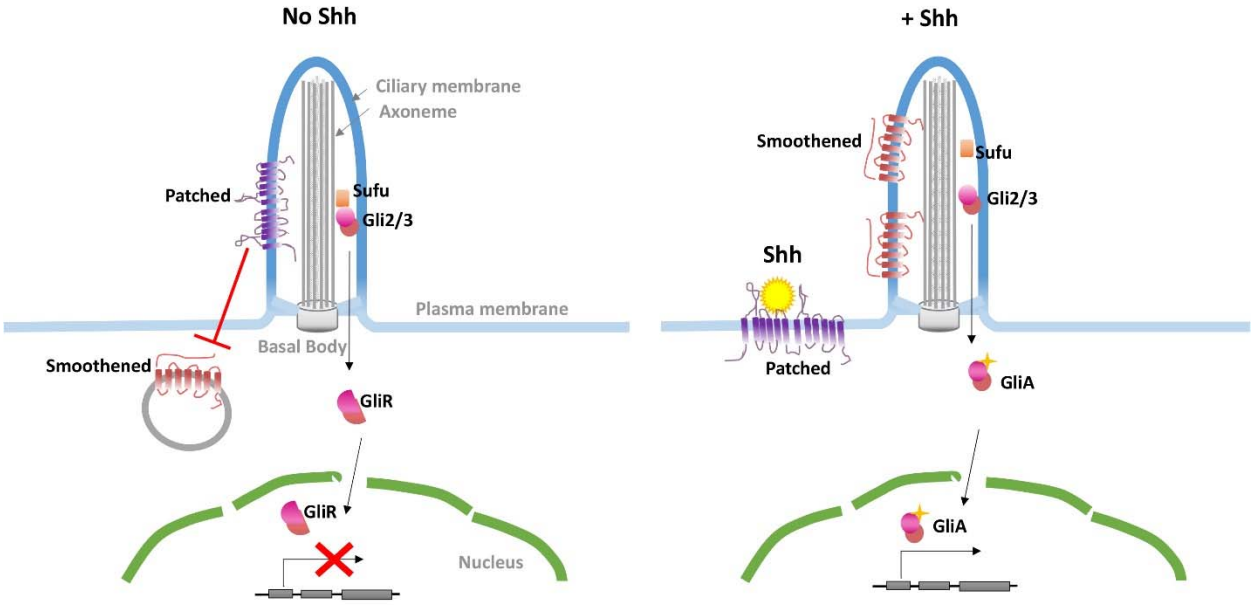

Fig 2. Simplified model of the cilia-based Hedgehog signaling pathway in mammals. In the absence of Sonic Hedgehog ligand (Shh), Patched receptor is localized in the ciliary membrane and prevents Smoothened GPCR entry into the cilium (left). The transcription factors Gli2/3 are processed into transcriptional repressors (GliR) that prevent activation of hedgehog target genes. In the presence of Shh (right), Patched exits the cilium and allows Smoothened to translocate into the cilium. This allows the Gli transcription factors to be activated (GliA) and upregulates transcription of hedgehog pathway genes (Wong and Reiter, 2008).

membrane. Ciliary Smoothened, through an unknown mechanism activates Gli2 and -3 (GliA), which can then translocate into the nucleus to activate Hh target genes (**Fig 2)** (Wong and Reiter, 2008).

More recently, an additional function has been attributed to cilia - secretion. Work done in *Chlamydomonas* and *Caenorhabditis elegans* shows that the cilium is a source of extracellular vesicles (ectosomes) that can function in inter-cellular communication in cell-autonomous and cell non-autonomous ways. In *Chlamydomonas*, vesicles released during mitotic division contain a lytic enzyme that degrades the mother cell wall, and allows the daughter cells to swim away (Wood et al., 2013). Vesicles shed from *C. elegans* cilia contain polycystic kidney disease proteins, polycystins 1 and 2, and alter the behavior of male animals, while vesicles lacking polycystin 2, derived from kinesin-3 klp6 mutant animals, do not. (Wang et al., 2014). These studies indicate that the cilium acts as both a transmitter and receiver of signals.

Form follows function

The axoneme or the microtubule core of the cilium is derived from the basal body, a modified centriole consisting of nine triplet microtubules arranged in a cartwheel (**Fig 3**). Each cell typically has two centriolar cylinders that can recruit pericentriolar matrix components to become a centrosome, which organizes the spindle microtubules during cell division. The centrosome (or centriolar pair) undergoes duplication during the S phase of the cell cycle and following maturation, each centrosome moves to the opposite poles of the cell to organize the spindle microtubules (Nigg and Stearns, 2011). In the centriolar pair, the older or “mother” centriole is clearly distinguishable from the daughter centriole due to the presence of additional distal and sub-distal appendages (**Fig 3**). Only the mother centriole is capable of forming a basal body that nucleates the axoneme, since it contains the nine distal appendages required for plasma membrane docking (Garcia and Reiter, 2016).

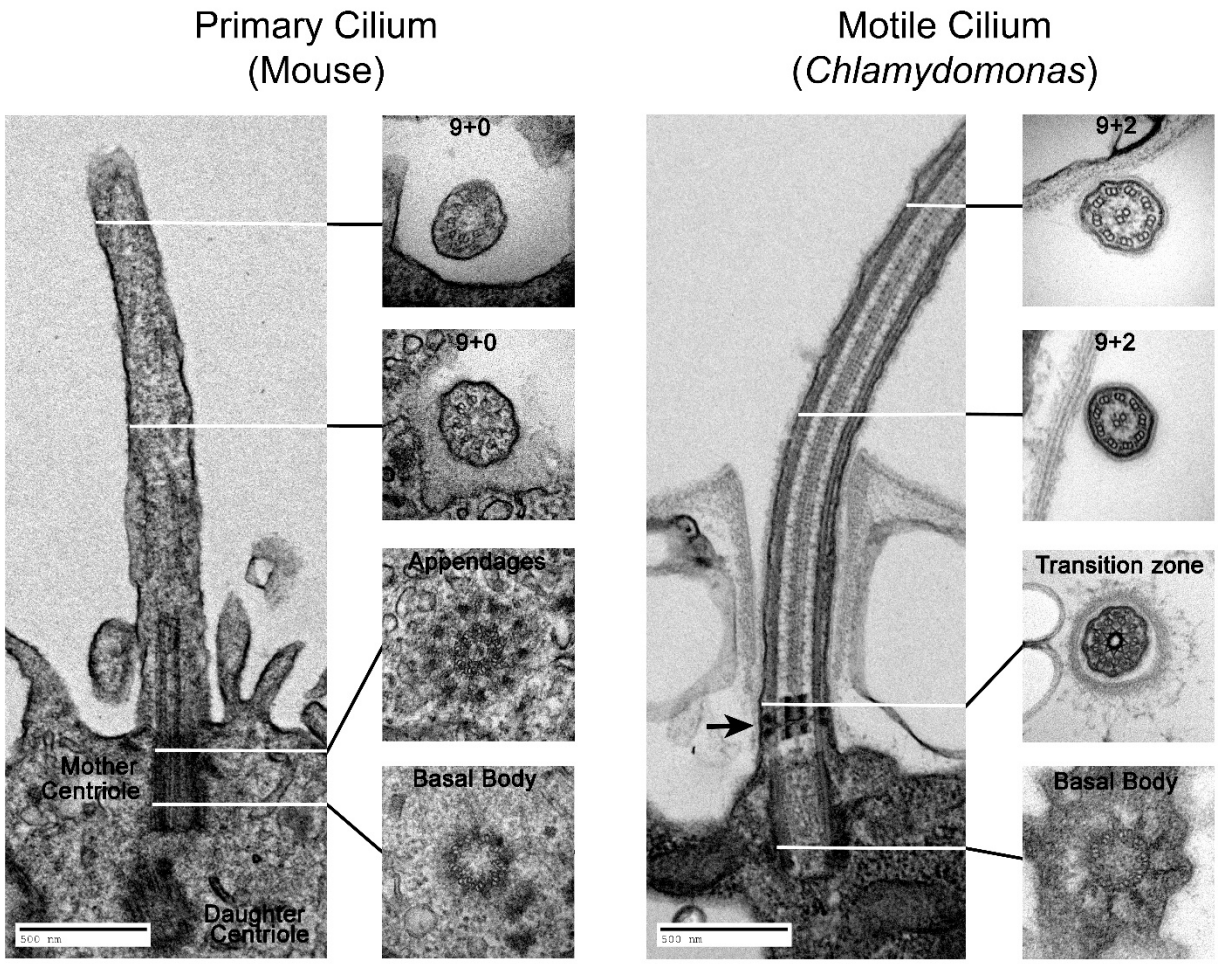

Fig 3. Primary and motile ciliary structures. Longitudinal and cross sections show the basal body, transition zone and axonemal structure of a primary (left) and a motile cilium (right). For the primary cilium, both mother and daughter centrioles are visible. The axoneme (9+0 in case of a primary cilium and 9+2 in case of a motile cilium) is templated from the basal body which contains nine triplet microtubules. The transition zone that acts as a ciliary gate, contains Y-linkers (arrow in right panel) that connect the membrane to the microtubules.

Out of the triplet microtubules in the basal body the two internal microtubules continue to form the axonemal core, leading to the nine outer doublet microtubules seen in primary cilia (also called the 9+0 configuration). Motile cilia, which have a 9+2 arrangement, additionally possess a central pair of microtubules and outer and inner dynein arms; the central pair has been implicated in regulating ciliary beat frequency (Lechtreck et al., 2008) (**Fig 3**). The central pair is not absolutely necessary for motility. The 9+0 cilia in the embryonic node display rotational movement and generate an asymmetric flow of morphogens, in turn generating left-right axis asymmetry in the developing embryo.

An emerging theme in cilia biology in recent years is the enormous diversity that exists in ciliary form and function. Categorizing cilia just on the basis of their axoneme configuration or ability to move now seems too simplistic. Just as 9+0 nodal cilia are motile, mechanosensory kinocilia in the ear have a 9+2 configuration, and yet are immotile (Schwander et al., 2010). The dendritic tips of olfactory sensory neurons assemble multiple cilia with a 9+2 configuration that are immotile and lack dynein arms. These olfactory cilia are enriched in odorant receptors and play a sensory role (Jenkins et al., 2009). Another highly specialized category of ciliated cells is the photoreceptor cells in the eye. In these sensory neurons, the dendrite terminates in a short 9+0 connecting cilium with membrane discs enriched with photoreceptors (called the outer segment) (Insinna and Besharse, 2008).

How do cells build a cilium?

The axoneme is enclosed by a membrane that is contiguous with the surrounding plasma membrane; nevertheless, a subset of proteins and lipids is selectively enriched in the cilium. How is the unique proteome and lipidome of the cilium generated and maintained? Since proteins are not synthesized in the ciliary matrix, cargo destined for this organelle must be recognized, sorted and trafficked from the cytoplasm or endomembrane system. The intraflagellar transport (IFT) machinery regulates the bi-directional movement of proteins into

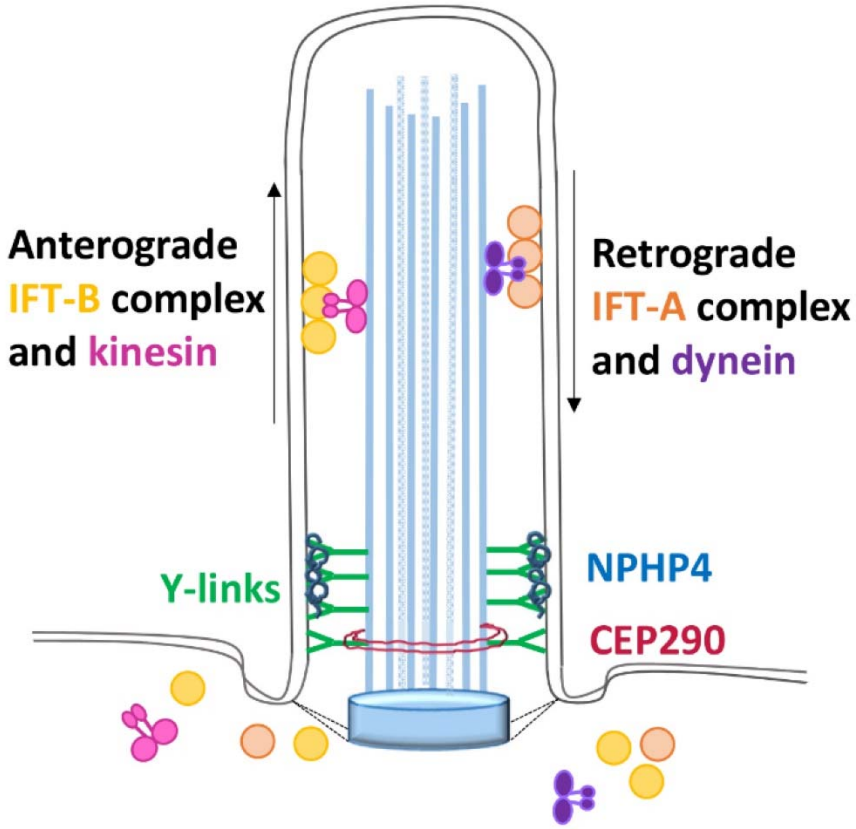

Fig 4. Schematic of the ciliary intraflagellar transport system. The model illustrates the general arrangement of the system required for ciliary assembly. Anterograde IFT particles (IFT-B in mammals) are moved by kinesin to deliver cargo from the cell body to the cilium, and retrograde IFT particles (IFT-A in mammals) and dynein motors return cargo from the cilium to the cell body along the doublet microtubules. The transition zone, including Y-links near the base, forms the ciliary gate to control protein entry and exit. Two components of the transition zone – nephrocystin-4 (NPHP4) and CEP290 are shown.

and out of the cilium (**Fig 4**). The multimeric anterograde IFT-B transport complex (which contains at least 16 subunits) transports cargo from the base to the tip of the cilium with the help of kinesin motor proteins. The multimeric retrograde IFT-A transport complex (which contains 6 subunits) associates with IFT dynein motors to export proteins out of the cilium. This bi-directional transport system is absolutely essential for ciliogenesis, as it carries building blocks such as tubulin, radial spoke proteins and dynein proteins. IFT-B and IFT-A are also essential for ciliary maintenance and disassembly. The trafficking of membrane proteins into the cilium poses additional challenges and another multimeric protein complex called the BBSome associates with IFT subunits to mediate their movement into and out of the cilium (Nachury et al., 2007; Lechtreck et al., 2009; Jin et al., 2010; Nachury et al., 2010). How IFT and BBS proteins recognize the wide range of cargo proteins they traffic into the cilium is still unclear.

While the IFT complex offers some selectivity to the proteins transported into the cilium, a means to exclude proteins from the cytoplasm and plasma membrane must also be in place. This is facilitated by barriers at the base of each cilium, one being the transition zone that lies distal to the basal body. Ultrastructurally, the transition zone is characterized by wedge shaped Y-linkers that attach the ciliary membrane to the doublet microtubules (**Fig 4**). Loss of transition zone components such as CEP290 and NPHP4 alters the protein composition of cilia (Craige et al., 2010; Awata et al., 2014; Li et al., 2016).

The process of ciliogenesis varies in different cell types (**Fig 5**). Many cells, such as the multiciliated epithelial cells of the lung and kidney, use the extracellular pathway of ciliogenesis. In this pathway, the basal body docks at the plasma membrane and the axoneme and ciliary membrane are then extended outward. In contrast, cells like fibroblasts and neural progenitor cells accomplish many of the early steps of ciliogenesis intracellularly (called the intracellular pathway). The sequence of events that comprise primary cilium biogenesis were described nearly 50 years ago by Sergei Sorokin using electron microscopy to visualize the process in

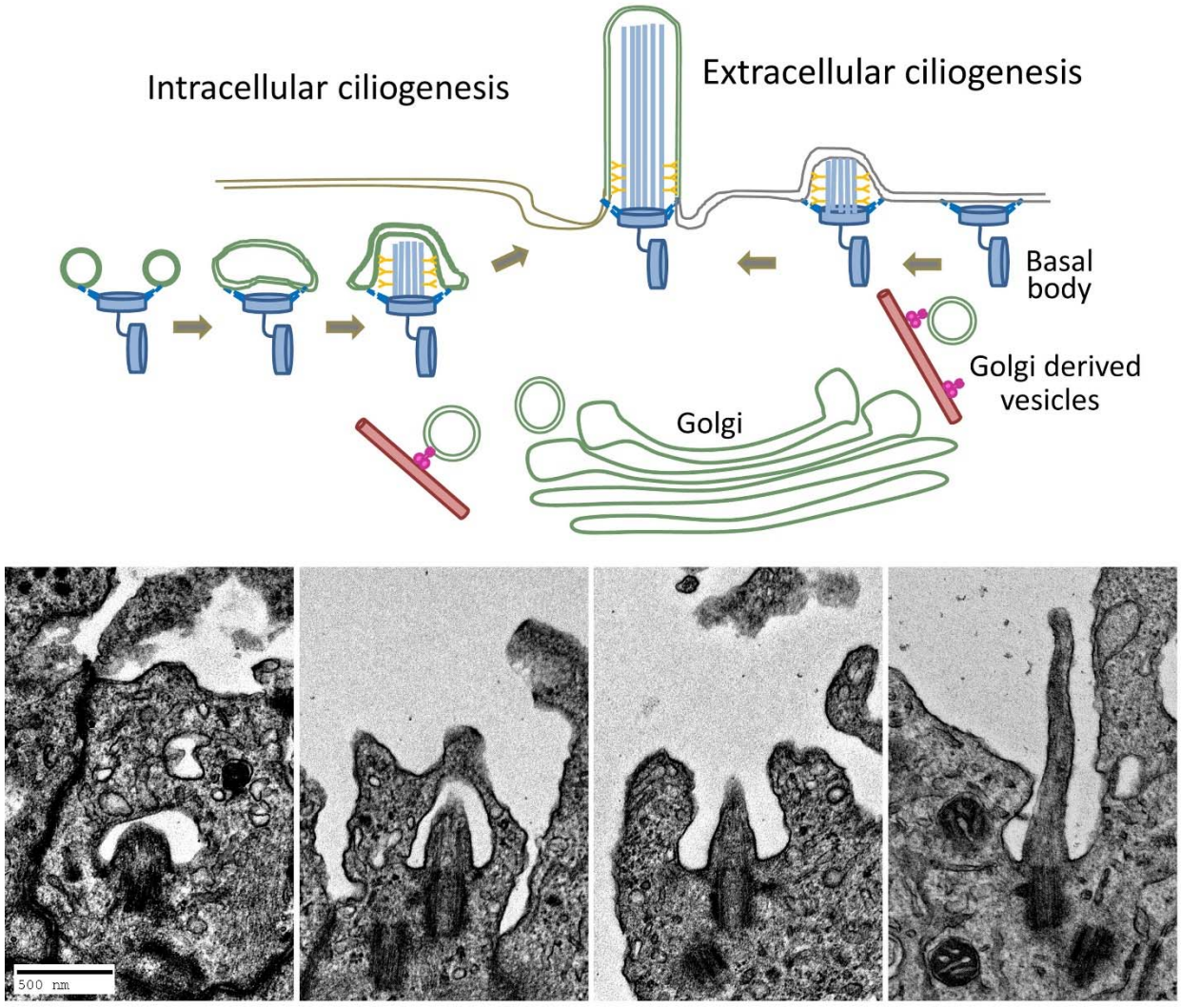

Fig 5. Pathways of ciliogenesis. Top panel: Schematic showing two different modes of ciliogenesis used by different cell types. Fibroblasts and neuronal progenitors assemble part of their cilium inside the cytoplasm (intracellular ciliogenesis). Epithelial cells and *Chlamydomonas* use the extracellular pathway of ciliogenesis, which starts with the docking of basal bodies at the plasma membrane. Golgi-derived vesicles deliver specific membrane proteins and lipids to the growing cilium. **Bottom panel**: Electron micrographs showing the different stages of intracellular ciliogenesis during the assembly of primary cilia in neural epithelial cells.

fibroblasts and smooth muscle cells (Sorokin, 1962). First, a Golgi derived vesicle, called a primary ciliary vesicle attaches to the distal appendages of the mother centriole. Second, the axoneme extends from the basal body and secondary vesicles fuse with the primary ciliary vesicle to accommodate the growing structure. The axoneme at this stage is covered by two membranes, the inner membrane, which will eventually become the ciliary membrane, and an outer membrane, called the sheath, which will fuse with the plasma membrane. After this structure docks to the plasma membrane and fusion of the sheath and the plasma membrane occurs, the axoneme emerges from the surface as it continues to elongate by a supply of building blocks and membrane (**Fig 5**). Recently, an intermediate step has been identified in this process - the distal appendages of the mother cilium first associate with smaller vesicles (called distal appendage vesicles), which fuse to give rise to the primary ciliary vesicle (Lu et al., 2015). Membrane shaping Eps15 homology domain proteins, EHD1/EHD3, along with several small Rab GTPase proteins, such as Rab8 and Rab11, are important for these early steps in ciliary vesicle formation. Although several Arf family GTPases have also been implicated in ciliogenesis, their exact mechanism of action remains unclear.

When cilia go awry

As expected, defects in cilium formation and function have severe consequences. Genetic disorders resulting in dysfunctional cilia are collectively known as ciliopathies, which are usually heterogeneous, multisystemic disorders with overlapping and distinct clinical manifestations (Brown and Witman, 2014). Defective motile cilia are seen in primary ciliary dyskinesia, which is characterized by impaired mucociliary clearance (due to dysfunctional cilia in the respiratory tract), *situs inversus* (abnormality in nodal cilia) and infertility (due to immotile sperm in men and impaired cilia in fallopian tubes in women). Defects in primary cilia lead to several degenerative, pleiotropic disorders with retinal, renal and neural manifestations. Mutations in the BBSome complex result in Bardet Biedl syndrome (BBS), which is characterized by retinal degeneration,

obesity, polydactyly and cystic kidneys. Defects in the renal ciliary proteins polycystin-1 and 2, which function as a mechanosensory complex to detect fluid flow, result in polycystic kidney disease (PKD), the most common inherited genetic disorder; patients develop fluid filled cysts in their kidneys, which worsen progressively with age, resulting in renal failure. Skeletal malformations are also shared between several ciliopathies. One severe example is seen in Jeune asphyxiating thoracic dystrophy (JATD), which results in respiratory insufficiency due to a constricted rib cage. Central nervous system abnormalities are hallmarks of Meckel syndrome and Joubert syndrome; intellectual disability and brain malformations are some of the characteristics of these diseases (Hildebrandt et al., 2011; Waters and Beales, 2011). As more causative genes for ciliopathies are determined, it is becoming apparent that genetic modifiers greatly impact the pathophysiology of disease (Yee et al., 2015). Genome wide analytical tools to probe mutational burden in ciliopathic patients might provide insight into these phenotypic modifiers.

Birth of an organelle

Cilia are evolutionarily ancient, well-conserved organelles present in almost all major eukaryotic phyla. Flagella (hereafter referred to as cilia) present on unicellular eukaryotes such as the green alga, *Chlamydomonas reinhardtii*, share many similarities in structure, composition and function with mammalian cilia. Seminal work providing insight into protein trafficking in cilia and ciliopathies has been accomplished using this organism, due to the ease of genetic and biochemical analysis. Furthermore, the diverse and evolutionarily distant model systems (green alga, *C. elegans*, zebrafish, and mice to name a few) used in ciliary research have contributed to our knowledge of the commonalities and differences in cilia function that arose during evolution. Phylogenetic analysis of ciliary trafficking proteins, signaling modules and structural components has proven to be immensely useful in our understanding of this complex organelle (Carvalho-Santos et al., 2011; Sung and Leroux, 2013; van Dam et al., 2013).

While tracing the evolutionary history of the cilium, the distribution of basal bodies and centrioles must also be considered. Although there are interesting variations on the presence and type of cilia and ciliary/axonemal structure, the most striking finding is the complete loss of cilia, ciliary genes and centrioles/basal bodies in angiosperms, most fungi and amoebae (Carvalho-Santos et al., 2011). In apicomplexans such as *Plasmodium*, where the cilium is preassembled in the cytoplasm, intraflagellar genes are lost, suggesting that genes for entire structures were eliminated when they were not required (Mitchell, 2016). In the flatworm, *Schmidtea mediterranea*, centrosomes are absent, although cilia are still assembled in terminally differentiated cells from basal bodies that are generated through the acentriolar pathway (Azimzadeh et al., 2012). *C. elegans* only possess primary cilia and lack motile cilia (Carvalho-Santos et al., 2011). Thus, as organisms evolved, the canonical cilium diversified, became more complex and adopted new functions.

Although the concept of a phylogenetic tree is fluid, especially in lower phyla due to the lack of complete and reliable genome sequences, it is surprising that no organisms discovered so far contain ‘evolutionarily intermediate’ forms of cilia. It is now accepted that the last eukaryotic common ancestor (LECA) possessed a sophisticated ancestral cilium capable of accomplishing both motile and sensory roles (Mitchell, 2016). What were the steps leading to the formation of an ancestral cilium? In order to assemble such an intricate and elaborate structure, the LECA must have had in place all of the required structural components (tubulins, radial spoke proteins), a functional membrane and protein trafficking system (including coat proteins, IFT proteins) and motor proteins (dyneins and kinesins).

It is also interesting to consider the evolutionary driving force behind the generation of this complex organelle. One of the current models suggests that formation of a sensory patch on the plasma membrane due to polarized trafficking from the endomembrane system might have been the precursor for the cilium (Satir et al., 2008). The basal body-derived microtubular core

presumably arose to provide structural stability to this ciliary prototype. It is not known if motility predated development of sensory function or if they co-evolved, but bringing cellular motility to an otherwise immotile organism could have served as a positive driving force (Mitchell, 2007).

More questions than answers

The rapid pace of research on ciliary biology and ciliopathies has raised many new questions. Recently, several G protein coupled receptors (GPCRs) have been localized to the ciliary membrane (Schou et al., 2015). Why are so many signaling proteins and receptors targeted to the cilium? What is the consequence of this localization and do downstream G-protein effectors also localize in the ciliary compartment?

What are the signaling pathways controlling ciliogenesis and how are they regulated in a cell-specific manner? Several positive and negative regulators of ciliogenesis have been identified, revealing an elaborate network of events that ultimately controls cilium assembly and length. At early steps of ciliogenesis, distal appendage protein CEP164 is essential for formation of the ciliary vesicle. CEP164 localizes to the centrioles in non-mitotic cells and recruits Rab8, a small GTPase, and its GDP/GTP exchange factor (GEF), Rabin8 (Schmidt et al., 2012). The subsequent step of axoneme elongation is considered to be under negative regulation, and requires the removal of inhibitory ‘cap’ proteins such as CP110 (Kleylein-Sohn et al., 2007). Kinases such as TTBK2 and MARK4, which regulate release of CP110 from the distal end of the centriole, have been described, but their exact mechanism of action is unclear (Goetz et al., 2012; Kuhns et al., 2013). The ubiquitin proteasome machinery is also emerging as a key player in the assembly and disassembly of cilia (Kasahara et al., 2014; Long et al., 2016).

In addition to these effector proteins, several highly conserved ciliary transcription factors that modulate expression of ciliary genes in different tissues have been discovered. The regulatory factor X (RFX) family of transcription factors regulate the assembly of primary and motile cilia

and forkhead box protein (FOXJ1) transcription factor is essential for motile ciliary assembly. Understanding the cross-talk between these transcription factors in different tissues and uncovering their target genes is vital to decoding ciliary assembly pathways (Choksi et al., 2014).

Another intriguing issue is the spatial control of ciliary assembly. How is the location at which a cilium or cilia appear in each cell determined? It is known that primary cilia assemble close to the Golgi, and are often submerged in a deep ciliary pocket. A recent study shows that a subset of sub-distal appendage proteins are dispensable for ciliogenesis, but disrupt centrosome cohesion and the close association of the primary cilium and Golgi, causing the cilium to emerge from the cell surface. These surface-localized primary cilia display altered mechanosensory properties (response to fluid flow) and localization of hedgehog signaling components (Mazo et al., 2016).

For generating an effective stroke to propel fluid, multiciliated cells must tightly regulate the location of hundreds of basal bodies to define ciliary positioning. The direction of basal body accessory structures, such as the basal foot and rootlet, determine the direction of ciliary beating. Planar cell polarity proteins such as Dishevelled, Vangl2, and cadherin proteins Celsr2 and Celsr3 are known to affect rotational polarity (parallel arrangement of rootlets within a multiciliated cell) and tissue level planar polarity (Park et al., 2008; Guirao et al., 2010; Tissir et al., 2010). Furthermore, loss of some planar cell polarity effector proteins also leads to defective ciliogenesis (Park et al., 2006). How the planar cell polarity and ciliogenesis pathways intersect in multiple cell types needs further exploration.

Finally, it is becoming clear that many ciliary proteins “moonlight”, playing essential roles in other cellular processes (Vertii et al., 2015). In dividing cells, IFT88 localizes at the spindle poles, where it recruits tubulin nucleating factors; loss of IFT88 leads to mitotic defects, suggesting it plays a critical non-ciliary role (Delaval et al., 2011). On the other hand, small

GTPases Rab8 and Rab11, well known regulators of endosomal trafficking, are essential for ciliogenesis. Active, GTP bound Rab11 recruits Rabin11, the GEF for Rab8, to the base of the cilium to promote primary ciliogenesis (Knodler et al., 2010). Another interesting example is the presence of ciliary proteins such as IFT20 in the immune synapse, a sensory patch on T-cells, which lack cilia. The immune synapse bears some striking similarities to the cilium; the centrosome and Golgi are positioned very close to the receptor-enriched synaptic membrane between the T-cell and antigen presenting cell. IFT20 is a primarily Golgi-localized component of the IFT complex, which is also present in the microtubule organizing center and post-Golgi vesicles. IFT20 localizes to the immune synapse; loss of IFT20 impairs signaling, possibly by impairing polarized trafficking from the Golgi (Finetti et al., 2009). In light of these findings, non-ciliary roles for ciliary proteins must be considered while assessing pathophysiology of ciliopathies.

REFERENCES

Arnaiz, O., Cohen, J., Tassin, A. M. and Koll, F. (2014). Remodeling Cildb, a popular database for cilia and links for ciliopathies. *Cilia* **3**, 9.

Arnaiz, O., Malinowska, A., Klotz, C., Sperling, L., Dadlez, M., Koll, F. and Cohen, J. (2009). Cildb: a knowledgebase for centrosomes and cilia. *Database (Oxford)* **2009**, bap022.

Awata, J., Takada, S., Standley, C., Lechtreck, K. F., Bellve, K. D., Pazour, G. J., Fogarty, K. E. and Witman, G. B. (2014). NPHP4 controls ciliary trafficking of membrane proteins and large soluble proteins at the transition zone. *J Cell Sci* **127**, 4714-4727.

Azimzadeh, J., Wong, M. L., Downhour, D. M., Sanchez Alvarado, A. and Marshall, W. F. (2012). Centrosome loss in the evolution of planarians. *Science* **335**, 461-463.

Bloodgood, R. A. (2010). Sensory reception is an attribute of both primary cilia and motile cilia. *J Cell Sci* **123**, 505-509.

Brown, J. M. and Witman, G. B. (2014). Cilia and Diseases. *Bioscience* **64**, 1126-1137.

Carvalho-Santos, Z., Azimzadeh, J., Pereira-Leal, J. B. and Bettencourt-Dias, M. (2011). Evolution: Tracing the origins of centrioles, cilia, and flagella. *J Cell Biol* **194**, 165-175.

Choksi, S. P., Lauter, G., Swoboda, P. and Roy, S. (2014). Switching on cilia: transcriptional networks regulating ciliogenesis. *Development* **141**, 1427-1441.

Craige, B., Tsao, C. C., Diener, D. R., Hou, Y., Lechtreck, K. F., Rosenbaum, J. L. and Witman, G. B. (2010). CEP290 tethers flagellar transition zone microtubules to the membrane and regulates flagellar protein content. *J Cell Biol* **190**, 927-940.

Davis, E. E., Brueckner, M. and Katsanis, N. (2006). The emerging complexity of the vertebrate cilium: new functional roles for an ancient organelle. *Dev Cell* **11**, 9-19.

Delaval, B., Bright, A., Lawson, N. D. and Doxsey, S. (2011). The cilia protein IFT88 is required for spindle orientation in mitosis. *Nat Cell Biol* **13**, 461-468.

Dobell, C. and Leeuwenhoek, A. v. (1932). Antony van Leeuwenhoek and his "Little animals"; being some account of the father of protozoology and bacteriology and his multifarious discoveries in these disciplines. New York,: Harcourt, Brace and company.

Finetti, F., Paccani, S. R., Riparbelli, M. G., Giacomello, E., Perinetti, G., Pazour, G. J., Rosenbaum, J. L. and Baldari, C. T. (2009). Intraflagellar transport is required for polarized recycling of the TCR/CD3 complex to the immune synapse. *Nat Cell Biol* **11**, 1332-1339.

Garcia, G., 3rd and Reiter, J. F. (2016). A primer on the mouse basal body. *Cilia* **5**, 17.

Goetz, S. C., Liem, K. F., Jr. and Anderson, K. V. (2012). The spinocerebellar ataxia-associated gene Tau tubulin kinase 2 controls the initiation of ciliogenesis. *Cell* **151**, 847-858.

Guirao, B., Meunier, A., Mortaud, S., Aguilar, A., Corsi, J. M., Strehl, L., Hirota, Y., Desoeuvre, A., Boutin, C., Han, Y. G. et al. (2010). Coupling between hydrodynamic forces and planar cell polarity orients mammalian motile cilia. *Nat Cell Biol* **12**, 341-350.

Hildebrandt, F., Benzing, T. and Katsanis, N. (2011). Ciliopathies. *N Engl J Med* **364**, 1533-1543.

Insinna, C. and Besharse, J. C. (2008). Intraflagellar transport and the sensory outer segment of vertebrate photoreceptors. *Dev Dyn* **237**, 1982-1992.

Jenkins, P. M., McEwen, D. P. and Martens, J. R. (2009). Olfactory cilia: linking sensory cilia function and human disease. *Chem Senses* **34**, 451-464.

Jin, H., White, S. R., Shida, T., Schulz, S., Aguiar, M., Gygi, S. P., Bazan, J. F. and Nachury, M. V. (2010). The conserved Bardet-Biedl syndrome proteins assemble a coat that traffics membrane proteins to cilia. *Cell* **141**, 1208-1219.

Johnson, N. T., Villalon, M., Royce, F. H., Hard, R. and Verdugo, P. (1991). Autoregulation of beat frequency in respiratory ciliated cells. Demonstration by viscous loading. *Am Rev Respir Dis* **144**, 1091-1094.

Kasahara, K., Kawakami, Y., Kiyono, T., Yonemura, S., Kawamura, Y., Era, S., Matsuzaki, F., Goshima, N. and Inagaki, M. (2014). Ubiquitin-proteasome system controls ciliogenesis at the initial step of axoneme extension. *Nat Commun* **5**, 5081.
Kleylein-Sohn, J., Westendorf, J., Le Clech, M., Habedanck, R., Stierhof, Y. D. and Nigg, E. A. (2007). Plk4-induced centriole biogenesis in human cells. *Dev Cell* **13**, 190-202.
Knodler, A., Feng, S., Zhang, J., Zhang, X., Das, A., Peranen, J. and Guo, W. (2010). Coordination of Rab8 and Rab11 in primary ciliogenesis. *Proc Natl Acad Sci U S A* **107**, 6346-6351.
Kuhns, S., Schmidt, K. N., Reymann, J., Gilbert, D. F., Neuner, A., Hub, B., Carvalho, R., Wiedemann, P., Zentgraf, H., Erfle, H. et al. (2013). The microtubule affinity regulating kinase MARK4 promotes axoneme extension during early ciliogenesis. *J Cell Biol* **200**, 505-522.
Lechtreck, K. F., Delmotte, P., Robinson, M. L., Sanderson, M. J. and Witman, G. B. (2008). Mutations in Hydin impair ciliary motility in mice. *J Cell Biol* **180**, 633-643.
Lechtreck, K. F., Johnson, E. C., Sakai, T., Cochran, D., Ballif, B. A., Rush, J., Pazour, G. J., Ikebe, M. and Witman, G. B. (2009). The *Chlamydomonas reinhardtii* BBSome is an IFT cargo required for export of specific signaling proteins from flagella. *J Cell Biol* **187**, 1117-1132.
Li, C., Jensen, V. L., Park, K., Kennedy, J., Garcia-Gonzalo, F. R., Romani, M., De Mori, R., Bruel, A. L., Gaillard, D., Doray, B. et al. (2016). MKS5 and CEP290 dependent assembly pathway of the ciliary transition zone. *PLoS Biol* **14**, e1002416.
Long, H., Zhang, F., Xu, N., Liu, G., Diener, D. R., Rosenbaum, J. L. and Huang, K. (2016). Comparative Analysis of Ciliary Membranes and Ectosomes. *Curr Biol*. **26**, 3327-3335
Lu, Q., Insinna, C., Ott, C., Stauffer, J., Pintado, P. A., Rahajeng, J., Baxa, U., Walia, V., Cuenca, A., Hwang, Y. S. et al. (2015). Early steps in primary cilium assembly require EHD1/EHD3-dependent ciliary vesicle formation. *Nat Cell Biol* **17**, 531.
Mazo, G., Soplop, N., Wang, W. J., Uryu, K. and Tsou, M. B. (2016). Spatial control of primary ciliogenesis by subdistal appendages alters sensation-associated properties of cilia. *Dev Cell* **39**, 424-437.
Mitchell, D. R. (2007). The evolution of eukaryotic cilia and flagella as motile and sensory organelles. *Adv Exp Med Biol* **607**, 130-140.
Mitchell, D. R. (2016). Evolution of Cilia. *Cold Spring Harb Perspect Biol*. Cilia, pp.369-380.
Nachury, M. V. (2014). How do cilia organize signalling cascades? *Philos Trans R Soc Lond B Biol Sci* **369**.
Nachury, M. V., Seeley, E. S. and Jin, H. (2010). Trafficking to the ciliary membrane: how to get across the periciliary diffusion barrier? *Annu Rev Cell Dev Biol* **26**, 59-87.
Nachury, M. V., Loktev, A. V., Zhang, Q., Westlake, C. J., Peranen, J., Merdes, A., Slusarski, D. C., Scheller, R. H., Bazan, J. F., Sheffield, V. C. et al. (2007). A core complex of BBS proteins cooperates with the GTPase Rab8 to promote ciliary membrane biogenesis. *Cell* **129**, 1201-1213.
Nigg, E. A. and Stearns, T. (2011). The centrosome cycle: Centriole biogenesis, duplication and inherent asymmetries. *Nat Cell Biol* **13**, 1154-1160.
Pan, J. and Snell, W. J. (2000). Signal transduction during fertilization in the unicellular green alga, *Chlamydomonas*. *Curr Opin Microbiol* **3**, 596-602.
Park, T. J., Haigo, S. L. and Wallingford, J. B. (2006). Ciliogenesis defects in embryos lacking inturned or fuzzy function are associated with failure of planar cell polarity and Hedgehog signaling. *Nat Genet* **38**, 303-311.
Park, T. J., Mitchell, B. J., Abitua, P. B., Kintner, C. and Wallingford, J. B. (2008). Dishevelled controls apical docking and planar polarization of basal bodies in ciliated epithelial cells. *Nat Genet* **40**, 871-879.
Satir, P., Mitchell, D. R. and Jekely, G. (2008). How did the cilium evolve? *Curr Top Dev Biol* **85**, 63-82.
Schmidt, K. N., Kuhns, S., Neuner, A., Hub, B., Zentgraf, H. and Pereira, G. (2012). Cep164 mediates vesicular docking to the mother centriole during early steps of ciliogenesis. *J Cell Biol* **199**, 1083-1101.
Schou, K. B., Pedersen, L. B. and Christensen, S. T. (2015). Ins and outs of GPCR signaling in primary cilia. *EMBO Rep* **16**, 1099-1113.

Schwander, M., Kachar, B. and Muller, U. (2010). Review series: The cell biology of hearing. *J Cell Biol* **190**, 9-20.
Shah, A. S., Ben-Shahar, Y., Moninger, T. O., Kline, J. N. and Welsh, M. J. (2009). Motile cilia of human airway epithelia are chemosensory. *Science* **325**, 1131-1134.
Sorokin, S. (1962). Centrioles and the formation of rudimentary cilia by fibroblasts and smooth muscle cells. *J Cell Biol* **15**, 363-377.
Sung, C. H. and Leroux, M. R. (2013). The roles of evolutionarily conserved functional modules in cilia-related trafficking. *Nat Cell Biol* **15**, 1387-1397.
Tissir, F., Qu, Y., Montcouquiol, M., Zhou, L., Komatsu, K., Shi, D., Fujimori, T., Labeau, J., Tyteca, D., Courtoy, P. et al. (2010). Lack of cadherins Celsr2 and Celsr3 impairs ependymal ciliogenesis, leading to fatal hydrocephalus. *Nat Neurosci* **13**, 700-707.
van Dam, T. J., Townsend, M. J., Turk, M., Schlessinger, A., Sali, A., Field, M. C. and Huynen, M. A. (2013). Evolution of modular intraflagellar transport from a coatomer-like progenitor. *Proc Natl Acad Sci U S A* **110**, 6943-6948.
Vertii, A., Bright, A., Delaval, B., Hehnly, H. and Doxsey, S. (2015). New frontiers: discovering cilia-independent functions of cilia proteins. *EMBO Rep* **16**, 1275-1287.
Wang, J., Silva, M., Haas, L. A., Morsci, N. S., Nguyen, K. C., Hall, D. H. and Barr, M. M. (2014). *C. elegans* ciliated sensory neurons release extracellular vesicles that function in animal communication. *Curr Biol* **24**, 519-525.
Waters, A. M. and Beales, P. L. (2011). Ciliopathies: an expanding disease spectrum. *Pediatr Nephrol* **26**, 1039-1056.
Wong, S. Y. and Reiter, J. F. (2008). The primary cilium at the crossroads of mammalian hedgehog signaling. *Curr Top Dev Biol* **85**, 225-260.
Wood, C. R., Huang, K., Diener, D. R. and Rosenbaum, J. L. (2013). The cilium secretes bioactive ectosomes. *Curr Biol* **23**, 906-911.
Yee, L. E., Garcia-Gonzalo, F. R., Bowie, R. V., Li, C., Kennedy, J. K., Ashrafi, K., Blacque, O. E., Leroux, M. R. and Reiter, J. F. (2015). Conserved genetic interactions between ciliopathy complexes cooperatively support ciliogenesis and ciliary signaling. *PLoS Genet* **11**, e1005627.

Chapter 2

60 Years of POMC: From POMC and α-MSH to PAM molecular oxygen, copper and vitamin C

Dhivya Kumar, Richard E. Mains and Betty A. Eipper

This chapter is a duplicate version of a review published in The Journal of Molecular Endocrinology. 2016 May; 56(4):T63-76.

ABSTRACT

A critical role for peptide C-terminal amidation was apparent when the first bioactive peptides were identified. The conversion of POMC into ACTH and then into αMSH, an amidated peptide, provided a model system for identifying the amidating enzyme. Peptidylglycine α-amidating monooxygenase (PAM), the only enzyme that catalyzes this modification, is essential; mice lacking PAM survive only until mid-gestation. Purification and cloning led to the discovery that the amidation of peptidylglycine substrates proceeds in two steps: peptidylglycine α-hydroxylating monooxygenase (PHM) catalyzes the copper and ascorbate-dependent α-hydroxylation of the peptidylglycine substrate; peptidyl-α-hydroxyglycine α-amidating lyase (PAL) cleaves the N-C bond, producing amidated product plus glyoxylate. Both enzymes are contained in the luminal domain of PAM, a type 1 integral membrane protein. The structures of both catalytic cores have been determined, revealing how they interact with metals, molecular oxygen and substrate to catalyze both reactions. Although not essential for activity, the intrinsically disordered cytosolic domain, is essential for PAM trafficking. A phylogenetic survey led to identification of bifunctional membrane PAM in *Chlamydomonas*, a unicellular eukaryote. Accumulating evidence points to a role for PAM in copper homeostasis and in retrograde signaling from the lumen of the secretory pathway to the nucleus. The discovery of PAM in cilia,

cellular antennae that sense and respond to environmental stimuli, suggests that much remains to be learned about this ancient protein.

POMC and PAM: Where it all began

Over the last three decades, we have amassed a great deal of information on the function, trafficking and biochemical properties of the only known peptide amidating enzyme, peptidylglycine α-amidating monooxygenase (PAM). Until its discovery in 1982, even the existence of such an enzyme was questioned (**Fig.1**). Based on the first biologically active peptides identified (vasopressin, oxytocin, α-MSH), it was clear that a C-terminal amide group was essential, but there was no reason to suspect that a mechanism other than transamination (such as in glutamine synthesis) might be in place. The discovery of glycine-extended precursors for amidated peptides such as αMSH, adipokinetic hormone and melittin raised the possibility that an enzyme recognizing the terminal glycine was involved in generating the mature amidated peptide (Harris and Lerner, 1957; Stone et al., 1976; Suchanek and Kreil, 1977).

Using a synthetic radiolabeled peptidylglycine substrate (based on the last three amino acid residues of the αMSH precursor), Bradbury et al. demonstrated the presence of an activity catalyzing the amidation reaction in secretory granules of bovine pituitaries (Bradbury et al., 1982). In this landmark study, the amide group nitrogen was shown to be derived from the glycine residue, ruling out the possibility of a transaminase reaction; the formation of glyoxylate during the reaction pointed to a hydroxylation step in the reaction mechanism (Bradbury et al., 1982).

Around this time, our laboratory was focused on understanding the tissue-specific differential processing of POMC. The proteases that produced the longer peptides (such as pro-γ-MSH, ACTH, JP and βLPH in corticotropes) or the shorter peptides (such as αMSH, γ-MSH and β-endorphin in melanotropes and hypothalamic POMC neurons) were of special interest. Establishing primary rat intermediate pituitary cultures seemed like a convenient way to characterize the production of αMSH from what was then known as pro-ACTH. In order to study

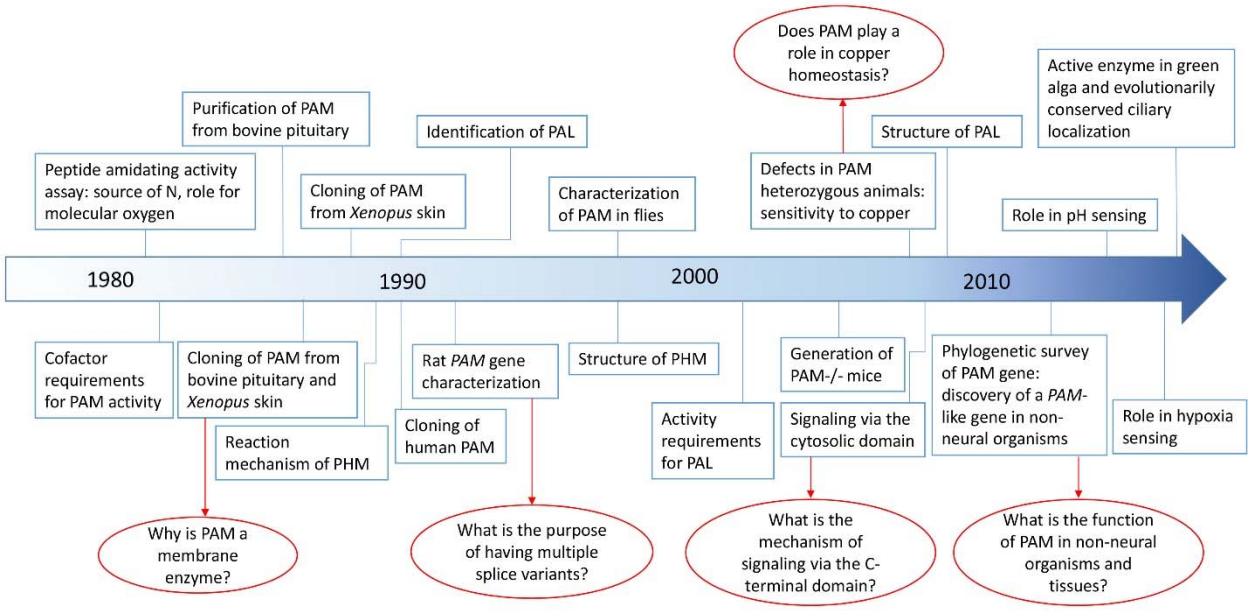

Figure 1. Timeline highlighting key developments leading from POMC processing studies to PAM. The landmark study of Bradbury et al. (1982) (Bradbury et al., 1982), provided a means of assaying peptide amidating activity in tissue lysates. Purification, cloning and structural/mechanistic studies focused on PAM and then expanded to include cell biological studies on secretory granule biogenesis, retrograde signaling from the granule lumen to the nucleus and the delivery of essential cofactors (ascorbate and copper) to the secretory pathway. Key unanswered questions are marked by red arrows.

secretion, it was important to culture cells in serum-free medium. However, it soon became obvious that serum contained a factor that was essential for the conversion of αMSH-Gly into amidated αMSH. Antibody specific for amidated αMSH was key in realizing that otherwise healthy pituitary cells maintained in serum-free medium performed all of the processing steps required for generating active α-MSH including proteolytic cleavage and acetylation, except for amidation (Eipper et al., 1983a; Glembotski et al., 1983). In order to identify the serum factor(s) required for amidation, we turned to the newly developed enzyme assay to take a closer look at the amidating enzyme.

As a first step, secretory granules were purified from rat and bovine anterior, intermediate and neural pituitary; β-endorphin immunoreactivity served as a convenient marker for granule fractions (Eipper et al., 1983b). Using the assay developed by Bradbury et al. in 1982, amidation activity could be detected in the secretory granules from all three regions. A simple experiment - determining the pH optimum - proved to be key in determining the co-factor requirements of the enzyme. Activity was greatly reduced in citrate and phosphate buffers, which can chelate metals, compared to sulfonic acid buffers. Subsequent experiments confirmed an essential role for copper (Eipper et al., 1983b). Similar to other copper-dependent enzymes involved in redox reactions requiring molecular oxygen, the amidation reaction was dependent on oxygen availability. The remarkable similarity of the amidation reaction to that of dopamine β-monooxygenase (DBM), which converts dopamine to norepinephrine in a copper, molecular oxygen and ascorbate (vitamin C) dependent manner, suggested that ascorbate might provide the reducing equivalents essential for peptide amidation. As predicted, ascorbate was a potent stimulator of peptide amidation catalyzed by peptidylglycine-α-amidating monooxygenase (PAM) (Eipper et al., 1983b). Knowing the cofactors required for its catalytic activity, we were not surprised that simply adding ascorbate to our serum-free medium allowed melanotropes to produce amidated αMSH. Peptidylglycine α-amidating monooxygenase (PAM; EC 1.14.17.3)

and dopamine β-monooxygenase (DBM; EC 1.14.17.1) were thought to form a family of related copper-dependent monooxygenases; this meant that the detailed structural and mechanistic studies carried out on DBM (Stewart and Klinman, 1988) could guide studies of PAM.

WHAT HAVE WE LEARNED ABOUT PAM SINCE ITS IDENTIFICATION?

Structure of the PAM gene

The flurry of activity that ensued centered on cloning the gene encoding PAM (**Fig.1**). The protein was purified from bovine pituitaries and used to generate antibodies (Murthy et al., 1986; Eipper et al., 1987). Having antibodies allowed identification of a cDNA encoding PAM using a phage expression library generated from bovine intermediate pituitary RNA (Eipper et al., 1987). At the same time, a cDNA encoding PAM was cloned from *Xenopus laevis* skin (Mizuno et al., 1987; Ohsuye et al., 1988). Analysis of the protein encoded by the PAM cDNA delivered a few surprises. As expected, a cleaved signal peptide was found, allowing entry of PAM into the secretory pathway lumen. The cDNA encoded a protein more than twice the size expected. Although the enzyme purified from pituitary was soluble, the cDNA encoded what was predicted to be a type 1 integral membrane protein – its single membrane spanning domain was followed by a short stretch of hydrophilic residues predicted to reside in the cytoplasm. Several pairs of basic amino acids - recognition sites for prohormone convertase-like endoproteases - were also present in the intraluminal part of the PAM protein. Several questions arose: Why would an enzyme catalyzing amidation of bioactive peptides include a transmembrane domain? Why did it include endoproteolytic cleavage sites and how did they affect its processing and activity? Efforts spanning over two decades have unraveled the answers to some of these puzzling questions.

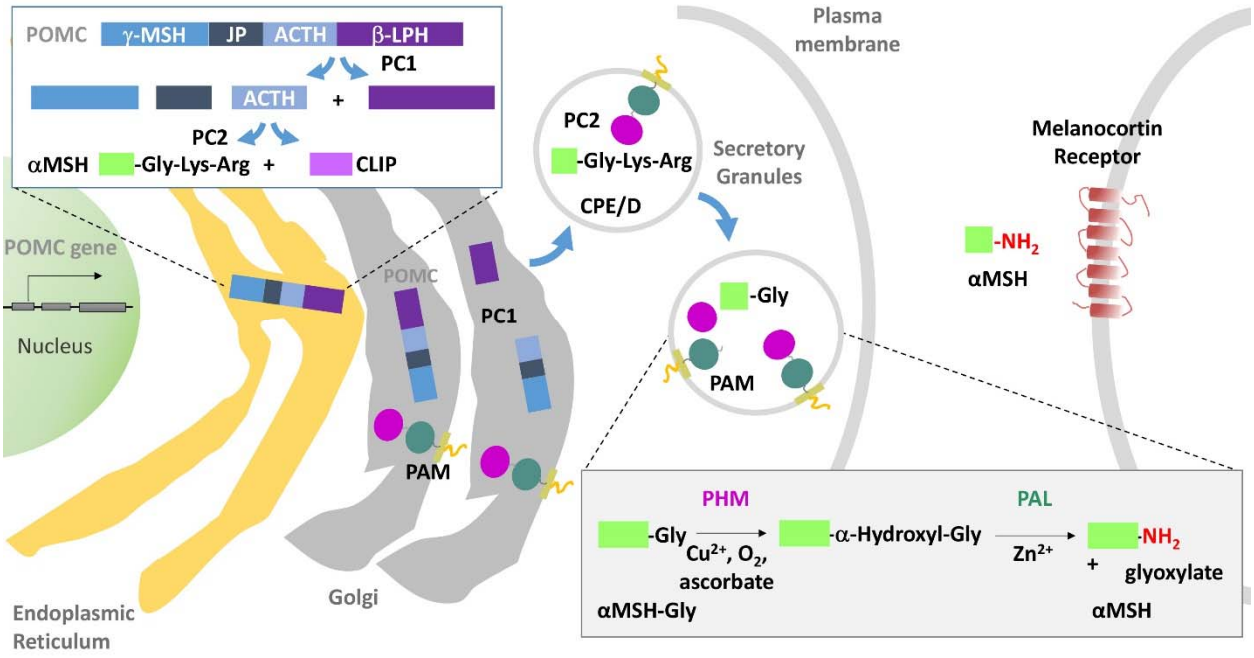

Figure 2. POMC processing: amidation of αMSH. Following the co-translational removal of its N-terminal signal sequence, POMC moves through the Golgi complex. As luminal pH begins to fall and prohormone convertase 1 (PC1) is activated, the first POMC cleavage produces ACTH biosynthetic intermediate and β-Lipotropin. Subsequent cleavages (upper left box), which occur largely in maturing secretory granules, separate Joining Peptide (JP) from ACTH; the C-terminus of JP can be amidated. Melanotropes, which express both PC1 and PC2, cleave ACTH(1-39) to produce an N-terminal fragment (precursor to αMSH) and CLIP (corticotropin-like intermediate lobe peptide). The production of αMSH requires a carboxypeptidase, PAM and an N-acetyltransferase (not shown). The sequential actions of PHM and PAL on αMSH-Gly are illustrated (lower right box).

A PAL for PHM

It was soon discovered that the PAM cDNA encoded two enzymatic domains, both of which were necessary to yield an amidated peptide (**Fig. 2**). Formation of an α-hydroxyglycine intermediate by the stereo-specific hydroxylation of the glycine-extended peptide precursor was proposed as the first step in the reaction mediated by PAM (Young and Tamburini, 1989). Although the second step of this reaction, cleavage of the N-C bond to yield amidated product is spontaneous in alkaline pH, it is impeded in the acidic environment of secretory granules. The stability of synthetic peptides terminating with a COOH-terminal α-hydroxyglyine residue was shown to decline at pH values above 6, with half-lives of 8 h at pH7.4 (Bundgaard and Kahns, 1991). An enzyme catalyzing N-C bond cleavage was identified in bovine neurointermediate pituitaries; it was found that the bovine PAM precursor also contained this enzymatic activity. Thus, the PAM gene encodes two enzymatic domains that function sequentially to generate amidated peptides: peptidyglycine α-hydroxylating monooxygenase (PHM; EC 1.14.17.3) and peptidyl-α-hydroxyglycine α-amidating lyase (PAL; 4.3.2.5) (Katopodis et al., 1990; Perkins et al., 1990). Studies with purified PAL protein revealed its pH optimum to be in the acidic range and its dependence on zinc (Eipper et al., 1991).

Apart from endoproteolytic processing, functionally different forms of PAM can also be generated by alternative splicing. The longest isoform (PAM-1) (**Fig. 3A**) contains the two enzymatic domains, a transmembrane domain, a cytosolic domain and an endoprotease-sensitive linker region between PHM and PAL. This endoprotease-sensitive region is not included in the PAM-2 isoform, and PHM and PAL are rarely separated by cleavage. A third major isoform (PAM-3) lacks both the endoproteolytic cleavage site and the transmembrane domain, allowing soluble, bifunctional PAM to be secreted. PAM expression is not limited to neuroendocrine tissues; PAM is expressed at widely varying levels in almost all mammalian cell types, with significant expression in airway epithelium, ependymal cells in the brain, endothelial

cells and adult atrium as well as brain and pituitary (Eipper et al., 1988; Oldham et al., 1992; Schafer et al., 1992). PAM expression is developmentally regulated; isoform-specific regulation is especially apparent in heart and neural tissues, suggesting that different isoforms have distinct functions (Braas et al., 1989; Stoffers et al., 1989; Stoffers et al., 1991; Eipper et al., 1992). Both in neurons and endocrine cells, soluble PHM and PAL are secreted along with neuropeptides and peptide hormones upon stimulation; PHM and PAL can be detected in serum and cerebrospinal fluid (Mains et al., 1985; Wand et al., 1985).

Cellular requirements for PAM activity

PAM activity requires the delivery of copper and ascorbate to the lumen of the secretory pathway. Cells devote considerable energy to compartmentalizing and tightly regulating the flow of copper, a transition metal that can participate in free radical formation. Copper transporters deliver copper to intracellular copper chaperones such as COX17 and Atox1, which deliver copper to specific acceptor proteins. For the secretory pathway, two P-type ATPases, ATP7A and ATP7B, receive copper from Atox1 and transport it into the lumen (Prohaska, 2008). No copper chaperones have been identified in the secretory pathway lumen and it has been suggested that PHM is metallated directly by the P-type ATPases (El Meskini et al., 2001; Otoikhian et al., 2012).While most organisms, including rodents, synthesize ascorbate from glucose, humans lack this ability and must acquire it from their diet. Two Na^+-dependent ascorbate transporters (SVCT1 and SVCT2) expressed in intestinal epithelial cells and neuroendocrine cells, respectively, import ascorbate into cells (Burzle and Hediger, 2012); neuroendocrine cells lack gulonolactone oxidase and must use SVCT2 to obtain ascorbate from the circulation. It is not known how ascorbate enters the secretory pathway lumen, but it is maintained in the reduced state by the action of cytochrome $b_{561,}$ which shuttles electrons across the secretory pathway membrane (Asada et al., 2005; Iliadi et al., 2008).

Another important factor necessary for amidation is the low pH of the secretory pathway lumen. Both PHM and PAL exhibit optimal activity under acidic conditions. Intraluminal pH is maintained by the proton pumping activity of the multi-subunit vacuolar or V-ATPase. In addition to its role in acidification, the V-ATPase plays a role in secretory granule biogenesis through its role in sorting of vesicular cargo (Sobota et al., 2009). This proton pump also relays information about amino acid levels in the interior of lysosomes to mTOR (mammalian Target of Rapamycin), a cytosolic Ser/Thr kinase that serves as a master energy regulator (Jewell et al., 2013). It is intriguing to consider a role for PAM in signaling nutritional status information from distal parts of the secretory pathway (glycine levels, for example) to mTOR through the V-ATPase.

Crystal structures and insights into mechanism of peptide amidation

As mentioned previously, the cofactor requirements for the PHM domain of PAM are strikingly similar to those of dopamine β-monooxygenase (DBM). The similarity extends to their amino acid sequences, with about 30% identity in the catalytic cores of the two molecules (Prigge et al., 1997). Another member of this small family of copper-dependent monooxygenases is the endoplasmic reticulum localized Monooxygenase X (MOX), predicted to hydroxylate an unidentified hydrophobic substrate (Xin et al., 2004). Of these three monooxygenases, PHM is the only one with a solved crystal structure (**Fig.3B** and **C**), providing key insights into reaction mechanism (Prigge et al., 1997; Prigge et al., 1999; Prigge et al., 2004). Only small structural differences were observed when the protein was crystallized in the reduced, oxidized or substrate bound form. The catalytic core of PHM has two domains, each composed primarily of eight antiparallel β-strands (**Fig.3B**). Resembling a jelly roll motif, each domain has a hydrophobic interior held together by disulfide linkages; the two domains are linked by a single polypeptide chain. Each domain has one copper binding site: the three His residues of the Cu_H site are in the N-terminal domain; the two His and one Met of the Cu_M site are in the C-terminal

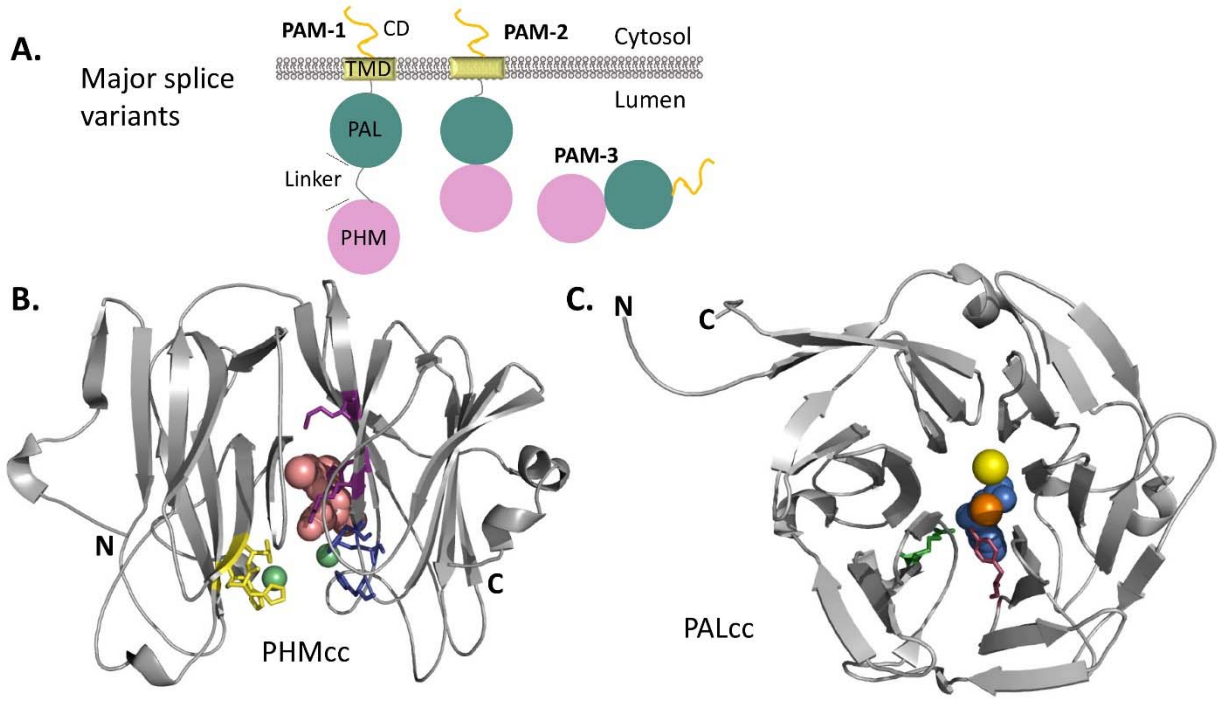

Figure 3. Major PAM Splice Variants and PHM and PAL Catalytic Core Structures. (A) The major splice variants (isoforms) of PAM are shown. While PAM-1 and PAM-2 are type 1 integral membrane proteins, PAM-3 is a soluble, secreted protein. (**B**) Crystal structure of rat PHM (PDB identifier: 1OPM) in the oxidized state bound to a substrate, N-acetyl-3,5-diiodotyrosylglycine (shown in pink), rendered here using PyMOL; bound copper, green spheres. The copper binding site in the N-terminal domain of PHM (Cu_H, in yellow) is separated from the copper binding site in the C-terminal domain (Cu_M, in blue) by an 11Å solvent filled cleft; the peptidylglycine substrate and molecular oxygen bind near Cu_M. Other essential catalytic residues involved in substrate binding (R^{240}, Y^{318}, M^{320}) are shown in purple. After considering many mechanisms, quantum mechanical tunneling is thought to facilitate electron transfer from the Cu_H site, through solvent, to the Cu_M site (Francisco et al., 2004; Klinman, 2006; McIntyre et al., 2010). (**B**). The structure of PAL (PDB identifier: 3FW0) crystallized in the presence of mercury ion (orange) instead of zinc to capture binding of a non-peptide substrate (alpha-hydroxyhippuric acid, in blue) is shown. The six-bladed β-propeller structure of PAL positions Zn near a key Tyr residue (shown in purple) and a key Arg residue (shown in green). The structurally important calcium ion is depicted as a yellow sphere (Chufan et al., 2009).

domain. An 11 Å solvent exposed hydrophilic cleft separates Cu_H from Cu_M; in two single electron steps, both sites are reduced. Molecular oxygen binds to the Cu_M site, with the peptidylglycine substrate bound close by; glycine is the only amino acid that can be accommodated and there is no indication that the distance between Cu_H and Cu_M varies during the reaction. The active site of PHM can accommodate large substrates (e.g. ubiquitin and selected immunoglobulin heavy chains) as well as fatty acyl glycines and other non-peptide substrates (Wilcox et al., 1999; Chew et al., 2005; Skulj et al., 2014).

The crystal structure of the catalytic core of PAL was solved about ten years later (**Fig.3C**): it is a six-bladed β-propeller, with long loops extending from the propeller surface (Chufan et al., 2009). The central cavity houses a calcium ion required for structural integrity and a zinc ion required for catalytic activity. The peptidyl-α-hydroxyglycine substrate binds close to the zinc, which is coordinated by three His residues. Well conserved tyrosine (Tyr^{654}) and arginine (Arg^{706}) residues play a critical role in catalysis (De et al., 2006; Chufan et al., 2009). As in the catalytic core of PHM, disulfide linkages play an essential role in the structural integrity of PAL. The N- and C-termini of PAL are positioned close to each other and its C-terminus is tethered to the membrane; the unique geometry of the β-propeller structure positions PHM close to the membrane to receive copper and ascorbate from transmembrane P-type ATPases and cytochrome b_{561}.

With the ability to produce active PHMcc and site directed mutants in mammalian cells, the unique properties of the two essential copper binding sites and the effects of pH on PHM were determined (Jaron et al., 2002; Siebert et al., 2005; Evans et al., 2006; Kline et al., 2013). The detailed mechanistic studies carried out previously on purified dopamine β-monooxygenase guided similar studies on PHMcc (Stewart and Klinman, 1988). The initial focus was on the 11 Å solvent filled gap separating the two essential copper binding sites. Cu_H, which has the properties expected of an electron transfer site, and Cu_M, which binds O_2 and is adjacent to the

peptidylglycine substrate, are both essential. After exploring multiple possibilities, the effects of temperature on intrinsic isotope effects and modeling studies have led to the consensus that PHM-dependent C(α)-H bond activation is dominated by quantum mechanical tunneling (Francisco et al., 2002; Francisco et al., 2004; Klinman, 2006; McIntyre et al., 2010). Efforts to develop inhibitors of PHM and PAL continue (Merkler et al., 2008; Langella et al., 2010). Disulfiram, a copper chelator reduces levels of amidated peptides in rat pituitary and cerebral cortex, presumably by inhibiting PHM activity (Mueller et al., 1993). A mechanism based suicide inhibitor, 4-phenyl-3-butenoic acid has been shown to inhibit PHM activity *in vivo* (Mueller et al., 1999). Other potent inhibitors include hippurate analogs and N-substituted homocysteine analogs (Erion et al., 1994; Merkler et al., 2008).

MORE THAN JUST AN ENZYME - A MULTI-TASKING PROTEIN

Evolutionary distribution of PAM

Amidated peptides are widespread, with roles in organisms with simple nervous systems, such as Hydra and Aplysia (Fujisawa et al., 1999; Grunder and Assmann, 2015). Furthermore, PAM has been characterized in sea anemone, fly and flatworm (Kolhekar et al., 1997; Williamson et al., 2000; Han et al., 2004; Mair et al., 2004). Although it was assumed that PAM co-evolved with the nervous system, recent studies suggest otherwise. A phylogenetic study identified PAM-like sequences in non-neural organisms such as *Amphimedon queenslandica*, a sponge, and *Trichoplax adhaerens*, a placozoan. Neuropeptide like sequences have been found in the *Trichoplax* genome and immunoreactivity to amidated peptides has been demonstrated in cells of *Trichoplax* (Jekely, 2013; Smith et al., 2014). Perhaps more surprising was finding PAM-like sequences in several green algal genomes; the presence of PAM in *Chlamydomonas reinhardtii*, *Volvox carteri* and *Ostreococcus tauri* raised the possibility that PAM evolved before the divergence of plants and animals (Attenborough et al., 2012). Active PAM enzyme has been

demonstrated in the unicellular green alga, *Chlamydomonas reinhardtii* raising the question of ancestral function (Kumar et al., 2015). Although amidated peptides have not been identified in green algae, the evolutionary conservation of components essential for PAM activity (copper homeostatic machinery, ascorbate synthesis, the V-ATPase) in eukaryotes certainly supports the possibility of amidation reactions occurring in these non-neural organisms. It is also possible that PAM amidates non-peptide substrates, or has a completely novel role distinct from those discovered in mammals.

The cytosolic domain of PAM

Although a cytosolic domain is not essential for PHM or PAL activity, the PAM gene in *Chlamydomonas reinhardtii* encodes a protein of identical topology (Kumar et al., 2015). Unlike soluble granule content proteins, granule membrane proteins are not secreted; after exocytosis and insertion into the plasma membrane, membrane PAM can be retrieved, traveling through the endocytic pathway in a regulated manner. In *Drosophila*, gene duplication is thought to have produced separate genes encoding soluble PHM, soluble PAL and membrane PAL.

Unlike the catalytic domains of PAM, its cytosolic domain is protease sensitive; the specific activity of PHM is increased following removal of the cytosolic domain. The cytosolic domain of PAM plays an essential role in its trafficking in mammalian cells; although soluble PHM and soluble PAL accumulate in secretory granules, PAM lacking its cytosolic domain accumulates on the plasma membrane (Tausk et al., 1992; Milgram et al., 1993). Furthermore, an epitope-tagged protein consisting of the transmembrane and cytosolic domains of PAM localizes to the trans Golgi network and secretory granules, indicating that it contains key trafficking information (El Meskini et al., 2001).

The cytosolic domain (86 residues in mammalian PAM) is unstructured and contains no characteristic motifs. It is sensitive to proteolytic degradation, a feature characteristic of

intrinsically disordered proteins involved in signaling, where the signal must be turned off just as rapidly as it is turned on (Rajagopal et al., 2009). Unstructured domains are often hubs of protein/protein interactions and multiple PAM cytosolic domain interactors have been identified. Kalirin and Trio, members of the Rho GDP/GTP exchange factor (Rho-GEF) family, play roles in cytoskeletal control and the maintenance of synapses. Uhmk1, a Ser/Thr kinase, phosphorylates the C-terminus of PAM and Rassf9, a member of the Ras-association domain family, plays a role in epidermal homeostasis (Alam et al., 1996; Lee et al., 2011). More recently, PAM has been shown to interact with the Adaptor Protein-1 (AP-1) Complex (Bonnemaison et al., 2015). The AP-1 complex belongs to a family of endosomal and secretory granule coat proteins that link cargo proteins to clathrin; both PAM and Atp7a, the P-type ATPase that transports copper into the TGN, interact with AP-1. Diminished AP-1 function affects PAM and Atp7a trafficking through the endocytic pathway. Antibodies to amidated (18 kDa fragment) and non-amidated POMC products allowed development of an assay to measure PAM activity in cells following manipulation of copper levels; cells with reduced AP-1 levels were more sensitive to copper restriction than control cells (Bonnemaison et al., 2014; Bonnemaison et al., 2015).

Mass spectrometry and two dimensional gel electrophoresis revealed multiple phosphorylation sites (Ser and Thr) in the cytosolic domain of PAM (Rajagopal et al., 2009). Phosphomimetic mutants revealed a role for phosphorylation in PAM trafficking through various biosynthetic and endocytic compartments. Development of an antibody specific to the C-terminal domain of PAM allowed identification of the various proteolytic fragments generated. Prohormone convertase-mediated cleavage of PAM in the secretory granules generates a slightly larger transmembrane/cytosolic domain fragment that γ-secretase-mediated cleavage of PAM. Both transmembrane/cytosolic domain fragments can be cleaved by γ-secretase; this intramembrane cleavage produces a short-lived, soluble 16 kDa fragment (sf-CD, soluble fragment of PAM

cytosolic domain) that accumulates in the nucleus (Rajagopal et al., 2009; Rajagopal et al., 2010). Upregulation of PAM-1 levels in a corticotrope cell line caused alterations in cell morphology, a reduction in secretagogue-responsiveness and altered expression of a subset of genes, including copper chaperones, aquaporin 1 and Slpi, a protease inhibitor (Francone et al., 2010). In addition to its enzymatic role, these studies indicate that PAM relays signals from the lumen of the secretory/endocytic pathway to the nucleus, in a manner similar to other type I integral membrane proteins in the endoplasmic reticulum such as SREBP and ATF6 (Rajagopal et al., 2012).

Lessons learned from knockout and heterozygous mice

Mice lacking both copies of *Pam* show no detectable peptide amidation activity and do not survive past mid-gestation, dying at e14.5 to e15.5 (Czyzyk et al., 2005). The *Pam* null embryos display severe edema, cardiac malformations and poor vasculature compared to wild type littermates. The heterozygous animals on the other hand, have half the wild type level of PAM activity and are viable. The heterozygous animals showed only minor changes in the levels of the amidated peptides tested, suggesting that the reduced levels of PAM in $PAM^{+/-}$ mice were sufficient to catalyze the amidation reaction (Czyzyk et al., 2005).

As they age, $PAM^{+/-}$ mice display increased adiposity compared to age matched wild type littermates. Glucose metabolism, which is regulated in part by amidated peptides, is impaired in older PAM heterozygous mice compared to wild type controls (Czyzyk et al., 2005). The $PAM^{+/-}$ animals demonstrate other behavioral deficits: they are unable to regulate body temperature, show increased anxiety-like behavior and are more susceptible to seizures compared to wild type mice. Moreover, wild type mice maintained on a copper restricted diet mimic many of the behavioral deficits observed in $PAM^{+/-}$ mice and supplemental dietary copper reverses some of the behavioral defects observed in $PAM^{+/-}$ animals (Bousquet-Moore et al., 2009; Bousquet-Moore et al., 2010). These data suggest that altered copper homeostasis contributes to the

behavioral defects observed in PAM heterozygous mice. A role for PAM in copper homeostasis had not previously been suspected.

Sensory roles of PAM

Comparative genomic analyses suggest that cuproproteins evolved following oxygenation of the Earth; thus PAM belongs to a small set of cuproenzymes with primitive roles predating multicellularity. As one of the few proteins dependent on a steady supply of copper and molecular oxygen for activity, PAM is well positioned to function as a sensor for these critical factors. As mentioned above, studies with mice lacking one copy of *Pam* and signaling mediated by PAM sf-CD suggest an involvement in copper sensing. Additional support for this hypothesis comes from studies using corticotrope cell lines. Depleting or overloading these cells with copper alters the trafficking of PAM through the secretory and endocytic pathways, but does not lead to its degradation, as in the case of other cuproproteins (De et al., 2007).

The absolute dependence of the amidation reaction on molecular oxygen has been known for a long time, but whether physiologically relevant changes in oxygen levels affected PHM activity was not known. A recent study shows that the ability of PAM to produce amidated products is as sensitive to changes in oxygen level as the prolyl hydroxylases that control the stability of hypoxia inducible factor (HIF), a key oxygen signaling protein. The speed and sensitivity with which PAM activity responds to hypoxia suggest a novel, paracrine signaling mechanism that could operate during oxygen homeostasis *in vivo* (Simpson et al., 2015).

The pH gradient in the lumen of the secretory pathway plays an essential role in the biosynthesis and processing of proteins. Enzymes like PAM, which operate late in the secretory pathway, display acidic pH optima, and the pH gradient in the luminal compartment often dictates which biosynthetic enzymes are active and which processing steps can occur. The protease-sensitive linker region that connects the catalytic core of PHM to the catalytic core of

PAL contains a cluster of histidine residues (His-Gly-His-His) that confer pH sensitivity (Vishwanatha et al., 2014). PAM lacking these histidine residues (Ala-Gly-Ala-Ala) is handled differently in corticotrope cell lines; instead of being recycled, endocytosed PAM lacking this His-cluster is rapidly degraded. The γ-secretase-mediated production of PAM sf-CD is largely eliminated and the morphological changes associated with PAM expression no longer occur.

WHAT THE FUTURE HOLDS FOR PAM BIOLOGY

The involvement of PAM in sensing environmental signals and generating factors involved in transcriptional regulation led us to expand our studies beyond the role of PAM as an amidating enzyme. Thus, there has been a paradigm shift in our understanding of this multi-tasking protein. We see understanding the role of PAM in non-neural tissues and organisms as key to uncovering all of the functions of this ancient, evolutionarily conserved protein. For instance, it will be interesting to determine the significance of abundant levels of PAM in the atrium, where it comprises about 1% of the total proteome (O'Donnell et al., 2003).

Mutations in the luminal copper transporting P-type ATPase, ATP7A, cause Menkes disease, a copper metabolism disorder characterized by neurodegeneration, mental retardation, connective tissue abnormalities and early childhood lethality. Several cuproenzymes, including PAM are affected by the loss of functional ATP7A. Using the mottled-brindled mouse, an animal model for Menkes disease, normal levels of PAM expression, but reduced levels of amidated peptides such as joining peptide, α-MSH and cholecystokinin were shown, suggesting that alterations in PAM activity might contribute to some of the phenotypes observed in these patients (Steveson et al., 2003). Altered PAM levels/activity have also been reported in the cerebrospinal fluid of multiple sclerosis and post-polio syndrome patients (Tsukamoto et al., 1995; Gonzalez et al., 2009). The ability to assay PAM activity in serum makes it an attractive biomarker candidate (Gaier et al., 2014).

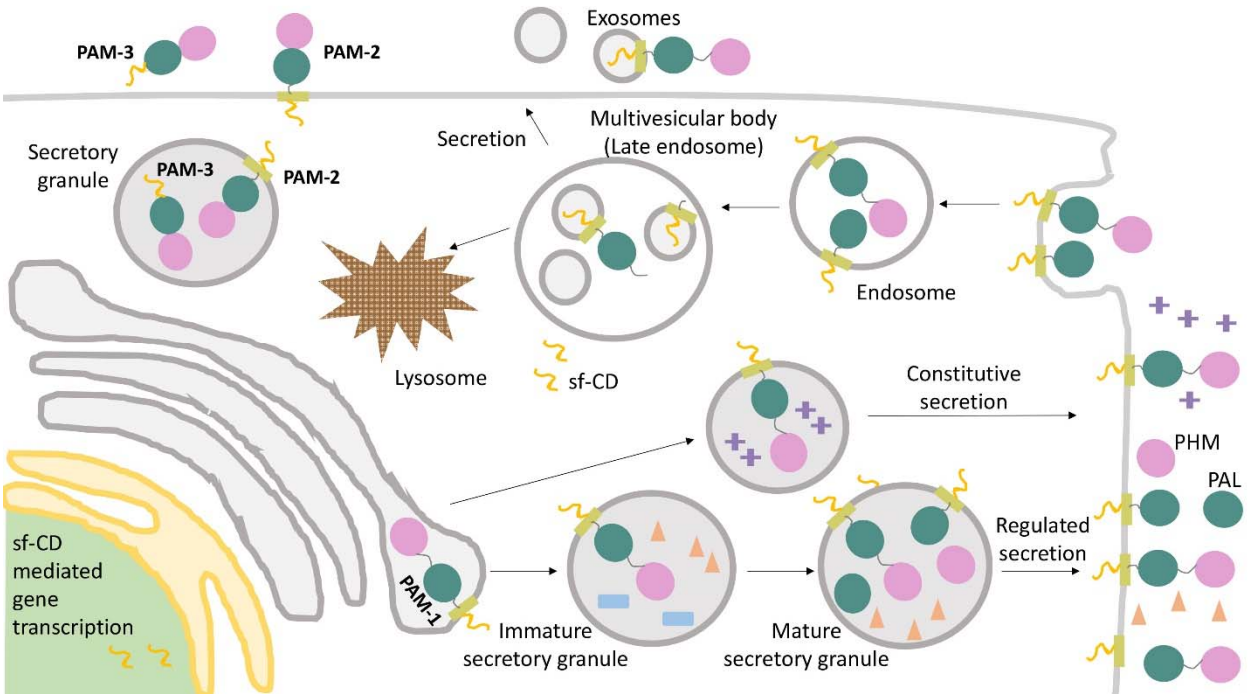

Figure 4. PAM trafficking. Membrane PAM (PAM-1, PAM-2) travels through both the biosynthetic and endocytic pathways; soluble PAM (PAM-3) is efficiently packaged into secretory granules and secreted. Cleavage of PAM in the biosynthetic pathway involves the prohormone convertases and cleavages at pairs of basic residues in the linker region between PHM and PAL and immediately following PAL. Cleavages on the cell surface and in the endocytic pathway involve α-secretase and γ-secretase. Phosphorylation of its cytosolic domain affects the ability of PAM to move from the limiting membrane of MVBs into the intraluminal vesicles. Endocytosed PAM can be returned to the trans-Golgi network, for re-entry into secretory granules, or degraded in lysosomes.

During its endocytic trafficking, PAM enters the intraluminal vesicles that characterize multivesicular bodies (**Fig. 4**); the fusion of multivesicular bodies with the plasma membrane results in release of these intraluminal vesicles, which are then known as exosomes (Rajagopal et al., 2010). Since they can be isolated from a variety of sources such as saliva, serum and urine, exosomes are being explored as a diagnostic tool (Simpson et al., 2009). PAM was identified in exosomes derived from human saliva and prostate cancer cells (Gonzalez-Begne et al., 2009; Minciacchi et al., 2015). It will be interesting to determine if PAM-containing exosome release is differentially regulated, especially during genetic or metabolic alterations.

PAM, cilia and POMC in obesity

A close look at the phylogenetic distribution of PAM suggested a strong correlation with the presence of cilia, leading us to explore the presence of PAM in this signaling organelle (Kumar et al., 2015). PAM localizes to primary and motile cilia in mammalian cells and to the motile cilium of *Chlamydomonas reinhardtii*, a unicellular eukaryote, suggesting an important, evolutionarily conserved role for PAM in this organelle (**Fig.5**). Cilia are tiny hair-like, microtubule-based organelles that extend from the cell surface of almost all mammalian cells. Primary cilia are critical sensory and signaling structures, important for sensing and responding to environmental stimuli. Multiple, motile cilia in unicellular eukaryotes, tracheal and ependymal cells play additional roles in cell motility and fluid propulsion. Acting as tiny reaction chambers, cilia compartmentalize signaling pathways and proteins. Ciliary protein entry and exit is tightly regulated by specialized trafficking pathways. Only proteins destined for the cilium are recognized by the intraflagellar trafficking machinery. Ciliary dysfunction affects a number of different tissues including kidney, heart and eyes, resulting in disorders collectively known as ciliopathies (Fliegauf et al., 2007).

The significance of POMC in energy homeostasis is clear: loss of POMC or melanocortin receptors, MC3R and MC4R, causes an obesity phenotype in mice, and mutations in *POMC*

result in obesity in humans (Hinney et al., 1998; Yaswen et al., 1999; Challis et al., 2004). The leptin/melanocortin system plays a central role in regulating feeding behavior and obesity. Leptin, a satiety hormone, is secreted by adipocytes in proportion to body fat and acts on POMC and NPY neurons in the hypothalamus to reduce food intake and promote thermogenesis. Increased POMC production as a result of leptin signaling leads to a rise in αMSH and βMSH levels; their binding to melanocortin receptors regulates energy balance (Sen Gupta et al., 2009).

A number of recent studies have shown that cilia play an important role in energy homeostasis. Several GPCRs, including melanin-concentrating hormone receptor-1 (MCHR1), localize to cilia (**Fig.5**), suggesting that G-protein signaling might occur in cilia (Berbari et al., 2008a). Furthermore, this localization is perturbed in mice lacking components of the BBSome (Berbari et al., 2008b). The BBSome, a multi-protein complex comprised of seven Bardet-Biedl Syndrome (BBS) proteins, is implicated in membrane protein trafficking and ciliary biogenesis (Jin and Nachury, 2009). Mutations in these BBS genes result in a ciliopathy (Bardet-Biedl Syndrome) characterized by mental retardation, retinopathy and renal defects. Obesity is also observed in these patients and mouse models of the disease, further strengthening the link between energy homeostasis and cilia (Sen Gupta et al., 2009).

Leptin signaling has recently been linked to the cilium - hyperphagic BBS mutant mice have increased levels of circulating leptin and are resistant to exogenous leptin treatment, even when weight matched with control animals (Rahmouni et al., 2008; Seo et al., 2009). Although the leptin receptor has not been localized to cilia, it interacts with components of the BBSome and loss of BBS components causes mislocalization of the leptin receptor in large vesicles (Seo et al., 2009). Further support for the importance of cilia in energy regulation comes from the conditional knockout of intraflagellar transport proteins, which leads to the loss of primary cilia in adult mice. Ablation of cilia only on POMC neurons causes mice to become hyperphagic and

obese; a model proposing the disruption of a feedback mechanism between leptin and somatostatin signaling that regulates satiety responses has been proposed (Davenport et al., 2007; Satir, 2007). These data are interesting, especially in light of the localization of PAM to cilia. It is currently not known if PAM localizes to cilia in POMC neurons, or if this localization is BBSome-mediated (**Fig.5**). It is also unclear if PAM performs a catalytic or signaling role in the cilium, but there is certainly a link between PAM and energy metabolism, as seen in the increased adiposity phenotype in older $PAM^{+/-}$ mice. Two genome wide association studies linked PAM to altered insulinogenic index and susceptibility to type 2 diabetes in Finnish and Icelandic populations, necessitating a closer look at altered energy homeostasis in the context of PAM (Huyghe et al., 2013; Steinthorsdottir et al., 2014).

ACKNOWLEDGEMENTS

We thank the graduate students, post-doctoral fellows and technicians with whom we have worked over the years for sharing their curiosity and passion for science. The expertise of our various collaborators has allowed us to expand our studies in ways we could not have imagined; special thanks go to Mario Amzel, Ninian Blackburn, Paul Taghert and Nils Back, without whom much of this work could not have been imagined.

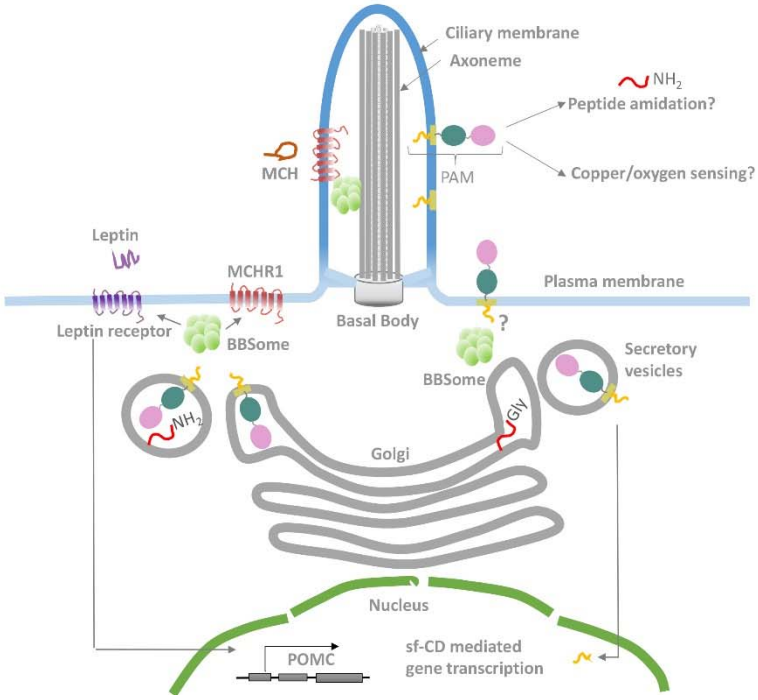

Figure 5. Model of PAM function in cilia. PAM localizes to cilia, where it may play roles in peptide amidation and sensing of copper or oxygen. Ciliary PAM may also be subjected to cleavages leading to the release of sf-CD and changes in gene expression. It is not known if the BBSome is essential for PAM trafficking into the ciliary compartment. However, trafficking of the melanocortin concentrating hormone receptor (MCHR1) into the cilium requires the BBSome and leptin receptor localization is affected by loss of BBS components. The leptin/melanocortin system is critical for establishing energy homeostasis. Leptin binding to its receptor leads to up-regulation of POMC and satiety responses. It is not known if PAM also plays a role in energy balance in POMC neurons.

REFERENCES

Alam, M. R., Caldwell, B. D., Johnson, R. C., Darlington, D. N., Mains, R. E. and Eipper, B. A. (1996). Novel proteins that interact with the COOH-terminal cytosolic routing determinants of an integral membrane peptide-processing enzyme. *J Biol Chem* **271**, 28636-28640.

Asada, A., Orii, H., Watanabe, K. and Tsubaki, M. (2005). Planarian peptidylglycine-hydroxylating monooxygenase, a neuropeptide processing enzyme, colocalizes with cytochrome b561 along the central nervous system. *FEBS J* **272**, 942-955.

Attenborough, R. M., Hayward, D. C., Kitahara, M. V., Miller, D. J. and Ball, E. E. (2012). A "neural" enzyme in nonbilaterian animals and algae: preneural origins for peptidylglycine alpha-amidating monooxygenase. *Mol Biol Evol* **29**, 3095-3109.

Berbari, N. F., Johnson, A. D., Lewis, J. S., Askwith, C. C. and Mykytyn, K. (2008a). Identification of ciliary localization sequences within the third intracellular loop of G protein-coupled receptors. *Mol Biol Cell* **19**, 1540-1547.

Berbari, N. F., Lewis, J. S., Bishop, G. A., Askwith, C. C. and Mykytyn, K. (2008b). Bardet-Biedl syndrome proteins are required for the localization of G protein-coupled receptors to primary cilia. *Proc Natl Acad Sci U S A* **105**, 4242-4246.

Bonnemaison, M., Back, N., Lin, Y., Bonifacino, J. S., Mains, R. and Eipper, B. (2014). AP-1A controls secretory granule biogenesis and trafficking of membrane secretory granule proteins. *Traffic* **15**, 1099-1121.

Bonnemaison, M. L., Back, N., Duffy, M. E., Ralle, M., Mains, R. E. and Eipper, B. A. (2015). Adaptor protein-1 complex affects the endocytic trafficking and function of peptidylglycine alpha-amidating monooxygenase, a luminal cuproenzyme. *J Biol Chem* **290**, 21264-21279.

Bousquet-Moore, D., Ma, X. M., Nillni, E. A., Czyzyk, T. A., Pintar, J. E., Eipper, B. A. and Mains, R. E. (2009). Reversal of physiological deficits caused by diminished levels of peptidylglycine alpha-amidating monooxygenase by dietary copper. *Endocrinology* **150**, 1739-1747.

Bousquet-Moore, D., Prohaska, J. R., Nillni, E. A., Czyzyk, T., Wetsel, W. C., Mains, R. E. and Eipper, B. A. (2010). Interactions of peptide amidation and copper: novel biomarkers and mechanisms of neural dysfunction. *Neurobiol Dis* **37**, 130-140.

Braas, K. M., Stoffers, D. A., Eipper, B. A. and May, V. (1989). Tissue specific expression of rat peptidylglycine alpha-amidating monooxygenase activity and mRNA. *Mol Endocrinol* **3**, 1387-1398.

Bradbury, A. F., Finnie, M. D. and Smyth, D. G. (1982). Mechanism of C-terminal amide formation by pituitary enzymes. *Nature* **298**, 686-688.

Bundgaard, H. and Kahns, A. H. (1991). Chemical stability and plasma-catalyzed dealkylation of peptidyl-alpha-hydroxyglycine derivatives--intermediates in peptide alpha-amidation. *Peptides* **12**, 745-748.

Burzle, M. and Hediger, M. A. (2012). Functional and physiological role of vitamin C transporters. *Curr Top Membr* **70**, 357-375.

Challis, B. G., Coll, A. P., Yeo, G. S., Pinnock, S. B., Dickson, S. L., Thresher, R. R., Dixon, J., Zahn, D., Rochford, J. J., White, A. et al. (2004). Mice lacking pro-opiomelanocortin are sensitive to high-fat feeding but respond normally to the acute anorectic effects of peptide-YY(3-36). *Proc Natl Acad Sci U S A* **101**, 4695-4700.

Chew, G. H., Galloway, L. C., McIntyre, N. R., Schroder, L. A., Richards, K. M., Miller, S. A., Wright, D. W. and Merkler, D. J. (2005). Ubiquitin and ubiquitin-derived peptides as substrates for peptidylglycine alpha-amidating monooxygenase. *FEBS Lett* **579**, 4678-4684.

Chufan, E. E., De, M., Eipper, B. A., Mains, R. E. and Amzel, L. M. (2009). Amidation of bioactive peptides: the structure of the lyase domain of the amidating enzyme. *Structure* **17**, 965-973.

Czyzyk, T. A., Ning, Y., Hsu, M. S., Peng, B., Mains, R. E., Eipper, B. A. and Pintar, J. E. (2005). Deletion of peptide amidation enzymatic activity leads to edema and embryonic lethality in the mouse. *Dev Biol* **287**, 301-313.
Davenport, J. R., Watts, A. J., Roper, V. C., Croyle, M. J., van Groen, T., Wyss, J. M., Nagy, T. R., Kesterson, R. A. and Yoder, B. K. (2007). Disruption of intraflagellar transport in adult mice leads to obesity and slow-onset cystic kidney disease. *Curr Biol* **17**, 1586-1594.
De, M., Ciccotosto, G. D., Mains, R. E. and Eipper, B. A. (2007). Trafficking of a secretory granule membrane protein is sensitive to copper. *J Biol Chem* **282**, 23362-23371.
De, M., Bell, J., Blackburn, N. J., Mains, R. E. and Eipper, B. A. (2006). Role for an essential tyrosine in peptide amidation. *J Biol Chem* **281**, 20873-20882.
Eipper, B. A., Glembotski, C. C. and Mains, R. E. (1983a). Selective loss of alpha-melanotropin-amidating activity in primary cultures of rat intermediate pituitary cells. *J Biol Chem* **258**, 7292-7298.
Eipper, B. A., Mains, R. E. and Glembotski, C. C. (1983b). Identification in pituitary tissue of a peptide alpha-amidation activity that acts on glycine-extended peptides and requires molecular oxygen, copper, and ascorbic acid. *Proc Natl Acad Sci U S A* **80**, 5144-5148.
Eipper, B. A., May, V. and Braas, K. M. (1988). Membrane-associated peptidylglycine alpha-amidating monooxygenase in the heart. *J Biol Chem* **263**, 8371-8379.
Eipper, B. A., Perkins, S. N., Husten, E. J., Johnson, R. C., Keutmann, H. T. and Mains, R. E. (1991). Peptidyl-alpha-hydroxyglycine alpha-amidating lyase. Purification, characterization, and expression. *J Biol Chem* **266**, 7827-7833.
Eipper, B. A., Green, C. B., Campbell, T. A., Stoffers, D. A., Keutmann, H. T., Mains, R. E. and Ouafik, L. (1992). Alternative splicing and endoproteolytic processing generate tissue-specific forms of pituitary peptidylglycine alpha-amidating monooxygenase (PAM). *J Biol Chem* **267**, 4008-4015.
Eipper, B. A., Park, L. P., Dickerson, I. M., Keutmann, H. T., Thiele, E. A., Rodriguez, H., Schofield, P. R. and Mains, R. E. (1987). Structure of the precursor to an enzyme mediating COOH-terminal amidation in peptide biosynthesis. *Mol Endocrinol* **1**, 777-790.
El Meskini, R., Galano, G. J., Marx, R., Mains, R. E. and Eipper, B. A. (2001). Targeting of membrane proteins to the regulated secretory pathway in anterior pituitary endocrine cells. *J Biol Chem* **276**, 3384-3393.
Erion, M. D., Tan, J., Wong, M. and Jeng, A. Y. (1994). Inhibition of peptidylglycine alpha-amidating monooxygenase by N-substituted homocysteine analogs. *J Med Chem* **37**, 4430-4437.
Evans, J. P., Blackburn, N. J. and Klinman, J. P. (2006). The catalytic role of the copper ligand H172 of peptidylglycine alpha-hydroxylating monooxygenase: a kinetic study of the H172A mutant. *Biochemistry* **45**, 15419-15429.
Fliegauf, M., Benzing, T. and Omran, H. (2007). When cilia go bad: cilia defects and ciliopathies. *Nat Rev Mol Cell Biol* **8**, 880-893.
Francisco, W. A., Knapp, M. J., Blackburn, N. J. and Klinman, J. P. (2002). Hydrogen tunneling in peptidylglycine alpha-hydroxylating monooxygenase. *J Am Chem Soc* **124**, 8194-8195.
Francisco, W. A., Wille, G., Smith, A. J., Merkler, D. J. and Klinman, J. P. (2004). Investigation of the pathway for inter-copper electron transfer in peptidylglycine alpha-amidating monooxygenase. *J Am Chem Soc* **126**, 13168-13169.
Francone, V. P., Ifrim, M. F., Rajagopal, C., Leddy, C. J., Wang, Y., Carson, J. H., Mains, R. E. and Eipper, B. A. (2010). Signaling from the secretory granule to the nucleus: Uhmk1 and PAM. *Mol Endocrinol* **24**, 1543-1558.
Fujisawa, Y., Furukawa, Y., Ohta, S., Ellis, T. A., Dembrow, N. C., Li, L., Floyd, P. D., Sweedler, J. V., Minakata, H., Nakamaru, K. et al. (1999). The Aplysia mytilus inhibitory peptide-related peptides: identification, cloning, processing, distribution, and action. *J Neurosci* **19**, 9618-9634.

Gaier, E. D., Kleppinger, A., Ralle, M., Covault, J., Mains, R. E., Kenny, A. M. and Eipper, B. A. (2014). Genetic determinants of amidating enzyme activity and its relationship with metal cofactors in human serum. *BMC Endocr Disord* **14**, 58.
Glembotski, C. C., Eipper, B. A. and Mains, R. E. (1983). Adrenocorticotropin(1-14)OH-related molecules in primary cultures of rat intermediate pituitary cells. Identification and role in the biosynthesis of alpha-melanotropin. *J Biol Chem* **258**, 7299-7304.
Gonzalez-Begne, M., Lu, B., Han, X., Hagen, F. K., Hand, A. R., Melvin, J. E. and Yates, J. R. (2009). Proteomic analysis of human parotid gland exosomes by multidimensional protein identification technology (MudPIT). *J Proteome Res* **8**, 1304-1314.
Gonzalez, H., Ottervald, J., Nilsson, K. C., Sjogren, N., Miliotis, T., Von Bahr, H., Khademi, M., Eriksson, B., Kjellstrom, S., Vegvari, A. et al. (2009). Identification of novel candidate protein biomarkers for the post-polio syndrome - implications for diagnosis, neurodegeneration and neuroinflammation. *J Proteomics* **71**, 670-681.
Grunder, S. and Assmann, M. (2015). Peptide-gated ion channels and the simple nervous system of Hydra. *J Exp Biol* **218**, 551-561.
Han, M., Park, D., Vanderzalm, P. J., Mains, R. E., Eipper, B. A. and Taghert, P. H. (2004). Drosophila uses two distinct neuropeptide amidating enzymes, dPAL1 and dPAL2. *J Neurochem* **90**, 129-141.
Harris, J. I. and Lerner, A. B. (1957). Amino-acid sequence of the alpha-melanocyte-stimulating hormone. *Nature* **179**, 1346-1347.
Hinney, A., Becker, I., Heibult, O., Nottebom, K., Schmidt, A., Ziegler, A., Mayer, H., Siegfried, W., Blum, W. F., Remschmidt, H. et al. (1998). Systematic mutation screening of the pro-opiomelanocortin gene: identification of several genetic variants including three different insertions, one nonsense and two missense point mutations in probands of different weight extremes. *J Clin Endocrinol Metab* **83**, 3737-3741.
Huyghe, J. R., Jackson, A. U., Fogarty, M. P., Buchkovich, M. L., Stancakova, A., Stringham, H. M., Sim, X., Yang, L., Fuchsberger, C., Cederberg, H. et al. (2013). Exome array analysis identifies new loci and low-frequency variants influencing insulin processing and secretion. *Nat Genet* **45**, 197-201.
Iliadi, K. G., Avivi, A., Iliadi, N. N., Knight, D., Korol, A. B., Nevo, E., Taylor, P., Moran, M. F., Kamyshev, N. G. and Boulianne, G. L. (2008). nemy encodes a cytochrome b561 that is required for *Drosophila* learning and memory. *Proc Natl Acad Sci U S A* **105**, 19986-19991.
Jaron, S., Mains, R. E., Eipper, B. A. and Blackburn, N. J. (2002). The catalytic role of the copper ligand H172 of peptidylglycine alpha-hydroxylating monooxygenase (PHM): a spectroscopic study of the H172A mutant. *Biochemistry* **41**, 13274-13282.
Jekely, G. (2013). Global view of the evolution and diversity of metazoan neuropeptide signaling. *Proc Natl Acad Sci U S A* **110**, 8702-8707.
Jewell, J. L., Russell, R. C. and Guan, K. L. (2013). Amino acid signalling upstream of mTOR. *Nat Rev Mol Cell Biol* **14**, 133-139.
Jin, H. and Nachury, M. V. (2009). The BBSome. *Curr Biol* **19**, R472-473.
Katopodis, A. G., Ping, D. and May, S. W. (1990). A novel enzyme from bovine neurointermediate pituitary catalyzes dealkylation of alpha-hydroxyglycine derivatives, thereby functioning sequentially with peptidylglycine alpha-amidating monooxygenase in peptide amidation. *Biochemistry* **29**, 6115-6120.
Kline, C. D., Mayfield, M. and Blackburn, N. J. (2013). HHM motif at the CuH-site of peptidylglycine monooxygenase is a pH-dependent conformational switch. *Biochemistry* **52**, 2586-2596.
Klinman, J. P. (2006). The copper-enzyme family of dopamine beta-monooxygenase and peptidylglycine alpha-hydroxylating monooxygenase: resolving the chemical pathway for substrate hydroxylation. *J Biol Chem* **281**, 3013-3016.

Kolhekar, A. S., Roberts, M. S., Jiang, N., Johnson, R. C., Mains, R. E., Eipper, B. A. and Taghert, P. H. (1997). Neuropeptide amidation in *Drosophila*: separate genes encode the two enzymes catalyzing amidation. *J Neurosci* **17**, 1363-1376.
Kumar, D., Blaby-Haas, C. E., Merchant, S. S., Mains, R. E., King, S. M. and Eipper, B. A. (2015). Cilia-associated bioactive peptide amidating activity preceded the emergence of multicellularity. *American Society for Cell Biology meeting, San Diego, California* **December 12-16**.
Langella, E., Pierre, S., Ghattas, W., Giorgi, M., Reglier, M., Saviano, M., Esposito, L. and Hardre, R. (2010). Probing the peptidylglycine alpha-hydroxylating monooxygenase active site with novel 4-phenyl-3-butenoic acid based inhibitors. *ChemMedChem* **5**, 1568-1576.
Lee, C. M., Yang, P., Chen, L. C., Chen, C. C., Wu, S. C., Cheng, H. Y. and Chang, Y. S. (2011). A novel role of RASSF9 in maintaining epidermal homeostasis. *PLoS One* **6**, e17867.
Mains, R. E., Myers, A. C. and Eipper, B. A. (1985). Hormonal, drug, and dietary factors affecting peptidyl glycine alpha-amidating monooxygenase activity in various tissues of the adult male rat. *Endocrinology* **116**, 2505-2515.
Mair, G. R., Niciu, M. J., Stewart, M. T., Brennan, G., Omar, H., Halton, D. W., Mains, R., Eipper, B. A., Maule, A. G. and Day, T. A. (2004). A functionally atypical amidating enzyme from the human parasite *Schistosoma mansoni*. *FASEB J* **18**, 114-121.
McIntyre, N. R., Lowe, E. W., Jr., Belof, J. L., Ivkovic, M., Shafer, J., Space, B. and Merkler, D. J. (2010). Evidence for substrate preorganization in the peptidylglycine alpha-amidating monooxygenase reaction describing the contribution of ground state structure to hydrogen tunneling. *J Am Chem Soc* **132**, 16393-16402.
Merkler, D. J., Asser, A. S., Baumgart, L. E., Carballo, N., Carpenter, S. E., Chew, G. H., Cosner, C. C., Dusi, J., Galloway, L. C., Lowe, A. B. et al. (2008). Substituted hippurates and hippurate analogs as substrates and inhibitors of peptidylglycine alpha-hydroxylating monooxygenase (PHM). *Bioorg Med Chem* **16**, 10061-10074.
Milgram, S. L., Mains, R. E. and Eipper, B. A. (1993). COOH-terminal signals mediate the trafficking of a peptide processing enzyme in endocrine cells. *J Cell Biol* **121**, 23-36.
Minciacchi, V. R., You, S., Spinelli, C., Morley, S., Zandian, M., Aspuria, P. J., Cavallini, L., Ciardiello, C., Reis Sobreiro, M., Morello, M. et al. (2015). Large oncosomes contain distinct protein cargo and represent a separate functional class of tumor-derived extracellular vesicles. *Oncotarget* **6**, 11327-11341.
Mizuno, K., Ohsuye, K., Wada, Y., Fuchimura, K., Tanaka, S. and Matsuo, H. (1987). Cloning and sequence of cDNA encoding a peptide C-terminal alpha-amidating enzyme from *Xenopus laevis*. *Biochem Biophys Res Commun* **148**, 546-552.
Mueller, G. P., Driscoll, W. J. and Eipper, B. A. (1999). In vivo inhibition of peptidylglycine-alpha-hydroxylating monooxygenase by 4-phenyl-3-butenoic acid. *J Pharmacol Exp Ther* **290**, 1331-1336.
Mueller, G. P., Husten, E. J., Mains, R. E. and Eipper, B. A. (1993). Peptide alpha-amidation and peptidylglycine alpha-hydroxylating monooxygenase: control by disulfiram. *Mol Pharmacol* **44**, 972-980.
Murthy, A. S., Mains, R. E. and Eipper, B. A. (1986). Purification and characterization of peptidylglycine alpha-amidating monooxygenase from bovine neurointermediate pituitary. *J Biol Chem* **261**, 1815-1822.
O'Donnell, P. J., Driscoll, W. J., Back, N., Muth, E. and Mueller, G. P. (2003). Peptidylglycine-alpha-amidating monooxygenase and pro-atrial natriuretic peptide constitute the major membrane-associated proteins of rat atrial secretory granules. *J Mol Cell Cardiol* **35**, 915-922.
Ohsuye, K., Kitano, K., Wada, Y., Fuchimura, K., Tanaka, S., Mizuno, K. and Matsuo, H. (1988). Cloning of cDNA encoding a new peptide C-terminal alpha-amidating enzyme having a putative membrane-spanning domain from Xenopus laevis skin. *Biochem Biophys Res Commun* **150**, 1275-1281.
Oldham, C. D., Li, C., Girard, P. R., Nerem, R. M. and May, S. W. (1992). Peptide amidating enzymes are present in cultured endothelial cells. *Biochem Biophys Res Commun* **184**, 323-329.

Otoikhian, A., Barry, A. N., Mayfield, M., Nilges, M., Huang, Y., Lutsenko, S. and Blackburn, N. J. (2012). Lumenal loop M672-P707 of the Menkes protein (ATP7A) transfers copper to peptidylglycine monooxygenase. *J Am Chem Soc* **134**, 10458-10468.
Perkins, S. N., Husten, E. J. and Eipper, B. A. (1990). The 108-kDA peptidylglycine alpha-amidating monooxygenase precursor contains two separable enzymatic activities involved in peptide amidation. *Biochem Biophys Res Commun* **171**, 926-932.
Prigge, S. T., Eipper, B. A., Mains, R. E. and Amzel, L. M. (2004). Dioxygen binds end-on to mononuclear copper in a precatalytic enzyme complex. *Science* **304**, 864-867.
Prigge, S. T., Kolhekar, A. S., Eipper, B. A., Mains, R. E. and Amzel, L. M. (1997). Amidation of bioactive peptides: the structure of peptidylglycine alpha-hydroxylating monooxygenase. *Science* **278**, 1300-1305.
Prigge, S. T., Kolhekar, A. S., Eipper, B. A., Mains, R. E. and Amzel, L. M. (1999). Substrate-mediated electron transfer in peptidylglycine alpha-hydroxylating monooxygenase. *Nat Struct Biol* **6**, 976-983.
Prohaska, J. R. (2008). Role of copper transporters in copper homeostasis. *Am J Clin Nutr* **88**, 826S-829S.
Rahmouni, K., Fath, M. A., Seo, S., Thedens, D. R., Berry, C. J., Weiss, R., Nishimura, D. Y. and Sheffield, V. C. (2008). Leptin resistance contributes to obesity and hypertension in mouse models of Bardet-Biedl syndrome. *J Clin Invest* **118**, 1458-1467.
Rajagopal, C., Mains, R. E. and Eipper, B. A. (2012). Signaling from the secretory granule to the nucleus. *Crit Rev Biochem Mol Biol* **47**, 391-406.
Rajagopal, C., Stone, K. L., Mains, R. E. and Eipper, B. A. (2010). Secretion stimulates intramembrane proteolysis of a secretory granule membrane enzyme. *J Biol Chem* **285**, 34632-34642.
Rajagopal, C., Stone, K. L., Francone, V. P., Mains, R. E. and Eipper, B. A. (2009). Secretory granule to the nucleus: role of a multiply phosphorylated intrinsically unstructured domain. *J Biol Chem* **284**, 25723-25734.
Satir, P. (2007). Cilia biology: stop overeating now! *Curr Biol* **17**, R963-965.
Schafer, M. K., Stoffers, D. A., Eipper, B. A. and Watson, S. J. (1992). Expression of peptidylglycine alpha-amidating monooxygenase (EC 1.14.17.3) in the rat central nervous system. *J Neurosci* **12**, 222-234.
Sen Gupta, P., Prodromou, N. V. and Chapple, J. P. (2009). Can faulty antennae increase adiposity? The link between cilia proteins and obesity. *J Endocrinol* **203**, 327-336.
Seo, S., Guo, D. F., Bugge, K., Morgan, D. A., Rahmouni, K. and Sheffield, V. C. (2009). Requirement of Bardet-Biedl syndrome proteins for leptin receptor signaling. *Hum Mol Genet* **18**, 1323-1331.
Siebert, X., Eipper, B. A., Mains, R. E., Prigge, S. T., Blackburn, N. J. and Amzel, L. M. (2005). The catalytic copper of peptidylglycine alpha-hydroxylating monooxygenase also plays a critical structural role. *Biophys J* **89**, 3312-3319.
Simpson, P. D., Eipper, B. A., Katz, M. J., Gandara, L., Wappner, P., Fischer, R., Hodson, E. J., Ratcliffe, P. J. and Masson, N. (2015). Striking oxygen sensitivity of the peptidylglycine alpha-amidating monooxygenase (PAM) in neuroendocrine cells. *J Biol Chem* **290**, 24891-24901.
Simpson, R. J., Lim, J. W., Moritz, R. L. and Mathivanan, S. (2009). Exosomes: proteomic insights and diagnostic potential. *Expert Rev Proteomics* **6**, 267-283.
Skulj, M., Pezdirec, D., Gaser, D., Kreft, M. and Zorec, R. (2014). Reduction in C-terminal amidated species of recombinant monoclonal antibodies by genetic modification of CHO cells. *BMC Biotechnol* **14**, 76.
Smith, C. L., Varoqueaux, F., Kittelmann, M., Azzam, R. N., Cooper, B., Winters, C. A., Eitel, M., Fasshauer, D. and Reese, T. S. (2014). Novel cell types, neurosecretory cells, and body plan of the early-diverging metazoan Trichoplax adhaerens. *Curr Biol* **24**, 1565-1572.
Sobota, J. A., Back, N., Eipper, B. A. and Mains, R. E. (2009). Inhibitors of the V0 subunit of the vacuolar H+-ATPase prevent segregation of lysosomal- and secretory-pathway proteins. *J Cell Sci* **122**, 3542-3553.

Steinthorsdottir, V., Thorleifsson, G., Sulem, P., Helgason, H., Grarup, N., Sigurdsson, A., Helgadottir, H. T., Johannsdottir, H., Magnusson, O. T., Gudjonsson, S. A. et al. (2014). Identification of low-frequency and rare sequence variants associated with elevated or reduced risk of type 2 diabetes. *Nat Genet* **46**, 294-298.
Steveson, T. C., Ciccotosto, G. D., Ma, X. M., Mueller, G. P., Mains, R. E. and Eipper, B. A. (2003). Menkes protein contributes to the function of peptidylglycine alpha-amidating monooxygenase. *Endocrinology* **144**, 188-200.
Stewart, L. C. and Klinman, J. P. (1988). Dopamine beta-hydroxylase of adrenal chromaffin granules: structure and function. *Annu Rev Biochem* **57**, 551-592.
Stoffers, D. A., Green, C. B. and Eipper, B. A. (1989). Alternative mRNA splicing generates multiple forms of peptidyl-glycine alpha-amidating monooxygenase in rat atrium. *Proc Natl Acad Sci U S A* **86**, 735-739.
Stoffers, D. A., Ouafik, L. and Eipper, B. A. (1991). Characterization of novel mRNAs encoding enzymes involved in peptide alpha-amidation. *J Biol Chem* **266**, 1701-1707.
Stone, J. V., Mordue, W., Batley, K. E. and Morris, H. R. (1976). Structure of locust adipokinetic hormone, a neurohormone that regulates lipid utilisation during flight. *Nature* **263**, 207-211.
Suchanek, G. and Kreil, G. (1977). Translation of melittin messenger RNA in vitro yields a product terminating with glutaminylglycine rather than with glutaminamide. *Proc Natl Acad Sci U S A* **74**, 975-978.
Tausk, F. A., Milgram, S. L., Mains, R. E. and Eipper, B. A. (1992). Expression of a peptide processing enzyme in cultured cells: truncation mutants reveal a routing domain. *Mol Endocrinol* **6**, 2185-2196.
Tsukamoto, T., Noguchi, M., Kayama, H., Watanabe, T., Asoh, T. and Yamamoto, T. (1995). Increased peptidylglycine alpha-amidating monooxygenase activity in cerebrospinal fluid of patients with multiple sclerosis. *Intern Med* **34**, 229-232.
Vishwanatha, K., Back, N., Mains, R. E. and Eipper, B. A. (2014). A histidine-rich linker region in peptidylglycine alpha-amidating monooxygenase has the properties of a pH sensor. *J Biol Chem* **289**, 12404-12420.
Wand, G. S., Ney, R. L., Mains, R. E. and Eipper, B. A. (1985). Characterization of peptide alpha-amidation activity in human cerebrospinal fluid and central nervous system tissue. *Neuroendocrinology* **41**, 482-489.
Wilcox, B. J., Ritenour-Rodgers, K. J., Asser, A. S., Baumgart, L. E., Baumgart, M. A., Boger, D. L., DeBlassio, J. L., deLong, M. A., Glufke, U., Henz, M. E. et al. (1999). N-acylglycine amidation: implications for the biosynthesis of fatty acid primary amides. *Biochemistry* **38**, 3235-3245.
Williamson, M., Hauser, F. and Grimmelikhuijzen, C. J. (2000). Genomic organization and splicing variants of a peptidylglycine alpha-hydroxylating monooxygenase from sea anemones. *Biochem Biophys Res Commun* **277**, 7-12.
Xin, X., Mains, R. E. and Eipper, B. A. (2004). Monooxygenase X, a member of the copper-dependent monooxygenase family localized to the endoplasmic reticulum. *J Biol Chem* **279**, 48159-48167.
Yaswen, L., Diehl, N., Brennan, M. B. and Hochgeschwender, U. (1999). Obesity in the mouse model of pro-opiomelanocortin deficiency responds to peripheral melanocortin. *Nat Med* **5**, 1066-1070.
Young, S. D. and Tamburini, P. P. (1989). Enzymatic peptidyl alpha-amidation proceeds through formation of an alpha-hydroxyglycine intermediate. *J Am Chem Soc* **111**, 1933-1934.

Chapter 3

Early eukaryotic origins for cilia-associated bioactive peptide amidating activity

Dhivya Kumar, Crysten E. Blaby-Haas, Sabeeha S. Merchant, Richard E. Mains, Stephen M. King, and Betty A. Eipper

This chapter is a duplicate version of a research article published in the Journal of Cell Science. 2016 Mar 1; 129 (5):943-56

ABSTRACT

Ciliary axonemes and basal bodies were present in the last eukaryotic common ancestor and play critical roles in sensing and responding to environmental cues. Peptidergic signaling, generally considered a metazoan innovation, is essential for organismal development and homeostasis. Peptidylglycine alpha-amidating monooxygenase (PAM) is crucial for the last step of bioactive peptide biosynthesis. However, identification of a complete PAM-like gene in green algal genomes suggests ancient evolutionary roots for bioactive peptide signaling. We demonstrate that the *Chlamydomonas reinhardtii* PAM gene encodes an active peptide amidating enzyme (CrPAM) that shares key structural and functional features with the mammalian enzyme, indicating that components of the peptide biosynthetic pathway predate multicellularity. In addition to its secretory pathway localization, CrPAM localizes to cilia and tightly associates with the axonemal superstructure, revealing a novel axonemal enzyme activity. This localization pattern is conserved in mammals, with PAM present in both motile and immotile sensory cilia. The conserved ciliary localization of PAM adds to the known signaling capabilities of the eukaryotic cilium and provides a potential mechanistic link between peptidergic signaling and endocrine abnormalities commonly observed in ciliopathies.

INTRODUCTION

A key feature of eukaryotic cells is extensive compartmentalization and separation of functional modalities. One such highly specialized organelle that is conserved in many eukaryotic cells is the cilium, a microtubule based extension that projects from the cell surface (Singla and Reiter, 2006; Fliegauf et al., 2007). Cilia and the basal bodies that give rise to their axonemal structure are ubiquitously distributed across major eukaryotic groups, with the exception of flowering plants, most fungi and amoebae (Johnson and Leroux, 2010; Carvalho-Santos et al., 2011). Although the membrane surrounding the microtubule-based axonemal core is continuous with the plasma membrane, the ciliary lipidome and proteome are distinct (Nachury et al., 2010; Hsiao et al., 2012). Amongst the proteins targeted to the cilium are signaling molecules and receptors involved in the response to environmental signals. Components of the Hedgehog and Wnt pathways, along with several G-protein coupled receptors, are selectively trafficked into the cilium by the motor-protein driven intraflagellar transport (IFT) system (Huangfu et al., 2003; Berbari et al., 2008; Wallingford and Mitchell, 2011; Mukhopadhyay and Rohatgi, 2014). The importance of cilia-based signaling is demonstrated by the wide array of cilia-related disorders that occur in vertebrates (Waters and Beales, 2011; Brown and Witman, 2014). Only motile cilia can generate motive force, but both motile and primary cilia perform sensory and signaling roles (Shah et al., 2009; Bloodgood, 2010; Warner et al., 2014).

Accumulating evidence suggests a link between cilia and peptidergic signaling, an ancient metazoan pathway. Neuropeptides regulate ciliary beating and influence larval swimming behavior in marine annelids (Conzelmann et al., 2011) and melanin concentrating hormone (MCH) regulates ciliary beat frequency in the ependymal cells that move cerebrospinal fluid in the ventricles (Conductier et al., 2013). In addition, the G-protein coupled receptors for neuropeptide Y (Npy2r, Npy5r), somatostatin (Sstr3) and kisspeptin (Kiss1r) localize to neuronal cilia (Loktev and Jackson, 2013). Interestingly, neuropeptide precursors have been identified in ciliated metazoans lacking a nervous system,

suggesting that regulation of ciliary motility was an ancestral function of peptide-based signaling (Jekely, 2011; Jekely, 2013).

In eukaryotes, neuropeptides are synthesized from precursors that have a signal sequence, thereby confining all subsequent processing steps to the secretory pathway lumen. Secretory pathway enzymes convert inactive precursors into smaller bioactive peptides capable of downstream signaling. Many bioactive metazoan peptides have an amidated C-terminus (Prigge et al., 2000). This modification requires a bifunctional enzyme, peptidylglycine α-amidating monooxygenase (PAM) (Fig. 1A). The peptidylglycine α-hydroxylating monooxygenase (PHM) domain hydroxylates the α-carbon of peptides with a C-terminal glycine; the peptidyl-α-hydroxyglycine α-amidating lyase (PAL) domain subsequently cleaves the C-N bond, producing glyoxylate and α-amidated product (Fig. 1A). Amidation, which is often essential for bioactivity, can reduce peptide turnover and increase receptor affinity. PAM is essential in metazoans; mice and flies lacking *PAM* die at mid-gestation or mid-larval stages, respectively (Kolhekar et al., 1997b; Czyzyk et al., 2005). *PAM* missense alleles have been associated with metabolic disorders (Huyghe et al., 2013; Steinthorsdottir et al., 2014).

The identification of *PAM*-like genes in ciliated green algal genomes and in *Amphimedon*, the simplest animal lacking a nervous system, suggests its presence in the last eukaryotic common ancestor (Attenborough et al., 2012). Like PAM, amidated peptides, which are especially prevalent in primitive nervous systems, have not been found in yeast or higher plants (Jekely, 2013). Thus, there is a striking correlation between organisms with cilia and organisms expressing PAM. Although its enzymatic functions in the secretory pathway lumen do not require a transmembrane or cytosolic domain, these features are conserved in algal PAM. The steady state localization of vertebrate PAM in the trans-Golgi network, secretory granules and endosomes reflects the secretion of soluble PAM and the endocytic trafficking of membrane PAM (Milgram et al., 1997). Examination of *Pam*$^{+/-}$ mice and neuroendocrine cells engineered for inducible expression of *Pam* revealed its signaling role. Following exocytosis,

active membrane PAM appears on the cell surface; after endocytosis, membrane PAM can be returned to granules or degraded. In the endocytic pathway, γ-secretase-mediated intramembrane cleavage can release a soluble fragment of the PAM cytosolic domain, which then translocates into the nucleus, leading to altered gene expression (Ciccotosto et al., 1999; Francone et al., 2010). With its requirement for copper and molecular oxygen, PAM may long have played a role in coordinating events in the luminal compartment, cytosol and surrounding environment.

The intriguingly similar co-occurrence of the *PAM* gene and cilia led us to investigate its properties in organisms where amidated peptides have not yet been described. Here we used *Chlamydomonas reinhardtii*, one of the premier organisms for studying ciliary function (for clarity, we use the term cilium instead of flagellum), to explore the significance of the correlation between PAM expression and the presence of cilia.

RESULTS

Identification of a *PAM* gene in *C. reinhardtii*

The PAM-like sequence previously predicted for *C. reinhardtii* lacked key residues in the PAL domain (Attenborough et al., 2012). Our analysis of sequenced *C. reinhardtii* ESTs and the subsequent release of an improved gene model revealed an additional exon, resulting in a domain organization for Cre03.g152850 (hereafter referred to as CrPAM) very similar to the mammalian PAM2 isoform (Fig. 1B). We confirmed this structure by sequencing CrPAM cDNA (Genbank KT033716). Two signal peptide prediction tools, SignalP (Petersen et al., 2011) and PredAlgo (Tardif et al., 2012), identified a 21-residue signal peptide in CrPAM, in agreement with the localization of PAM in the secretory pathway. We found no evidence of *CrPAM* alternative splicing in EST libraries and RNA-Seq data. Like mammalian PAM, CrPAM is predicted to contain a transmembrane domain followed by a cytosolic domain (Fig. 1B). Alignment of the amino acid sequence of CrPAM with several metazoan PAM sequences revealed that all the residues essential for the catalytic activities of PHM and PAL were conserved, with two copper binding sites in PHM and binding sites for Zn^{2+} and Ca^{2+} in PAL (Fig. 1B,

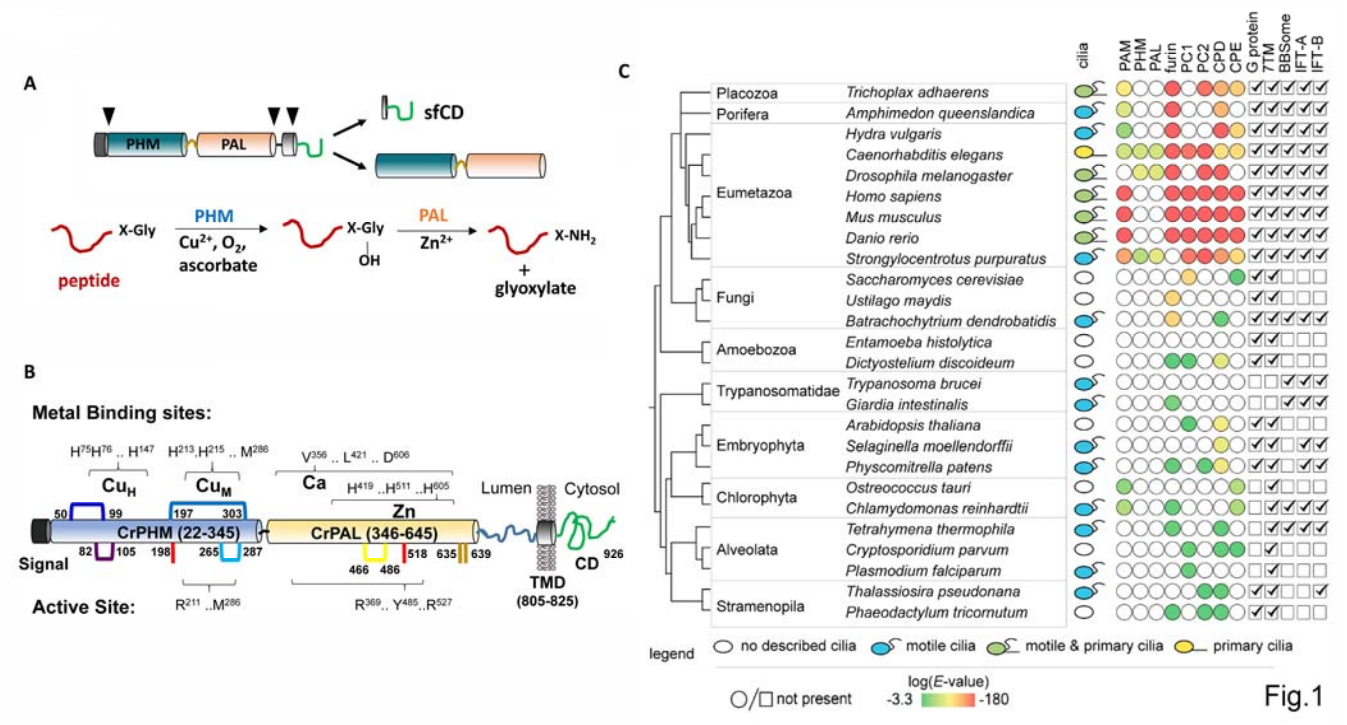

Fig. 1. CrPAM protein. (A) Schematic of mammalian PAM2 protein and the amidation reaction. Sequential processing of a glycine-extended peptide by PHM and PAL and their co-factor requirements are shown. Black arrowheads point to sites cleaved in the endoplasmic reticulum, secretory granules and endocytic pathway, removing the signal sequence and separating the enzymatic domains from the transmembrane domain or generating a soluble cytoplasmic domain fragment (sfCD), respectively. (B) Domains of CrPAM and predicted key catalytic residues in CrPHM and CrPAL are highlighted; predicted disulfide linkages are shown and cysteine residues unique to CrPAM are highlighted in red or brown. (C) Identification of protein homologs and co-occurrence with described cilia. Type of cilia (or absence thereof) for each organism is based on a literature search (Carvalho-Santos et al., 2011; van Dam et al., 2013). Proteins with similarity to human PAM, furin, PC1/3, PC2, CPD and CPE were determined using NCBI Blastp (default parameters; Table S2 lists all the uniprot IDs used in this analysis). The presence of a bifunctional ortholog of human PAM (PHM and PAL domains in a single protein) is indicated in the column labeled PAM. If the Blastp hit is a monofunctional protein (contains either PHM or PAL) that hit is indicated in the columns labeled PHM or PAL, as appropriate. An *E*-value of 1E-3 was used as a cutoff, and only the top (based on E-value) non-redundant protein sequence was reported (a hit is represented as a filled circle; the color represents the *E*-value between the hit and the human query sequence). The presence of heterotrimeric G proteins (α, β and γ subunits) and seven transmembrane domain receptors based on a literature search is indicated with a check mark. Data for BBSome, IFT-A and IFT-B components were from (van Dam et al., 2013). Organisms that contained even one coat protein complex component received a check mark.

S1 and S2). Four potential *N*-linked glycosylation sites were identified in CrPAM, two in the CrPHM domain and two between the CrPAL domain and the transmembrane domain. Single Cys residues in the CrPHM and CrPAL domains lack homologs in mammalian PAM and could remain free or participate in disulfide bond formation (red and brown in Fig. 1B).

Attenborough et al. (2012) attributed their identification of organisms with genes encoding bifunctional PAM, monofunctional PHM and monofunctional PAL (as in *D. melanogaster* and *C. elegans*) to an early gene duplication. We revisited the phylogenetic distribution and found a striking correlation between the presence of cilia and bifunctional PAM or monofunctional PHM and PAL (Fig. 1C). Our analysis included organisms analyzed previously for the presence of cilia and key ciliary trafficking components, IFT-A, IFT-B and BBSomes (Carvalho-Santos et al., 2011; van Dam et al., 2013). These evolutionarily conserved coat-like proteins play crucial roles in ciliogenesis and in localization of signaling proteins required for proper ciliary function. Although not every ciliated organism in this analysis contains PAM, organisms that have PAM generally have cilia. Organisms lacking cilia such as red algae, most fungi, amoebae and land plants lack PAM. An exception was noted for the green alga *Ostreococcus tauri* that is purported not to have cilia, but has retained a *PAM* gene. Interestingly, several of the ciliated organisms lacking PAM have also lost one or more components of the IFT and BBS sub-complexes (Fig.1C).

We surveyed these same organisms for other peptide processing pathway components, such as enzymes operating upstream of PAM (prohormone convertases and carboxypeptidases) and downstream targets of bioactive peptides (seven transmembrane receptors and heterotrimeric G-proteins). Overall, genomes of organisms encoding a PAM-like protein also encode other putative components of the peptide biosynthetic pathway (Fig. 1C and Table S2). While *C. reinhardtii* lacks heterotrimeric G proteins, other organisms expressing PAM encode both heterotrimeric G proteins and 7 transmembrane domain receptors. Collectively, this analysis strengthens the connection between the presence of cilia and peptide amidation.

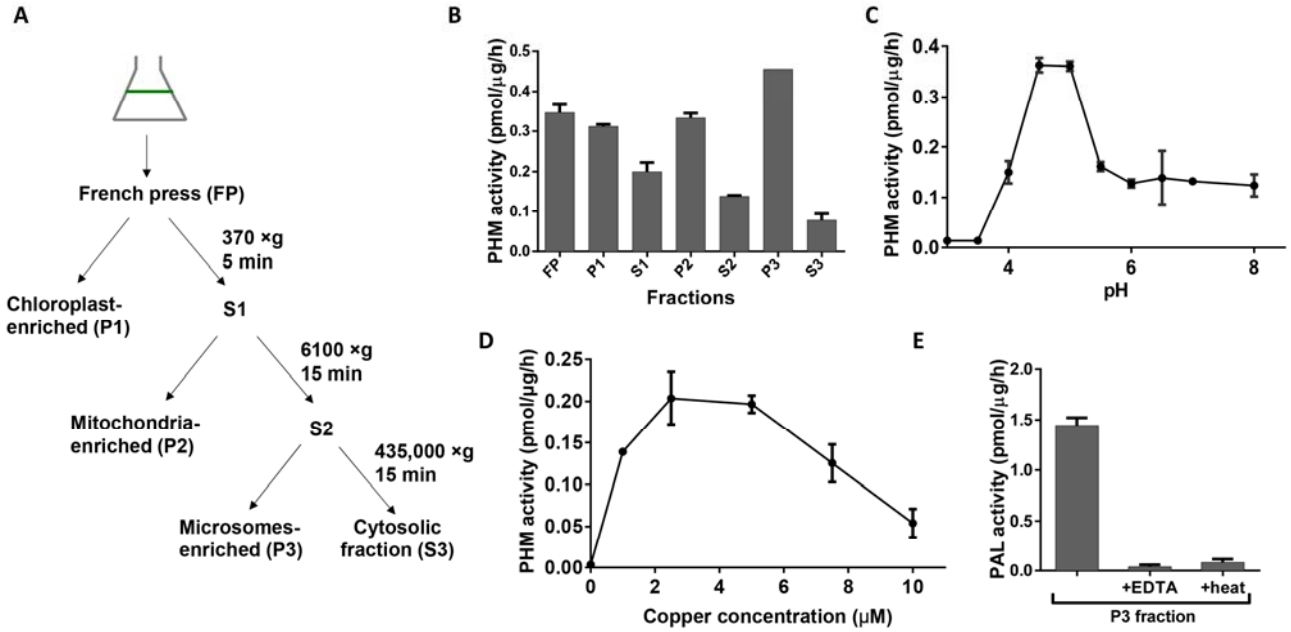

Fig. 2. *C. reinhardtii* cell lysates contain active PAM. (A) Schematic of the subcellular fractionation protocol used to enrich for different organelles from *C. reinhardtii* homogenates. (B) PHM activity was detected in all fractions, with the highest specific activity in the microsomal fraction (P3). (C) Microsomal PHM activity plotted as a function of pH. (D) PHM activity in the P3 fraction was greatest at 2.5-5 μM copper. (E) The same microsomal fraction displayed PAL activity that was inhibited by a divalent metal ion chelator (EDTA) or by heat (5 min at 100^0C).

Characterization of PAM activity in *C. reinhardtii* lysates

Our sequence analyses predicted an active PAM enzyme that localized to the secretory pathway in *C. reinhardtii*. To test this prediction, we subjected homogenates of wild-type CC124 *C. reinhardtii* cells to differential centrifugation (Fig. 2A). The fractions were tested for PHM activity using an *in vitro* assay that measures the conversion of a synthetic tripeptide substrate (Acetyl-Tyr-Val-Gly) into amidated product (Acetyl-Tyr-Val-NH_2). PHM activity was measurable in all fractions, with the highest specific activity in the particulate fraction containing small membrane fragments derived from multiple subcellular organelles (Fig. 2B) (Klein et al., 1983; El Meskini et al., 2000).

Mammalian PAM is optimally active at low pH, consistent with its presence in the secretory pathway lumen and mature secretory granules (luminal pH ~5), but remains active at neutral pH. We tested the effect of pH on PHM activity in *C. reinhardtii* lysates and found optimum activity at pH 4.5-5.0, with significant activity at pH 7 and above (Fig. 2C) (Husten and Eipper, 1994). *C. reinhardtii* PHM activity was also dependent on copper, with little activity observed in the absence of exogenous copper. As for the mammalian enzyme, higher concentrations of copper were inhibitory, presumably due to oxidation of the enzyme (Fig. 2D) (Eipper et al., 1983). PAL activity, which is Zn^{2+}- dependent, was detected in the same microsomal fraction and was greatly reduced by addition of a divalent metal ion chelator; PAL activity was also eliminated by heating at 100^0C for 5 min (Fig. 2E).

Expression of CrPAM in mammalian cells

To assess the properties of CrPAM, we transiently expressed the full-length cDNA in HEK-293T cells, which produce very little endogenous PHM activity. PHM activity was then readily detected in cell lysates and spent medium (Fig. 3A); the latter observation indicates that luminal domain cleavage of CrPAM occurred, generating soluble enzyme that was secreted, as observed for mammalian PAM. To assess this possibility, we generated antibodies to the C-terminus of CrPAM, which will detect intact CrPAM and any cell-associated fragments generated by the proteolytic cleavages that must occur

before active enzyme can be secreted. A cross-reactive band appeared in lysates from transfected HEK-293T and AtT-20 cells, a neuroendocrine cell line that stores the products of proopiomelanocortin cleavage in secretory granules (Fig. 3B); its apparent molecular mass, 117 ± 6 kDa, suggested that some of the potential *N*-glycosylation sites were utilized (predicted mass for CrPAM lacking its signal peptide, 97.2 kDa). In addition, a 16 kDa fragment was detected in lysates prepared from both cell types; cleavage between CrPAL and the transmembrane domain (as occurs in mammalian PAM) could generate a C-terminal fragment of this mass (CrTMD-CD), along with soluble bifunctional enzyme, which would be secreted (Rajagopal et al., 2010). The products produced by AtT-20 cells expressing rat PAM1 (rPAM1) and detected with antibodies to its C-terminus are shown for comparison.

The pH optimum of PHM secreted by HEK-293T cells expressing CrPAM was similar to that observed in the microsomal fraction of *C. reinhardtii* lysates (Fig. 3C). A copper chelator was added to the reaction mixture containing spent medium from CrPAM transfected and non-transfected (NT) cells and individual divalent metals were added in excess. CrPHM activity increased significantly only when copper was added to CrPAM spent medium along with the chelator; no other metal increased activity above baseline (marked “0) (Fig. 3D). Similar to mammalian PHM, CrPAM secreted by HEK-293T cells required a single electron donor (ascorbate) for activity (Fig. 3E). PAL activity was also detected in these lysates and was eliminated by heat or the addition of EDTA. In contrast to PHM, PAL activity was not detected in HEK-293T cell medium; two potential endoprotease cleavage sites within the predicted CrPAL catalytic core (Fig. S2) might account for the secretion of active PHM without the secretion of active PAL (Fig. 3F).

To characterize endogenous CrPAM, we tested the ability of affinity-purified C-terminal CrPAM antibodies to immunoprecipitate cross-reactive protein and PHM activity from *C. reinhardtii* lysates. PHM activity and a 117 kDa protein were detected in lysates prepared using non-ionic detergent (Fig. 3G). To determine whether the 117 kDa band represented CrPAM, lysates were incubated with affinity-

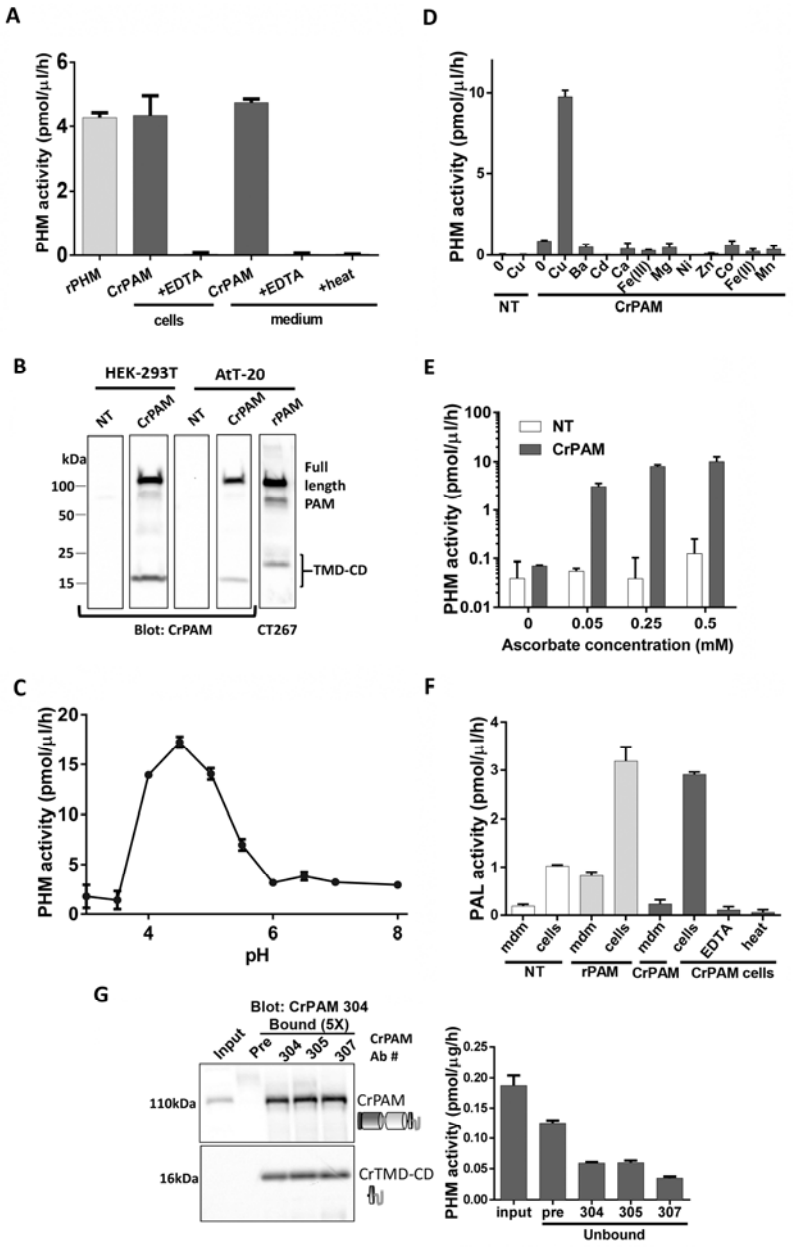

Fig. 3. CrPAM encodes active PAM. (A) PHM activity was detected in spent media and cell extracts of transiently transfected HEK-293T cells expressing CrPAM cDNA. The presence of EDTA or heating the sample (100°C, 5 min) reduced activity in cell extracts and spent media. (B) Immunoblot analysis of HEK-293T and AtT-20 cell lysates using antibody generated against the C-terminal domain of CrPAM (#304). Bands at 117 kDa and 16 kDa were detected only in transfected cell lysates. Lysate from AtT-20 cells expressing rPAM1 immunoblotted with a C-terminal antibody (CT267) is shown for reference. (C) pH dependence of PHM activity in spent medium from HEK-293T cells transiently expressing CrPAM. (D) Spent medium from non-transfected (NT) or CrPAM transfected HEK-293-T cells showed little or no PHM activity when a copper chelator (2 µM diethyldithiocarbamate) was added to the reaction mixture. The indicated metal salts (10 µM) were added to the reaction mixture in addition to the chelator; PHM activity increased significantly only when copper was added. (E) CrPHM activity was dependent on inclusion of ascorbate in the reaction (note the log scale); other single electron donors also support the activity of rat PHM (Prigge et al., 2000). (F) PAL activity was detected in lysates of

HEK-293T cells transiently expressing rPAM or CrPAM (NT, non-transfected control). PAL activity in lysates of HEK-293T cells expressing CrPAM was greatly reduced by the addition of EDTA (5 mM) or by heating the lysate. (G) Immunoprecipitation of CrPAM from *C. reinhardtii* cell lysates using affinity-purified C-terminal antibodies (Ab #304, #305 and #307) or pre-immune sera (Pre, as a control) showed enrichment of a 117 kDa band in the bound fractions, which were obtained from five times more material than the input. A 16 kDa fragment (CrTMD-CD) was also seen in the bound fractions, indicating some cleavage of the full-length protein and separation of the enzymatic domains (which will not be bound by this antibody) from the cytosolic domain; the mid-region of the blot, which contained the antibody heavy chain, is not shown. Immunoprecipitation reduced the amount of PHM activity in the unbound fractions compared to the input and pre-immune control.

purified antibody to the C-terminus of CrPAM. Unbound fractions were assayed for PHM activity and bound fractions were fractionated by SDS-PAGE and visualized using one of the affinity-purified antibodies. PHM activity was partially removed from the unbound fraction; while our C-terminal CrPAM antibody would be expected to bind intact CrPAM, any soluble proteins produced by its cleavage would not be recognized. A 117 kDa band was enriched in the bound fraction by all three affinity-purified antibodies (#304, #305 and #307) but not by pre-immune serum (Fig. 3G). In addition, a 16 kDa band, the mass expected for CrTMD-CD, was enriched by all three affinity-purified antibodies. These data are consistent with the conclusion that CrPAM, like the mammalian enzyme, was subject to endoproteolytic cleavage at a juxtamembrane luminal site.

Localization of CrPAM in mammalian neuroendocrine cells

In specialized secretory cells, peptide hormones and their processing enzymes enter the regulated secretory pathway and are stored in secretory granules. Since this pathway is well characterized in AtT-20 corticotrope tumor cells, we generated AtT-20 lines stably expressing CrPAM. In order to reduce signal from CrPAM diffusely distributed in the endoplasmic reticulum, wildtype AtT-20 cells and AtT-20 cells expressing CrPAM or rPAM1 were treated with cycloheximide for 1 hour before fixation (Sobota et al., 2006). Localization of CrPAM to the region enriched in GM-130, a cis-Golgi marker, was readily apparent (Fig. 4A; white arrows). As observed for PAM1, whose perinuclear localization reflects its presence in the TGN, immature secretory granules and endosomes (Milgram et al., 1997), staining for CrPAM was not coincident with GM-130. Secretory granules were visualized using an antibody specific for the C-terminus of the endogenous hormone, ACTH (Fig. 4B); granules were prevalent at the tips of cellular processes (green arrows). Using affinity-purified CrPAM and rPAM C-terminal antibodies, both proteins could be seen to co-localize with ACTH. Despite the evolutionary distance between rPAM and CrPAM, both proteins were similarly localized to multiple subcellular compartments in mouse corticotrope tumor cells.

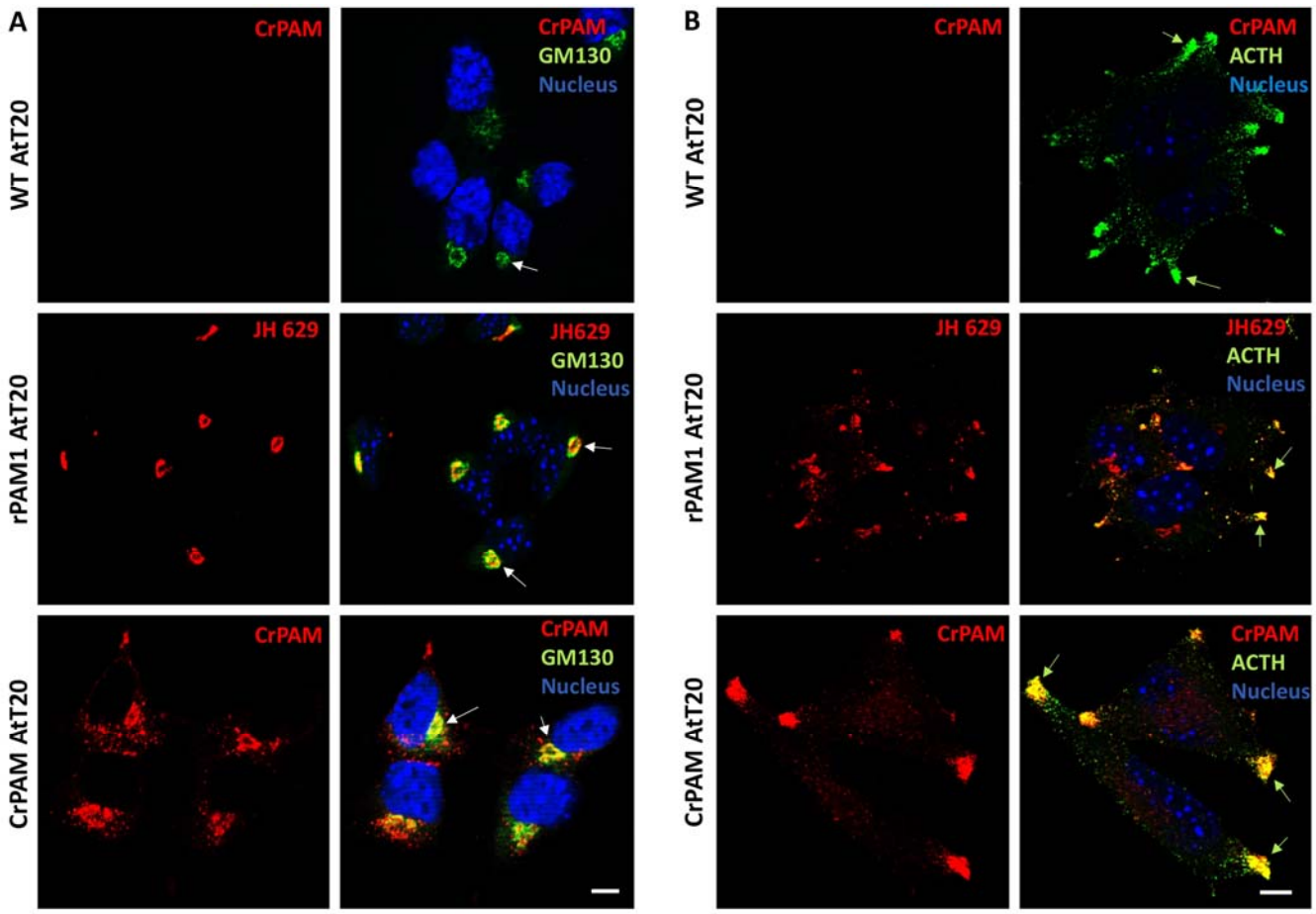

Fig. 4. Expression of CrPAM in mammalian neuroendocrine cells. Wild-type AtT-20 cells (WT) and stable lines expressing rPAM1 or CrPAM were fixed, permeabilized and stained for GM130 (A), a Golgi marker, or ACTH (B) a granule marker, using a FITC-tagged secondary antibody; cells were pretreated with 10 μM cycloheximide for 1 h (Sobota et al., 2006). WT and CrPAM expressing cells were stained using affinity-purified CrPAM C-terminal antibody; no background was observed in WT AtT-20 cells (upper panel, A and B). rPAM1 AtT-20 cells were stained with antibody to the linker region of mammalian PAM (JH629). PAM staining was visualized using Cy3-tagged secondary antibody. (A) Optical sections through the Golgi area showed perinuclear staining in rPAM1 and CrPAM expressing cells that partially co-localized with GM130 (white arrows). (B) In optical sections near the bottom of each cell, both rPAM1 and CrPAM were identified at the tips of cellular processes, where ACTH-containing granules accumulated (green arrows). Scale bar, 10 μm. Nuclei were visualized with Hoechst stain.

Expression and localization of endogenous CrPAM

The localization of endogenous CrPAM was established using immunofluorescence microcopy. In *C. reinhardtii* CC4351 cells, CrPAM localized to discrete vesicular structures in the cell body (Fig. 5A, Left). To confirm staining specificity, we preincubated the antibody with the antigenic peptide; the fluorescence intensity was greatly reduced (Fig. 5A, Right). Since CrPAM expressed in mammalian cells displayed strong localization to the perinuclear area occupied by the Golgi complex, we hypothesized that the vesicular staining pattern obtained for CrPAM represented the Golgi complex. Indeed, the localization of CrPAM in *C. reinhardtii* strongly resembled that of Arf1, a Golgi resident protein (Fig. 5B) (Dentler, 2013; Komsic-Buchmann et al., 2014). *C. reinhardtii* contains distinct Golgi stacks that are polarized and located close to the nucleus (Zhang and Robinson, 1986; Hummel et al., 2007). Treatment of cells with Brefeldin A, an ER to Golgi transport inhibitor, disrupted the strong vesicular staining observed with the CrPAM antibody (not shown), further confirming its Golgi localization. Unexpectedly, we also detected CrPAM staining in cilia, where it overlapped with staining for acetylated α-tubulin (Fig. 5A, Left); ciliary CrPAM staining was also blocked by pre-incubation with the antigenic peptide (Fig. 5A, Right). We obtained similar staining patterns with two other affinity-purified antibodies generated against the C-terminal domain of CrPAM (#304 and #305).

To confirm the presence of CrPAM in cilia, we stained detached cilia obtained from wild type CC124 *C. reinhardtii* cells. We observed punctate localization of CrPAM along the length of the cilia (Fig. 5C, Left). The signal was greatly reduced when the blocking peptide was used (Fig. 5C, Right). To determine the topology of CrPAM in the ciliary membrane, we incubated CC4351 *C. reinhardtii* cells with antibodies to CrPAM and acetylated tubulin or the major surface glycoprotein, FMG1. Staining for CrPAM and acetylated tubulin was observed in cilia only after the cells were permeabilized with Triton X-100 (TX-100); staining for these antigens was not observed when detergent was omitted (Fig. 5D). As expected, staining for FMG1, a cell surface marker, was observed in both permeabilized and non-permeabilized cells (Fig. 5E). Our immunofluorescence data showed that the C-terminal domain of

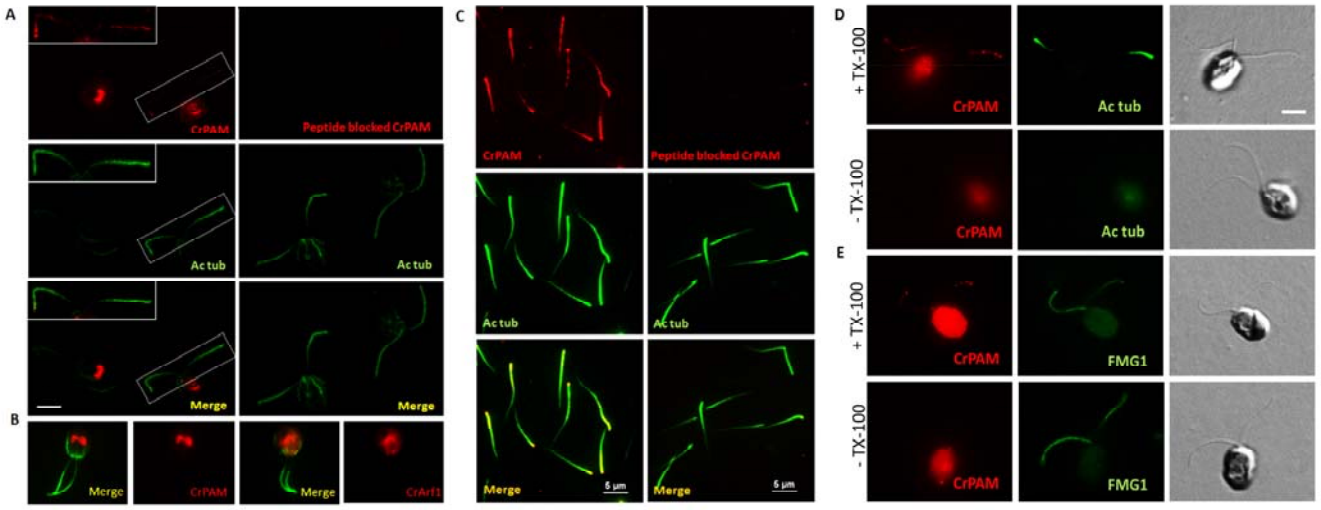

Fig. 5. CrPAM localizes to Golgi area and cilia in cell wall deficient CC4351 *C. reinhardtii* cells. (A) Confocal images of *C. reinhardtii* cells fixed, permeabilized and immunostained with affinity-purified antibody to CrPAM and acetylated tubulin (Left) and the corresponding peptide-blocked control (Right). CrPAM displayed tubulovesicular localization at the center of the cell body and punctate staining along the length of the cilia (white box and inset) that overlapped with acetylated tubulin. Scale bar, 5 μm. The CrPAM signal in the cell body and cilia was eliminated when antibody was pre-incubated with the antigenic peptide. (B) CrPAM staining in the cell body of fixed and permeabilized cells resembled CrArf1 staining. (C) Cilia isolated from CC124 *C. reinhardtii* were fixed, permeabilized and immunostained for CrPAM and acetylated tubulin (Left); cilia prepared in the same manner but visualized using CrPAM antibody pre-incubated with antigenic peptide served as a specificity control (Right). The punctate ciliary CrPAM staining was eliminated when the CrPAM antibody was blocked with peptide. Scale bar, 5 μm. (D and E) Fixed *C. reinhardtii* were incubated with antibodies to CrPAM and acetylated tubulin (D) or FMG1 (E) in the presence (+TX-100) or absence (-TX-100) of detergent; images for both treatments were acquired under identical conditions. Differential interference contrast images (right panels) allowed identification of cilia. CrPAM and tubulin staining was only observed in TX-100 treated cells. Scale bar, 5 μm.

CrPAM was present in the ciliary matrix, suggesting that the catalytic domains were exposed on the ciliary surface.

Knowing that endoproteolytic cleavages could separate its enzymatic domains from the C-terminus of CrPAM, we immunoblotted whole cilia isolated from wild type CC124 *C. reinhardtii* cells with our CrPAM antibody (Fig. 6A). Three bands (150, 70 and 50 kDa) were detected by the C-terminal specific antibody (control lane); none were present when the antibody was preincubated with blocking peptide (peptide lane). The two smaller fragments would be predicted to lack the PHM domain. Thus, ciliary CrPAM is a mixture of full-length and cleaved forms. The apparent masses observed suggest that CrPAM undergoes additional post-translational modifications (e.g. N- and O-linked glycosylation, phosphorylation), as documented for rPAM, before entering the cilium. Endoproteolytic cleavage might also generate membrane anchored forms of PHM and PAL that lack the C-terminal domain and would not be detected by our antibodies (Fig 6A).

To further explore the association of CrPAM with cilia, we turned to PHM assays; we sequentially treated detached wild type *C. reinhardtii* cilia with Triton X-100 to solubilize ciliary membrane proteins and matrix components, followed by 0.6 M NaCl and then 0.6 M KI to extract proteins that were more tightly bound to the axoneme (Fig. 6B). Remarkably, CrPHM activity was recovered in the 0.6 M NaCl fraction, but not in the initial detergent soluble (TX-100) fraction (Fig. 6C). This indicates that CrPAM either directly or indirectly associates with the axoneme; potentially both full-length CrPAM and cleaved forms containing the PHM domain but lacking the C-terminal domain could contribute to the activity measured. Thus, our results reveal the presence of a novel axoneme-associated enzyme activity in cilia. To further define the localization of CrPAM in cilia, we used immuno-electron microscopy. Isolated cilia were incubated with affinity-purified CrPAM antibody, which was then visualized using 15 nm gold-tagged secondary antibody (Fig. 6D). In ultrathin sections of cilia stained with the CrPAM antibody, gold particles were observed along the axoneme and were closely associated with outer doublet microtubules. Very few gold particles were observed either on cilia or in the background in the absence

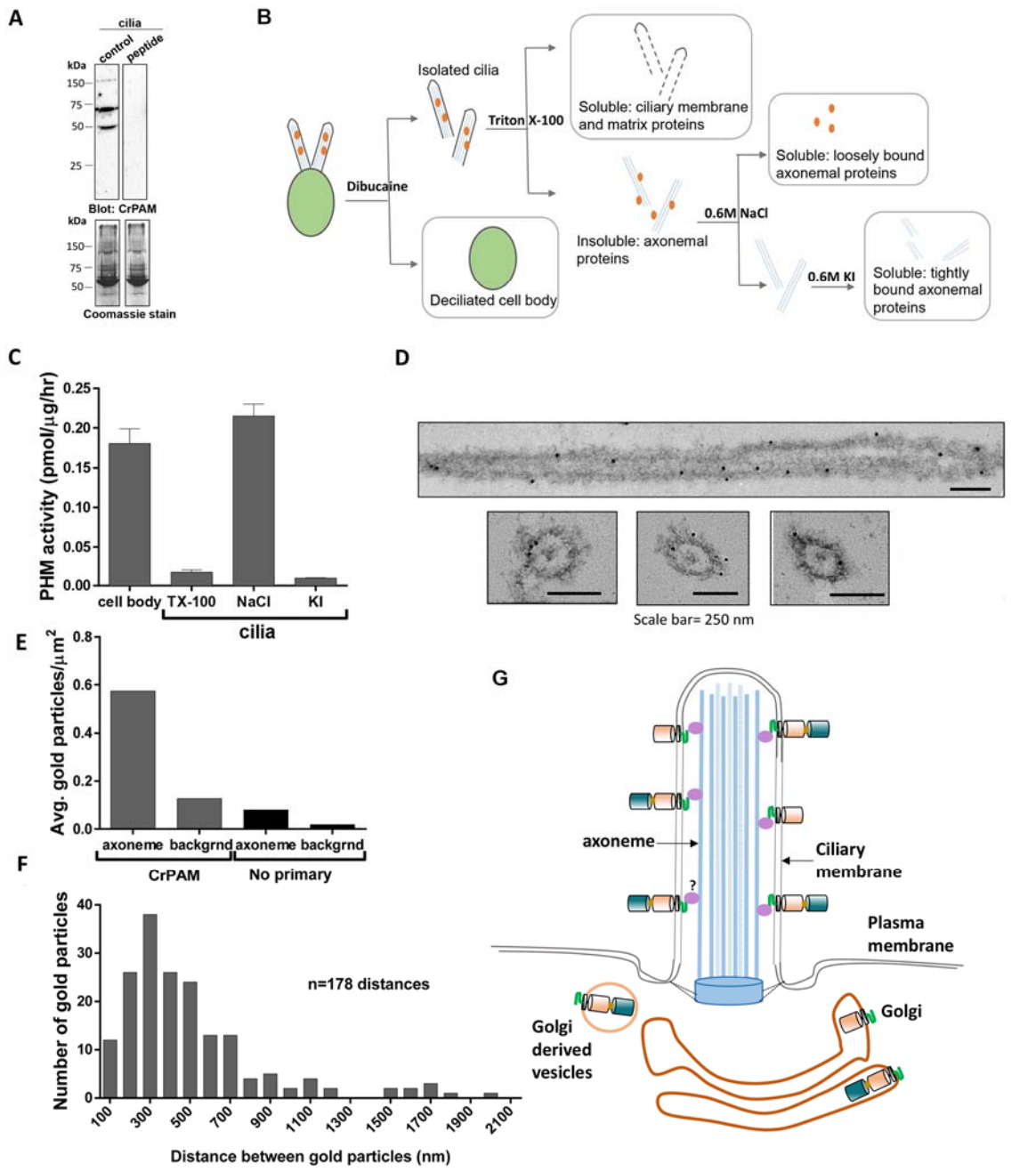

Fig. 6. CrPAM associates with the axoneme. (A) Isolated *C. reinhardtii* cilia extracted in SDS-lysis buffer were electrophoresed in a 10% polyacrylamide gel and immunoblotted with CrPAM C-terminal antibody (control) and antibody preincubated with a blocking peptide (peptide). Coomassie stain shows equal loading. The C-terminal antibody detects three specific bands in the cilium; note that membrane anchored enzymatic products of CrPAM cleavage lacking the C-terminal domain might also be present but would not be recognized by this antibody. (B) Schematic of fractionation scheme used to enrich for proteins associated with different ciliary sub-structures. Wild-type CC124 *C. reinhardtii* cilia were sequentially treated with buffers containing 1% Triton X-100 (to solubilize ciliary membrane and matrix proteins), 0.6 M NaCl (to solubilize proteins associated with the axoneme) and 0.6 M KI (to solubilize the axoneme and tightly bound proteins); salt extracted fractions were desalted and concentrated before analysis. Deciliated cell bodies were solubilized in 1% Triton X-100. (C) PHM specific activity in

Triton X-100 (TX-100) and salt extracted fractions obtained from cilia and cell bodies with the fractionation scheme described in (B). (D) ImmunoEM images of CrPAM localization in detached cilia from wild type CC124 *C. reinhardtii*. Gold particles were observed on or very close to the axonemal surface in both longitudinal and transverse sections. Scale bar, 250 nm. (E) The average density of gold particles in the axoneme and background regions was quantified for axonemes stained using the CrPAM antibody and control (No primary). Gold particles separated by more than 20 nm from the axoneme were considered background. The area of each background and axonemal region analyzed was measured; at least 50 axonemes and background regions were quantified for each set. The axonemal membrane is not visible because osmication was not performed. (F) To search for periodicity in the CrPAM staining along cilia, the distance between adjacent gold particles was determined using the distance measurement tool in Metamorph. Only gold particles on the same side of the axoneme were included in this analysis. The histogram was created using a 100 nm bin size and Graphpad Prism software. (G) Model of CrPAM localization in Golgi and cilia in *C. reinhardtii*. Multiple forms of CrPAM generated by proteolytic processing are present in the cilium and cell body (only the full length form and CrPAL membrane anchored forms are shown). The C-terminal domain resides in the cytoplasm in the cell body and in the ciliary matrix. The tight association of CrPAM with the axoneme could be indirectly mediated by unknown protein(s) depicted in purple.

of primary antibody (Fig. 6E). Gold labeling suggested periodicity, with a peak inter-particle distance of ~300 nm along the cilium (Fig. 6F). Based on these results, we conclude that CrPAM is a Golgi-localized protein that is also targeted to the cilium and associates closely with the ciliary axoneme in *C. reinhardtii* cells (Fig. 6G).

Identification of endogenous PAM in motile and sensory mammalian cilia

C. reinhardtii cilia share many biochemical and structural characteristics with mammalian cilia. We therefore asked whether PAM localized to mammalian cilia. Notably, PAM gene expression has been reported in the ventricular layer of the brain, where the multiple motile cilia on ependymal cells move the cerebrospinal fluid (Schafer et al., 1992; Zhang et al., 1997) . We isolated rodent ependymal cells and performed immunostaining with validated antibodies to several different domains of rPAM. Strikingly, punctate staining for PAM was apparent throughout the length of the cilia, which were co-stained for acetylated tubulin; similar patterns were observed with antibodies to the linker, CD and PHM domains of rPAM (Fig. 7A).

To confirm the general presence of PAM in motile cilia, rat tracheal epithelial cells were isolated and stained simultaneously with antisera to PAM and acetylated tubulin (Fig. 7B, Left). Confocal microscopy revealed punctate PAM staining at the base of the cilia and foci of staining distributed along the ciliary length. Staining specificity was verified by preincubating the PAM antibody with blocking peptide (Fig. 7B, Right). PAM staining at the base of the cilia in these multiciliated cells was adjacent to the basal bodies, which were revealed by staining for γ-tubulin (Fig. 7C). A similar localization pattern was reported for IFT20, a primarily Golgi localized component of the intraflagellar transport pathway, in airway epithelial cells (Jurczyk et al., 2004).

Spermatozoa rely on a highly-specialized flagellum for motility. PAM localization in this type of motile cilium was confirmed by immunostaining for PAM and acetylated tubulin (Fig. 7D). We observed a similar localization pattern with two other previously validated mammalian PAM antibodies.

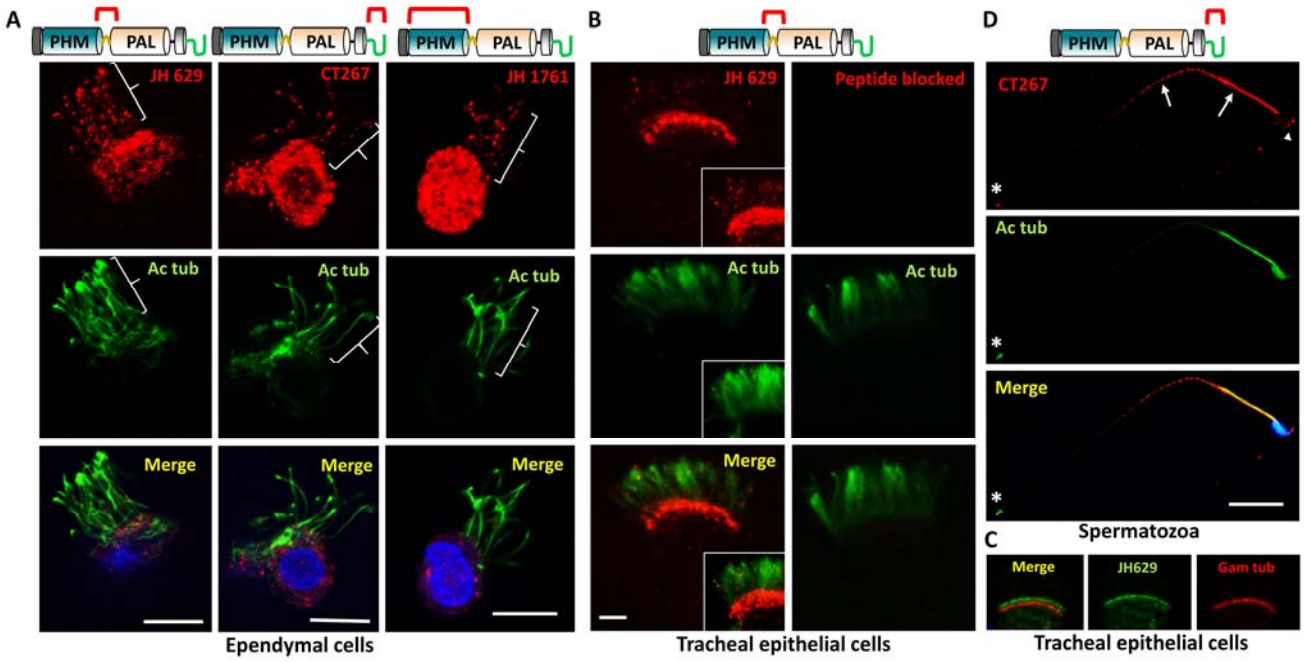

Fig. 7. PAM localizes to motile cilia in mammalian cells. (A) Rat ependymal cells were immunostained with antibodies to acetylated tubulin and mammalian PAM linker region (JH629), C-terminal domain (CT267) or PHM domain (JH1761); red brackets on PAM model show the antigen used to generate each antibody. Punctate PAM staining was observed along the length of the cilia using all three antibodies (white brackets). Scale bar, 10 μm. (B) Left. Rat tracheal epithelial cells were immunostained with antibodies to acetylated tubulin and PAM (JH629). Staining for PAM was observed at the base of the cilia and foci of staining were observed in the cilia. Right. Staining was greatly reduced when blocking peptide was present. Scale bar, 2 μm. (C) Tracheal epithelial cells were stained simultaneously for PAM (JH629) and γ-tubulin (Gam tub), a basal body marker. (D) Spermatozoa from wild type mice were immunostained with antibodies to acetylated tubulin and mammalian PAM (CT267). Punctate localization of PAM along the length of the axoneme (white arrows), at the tip of the tail (asterisk) and in the acrosomal vesicle (white arrowhead) was observed. Scale bar, 20 μm.

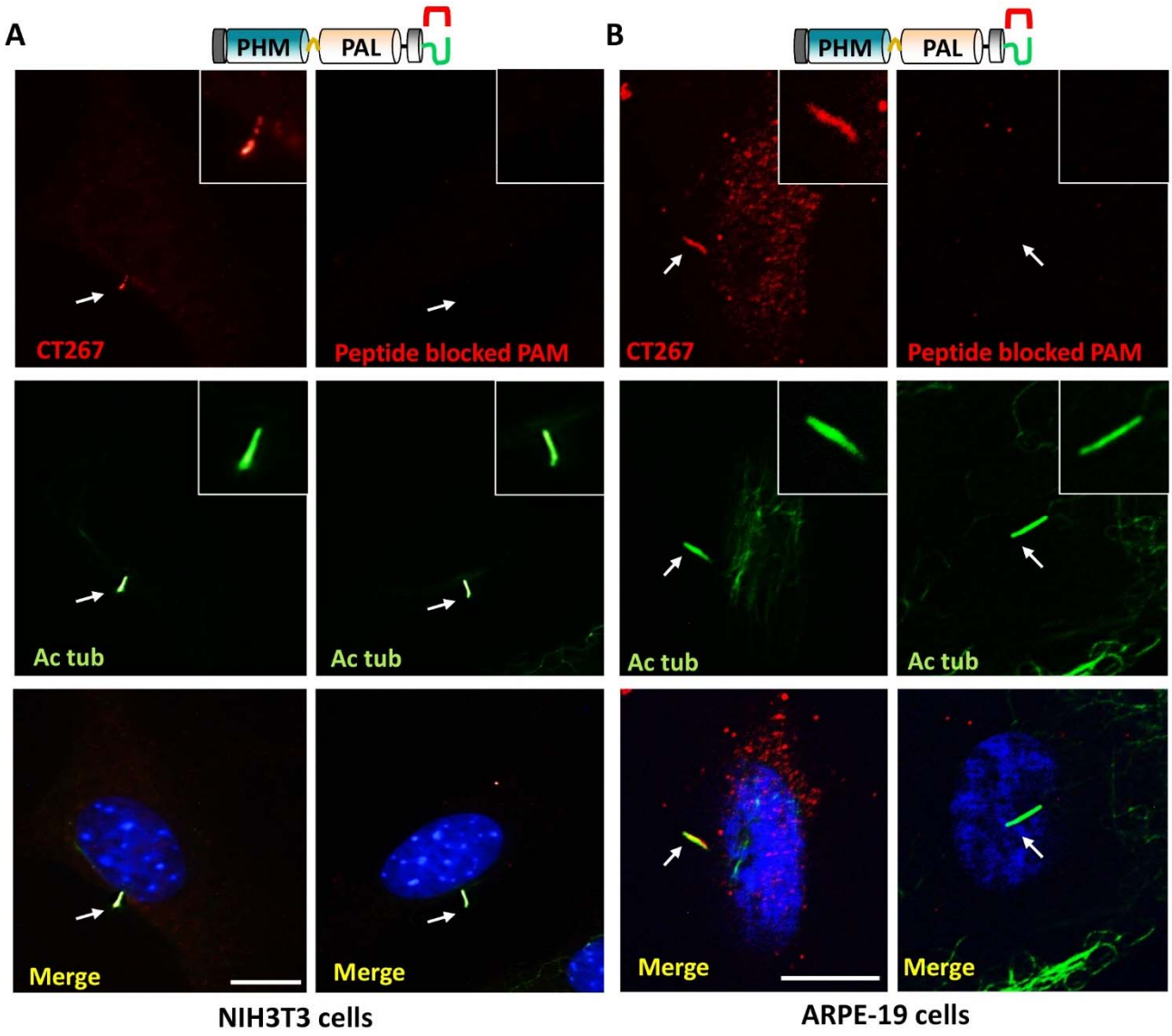

Fig. 8. PAM localizes to sensory cilia in mammalian cells. (A) Left. Serum starved NIH3T3 cells immunostained with antibody to acetylated tubulin and the C-terminus of mammalian PAM (CT267) displayed PAM staining along the length of the cilium (white arrow points to the cilium). Scale bar, 10 μm. Right. PAM protein could not be detected when the antibody was preincubated with the antigenic peptide. (B) Left. Human retinal pigment epithelial cells immunostained with antibodies to the C-terminus of mammalian PAM (CT267) and acetylated tubulin displayed similar localization of PAM in the cilium (white arrow points to the cilium). Right. Incubating the PAM antibody with antigenic peptide decreased signal observed in the cilium. Scale bar, 10 μm.

Interestingly, we also observed PAM localization to the acrosomal vesicle, which houses proteolytic enzymes required for fertilization, and a stronger signal at the very tip of the tail, where the axoneme is not surrounded by the outer dense fibers.

Most cell types possess immotile, primary cilia that play critical roles in signaling and sensing environmental cues. We reasoned that the presence or absence of PAM in primary cilia could indicate whether PAM played a role in motility or a more general role in signaling. Primary cilia were induced in NIH3T3 fibroblast cells by serum starvation and stained with antibodies to acetylated tubulin and PAM (Fig. 8A, Left). Primary cilia detected with acetylated tubulin staining also displayed PAM staining along their length (arrow marks the tip of the cilium). We confirmed the specificity of PAM staining by incubating the antibody with blocking peptide (Fig. 8A, Right).

Retinal pigment epithelial cell lines, which have well characterized sensory cilia, produce neuropeptide precursors and mature neuropeptides such as neuropeptide Y, which is amidated (Ammar et al., 1998). We used a human retinal pigment epithelial cell line (ARPE-19) to determine if PAM was targeted to these sensory cilia. PAM again localized to the cilium, where it overlapped with acetylated tubulin staining (arrow marks the tip of the cilium) (Fig. 8B, Left). The ciliary PAM signal was reduced when the antigenic peptide was used along with the antibody (Fig. 8B, Right).

DISCUSSION

C. reinhardtii genome encodes an active prohormone processing enzyme

A previous phylogenetic study identified *PAM*-like genes in several green algal genomes including *Chlamydomonas reinhardtii*, *Volvox carteri* and *Ostreococcus tauri* (Attenborough et al., 2012). We report here the characterization of an active peptide amidating monooxygenase in *C. reinhardtii* (Cre03.g152850). The CrPHM and CrPAL proteins exhibit 37% and 32% identity to the catalytic cores of human PHM and PAL, respectively (Fig. S1 and S2). As expected, CrPAM exhibited a stringent requirement for ascorbate and copper. Supplying ascorbate and copper to the lumen of the secretory

pathway requires transporters. The copper handling machinery in *C. reinhardtii* is similar to that in all eukaryotic cells (Merchant et al., 2006; Page et al., 2009; Blaby-Haas and Merchant, 2012). Cytosolic chaperones deliver the copper they receive from plasma membrane transporters to two highly conserved copper transporting P-type ATPases. *C. reinhardtii*, which synthesizes ascorbate, uses cytochrome b_{561} to regenerate reduced ascorbate in the secretory pathway lumen (Urzica et al., 2012). Optimal PAM activity occurs under acidic conditions, which are created by the vacuolar ATPase (V-ATPase), which is also highly conserved in *C. reinhardtii* (Table S1).

The presence of *PAM* in *C. reinhardtii* and metazoans suggests its presence in a shared ancestor and thus ancient evolutionary roots for its functions. Previous studies demonstrated conservation of the exon/intron organization of *PAM* in metazoans, with similar intron phasing and exon start sites in rat, *Drosophila* and Cnidaria (Kolhekar et al, 1997, Williamson et al, 2000). As expected, *CrPAM* had fewer and smaller introns than *rPAM*. Furthermore, we found essentially no alignment of exon/intron junctions between *C. reinhardtii* and metazoans.

Remarkably, despite the evolutionary distance separating mammals and green algae, CrPAM was trafficked and processed much like mammalian PAM when expressed in a murine neuroendocrine cell line. The specific activity observed for PHM in *C. reinhardtii* and neuroendocrine cell lysates was comparable (Ciccotosto et al., 1999). The active sites of mammalian and *C. reinhardtii* PHM appear to be very similar (Prigge et al., 1997); any penultimate residue in a peptide substrate can be accommodated. Classically, prohormone processing involves the cleavage of secretory pathway proteins by subtilisin-like prohormone convertases, which recognize pairs of basic residues, followed by removal of C-terminal Lys/Arg residues by carboxypeptidase B-like enzymes (CPE and CPD); all have been identified in *C. reinhardtii* (Fig. 1C and Table S1).

Ancestral form of PAM was membrane tethered

The ability of PAM to produce amidated peptides requires only its luminal domains (Milgram et al., 1994). The identification of a membrane tethered, bifunctional PAM protein with a cytosolic domain in *C. reinhardtii* suggests that the ancestral protein had this topology and that it was important for function. The transmembrane/cytosolic domain of rPAM plays an essential role in its trafficking in the biosynthetic and endocytic pathways. When the cytosolic domain is truncated, rPAM is largely localized to the plasma membrane (Milgram et al., 1993). Phosphorylation at multiple sites in the cytosolic domain of PAM controls its entry into the intraluminal vesicles of multivesicular bodies and its return to the trans-Golgi network (Back et al., 2010)

In mammals and *Chlamydomonas*, PAM exists as a mixture of full-length and N-terminally truncated forms in which the luminal catalytic domains have been separated from the transmembrane/cytosolic domain. In AtT-20 cells, the transmembrane/cytosolic domain fragments of rPAM are subject to γ-secretase-mediated cleavage, generating a soluble fragment of the cytosolic domain that accumulates in the nucleus (Francone et al., 2010; Rajagopal et al., 2010). AtT-20 cells engineered to allow doxycycline-inducible expression of rPAM demonstrated that increased expression of PAM caused changes in cytoskeletal organization and gene expression (Ciccotosto et al., 1999; Francone et al., 2010). These observations imply an ancient signaling role for PAM; its sensitivity to molecular oxygen, pH, copper, ascorbate and amino acids suggest several fundamental signaling pathways in which PAM could function.

Studies of PAM knockout mice (PAM^{KO}) also suggest that its role extends beyond its ability to produce amidated peptides. While PAM^{KO} mice fail to survive past mid-gestation, PAM heterozygotes ($PAM^{+/-}$) survive to adulthood; with half the normal level of PAM protein and activity, levels of amidated product peptides declined only slightly, suggesting that there is usually an excess of PAM activity (Bousquet-Moore et al., 2009). Nevertheless, $PAM^{+/-}$ mice exhibit an inability to vasoconstrict in a cold environment, increased adiposity, increased anxiety-like behavior, defects in copper homeostasis and

altered synaptic transmission (Bousquet-Moore et al., 2009; Bousquet-Moore et al., 2010; Gaier et al., 2010; Gaier et al., 2014). Mice maintained on a low copper diet mirrored some of the defects observed in PAM$^{+/-}$ mice; several deficits were reversed by a copper-supplemented diet (Bousquet-Moore et al., 2009; Gaier et al., 2010; Gaier et al., 2014). These observations are consistent with a role for PAM in communicating information about secretory pathway function to cytosolic effectors and to the nucleus.

PAM is included in a conserved set of Golgi-cilia proteins

The identification of PAM in cilia, an organelle dedicated to signaling and sensing environmental cues, also supports its signaling role. Localization of PAM to the cilia of several different mammalian cell types and *C. reinhardtii* highlights the importance of its presence in this cellular compartment. Although studies have focused on its neuroendocrine functions, PAM is expressed in tissues where cilia play essential roles (e.g., heart and olfactory epithelium) (Schafer et al., 1992; Zhang et al., 1997; Koefoed et al., 2014).

Also noteworthy is the widespread distribution of *PAM* in ciliated organisms and *PAM* gene loss in non-ciliated higher plants and fungi (Fig. 1C). Thus, it is possible that the last common ancestor of plants and animals contained both a *PAM* gene and cilia, with present day green algae maintaining *PAM* coincident with the presence of cilia. This correlation is not perfect, as *Ostreococcus tauri* contains a PAM-like protein, but lacks cilia. However, the occurrence of axonemal inner dynein arm heavy chain genes in *Ostreococcus* has been reported, raising the possibility that loss of ciliary components is incomplete and that remnants of a cilium may still exist (Wickstead and Gull, 2007). Alternatively, as suggested for *Chlorella*, which encodes nearly all ciliary outer dynein arm components (and a *PAM* gene), some green algae may have cilia at specific developmental stages that have not yet been observed; indeed, many cilia-related genes that are absent in land plants are conserved in these algae (Blanc et al., 2010).

The anomalies in the correlation of PAM and cilia extend to ciliated organisms such as the embryophyte, *Physcomitrella patens,* the chytrid fungus, *Batrachochytrium dedrobatidis,* alveolates such as *Tetrahymena thermophila* and trypanosomes such as *Trypanosoma brucei.* One explanation for the lack of a *PAM* gene in several of these ciliated organisms is their apparent use of cilia primarily for gamete or organismal motility rather than in a sensory or signaling capacity. Second, loss of *PAM* in some of these organisms (such as *Thalassiosira pseudonana*) closely parallels loss of some or all of the intraflagellar transport proteins, especially the BBSome subunits (Fig. 1C) (van Dam et al., 2013). Furthermore, these ciliated organisms are closely related to species (such as *Cryptosporidium parvum* and *Phaeodactylum tricornutum*) where complete loss of the IFT system and cilium have occurred. This correlation led to the proposal of a step-wise gain and loss of ciliary coat protein components, with the BBSome being the most recently acquired and thus, the first in line to be lost in lineages that subsequently lost the cilium completely (van Dam et al., 2013).

Several studies show that the Golgi complex and cilia are intricately linked; like most membrane proteins, those destined for the cilium must traverse the Golgi complex, where they are sorted into cilia-bound vesicles. It is important to note that the majority of the PAM protein in *C. reinhardtii* was found in the Golgi complex, with only a small fraction localized to the cilium. A similar distribution has been noted for IFT20, the Golgi localized component of the intraflagellar transport pathway required for proper ciliogenesis and trafficking of cilia localized proteins such as polycystin-2 (Follit et al., 2006).

Also intriguing is the association of CrPAM with the axonemal superstructure. The topology of CrPAM in the cilium places its C-terminal domain in the ciliary matrix or cilioplasm, suggesting that this domain is involved in a direct or indirect interaction with microtubules. While most membrane proteins (e.g., FMG1) and trafficking proteins (e.g., BBSome and IFT components) appear in the membrane/matrix fraction, the inner and outer dynein arms are solubilized by 0.6 M NaCl and the radial spokes require an even stronger lyotrope (0.6 M KI) for solubilization (Huang et al., 2007; King, 2013). CrPKD2, the *Chlamydomonas* homolog of polycystin-2, a 6 transmembrane domain ion channel, exhibits a similar

axonemal association (Huang et al., 2007). Like CrPAM, CrPKD2 and several other ciliary proteins are subject to proteolytic processing, generating fragments with distinct roles. Full-length CrPKD2 is found in the cell body, but not in the cilium, where two lower molecular weight fragments are observed (Huang et al., 2007).

What was the ancestral function of PAM?

Our demonstration of an active component of the peptide biosynthetic pathway in *C. reinhardtii* raises the question of whether this organism uses bioactive peptides for signaling; as noted above, genes encoding other essential processing enzymes as well as potential neuropeptide precursors are present (Fig. 1C). Although heterotrimeric G-proteins have not been found in *C. reinhardtii*, atypical GPCRs that employ distinct mechanisms of downstream signaling are present (Urano and Jones, 2013; Urano and Jones, 2014). Based on its localization and processing, CrPAM could produce amidated products in the lumen of the secretory pathway or on the ciliary surface. Active PAM has been identified on the surface of mammalian cells (Tausk et al., 1992) and in serum. Both CrPHM and CrPAL activities were detected in spent medium of mammalian cells expressing CrPAM. The topology of the protein in the cilium places the enzymatic domains in the extracellular milieu. *Chlamydomonas reinhardtii* grows above pH 3 and exhibits maximal growth rates in the range pH 5.5 - 8.5, conditions where both PHM and PAL can be active (Messerli et al., 2005). Extracellular environments containing oxygen and single electron donors may well support PAM enzyme activity.

A key question is the functional advantage of trafficking a peptide processing enzyme to the ciliary compartment. Characterization of $PAM^{+/-}$ mice has suggested a role of PAM in copper homeostasis. The ability of cells to amidate peptides was recently shown to be responsive to physiologically relevant changes in oxygen tension, leading to the suggestion of PAM-mediated hypoxia signaling mechanisms (Simpson et al., 2015). PAM could act as a copper and/or oxygen sensor in the cilium and transmit that information to the nucleus. Certainly, the ability of the soluble C-terminal domain of PAM to signal to the

nucleus coupled with the ability to generate bioactive peptides positions it as a potential sensor for these key environmental signals, crucial for organismal survival.

MATERIAL AND METHODS:

Cell Culture: *Chlamydomonas reinhardtii* strains CC124 mt- and CC4351 (*cw15 arg7-8*) obtained from the *Chlamydomonas* Resource Center were cultured in R medium and Tris-acetate-phosphate (TAP) medium supplemented with arginine as necessary (Witman, 1986). Cells were grown under a 12:12 h light/dark cycle at 22^0C and aerated with 95% air 5% CO_2.

NIH-3T3 and ARPE-19 cells were maintained in DMEM/F12 medium containing 10% fetal calf serum (Hyclone), 100 units/mL penicillin/streptomycin and 25 mM Hepes, pH 7.4 at 37^0C in a 5% CO_2 incubator. AtT-20 mouse corticotrope tumor cells and pEAK-RAPID HEK-293T cells were maintained as described (Bonnemaison et al., 2014).

Cloning and Molecular Biology: Oligo dT-primed template cDNA was prepared from wild type CC124 mt- *C. reinhardtii* genomic DNA using Superscript III (Life Technologies). The full length CrPAM coding region (accession number KT033716) was subcloned into pCI-neo (Promega) and verified by sequencing. For generating antibodies, a synthetic codon optimized DNA fragment encoding the C-terminal domain of CrPAM (CrCD) was ligated into a pGEX-6P3 vector to generate a GST-CrCD and used to transform BL21 *E. coli*.

Transient transfections of AtT-20 and pEAK-Rapid HEK293T cells were performed using Lipofectamine 2000 (Invitrogen) or TransIT-2020 (Mirus Bio). Stable cell lines were generated as described (Vishwanatha et al., 2014). For analyzing spent media, cells were incubated overnight in complete serum-free medium. Cell lysates were prepared in low ionic strength buffer containing 1% Triton-X100 and protease inhibitors; soluble fractions (14,000 rpm, 10 min) were used for enzyme assays. For immunoblot analyses, cells were collected in serum free medium, pelleted and solubilized in SDS lysis

buffer. Samples (equal protein) were analyzed using standard electrophoretic and immunoblotting techniques.

***C. reinhardtii* cilia isolation and fractionation:** CC124 mt- cells were deciliated with dibucaine (Witman, 1986; King, 1995). Isolated cilia in HMS (10 mM Hepes, pH 7.4, 5 mM $MgSO_4$, 4% sucrose) were sequentially extracted with NaTES-mannitol buffer containing 1% Triton X-100, 0.6 M NaCl and 0.6 M KI. Samples were concentrated and desalted using Amicon concentrators (10 kDa cut off) for determination of enzyme activity. For immunostaining, isolated cilia were placed onto polylysine coated coverslips and processed as described below. Isolated cilia were pelleted and mixed with equal volumes of DTT/sodium bicarbonate buffer (0.1 M DTT, 0.1 M $NaHCO_3$ containing protease inhibitors) and SDS/sucrose buffer (5% SDS and 30% sucrose) for western blotting. Peptide blocking experiments were performed by preincubating the primary antibody with an excess of synthetic peptide derived from the C-terminal sequence of CrPAM for 1 hr at room temperature.

Immunofluorescence: *C. reinhardtii* (strain CC4351) were mixed with an equal volume of 4% paraformaldehyde prepared in 30 mM Hepes, 5 mM EGTA, 5 mM $MgSO_4$, 25 mM KCl, 4% sucrose, pH 7.0 for 30 minutes at room temperature, placed onto polylysine-coated multichamber slides (Labtek) and permeabilized with PBS containing 0.5% Triton X-100 (this step was omitted in cells labeled "–TX-100" in Fig. 5 D, E). Cells were blocked with 3% fish skin gelatin, 1% BSA, 0.1% Tween20 in PBS for 1hr at room temperature. Primary antibodies were prepared in blocking buffer and cells incubated overnight at 4^0C or 1hr at room temperature for the topology experiment. Cells were incubated in secondary antibodies (Jackson ImmunoResearch) prepared in blocking buffer for 1-2hr at room temperature. Coverslips were mounted with ProLong Gold antifade mounting medium (Life Technologies).

Mammalian cells were fixed, permeabilized and stained as described previously (Bonnemaison et al., 2014). Tracheal cells (Pedersen et al., 2007), and ependymal cells were isolated from adult rats (Grondona et al., 2013). Adult mouse sperm were obtained from the cauda epididymis. Primary cells

fixed in solution were allowed to adhere to polylysine coated coverslips and stained as described above. All experiments were conducted with approved protocols from the UCHC Institutional Animal Care and Use Committees, in accordance with National Institutes of Health guidelines for animal care and the ARRIVE guidelines.

Images were obtained using a Zeiss Axiovert 200M microscope with 40×, 63× and 100× oil objectives and AxioVision software; optical sections were collected with the Zeiss ApoTome module. Confocal images were collected using the Zeiss LSM 510-Meta with an oil immersion 63× or 100× Plan Apochromat objective (NA 1.4) and LSM software. Detached cilia were imaged using a Nikon TE300 epifluorescence microscope with a 63× oil objective. Antibodies used included: CrPAM (1:500-1:1000, this study), CrArf1 (1:4000, Agrisera), acetylated tubulin clone 6-11B-1 (1:2000, Santa Cruz), rPAM1 exon 16, JH629 (1:1000 - 1:3000) (Yun et al., 1995), rPAM1 PHM, JH1761 (1:1000) (Milgram et al., 1997), rPAM1 C-terminus, CT267 (1:400 - 1:1000) (Rajagopal et al., 2009), ACTH(1-39) C-terminus monoclonal (1:100, Novocastra), FMG1 (1:200) (Bloodgood et al., 1986) and GM130 monoclonal (1:1000, BD Biosciences). Hoechst nuclear stain (1:1000, Invitrogen) was used where indicated.

Subcellular fractionation of *Chlamydomonas* cells: Wildtype CC124 mt- *C. reinhardtii* were pelleted, washed and resuspended in HMN buffer (30 mM Hepes pH 7.4, 5 mM $MgSO_4$ and 100 mM NaCl) containing a protease inhibitor cocktail and PMSF. The concentrated cell suspension was disrupted by passage through a French press. Fractions were obtained using a modified differential centrifugation protocol (Klein et al., 1983). After a 370 x *g* five minute spin, the supernatant was centrifuged at 6100 x *g* for 15 minutes; this supernatant was centrifuged at 435,000 x *g* in a TL100 centrifuge (Beckman) for 15 minutes. All pellet fractions were solubilized in low ionic strength buffer (20 mM NaTES, 10 mM mannitol, pH 7.4) containing 1% Triton-X100 and protease inhibitors before use in enzyme assays.

Antibody generation and validation: Purified CrCD (1.5 mg) was mixed with a synthetic peptide derived from the C-terminus of CrPAM (KRSTAEVEAARERERLLRSGP; 1.5 mg; Biomatik), conjugated to keyhole limpet hemocyanin using 0.3% glutaraldehyde (4 mg; Enzo Life Sciences), and used to

immunize three rabbits (#304, 305 and 307; Covance). Affinity-purification was performed using Affi-Gel-10 beads conjugated to CrCD or the synthetic peptide. For immunoprecipitation, affinity-purified antibodies and preimmune sera were added to *C. reinhardtii* lysates and incubated overnight at 4^0C; samples were clarified and supernatants incubated with protein A agarose beads. Bound proteins were eluted with Laemmli sample buffer; unbound fractions were used to determine PHM activity.

Enzyme assays: PHM and PAL assays were carried out as described (Kolhekar et al., 1997a) using trace amounts of [^{125}I]-labeled-Ac-Tyr-Val-Gly (PHM substrate) or [^{125}I]-labeled-Ac-Tyr-Val-(OH)-Gly and the corresponding unlabeled peptide (0.5 μM).

Immunogold electron microscopy: Detached cilia were fixed in 4% EM grade paraformaldehyde for 20 minutes at room temperature, washed in PBS buffer and collected by centrifugation. The pellet was dehydrated in ethanol at -20^0C and embedded in LR gold. Thin sections (70-80 nm) were mounted on formvar-coated mesh nickel grids, and incubated for 30 mins at room temperature in blocking buffer (1% BSA and 0.05% Triton X-100 in PBS).

Sections were incubated overnight at 4^{o}C in primary antibody (affinity-purified CT307, 1:10) in blocking buffer. Following three washes in PBS and one in blocking buffer, sections were incubated for 60 mins in goat anti-rabbit IgG conjugated to 15 nm gold (1:10, EM sciences). Grids were rinsed three times in PBS and post stained with 3% uranyl acetate and lead acetate. Sections were imaged using a Hitachi H-7650 transmission electron microscope. Gold particle density and spacing were quantified using Metamorph. For determination of gold particle density, 50 longitudinal cilia sections and background were manually traced and the number of gold particles and area calculated for both. Periodicity measurements were performed using the manual distance measurement tool in Metamorph.

ACKNOWLEDGMENTS

We thank Dr. Andrew Taylor, Boston University, for ARPE-19 cells, Dr. Branch Craige, UMass Medical School, for an aliquot of the CrArf1 antibody, Dr. Robert Bloodgood, University of Virginia, for an aliquot of the FMG1 antibody and Dr. Laurinda Jaffe, UConn Health Center for tracheal tissue. Many thanks to Yanping Wang, Darlene D'Amato and Ramila Patel-King for laboratory assistance and other Neuropeptide Laboratory members for their support. This work was supported by grants DK032949 (BAE), GM051293 (SMK), GM100753 (CEB) and GM042143 (SSM) from the National Institutes of Health.

AUTHOR CONTRIBUTIONS

Crysten E. Blaby-Haas performed the bioinformatics analysis in Sabeeha Merchant's labortory. Dhivya Kumar performed the remaining experiments under the guidance of Betty Eipper, Stephen King and Richard Mains.

REFERENCES:

Ammar, D. A., Hughes, B. A. and Thompson, D. A. (1998). Neuropeptide Y and the retinal pigment epithelium: receptor subtypes, signaling, and bioelectrical responses. *Invest Ophthalmol Vis Sci* **39**, 1870-1878.

Attenborough, R. M., Hayward, D. C., Kitahara, M. V., Miller, D. J. and Ball, E. E. (2012). A "neural" enzyme in nonbilaterian animals and algae: preneural origins for peptidylglycine alpha-amidating monooxygenase. *Mol Biol Evol* **29**, 3095-3109.

Back, N., Rajagopal, C., Mains, R. E. and Eipper, B. A. (2010). Secretory granule membrane protein recycles through multivesicular bodies. *Traffic* **11**, 972-986.

Berbari, N. F., Johnson, A. D., Lewis, J. S., Askwith, C. C. and Mykytyn, K. (2008). Identification of ciliary localization sequences within the third intracellular loop of G protein-coupled receptors. *Mol Biol Cell* **19**, 1540-1547.

Blaby-Haas, C. E. and Merchant, S. S. (2012). The ins and outs of algal metal transport. *Biochim Biophys Acta* **1823**, 1531-1552.

Blanc, G., Duncan, G., Agarkova, I., Borodovsky, M., Gurnon, J., Kuo, A., Lindquist, E., Lucas, S., Pangilinan, J., Polle, J. et al. (2010). The *Chlorella variabilis* NC64A genome reveals adaptation to photosymbiosis, coevolution with viruses, and cryptic sex. *Plant Cell* **22**, 2943-2955.

Bloodgood, R. A. (2010). Sensory reception is an attribute of both primary cilia and motile cilia. *J Cell Sci* **123**, 505-509.

Bloodgood, R. A., Woodward, M. P. and Salomonsky, N. L. (1986). Redistribution and shedding of flagellar membrane glycoproteins visualized using an anti-carbohydrate monoclonal antibody and concanavalin A. *J Cell Biol* **102**, 1797-1812.

Bonnemaison, M., Bäck, N., Lin, Y., Bonifacino, J. S., Mains, R. and Eipper, B. (2014). AP-1A controls secretory granule biogenesis and trafficking of membrane secretory granule proteins. *Traffic* **15**, 1099-1121.

Bousquet-Moore, D., Ma, X. M., Nillni, E. A., Czyzyk, T. A., Pintar, J. E., Eipper, B. A. and Mains, R. E. (2009). Reversal of physiological deficits caused by diminished levels of peptidylglycine alpha-amidating monooxygenase by dietary copper. *Endocrinology* **150**, 1739-1747.

Bousquet-Moore, D., Prohaska, J. R., Nillni, E. A., Czyzyk, T., Wetsel, W. C., Mains, R. E. and Eipper, B. A. (2010). Interactions of peptide amidation and copper: novel biomarkers and mechanisms of neural dysfunction. *Neurobiol Dis* **37**, 130-140.

Brown, J. M. and Witman, G. B. (2014). Cilia and Diseases. *Bioscience* **64**, 1126-1137.

Carvalho-Santos, Z., Azimzadeh, J., Pereira-Leal, J. B. and Bettencourt-Dias, M. (2011). Evolution: Tracing the origins of centrioles, cilia, and flagella. *J Cell Biol* **194**, 165-175.

Ciccotosto, G. D., Schiller, M. R., Eipper, B. A. and Mains, R. E. (1999). Induction of integral membrane PAM expression in AtT-20 cells alters the storage and trafficking of POMC and PC1. *J Cell Biol* **144**, 459-471.

Conductier, G., Brau, F., Viola, A., Langlet, F., Ramkumar, N., Dehouck, B., Lemaire, T., Chapot, R., Lucas, L., Rovere, C. et al. (2013). Melanin-concentrating hormone regulates beat frequency of ependymal cilia and ventricular volume. *Nat Neurosci* **16**, 845-847.

Conzelmann, M., Offenburger, S. L., Asadulina, A., Keller, T., Munch, T. A. and Jekely, G. (2011). Neuropeptides regulate swimming depth of Platynereis larvae. *Proc Natl Acad Sci U S A* **108**, E1174-1183.

Czyzyk, T. A., Ning, Y., Hsu, M. S., Peng, B., Mains, R. E., Eipper, B. A. and Pintar, J. E. (2005). Deletion of peptide amidation enzymatic activity leads to edema and embryonic lethality in the mouse. *Dev Biol* **287**, 301-313.

Dentler, W. (2013). A role for the membrane in regulating *Chlamydomonas* flagellar length. *PLoS One* **8**, e53366.

Eipper, B. A., Glembotski, C. C. and Mains, R. E. (1983). Bovine intermediate pituitary alpha-amidation enzyme: preliminary characterization. *Peptides* **4**, 921-928.

El Meskini, R., Mains, R. E. and Eipper, B. A. (2000). Cell type-specific metabolism of peptidylglycine alpha-amidating monooxygenase in anterior pituitary. *Endocrinology* **141**, 3020-3034.
Fliegauf, M., Benzing, T. and Omran, H. (2007). When cilia go bad: cilia defects and ciliopathies. *Nat Rev Mol Cell Biol* **8**, 880-893.
Follit, J. A., Tuft, R. A., Fogarty, K. E. and Pazour, G. J. (2006). The intraflagellar transport protein IFT20 is associated with the Golgi complex and is required for cilia assembly. *Mol Biol Cell* **17**, 3781-3792.
Francone, V. P., Ifrim, M. F., Rajagopal, C., Leddy, C. J., Wang, Y., Carson, J. H., Mains, R. E. and Eipper, B. A. (2010). Signaling from the secretory granule to the nucleus: Uhmk1 and PAM. *Mol Endocrinol* **24**, 1543-1558.
Gaier, E. D., Rodriguiz, R. M., Zhou, J., Ralle, M., Wetsel, W. C., Eipper, B. A. and Mains, R. E. (2014). In vivo and in vitro analyses of amygdalar function reveal a role for copper. *J Neurophysiol* **111**, 1927-1939.
Gaier, E. D., Rodriguiz, R. M., Ma, X. M., Sivaramakrishnan, S., Bousquet-Moore, D., Wetsel, W. C., Eipper, B. A. and Mains, R. E. (2010). Haploinsufficiency in peptidylglycine alpha-amidating monooxygenase leads to altered synaptic transmission in the amygdala and impaired emotional responses. *J Neurosci* **30**, 13656-13669.
Grondona, J. M., Granados-Duran, P., Fernandez-Llebrez, P. and Lopez-Avalos, M. D. (2013). A simple method to obtain pure cultures of multiciliated ependymal cells from adult rodents. *Histochem Cell Biol* **139**, 205-220.
Hsiao, Y. C., Tuz, K. and Ferland, R. J. (2012). Trafficking in and to the primary cilium. *Cilia* **1**, 4.
Huang, K., Diener, D. R., Mitchell, A., Pazour, G. J., Witman, G. B. and Rosenbaum, J. L. (2007). Function and dynamics of PKD2 in *Chlamydomonas reinhardtii* flagella. *J Cell Biol* **179**, 501-514.
Huangfu, D., Liu, A., Rakeman, A. S., Murcia, N. S., Niswander, L. and Anderson, K. V. (2003). Hedgehog signalling in the mouse requires intraflagellar transport proteins. *Nature* **426**, 83-87.
Hummel, E., Schmickl, R., Hinz, G., Hillmer, S. and Robinson, D. G. (2007). Brefeldin A action and recovery in *Chlamydomonas* are rapid and involve fusion and fission of Golgi cisternae. *Plant Biol (Stuttg)* **9**, 489-501.
Husten, E. J. and Eipper, B. A. (1994). Purification and characterization of PAM-1, an integral membrane protein involved in peptide processing. *Arch Biochem Biophys* **312**, 487-492.
Huyghe, J. R., Jackson, A. U., Fogarty, M. P., Buchkovich, M. L., Stancakova, A., Stringham, H. M., Sim, X., Yang, L., Fuchsberger, C., Cederberg, H. et al. (2013). Exome array analysis identifies new loci and low-frequency variants influencing insulin processing and secretion. *Nat Genet* **45**, 197-201.
Jekely, G. (2011). Origin and early evolution of neural circuits for the control of ciliary locomotion. *Proceedings. Biological sciences / The Royal Society* **278**, 914-922.
Jekely, G. (2013). Global view of the evolution and diversity of metazoan neuropeptide signaling. *Proc Natl Acad Sci U S A* **110**, 8702-8707.
Johnson, J. L. and Leroux, M. R. (2010). cAMP and cGMP signaling: sensory systems with prokaryotic roots adopted by eukaryotic cilia. *Trends Cell Biol* **20**, 435-444.
Jurczyk, A., Gromley, A., Redick, S., San Agustin, J., Witman, G., Pazour, G. J., Peters, D. J. and Doxsey, S. (2004). Pericentrin forms a complex with intraflagellar transport proteins and polycystin-2 and is required for primary cilia assembly. *J Cell Biol* **166**, 637-643.
King, S. M. (1995). Large-scale isolation of *Chlamydomonas* flagella. *Methods Cell Biol* **47**, 9-12.
King, S. M. (2013). Biochemical and physiological analysis of axonemal dyneins. *Methods Enzymol* **524**, 123-145.
Klein, U., Chen, C., Gibbs, M. and Platt-Aloia, K. A. (1983). Cellular fractionation of *Chlamydomonas reinhardii* with emphasis on the isolation of the chloroplast. *Plant Physiol* **72**, 481-487.
Koefoed, K., Veland, I. R., Pedersen, L. B., Larsen, L. A. and Christensen, S. T. (2014). Cilia and coordination of signaling networks during heart development. *Organogenesis* **10**, 108-125.
Kolhekar, A. S., Mains, R. E. and Eipper, B. A. (1997a). Peptidylglycine alpha-amidating monooxygenase: an ascorbate-requiring enzyme. *Methods Enzymol* **279**, 35-43.
Kolhekar, A. S., Roberts, M. S., Jiang, N., Johnson, R. C., Mains, R. E., Eipper, B. A. and Taghert, P. H. (1997b). Neuropeptide amidation in *Drosophila*: separate genes encode the two enzymes catalyzing amidation. *J Neurosci* **17**, 1363-1376.

Komsic-Buchmann, K., Wostehoff, L. and Becker, B. (2014). The contractile vacuole as a key regulator of cellular water flow in *Chlamydomonas reinhardtii*. *Eukaryotic cell* **13**, 1421-1430.
Loktev, A. V. and Jackson, P. K. (2013). Neuropeptide Y family receptors traffic via the Bardet-Biedl syndrome pathway to signal in neuronal primary cilia. *Cell reports* **5**, 1316-1329.
Merchant, S. S., Allen, M. D., Kropat, J., Moseley, J. L., Long, J. C., Tottey, S. and Terauchi, A. M. (2006). Between a rock and a hard place: trace element nutrition in *Chlamydomonas*. *Biochim Biophys Acta* **1763**, 578-594.
Messerli, M. A., Amaral-Zettler, L. A., Zettler, E., Jung, S. K., Smith, P. J. and Sogin, M. L. (2005). Life at acidic pH imposes an increased energetic cost for a eukaryotic acidophile. *J Exp Biol* **208**, 2569-2579.
Milgram, S. L., Mains, R. E. and Eipper, B. A. (1993). COOH-terminal signals mediate the trafficking of a peptide processing enzyme in endocrine cells. *J Cell Biol* **121**, 23-36.
Milgram, S. L., Eipper, B. A. and Mains, R. E. (1994). Differential trafficking of soluble and integral membrane secretory granule-associated proteins. *J Cell Biol* **124**, 33-41.
Milgram, S. L., Kho, S. T., Martin, G. V., Mains, R. E. and Eipper, B. A. (1997). Localization of integral membrane peptidylglycine alpha-amidating monooxygenase in neuroendocrine cells. *J Cell Sci* **110 (Pt 6)**, 695-706.
Mukhopadhyay, S. and Rohatgi, R. (2014). G-protein-coupled receptors, Hedgehog signaling and primary cilia. *Semin Cell Dev Biol* **33**, 63-72.
Nachury, M. V., Seeley, E. S. and Jin, H. (2010). Trafficking to the ciliary membrane: how to get across the periciliary diffusion barrier? *Annu Rev Cell Dev Biol* **26**, 59-87.
Page, M. D., Kropat, J., Hamel, P. P. and Merchant, S. S. (2009). Two *Chlamydomonas* CTR copper transporters with a novel cys-met motif are localized to the plasma membrane and function in copper assimilation. *Plant Cell* **21**, 928-943.
Pedersen, L. B., Rompolas, P., Christensen, S. T., Rosenbaum, J. L. and King, S. M. (2007). The lissencephaly protein Lis1 is present in motile mammalian cilia and requires outer arm dynein for targeting to *Chlamydomonas* flagella. *J Cell Sci* **120**, 858-867.
Petersen, T. N., Brunak, S., von Heijne, G. and Nielsen, H. (2011). SignalP 4.0: discriminating signal peptides from transmembrane regions. *Nature methods* **8**, 785-786.
Prigge, S. T., Mains, R. E., Eipper, B. A. and Amzel, L. M. (2000). New insights into copper monooxygenases and peptide amidation: structure, mechanism and function. *Cell Mol Life Sci* **57**, 1236-1259.
Prigge, S. T., Kolhekar, A. S., Eipper, B. A., Mains, R. E. and Amzel, L. M. (1997). Amidation of bioactive peptides: the structure of peptidylglycine alpha-hydroxylating monooxygenase. *Science* **278**, 1300-1305.
Rajagopal, C., Stone, K. L., Mains, R. E. and Eipper, B. A. (2010). Secretion stimulates intramembrane proteolysis of a secretory granule membrane enzyme. *J Biol Chem* **285**, 34632-34642.
Rajagopal, C., Stone, K. L., Francone, V. P., Mains, R. E. and Eipper, B. A. (2009). Secretory granule to the nucleus: role of a multiply phosphorylated intrinsically unstructured domain. *J Biol Chem* **284**, 25723-25734.
Schafer, M. K., Stoffers, D. A., Eipper, B. A. and Watson, S. J. (1992). Expression of peptidylglycine alpha-amidating monooxygenase (EC 1.14.17.3) in the rat central nervous system. *J Neurosci* **12**, 222-234.
Shah, A. S., Ben-Shahar, Y., Moninger, T. O., Kline, J. N. and Welsh, M. J. (2009). Motile cilia of human airway epithelia are chemosensory. *Science* **325**, 1131-1134.
Simpson, P. D., Eipper, B. A., Katz, M. J., Gandara, L., Wappner, P., Fischer, R., Hodson, E. J., Ratcliffe, P. J. and Masson, N. (2015). Striking oxygen sensitivity of the peptidylglycine alpha-amidating monooxygenase (pam) in neuroendocrine cells. *J Biol Chem*.
Singla, V. and Reiter, J. F. (2006). The primary cilium as the cell's antenna: signaling at a sensory organelle. *Science* **313**, 629-633.
Sobota, J. A., Ferraro, F., Back, N., Eipper, B. A. and Mains, R. E. (2006). Not all secretory granules are created equal: Partitioning of soluble content proteins. *Mol Biol Cell* **17**, 5038-5052.

Steinthorsdottir, V., Thorleifsson, G., Sulem, P., Helgason, H., Grarup, N., Sigurdsson, A., Helgadottir, H. T., Johannsdottir, H., Magnusson, O. T., Gudjonsson, S. A. et al. (2014). Identification of low-frequency and rare sequence variants associated with elevated or reduced risk of type 2 diabetes. *Nat Genet* **46**, 294-298.
Tardif, M., Atteia, A., Specht, M., Cogne, G., Rolland, N., Brugiere, S., Hippler, M., Ferro, M., Bruley, C., Peltier, G. et al. (2012). PredAlgo: a new subcellular localization prediction tool dedicated to green algae. *Mol Biol Evol* **29**, 3625-3639.
Tausk, F. A., Milgram, S. L., Mains, R. E. and Eipper, B. A. (1992). Expression of a peptide processing enzyme in cultured cells: truncation mutants reveal a routing domain. *Mol Endocrinol* **6**, 2185-2196.
Urano, D. and Jones, A. M. (2013). "Round up the usual suspects": a comment on nonexistent plant G protein-coupled receptors. *Plant Physiol* **161**, 1097-1102.
Urano, D. and Jones, A. M. (2014). Heterotrimeric G protein-coupled signaling in plants. *Annu Rev Plant Biol* **65**, 365-384.
Urzica, E. I., Adler, L. N., Page, M. D., Linster, C. L., Arbing, M. A., Casero, D., Pellegrini, M., Merchant, S. S. and Clarke, S. G. (2012). Impact of oxidative stress on ascorbate biosynthesis in *Chlamydomonas* via regulation of the VTC2 gene encoding a GDP-L-galactose phosphorylase. *J Biol Chem* **287**, 14234-14245.
van Dam, T. J., Townsend, M. J., Turk, M., Schlessinger, A., Sali, A., Field, M. C. and Huynen, M. A. (2013). Evolution of modular intraflagellar transport from a coatomer-like progenitor. *Proc Natl Acad Sci U S A* **110**, 6943-6948.
Vishwanatha, K., Back, N., Mains, R. E. and Eipper, B. A. (2014). A histidine-rich linker region in peptidylglycine alpha-amidating monooxygenase has the properties of a pH sensor. *J Biol Chem* **289**, 12404-12420.
Wallingford, J. B. and Mitchell, B. (2011). Strange as it may seem: the many links between Wnt signaling, planar cell polarity, and cilia. *Genes Dev* **25**, 201-213.
Warner, J. F., McCarthy, A. M., Morris, R. L. and McClay, D. R. (2014). Hedgehog signaling requires motile cilia in the sea urchin. *Mol Biol Evol* **31**, 18-22.
Waters, A. M. and Beales, P. L. (2011). Ciliopathies: an expanding disease spectrum. *Pediatr Nephrol* **26**, 1039-1056.
Wickstead, B. and Gull, K. (2007). Dyneins across eukaryotes: a comparative genomic analysis. *Traffic* **8**, 1708-1721.
Witman, G. B. (1986). Isolation of *Chlamydomonas* flagella and flagellar axonemes. *Methods Enzymol* **134**, 280-290.
Yun, H. Y., Milgram, S. L., Keutmann, H. T. and Eipper, B. A. (1995). Phosphorylation of the cytosolic domain of peptidylglycine alpha-amidating monooxygenase. *J Biol Chem* **270**, 30075-30083.
Zhang, J., Zheng, M., Eipper, B. A. and Pintar, J. E. (1997). Embryonic and uterine expression patterns of peptidylglycine alpha-amidating monooxygenase transcripts suggest a widespread role for amidated peptides in development. *Dev Biol* **192**, 375-391.
Zhang, Y.-H. and Robinson, D. G. (1986). The endomembranes of *Chlamydomonas reinhardii*: A comparison of the wildtype with the wall mutants CW 2 and CW 15. *Protoplasma* **133**, 186-194.

SUPPLEMENTARY FILES

Fig. S1: PHM domain alignment. Alignments were made using ClustalW2 (EMBL-EBI) and regions corresponding to the catalytic core of rat PHM. The sequences used were: *Chlamydomonas reinhardtii* PAM (CrPAM, KT033716), *Schistosoma mansoni* PHM (SchPHM, AA018222), *Schistosoma mansoni* PAM (SchPAM, CCD77525), *Aplysia californica* PAM (AcPAM, AAF67216), *Drosophila melanogaster* PHM (dPHM, AAF47127), *Rattus norvegicus* PAM (rPAM, P14925) and *Homo sapiens* PAM (hPAM, P19021). Residues important for catalytic activity (R^{240}, N^{316} and Y^{318} in rat PAM) are highlighted in turquoise. The two copper binding sites, Cu_H (His^{107}, His^{108} and His^{172} in rat PAM) and Cu_M (His^{242}, His^{244} and Met^{314} in rat PAM) are highlighted in pink and green, respectively. Cysteine residues are highlighted in red; potential N-linked glycosylation sites in CrPHM are underlined.

Fig. S2: PAL domain alignment. Alignments were made using ClustalW2 (EMBL-EBI) and regions corresponding to the catalytic core of rat PAL. The sequences used were: *Chlamydomonas reinhardtii* PAM (CrPAM, KT033716), *Schistosoma mansoni* PAL (SchPAL, ACN42951.1), *Aplysia californica* PAM (AcPAM, AAF67216), *Drosophila melanogaster* PAL1 (dPAL1, ACL83084), *Drosophila melanogaster* PAL2 (dPAL2, AHN56571), *Rattus norvegicus* PAM (rPAM, P14925) and *Homo sapiens* PAM (hPAM, P19021). The *Schistosoma* PAM sequence (CCD77525), which only includes a partial PAL domain, was not included in this analysis. The only adjustment made to the alignment was moving and lengthening one gap in CrPAM to allow alignment of the final residues involved in Zn^{2+} and Ca^{2+} binding to rat PAL. Residues involved in binding Zn^{2+} (H^{585}, H^{690} and H^{786} in rat PAM) are shown in purple, Ca^{2+} (V^{520}, L^{587} and D^{787} in rat PAM) in green and active site residues (R^{533}, Y^{654} and R^{706} in rat PAM) in cobalt. Cys residues are highlighted in red; pairs of basic amino acids are shown in bold Italics. The putative glycosylation sites in CrPAM occur after the PAL domain.

Fig S1

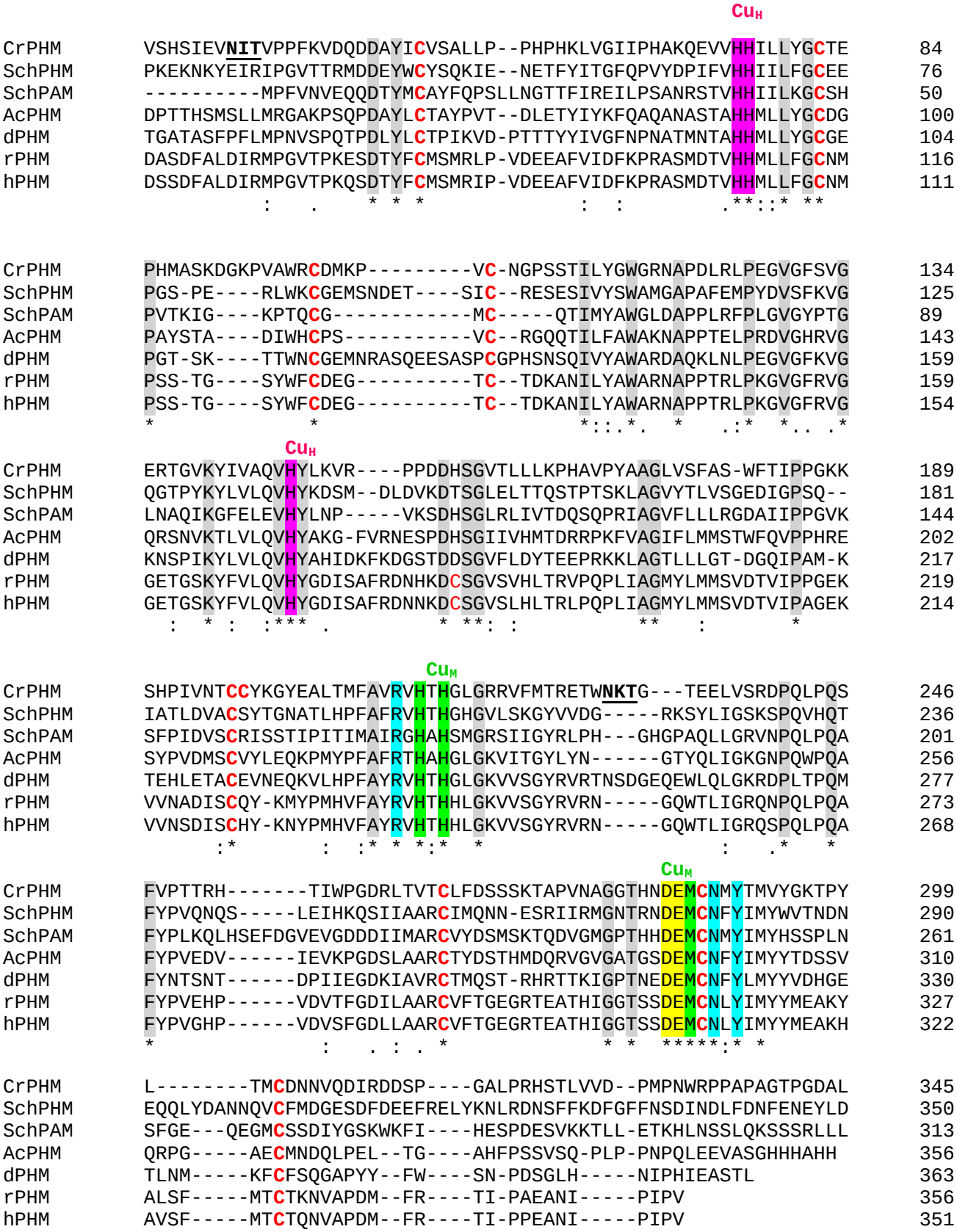
CuH
CrPHM VSHSIEVNITVPPFKVDQDDAYICVSALLP--PHPHKLVGIIPHAKQEVVHHILLYGCTE 84
SchPHM PKEKNKYEIRIPGVTTRMDDEYWCYSQKIE--NETFYITGFQPVYDPIFVHHIILFGCEE 76
SchPAM ----------MPFVNVEQQDTYMCAYFQPSLLNGTTFIREILPSANRSTVHHIILKGCSH 50
AcPHM DPTTHSMSLLMRGAKPSQPDAYLCTAYPVT--DLETYIYKFQAQANASTAHHMLLYGCDG 100
dPHM TGATASFPFLMPNVSPQTPDLYLCTPIKVD-PTTTYYIVGFNPNATMNTAHHMLLYGCGE 104
rPHM DASDFALDIRMPGVTPKESDTYFCMSMRLP-VDEEAFVIDFKPRASMDTVHHMLLFGCNM 116
hPHM DSSDFALDIRMPGVTPKQSDTYFCMSMRIP-VDEEAFVIDFKPRASMDTVHHMLLFGCNM 111
CrPHM PHMASKDGKPVAWRCDMKP---------VC-NGPSSTILYGWGRNAPDLRLPEGVGFSVG 134
SchPHM PGS-PE----RLWKCGEMSNDET----SIC--RESESIVYSWAMGAPAFEMPYDVSFKVG 125
SchPAM PVTKIG----KPTQCG-----------MC-----QTIMYAWGLDAPPLRFPLGVGYPTG 89
AcPHM PAYSTA----DIWHCPS----------VC--RGQQTILFAWAKNAPPTELPRDVGHRVG 143
dPHM PGT-SK----TTWNCGEMNRASQEESASPCGPHSNSQIVYAWARDAQKLNLPEGVGFKVG 159
rPHM PSS-TG----SYWFCDEG---------TC--TDKANILYAWARNAPPTRLPKGVGFRVG 159
hPHM PSS-TG----SYWFCDEG---------TC--TDKANILYAWARNAPPTRLPKGVGFRVG 154
CuH
CrPHM ERTGVKYIVAQVHYLKVR----PPDDHSGVTLLLKPHAVPYAAGLVSFAS-WFTIPPGKK 189
SchPHM QGTPYKYLVLQVHYKDSM--DLDVKDTSGLELTTQSTPTSKLAGVYTLVSGEDIGPSQ-- 181
SchPAM LNAQIKGFELEVHYLNP-----VKSDHSGLRLIVTDQSQPRIAGVFLLLRGDAIIPPGVK 144
AcPHM QRSNVKTLVLQVHYAKG-FVRNESPDHSGIIVHMTDRRPKFVAGIFLMMSTWFQVPPHRE 202
dPHM KNSPIKYLVLQVHYAHIDKFKDGSTDDSGVFLDYTEEPRKKLAGTLLLGT-DGQIPAM-K 217
rPHM GETGSKYFVLQVHYGDISAFRDNHKDCSGVSVHLTRVPQPLIAGMYLMMSVDTVIPPGEK 219
hPHM GETGSKYFVLQVHYGDISAFRDNNKDCSGVSLHLTRLPQPLIAGMYLMMSVDTVIPAGEK 214
CuM
CrPHM SHPIVNTCCYKGYEALTMFAVRVHTHGLGRRVFMTRETWNKTG---TEELVSRDPQLPQS 246
SchPHM IATLDVACSYTGNATLHPFAFRVHTHGHGVLSKGYVVDG-----RKSYLIGSKSPQVHQT 236
SchPAM SFPIDVSCRISSTIPITIMAIRGHAHSMGRSIIGYRLPH---GHGPAQLLGRVNPQLPQA 201
AcPHM SYPVDMSCVYLEQKPMYPFAFRTHAHGLGKVITGYLYN------GTYQLIGKGNPQWPQA 256
dPHM TEHLETACEVNEQKVLHPFAYRVHTHGLGKVVSGYRVRTNSDGEQEWLQLGKRDPLTPQM 277
rPHM VVNADISCQY-KMYPMHVFAYRVHTHHLGKVVSGYRVRN-----GQWTLIGRQNPQLPQA 273
hPHM VVNSDISCHY-KNYPMHVFAYRVHTHHLGKVVSGYRVRN-----GQWTLIGRQSPQLPQA 268
CuM
CrPHM FVPTTRH-------TIWPGDRLTVTCLFDSSSKTAPVNAGGTHNDEMCNMYTMVYGKTPY 299
SchPHM FYPVQNQS-----LEIHKQSIIAARCIMQNN-ESRIIRMGNTRNDEMCNFYIMYWVTNDN 290
SchPAM FYPLKQLHSEFDGVEVGDDDIIMARCVYDSMSKTQDVGMGPTHHDEMCNMYIMYHSSPLN 261
AcPHM FYPVEDV------IEVKPGDSLAARCTYDSTHMDQRVGVGATGSDEMCNFYIMYYTDSSV 310
dPHM FYNTSNT------DPIIEGDKIAVRCTMQST-RHRTTKIGPTNEDEMCNFYLMYYVDHGE 330
rPHM FYPVEHP------VDVTFGDILAARCVFTGEGRTEATHIGGTSSDEMCNLYIMYYMEAKY 327
hPHM FYPVGHP------VDVSFGDLLAARCVFTGEGRTEATHIGGTSSDEMCNLYIMYYMEAKH 322
CrPHM L--------TMCDNNVQDIRDDSP----GALPRHSTLVVD--PMPNWRPPAPAGTPGDAL 345
SchPHM EQQLYDANNQVCFMDGESDFDEEFRELYKNLRDNSFFKDFGFFNSDINDLFDNFENEYLD 350
SchPAM SFGE---QEGMCSSDIYGSKWKFI----HESPDESVKKTLL-ETKHLNSSLQKSSSRLLL 313
AcPHM QRPG-----AECMNDQLPEL--TG----AHFPSSVSQ-PLP-PNPQLEEVASGHHHAHH 356
dPHM TLNM-----KFCFSQGAPYY--FW----SN-PDSGLH-----NIPHIEASTL 363
rPHM ALSF-----MTCTKNVAPDM--FR----TI-PAEANI-----PIPV 356
hPHM AVSF-----MTCTQNVAPDM--FR----TI-PPEANI-----PIPV 351

Fig. S2

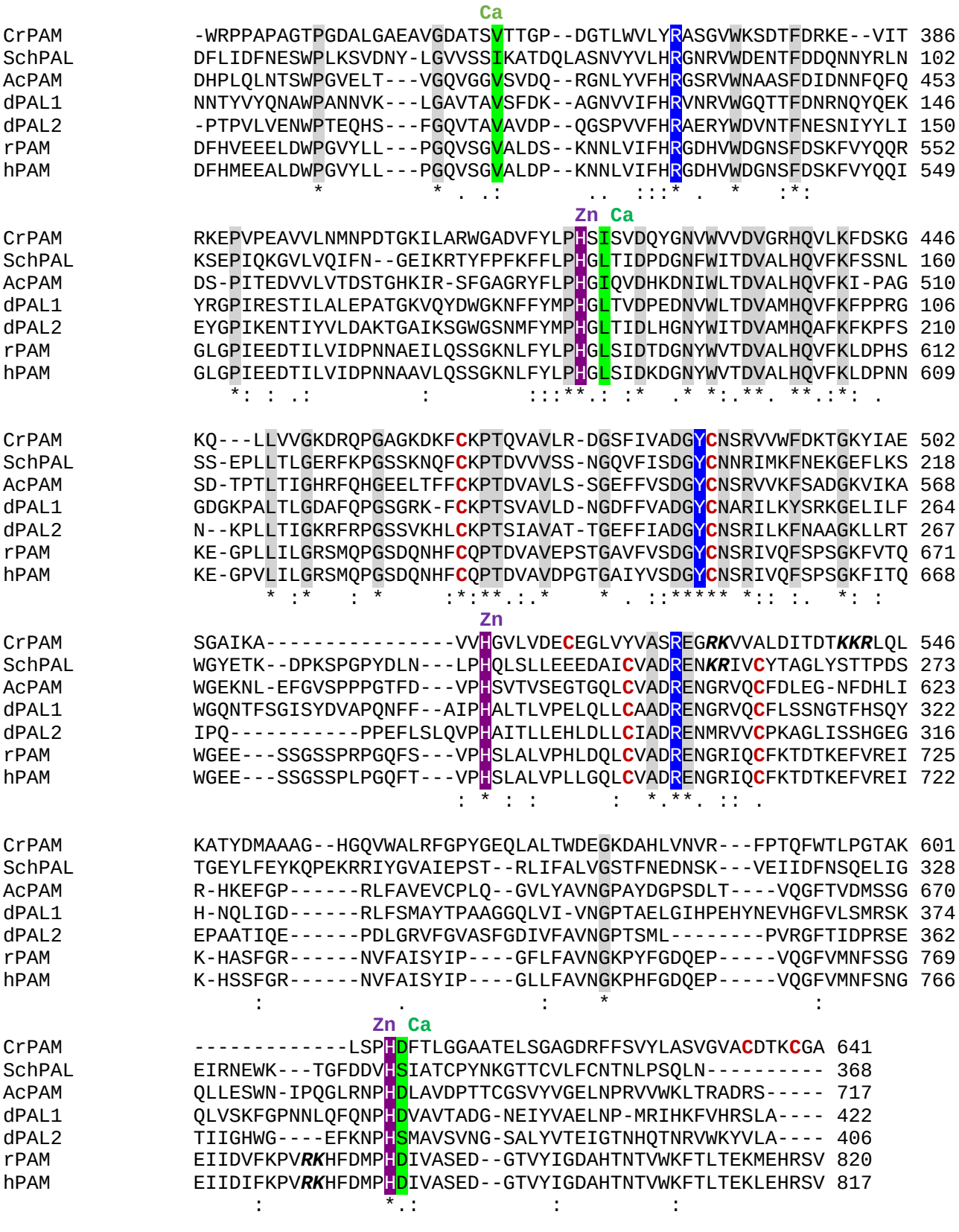
Ca
CrPAM -WRPPAPAGTPGDALGAEAVGDATSVTTGP--DGTLWVLYRASGVWKSDTFDRKE--VIT 386
SchPAL DFLIDFNESWPLKSVDNY-LGVVSSIKATDQLASNVYVLHRGNRVWDENTFDDQNNYRLN 102
AcPAM DHPLQLNTSWPGVELT---VGQVGGVSVDQ--RGNLYVFHRGSRVWNAASFDIDNNFQFQ 453
dPAL1 NNTYVYQNAWPANNVK---LGAVTAVSFDK--AGNVVIFHRVNRVWGQTTFDNRNQYQEK 146
dPAL2 -PTPVLVENWPTEQHS---FGQVTAVAVDP--QGSPVVFHRAERYWDVNTFNESNIYYLI 150
rPAM DFHVEEELDWPGVYLL---PGQVSGVALDS--KNNLVIFHRGDHVWDGNSFDSKFVYQQR 552
hPAM DFHMEEALDWPGVYLL---PGQVSGVALDP--KNNLVIFHRGDHVWDGNSFDSKFVYQQI 549
Zn Ca
CrPAM RKEPVPEAVVLNMNPDTGKILARWGADVFYLPHSISVDQYGNVWVVDVGRHQVLKFDSKG 446
SchPAL KSEPIQKGVLVQIFN--GEIKRTYFPFKFFLPHGLTIDPDGNFWITDVALHQVFKFSSNL 160
AcPAM DS-PITEDVVLVTDSTGHKIR-SFGAGRYFLPHGIQVDHKDNIWLTDVALHQVFKI-PAG 510
dPAL1 YRGPIRESTILALEPATGKVQYDWGKNFFYMPHGLTVDPEDNVWLTDVAMHQVFKFPPRG 106
dPAL2 EYGPIKENTIYVLDAKTGAIKSGWGSNMFYMPHGLTIDLHGNYWITDVAMHQAFKFKPFS 210
rPAM GLGPIEEDTILVIDPNNAEILQSSGKNLFYLPHGLSIDTDGNYWVTDVALHQVFKLDPHS 612
hPAM GLGPIEEDTILVIDPNNAAVLQSSGKNLFYLPHGLSIDKDGNYWVTDVALHQVFKLDPNN 609
CrPAM KQ---LLVVGKDRQPGAGKDKFCKPTQVAVLR-DGSFIVADGYCNSRVVWFDKTGKYIAE 502
SchPAL SS-EPLLTLGERFKPGSSKNQFCKPTDVVVSS-NGQVFISDGYCNNRIMKFNEKGEFLKS 218
AcPAM SD-TPTLTIGHRFQHGEELTFFCKPTDVAVLS-SGEFFVSDGYCNSRVVKFSADGKVIKA 568
dPAL1 GDGKPALTLGDAFQPGSGRK-FCKPTSVAVLD-NGDFFVADGYCNARILKYSRKGELILF 264
dPAL2 N--KPLLTIGKRFRPGSSVKHLCKPTSIAVAT-TGEFFIADGYCNSRILKFNAAGKLLRT 267
rPAM KE-GPLLILGRSMQPGSDQNHFCQPTDVAVEPSTGAVFVSDGYCNSRIVQFSPSGKFVTQ 671
hPAM KE-GPVLILGRSMQPGSDQNHFCQPTDVAVDPGTGAIYVSDGYCNSRIVQFSPSGKFITQ 668
Zn
CrPAM SGAIKA----------------VVHGVLVDECEGLVYVASREGRKVVALDITDTKKRLQL 546
SchPAL WGYETK--DPKSPGPYDLN---LPHQLSLLEEEDAICVADRENKRIVCYTAGLYSTTPDS 273
AcPAM WGEKNL-EFGVSPPPGTFD---VPHSVTVSEGTGQLCVADRENGRVQCFDLEG-NFDHLI 623
dPAL1 WGQNTFSGISYDVAPQNFF--AIPHALTLVPELQLLCAADRENGRVQCFLSSNGTFHSQY 322
dPAL2 IPQ-----------PPEFLSLQVPHAITLLEHLDLLCIADRENMRVVCPKAGLISSHGEG 316
rPAM WGEE---SSGSSPRPGQFS---VPHSLALVPHLDQLCVADRENGRIQCFKTDTKEFVREI 725
hPAM WGEE---SSGSSPLPGQFT---VPHSLALVPLLGQLCVADRENGRIQCFKTDTKEFVREI 722
Zn Ca
CrPAM KATYDMAAAG--HGQVWALRFGPYGEQLALTWDEGKDAHLVNVR---FPTQFWTLPGTAK 601
SchPAL TGEYLFEYKQPEKRRIYGVAIEPST--RLIFALVGSTFNEDNSK---VEIIDFNSQELIG 328
AcPAM R-HKEFGP------RLFAVEVCPLQ--GVLYAVNGPAYDGPSDLT----VQGFTVDMSSG 670
dPAL1 H-NQLIGD------RLFSMAYTPAAGGQLVI-VNGPTAELGIHPEHYNEVHGFVLSMRSK 374
dPAL2 EPAATIQE------PDLGRVFGVASFGDIVFAVNGPTSML--------PVRGFTIDPRSE 362
rPAM K-HASFGR------NVFAISYIP----GFLFAVNGKPYFGDQEP-----VQGFVMNFSSG 769
hPAM K-HSSFGR------NVFAISYIP----GLLFAVNGKPHFGDQEP-----VQGFVMNFSNG 766
CrPAM ------------LSPHDFTLGGAATELSGAGDRFFSVYLASVGVACDTKCGA 641
SchPAL EIRNEWK---TGFDDVHSIATCPYNKGTTCVLFCNTNLPSQLN---------- 368
AcPAM QLLESWN-IPQGLRNPHDLAVDPTTCGSVYVGELNPRVVWKLTRADRS----- 717
dPAL1 QLVSKFGPNNLQFQNPHDVAVTADG-NEIYVAELNP-MRIHKFVHRSLA---- 422
dPAL2 TIIGHWG----EFKNPHSMAVSVNG-SALYVTEIGTNHQTNRVWKYVLA---- 406
rPAM EIIDVFKPVRKHFDMPHDIVASED--GTVYIGDAHTNTVWKFTLTEKMEHRSV 820
hPAM EIIDIFKPVRKHFDMPHDIVASED--GTVYIGDAHTNTVWKFTLTEKLEHRSV 817

Table S1: Predicted *Chamydomonas reinhardtii* homologs of key human proteins known to be involved in prohormone processing. Gene identifiers from the Phytozyme website, molecular weights and percent identity to mammalian counterparts are shown.

Mammalian gene (human)	**Chlamydomonas gene(s)**	**MW Chlamy protein (kDa)**	**% identity Chlamy: mammal**
PCSK3=Furin PCSK1=PC1 PCSK2=PC2 PCSK4=PACE4	Cre04.g213400.t1.2 Cre09.g393350.t1.2 Cre01.g049950.t1.1 Cre16.g685300.t1.2	56 27 123 197	27.5 (part of furin) 27.2 (part of PC1) Sporangin=21.2 23.7
CTSH=hCT-H CTSL1=hCT-L1 CTSL2=hCT-L2	Cre01.g010832.t1.1 Cre07.g333000.t1.1 Cre08.g358522.t1.1 Cre09.g407700.t1.2 Cre05.g247851.t1.1	66 71 69 54 53	30.8-40.2 (for the 5 Chlamydomonas genes against the 3 target human genes)
CPE CPD	Cre07.g335900.t1.2 Cre06.g309450.t1.2	56 67	28.2-32.9 for CPE/D
ATP7A ATP7B	Cre16.g682369.t1.1 Cre09.g406400.t1.1	122 153	33.0-40.1 for A/B
VATA=V-ATPaseV1A	Cre10.g461050.t1.2	68	69.0
VPP1=V-ATPaseV0a	Cre04.g220350.t2.1 Cre09.g402500.t1.2 Cre11.g467705.t1.1	96 97 99	40.9-45.2
CYB561= Cytochrome b561	Cre06.g280100.t1.2	26	25.6

Table S2: Uniprot ID potential peptide processing enzymes in different species used in the construction of Fig. 1C.

Genome	query	UniProtKB ID (unless otherwise noted)	
Amphimedon queenslandica	furin	I1FG34	I1FG34_AMPQE
Amphimedon queenslandica	CPD	I1G9I1	I1G9I1_AMPQE
Arabidopsis thaliana	CPD	Q9M9H7	Q9M9H7_ARATH
Arabidopsis thaliana	PC1	Q0WUG6	SBT61_ARATH
Batrachochytrium dendrobatidis	furin	F4P3C2	F4P3C2_BATDJ
Batrachochytrium dendrobatidis	CPD	F4P5C4	F4P5C4_BATDJ
Caenorhabditis elegans	furin	O17798	FKPC1_CAEEL
Caenorhabditis elegans	PC2	G5ECN9	G5ECN9_CAEEL
Caenorhabditis elegans	PC1	P51559	BLI4_CAEEL
Caenorhabditis elegans	CPE	O17754	O17754_CAEEL
Caenorhabditis elegans	CPD	P91359	P91359_CAEEL
Cryptosporidium parvum	PC1	Q5CWJ3	Q5CWJ3_CRYPI
Cryptosporidium parvum	CPD	Q5CT20	Q5CT20_CRYPI
Cryptosporidium parvum	CPE	Q5CPT2	Q5CPT2_CRYPI
Danio rerio	CPD	E7F254	E7F254_DANRE
Danio rerio	CPE	Q6NSM5	Q6NSM5_DANRE
Danio rerio	furin	F1QKU2	F1QKU2_DANRE
Danio rerio	PC1	B6VCA1	B6VCA1_DANRE
Danio rerio	PC2	F1QWV9	F1QWV9_DANRE
Dictyostelium discoideum	CPD	Q54I77	Q54I77_DICDI
Dictyostelium discoideum	furin	Q55E86	Q55E86_DICDI
Dictyostelium discoideum	PC1	Q54SL5	Q54SL5_DICDI
Drosophila melanogaster	CPD	P42787	CPD_DROME
Drosophila melanogaster	furin	P26016	FUR11_DROME
Drosophila melanogaster	PC2	Q9VBC7	Q9VBC7_DROME
Giardia intestinalis	furin	E2RTR3	E2RTR3_GIAIC
Homo sapiens	Furin	P09958	FURIN_HUMAN
Homo sapiens	PC1	P29120	NEC1_HUMAN
Homo sapiens	PC2	P16519	NEC2_HUMAN
Homo sapiens	CPD	O75976	CBPD_HUMAN
Homo sapiens	CPE	P16870	CBPE_HUMAN
Mus musculus	CPD	O89001	CPD_MOUSE
Mus musculus	CPE	Q00493	CBPE_MOUSE
Mus musculus	furin	P23188	FURIN_MOUSE
Mus musculus	PC1	P63239	NEC1_MOUSE
Mus musculus	PC2	P21661	NEC2_MOUSE

Ostreococcus tauri	CPE	A0A090N476	A0A090N476_OSTTA
Phaeodactylum tricornutum	CPD	B7G3L4	B7G3L4_PHATC
Phaeodactylum tricornutum	furin	B7G7C6	B7G7C6_PHATC
Phaeodactylum tricornutum	PC2	B7G7A9	B7G7A9_PHATC
Physcomitrella patens subsp. patens	CPD	A9RL00	A9RL00_PHYPA
Physcomitrella patens subsp. patens	furin	A9U6I5	A9U6I5_PHYPA
Physcomitrella patens subsp. patens	PC2	A9U6C3	A9U6C3_PHYPA
Plasmodium falciparum	PC1	W7K4R7	W7K4R7_PLAFO
Saccharomyces cerevisiae	PC1	P13134	KEX2_YEAST
Saccharomyces cerevisiae	CPE	P38836	ECM14_YEAST
Selaginella moellendorffii	CPD	D8RFC7	D8RFC7_SELML
Strongylocentrotus purpuratus	PC2	W4Z6P7	W4Z6P7_STRPU
Strongylocentrotus purpuratus	PC1	W4XGU9	W4XGU9_STRPU
Strongylocentrotus purpuratus	CPD	W4YVC8	W4YVC8_STRPU
Strongylocentrotus purpuratus	CPE	W4XW74	W4XW74_STRPU
Tetrahymena thermophila	furin	I7MD46	I7MD46_TETTS
Tetrahymena thermophila	CPD	Q24GJ2	Q24GJ2_TETTS
Thalassiosira pseudonana	CPD	B8LEJ7	B8LEJ7_THAPS
Thalassiosira pseudonana	PC2	B5YMF0	B5YMF0_THAPS
Trichoplax adhaerens	furin	B3RSJ2	B3RSJ2_TRIAD
Trichoplax adhaerens	PC2	B3RSI8	B3RSI8_TRIAD
Trichoplax adhaerens	CPD	B3SAM1	B3SAM1_TRIAD
Trichoplax adhaerens	CPE	B3RVW8	B3RVW8_TRIAD
Ustilago maydis	furin	jgi|Ustma1|2843|UM02843	JGI
Chlamydomonas reinhardtii	furin	Cre04.g213400.t1.2	Phytozome
Chlamydomonas reinhardtii	CPE	Cre07.g335900.t1.2	Phytozome
Hydra vulgaris	furin	LOC100205483	Hydra DB
Hydra vulgaris	CPE	LOC100208105	Hydra DB
Hydra vulgaris	CBPD	LOC100213926	Hydra DB

Chapter 4

A Bioactive Peptide Amidating Enzyme Is Required for Ciliogenesis

Dhivya Kumar, Daniela Strenkert, Ramila S. Patel-King, Michael T. Leonard, Sabeeha S. Merchant, Richard E. Mains, Stephen M. King and Betty A. Eipper

This chapter was submitted for publication in eLife in its present form and is currently under review.

ABSTRACT

The pathways controlling cilium biogenesis in different cell types have not been fully elucidated. We recently identified peptidylglycine α-amidating monooxygenase (PAM), an enzyme required for generating amidated bioactive signaling peptides, in cilia of *Chlamydomonas* and mammalian cells. Here, we show that PAM is required for the normal assembly of motile and primary cilia in *Chlamydomonas*, planaria and mice. *Chlamydomonas* PAM knockdown lines failed to assemble cilia beyond the transition zone, had abnormal Golgi architecture and altered levels of cilia assembly components. Decreased PAM gene expression reduced motile ciliary density on the ventral surface of planaria and resulted in the appearance of cytosolic axonemes lacking a ciliary membrane. The architecture of primary cilia on neuroepithelial cells in $PAM^{-/-}$ mouse embryos was also aberrant. Our data suggest that alterations in post-Golgi trafficking contribute to the observed ciliogenesis defects and provide an unanticipated and highly conserved link between PAM, amidation and ciliary assembly.

INTRODUCTION

Cilia are ancient microtubule-based organelles derived from the basal body, and were present in the last eukaryotic common ancestor (Carvalho-Santos et al., 2011). The signaling potential of primary cilia and the added ability of motile cilia to generate propulsive force established them as key organelles required for the development and homeostasis of diverse cell types. The protein and lipid complements of the cilium are distinct from the rest of the cell; more than 700 proteins and specific lipids such as sterols are enriched in this intricate structure. Thus, the biogenesis and maintenance of these complex organelles is a tightly regulated cell type specific event (Hsiao et al., 2012; Nachury et al., 2010). Disruption of ciliogenesis or ciliary function leads to ciliopathies, a group of multisystemic diseases that have partially overlapping, often severe phenotypes, highlighting the importance of understanding these processes in different cells (Brown and Witman, 2014; Fliegauf et al., 2007; Waters and Beales, 2011).

The roles of microtubule motors and intraflagellar transport (IFT) proteins in trafficking the cargo proteins required to build and maintain ciliary architecture have been well described. The growing cilium also relies on the delivery of membrane vesicles and proteins derived from the Golgi and disruption of the secretory pathway by Brefeldin A inhibits ciliogenesis (Dentler, 2013; Haller and Fabry, 1998). Additionally, proteins and complexes involved in polarized vesicular trafficking such as the clathrin adaptor protein-1 complex (AP1), Rabs and Arf/Arl proteins, the exocyst and BBS complexes are critical for cilium biogenesis (Hsiao et al., 2012; Nachury et al., 2007; Zuo et al., 2009). The signaling processes coordinating these pathways and regulating ciliogenesis are poorly understood.

Peptidylglycine α-amidating monooxygenase (PAM), a secretory pathway-localized enzyme, catalyzes one of the final steps in the biosynthesis of many signaling peptides (Kumar et al., 2016b). PAM-catalyzed C-terminal amidation confers bioactivity to secreted peptides such as oxytocin, vasopressin and neuropeptide Y. The two enzymatic domains of PAM act sequentially

on glycine-extended peptide precursors. Peptidylglycine α-hydroxylating monooxygenase (PHM) catalyzes the copper and ascorbate dependent hydroxylation of the α-carbon of the terminal glycine, and peptidyl-α-hydroxyglycine α-amidating lyase (PAL) cleaves the N-C bond, generating glyoxylate and the α-amidated peptide. PAM is a type I integral membrane protein containing a cytosolic domain that is not essential for catalytic activity, but necessary for routing the enzyme through the secretory and endocytic pathways (Milgram et al., 1993).

Based on a phylogenetic study identifying PAM-like genes in green algal genomes, we recently demonstrated the presence of active enzyme in the unicellular eukaryote, *Chlamydomonas reinhardtii* (Attenborough et al., 2012; Kumar et al., 2016a). Despite the evolutionary distance between green algae and mammals, the biochemical properties of *C. reinhardtii* PAM (CrPAM) are remarkably similar to those of rat PAM. In both species, the full-length enzyme is membrane tethered, with its two catalytic domains, PHM and PAL, residing in the secretory pathway lumen. We also demonstrated that the catalytic domains of CrPAM can be separated from its transmembrane and cytosolic domains, leading to the generation of soluble bifunctional enzyme that can be secreted from cells (Kumar et al., 2016a).

The striking evolutionary co-occurrence of organisms containing PAM-like genes and cilia prompted us to explore PAM localization in *C. reinhardtii*, a premier reference organism for ciliary studies. Using an antibody recognizing the cytosolic domain of CrPAM, we localized the enzyme to the Golgi and to cilia (*aka* flagella). The ciliary localization of PAM was also observed in mammalian cells with motile or primary cilia (tracheal epithelial cells, fibroblasts, spermatozoa) (Kumar et al., 2016a). Furthermore, in *C. reinhardtii* cilia, PAM activity displayed an unexpected, strong biochemical association with the axonemal superstructure (Kumar et al., 2016a). Together, these observations in multiple cell types suggested that PAM has a novel and highly conserved signaling or sensory function in eukaryotic cilia. Here, we demonstrate that

PAM plays a key conserved role during the early steps of ciliogenesis, revealing a novel link between amidation and cilium assembly in multiple cell types.

RESULTS

Knockdown of PAM expression disrupts ciliogenesis in *C. reinhardtii*

To explore the function of PAM in *C. reinhardtii*, we designed an artificial microRNA (amiRNA) targeted to the 5' region of the CrPAM gene (Fig 1 A); expression was under control of the strong, constitutive promoter, HSP70A-RBSC2 (Molnar et al., 2009; Schroda et al., 2000). CrPAM protein expression was assessed by western blot analysis of whole cell lysates; seven transformants and two empty vector controls were chosen for further phenotypic analysis. Phase-contrast microscopy revealed that all seven knockdown strains were immotile and lacked cilia. Two strains (PAM-amiRNA # 3 and # 8) were selected for detailed analysis. Lysates of both strains contained reduced amounts of PAM protein (Fig 1 B). Enzyme assays showed reduced levels of PHM and PAL activity in both strains (Fig 1 C). Compared to empty vector transformed control strains, activity was reduced to about 30% and 10% in PAM-amiRNA #3 and #8, respectively.

We next used immunostaining for CrPAM and acetylated tubulin to compare PAM-amiRNA and empty vector *C. reinhardtii* cells. Images procured under similar exposure settings confirmed reduction of CrPAM levels in PAM-amiRNA strain #8 when compared to the empty vector control strain (Fig 1 D). As reported previously (Kumar et al., 2016a), most of the PAM protein localized to the Golgi (Fig 1 D), while a small fraction was present along the length of the cilia (inset in Fig 1 D) in the empty vector controls. Most strikingly, staining for acetylated tubulin confirmed the absence of cilia in both knockdown lines. Although cilia were robustly stained in control cells, only cell body microtubules were visible in the PAM-amiRNA cells (Fig 1 D). To explore the possibility of the formation of short ciliary stubs in the PAM-amiRNA mutants, we

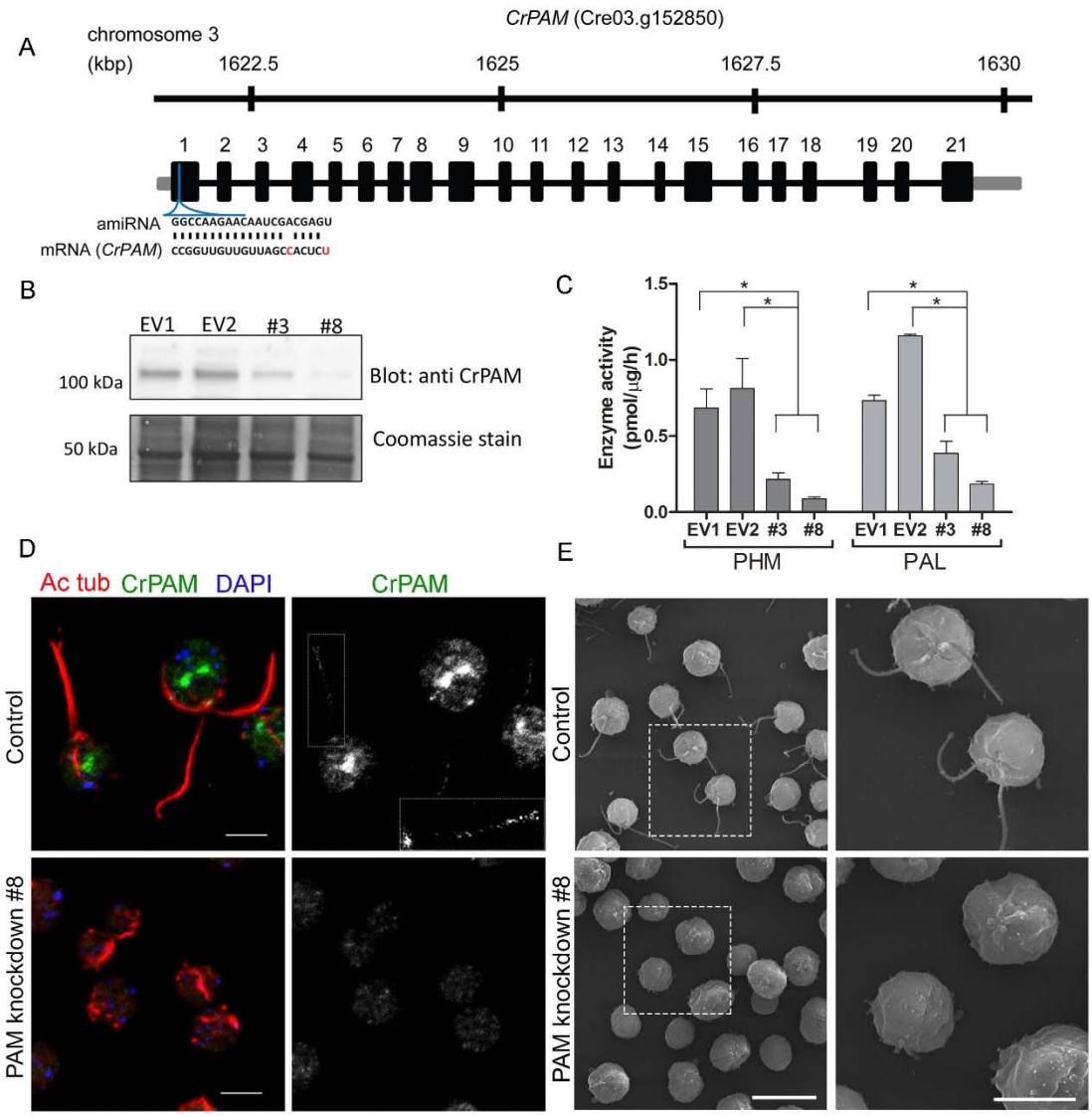

Fig 1. Knockdown of PAM disrupts ciliogenesis in *C. reinhardtii* (A) Schematic showing CrPAM (Cre03.g152850) gene structure and amiRNA target sequence at the 5' end of the CrPAM mRNA. 5'- and 3'-untranslated regions (gray bars), exons (numbered rectangles) and introns (black lines) drawn to scale. (B) Cell lysates prepared from control strains transformed with empty vector (EV1 and EV2) and knockdown strains transformed with the CrPAM amiRNA construct (#3 and #8) were subjected to western blot analysis using an antibody to the C-terminal domain of CrPAM. Top panel shows reduction of CrPAM band intensity (110 kDa) in the two knockdown strains. Coomassie staining of the membrane (bottom panel) shows equal loading. (C) PHM and PAL specific activities in cell lysates from triplicate assays (mean ± SD). Asterisks indicate $p < 0.05$ in a one-way Anova. (D) Immunofluorescence images of *C. reinhardtii* control and PAM amiRNA #8 cells stained with antibodies to acetylated tubulin (red) and CrPAM (green) acquired at equal exposure. Right panels show CrPAM staining in the cilium (inset) and Golgi, which is lost in knockdown cells. Acetylated tubulin staining shows loss of cilia; cortical microtubules are still visible in knockdown cells. Scale bar, 5 μm. (E) Scanning electron micrographs of control (top panels) and PAM amiRNA #8 cells (bottom panels) at low (left panels, scale bar, 10 μm) and high (right panels, scale bar, 5 μm) magnification.

utilized scanning electron microscopy. Most control cells had two cilia that were each ~10 μm in length. In contrast, cilia were never observed on cells of either knockdown strain; only short ciliary stubs were visible. PAM-amiRNA cells otherwise appeared morphologically normal in size and shape (Fig 1 E).

These results were consistent with a key role for PAM in regulating ciliogenesis in *C. reinhardtii* cells. The cytosolic domain of mammalian PAM is not required for enzyme activity, but controls its endocytic trafficking, and acts as a hub for various cytosolic protein interactions (Milgram et al., 1993; Prigge et al., 1997). To determine whether this PAM domain was required, we procured an insertional mutant from the indexed *C. reinhardtii* mutant library (Li et al., 2016a) in which the CrPAM cytosolic domain was disrupted. The *C. reinhardtii* insertional mutant obtained (CrPAM-ΔCD) encoded a protein lacking the final 73 residues of the 101-residue cytosolic domain of CrPAM; the first 28 residues of the cytosolic domain were followed by an 18 amino acid sequence derived from the insertion cassette (Fig 2 A). Lysates prepared from the CrPAM-ΔCD mutant strain exhibited significantly more PHM and PAL enzyme activity than the control CC4533 strain (Fig 2 B). As expected, antibody specific for the cytosolic domain of CrPAM failed to detect any cross-reactive protein in CrPAM-ΔCD lysates. Using a newly generated antibody to the luminal enzymatic domains of CrPAM, bands of the expected mass were detected in control and CrPAM-ΔCD lysates (Fig 2 C). Levels of CrPAM-ΔCD protein exceeded levels of CrPAM protein, perhaps reflecting its altered trafficking and turnover (Fig 2 B, C). The CrPAM-ΔCD cells were motile, with cilia that were similar in length to control cells (9.4 ± 0.2 μm for CC4533 and 9.5 ± 0.2 μm for CrPAM-ΔCD cells; $n > 80$ for each strain) (Fig 2 D). Transmission electron microscopy revealed no apparent ultrastructural defects in the cilia of CrPAM-ΔCD cells (Fig 2 E). The fact that CrPAM does not require an intact C-terminus in order to support ciliogenesis suggests that the catalytic cores may provide the essential ciliogenic factor.

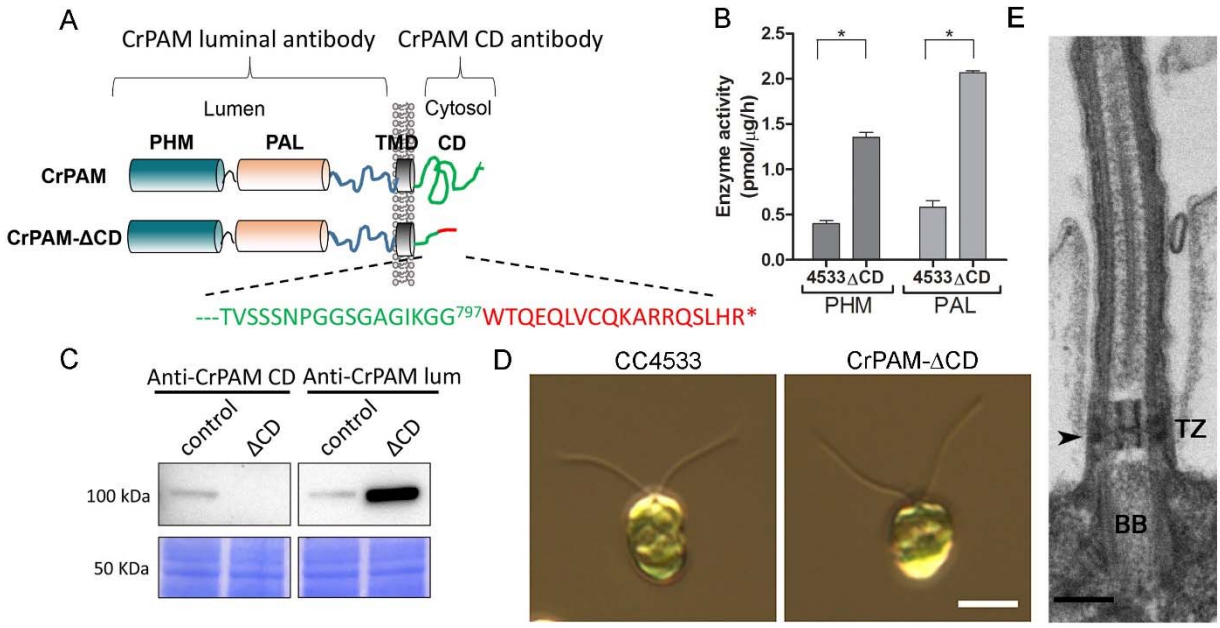

Fig 2. *C. reinhardtii* strain lacking the C-terminal domain of PAM assembles cilia (A) Schematic showing disruption of the cytosolic domain of CrPAM in the CrPAM-ΔCD strain. Residues corresponding to the C-terminus of CrPAM (green) and insertion cassette (red) are shown. (B) PHM and PAL specific activities in control (CC4533) and CrPAM-ΔCD strain lysates (mean ± SD). Both PHM and PAL activity increased in CrPAM-ΔCD cells ($p < 0.05$ using unpaired t-test). (C) Western blot of control and CrPAM-ΔCD strain lysates with C-terminal domain and luminal antibodies. As predicted by its sequence, CrPAM-ΔCD could be detected by the PAM luminal domain antibody, but not by the PAM cytosolic domain antibody. (D) Differential interference contrast images of control and CrPAM-ΔCD cells showing the presence of cilia in both (Scale bar, 5 μm). (E) Transmission electron micrograph showing normal ciliary structure in CrPAM-ΔCD strain. Basal body (BB), transition zone (TZ) and Y-linkers (arrowhead) appear normal (Scale bar, 200 nm).

C. reinhardtii PAM knockdown cells fail to assemble cilia beyond the transition zone

We next assessed the ultrastructural defects resulting from PAM deficiency in *C. reinhardtii* cells. Compared to the normal ciliary morphology observed in longitudinal sections of control cells (Fig 3 A), we observed only short ciliary stubs in PAM knockdown cells. The basal bodies appeared normal, however, we were unable to observe normal axonemal structures extending beyond the transition zone in these cells (Fig 3 B-E). Most of the short ciliary stubs seen in PAM knockdown cells contained accumulations of electron dense material; some also had randomly oriented fragments of microtubules (arrows in Fig 3 B and C). In both longitudinal and cross-sections, most features of the transition zone looked quite similar in PAM-deficient and control cells. Strikingly though, a deficit was apparent in the Y linkers of PAM-deficient cells. Wedge-shaped Y linkers, which connect the microtubules to the membrane and regulate protein entry into the cilium (arrowheads in Fig 3 A), were readily apparent in longitudinal sections through the transition zone of control cilia. However, we were unable to find Y linkers in the transition zones of PAM knockdown cells (Fig 3 B-D). Overall, the phenotypes observed in the PAM knockdown cells closely mirrored those previously reported for several IFT and transition zone mutants (Craige et al., 2010; Hou et al., 2007; Pazour et al., 2000).

PAM is necessary for ciliary motility in metazoans

To test whether this unexpected role for PAM in ciliogenesis was conserved in metazoans, we utilized RNAi mediated gene knockdown in the planarian *Schmidtea mediterranea*, which has a ciliated ventral epithelium used for gliding locomotion. The *S. mediterranea* genome encodes a bifunctional PAM protein with a transmembrane domain and cytosolic domain, a soluble PHM protein and a soluble PAL protein (Fig 4 A). To assess the role of bifunctional PAM and soluble PHM, we designed RNAi vectors targeted to each gene (Fig 4 A); soluble PAL, which would presumably function downstream of soluble PHM, was not targeted. Groups of planarians possessing a ciliated ventral epithelium were fed with bacteria containing either the empty

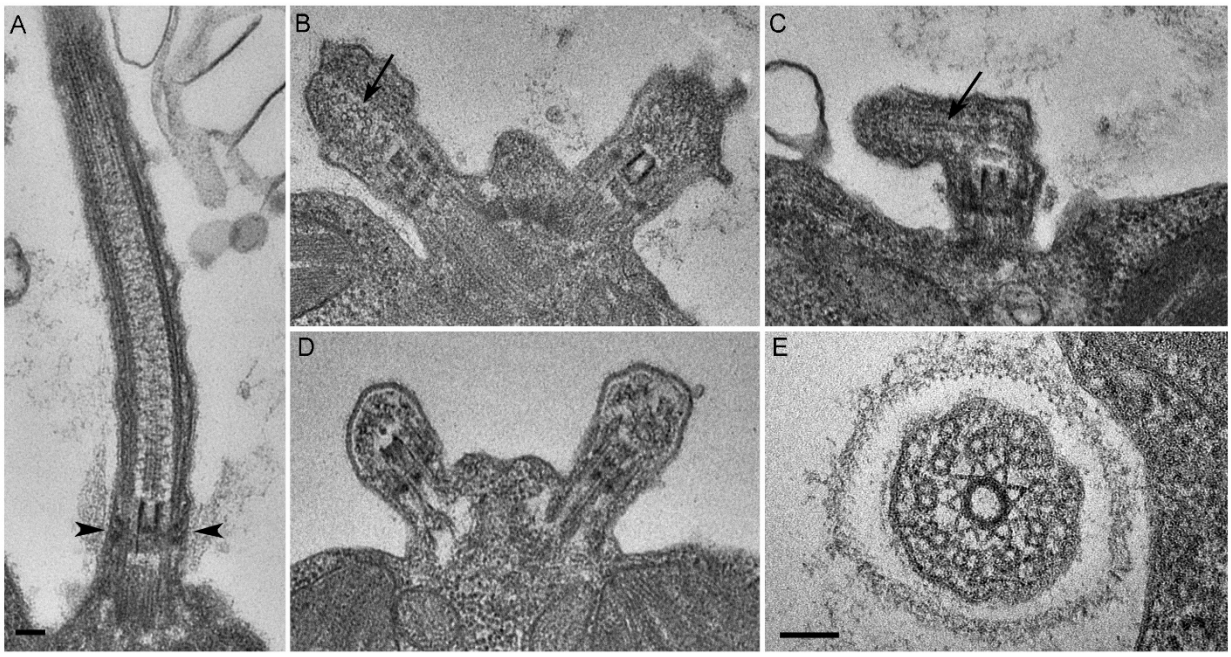

Fig 3. *C. reinhardtii* PAM knockdown cells fail to assemble cilia beyond the transition zone (A) Transmission electron micrograph of control cilium showing an ultrastructurally normal basal body, transition zone and axoneme. Wedge shaped Y linkers connecting the microtubules to the membrane in the transition zone are visible (arrowheads). (B-D) Examples of ciliary stubs seen in PAM knockdown cells. Longitudinal sections through the anterior portion of the cell show an ultrastructurally normal basal body, although Y linkers appeared to be disrupted. Electron dense material accumulated in the stubs (B, C and D) and microtubule fragments (arrows in B and C) were randomly oriented. (E) Cross-section of a transition zone from PAM amiRNA cell showed stellate centrin fibers and outer doublet microtubules surrounded by a ciliary membrane. Electron dense material fills the space between the microtubules and the membrane (Scale bar, 100 nm).

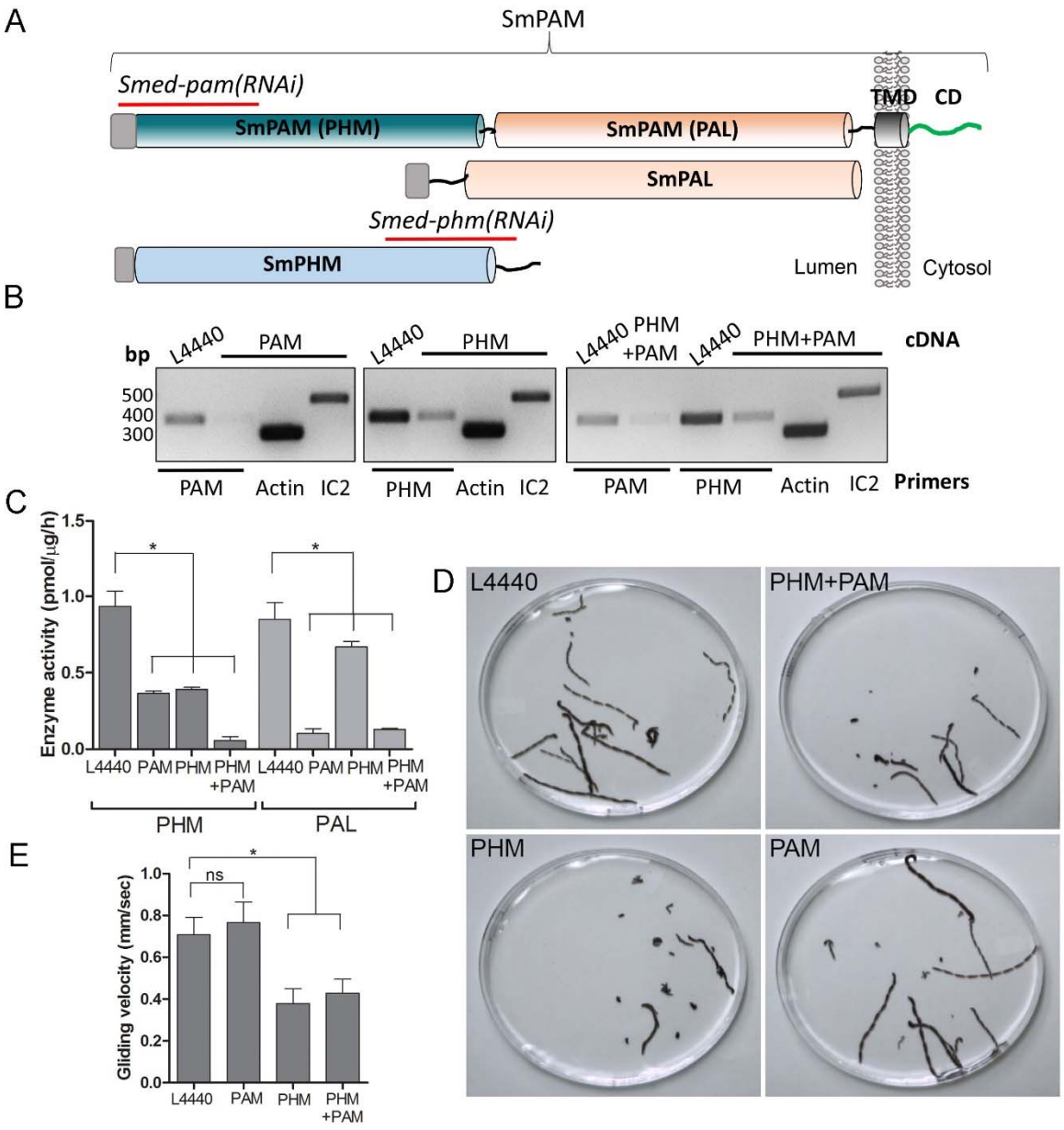

Fig 4. Knockdown of PHM gene in planaria causes motility defects (A) Schematic of *S. mediterrania* bifunctional PAM, monofunctional PAL and monofunctional PHM showing the regions used to generate RNAi constructs (red lines). Signal sequences, grey; transmembrane domain in SmPAM, black; cytosolic domain, CD. (B) RT-PCR analysis of mRNA from flatworms fed with the L4440, PAM, PHM or PHM+PAM dsRNA. The cDNA source is shown above the image, and the primer pairs used for RT-PCR are listed below the image. Actin and dynein IC2 primers were used as controls. (C) PHM and PAL specific activities in planarian lysates plotted as mean ± SD from triplicate assays (asterisks indicate $p < 0.05$ in a one-way Anova). (D) Overlays of frames from deconvolved videos of control and RNAi planaria showing the tracks taken over 60 seconds. (E) PHM and PHM+PAM RNAi animals displayed reduced gliding velocities plotted as mean± SEM compared to L4440 and PAM RNAi animals (asterisks indicate $p < 0.05$ in an unpaired t test).

vector control plasmid (L4440), the *Smed-phm(RNAi),* the *Smed-pam(RNAi)* or a mixture of bacterial cells expressing both the *Smed-phm* and *Smed-pam* RNAi vectors for three weeks. Gene expression was monitored using RT-PCR. Reductions in PAM and/or PHM mRNA were observed as expected in animals fed with *Smed-phm(RNAi)* or *Smed-pam(RNAi)* or a mixture of both; actin and outer arm dynein IC2 mRNA levels were unaltered (Fig 4 B). To monitor the success of our knockdown strategy, PHM and PAL enzyme activities were monitored in lysates. Both PHM and PAL activities were readily detected in L4440 lysates (Fig 4 C). PHM activity was reduced to ~40% in *Smed-pam(RNAi)* and *Smed-phm(RNAi)* animals (Fig 4 C). Knockdown of both *Smed-pam* and *Smed-phm* reduced PHM specific activity to less than 10% of control. As expected, PAL activity was reduced in lysates prepared from *Smed-pam* and the double knockdown animals, but not in *Smed-phm(RNAi)* planaria. Our results also show that most of the PAL enzyme activity was derived from the bifunctional enzyme (Fig 4 C).

Since cilia are required for gliding locomotion in *S. mediterranea*, we assessed motility using live video microscopy (Supplementary Video S1 and Fig 4 D). Compared to the controls, a greater percentage of animals were immotile. The *Smed-phm(RNAi)* planaria also exhibited more frequent reorientation of gliding direction compared to the other experimental and control groups (Fig 4 D). Interestingly, gliding velocity for *Smed-pam(RNAi)* animals was comparable to L4440 controls (≈ 0.7 mm/s), while gliding velocities for *Smed-phm(RNAi)* and the double knockdown animals were lower (≈ 0.4 mm/s) (Fig 4 E)., Planarians completely devoid of cilia move at velocities similar to those of the *Smed-phm(RNAi)* and *Smed-phm+pam(RNAi)* animals by using muscular contractions to propel their bodies forward (Rompolas et al., 2010). These results suggested that PHM activity was necessary for normal motility behavior in planarians.

To explore the defects in gliding behavior in RNAi-fed planarians, we used high frame-rate video microscopy to analyze ciliary beat frequency (CBF). As observed previously, cilia in L4440 control animals had a CBF of ≈ 26 Hz (Rompolas et al., 2010). In PHM and double knockdown

animals, CBF was decreased to ≈ 18 Hz and ≈ 17 Hz, respectively. The CBF in the *Smed-pam(RNAi)* knockdown animals was ≈ 30 Hz, consistent with the normal gliding velocity measured for this experimental group (Fig 4 E). The waveform of cilia in the double knockdown animals appeared to be dramatically different from control animals, with restricted motion compared to the highly coordinated smooth waveform of control cilia (Supplementary Video S2).

PAM is necessary for ciliogenesis in metazoans

We next assessed ciliary morphology in the groups of planarians fed with bacteria expressing dsRNA. Scanning electron microscopy revealed dense, tightly packed cilia covering the entire ventral surface of L4440 control animals (Fig 5 A). In stark contrast, knockdown of both PHM and PAM resulted in a severe reduction in ciliary density; planarian cilia undergo constant remodeling and ciliary loss is due to the failure of this process (Rompolas et al., 2010) (Fig 5 A). Flatworms receiving only *Smed-phm(RNAi)* or *Smed-pam(RNAi)* displayed intermediate phenotypes. Ciliary length was very heterogeneous in the RNAi-fed animals - short cilia were interspersed with cilia of normal length, presumably due to variations in the ciliary remodeling process (Fig 5 A). As loss of PHM activity alone resulted in a ciliogenesis defect in planaria, these results further underscore the potential role of amidating activity in this process.

Transmission electron microscopy also revealed pleomorphic defects resulting from the loss of PHM or both PHM and PAM in RNAi-fed planarians. In cross-sections, cilia with a normal 9+2 axonemal structure, containing outer and inner dynein arms, were observed in all samples (Fig 5 B-D). Occasionally, in the *Smed-phm(RNAi)* and *Smed-phm+pam(RNAi)* samples, the doublet microtubule organization was altered; singlet microtubules were sometimes observed along with doublet microtubules and in other cases the number of microtubules was aberrant (Fig 5 E, F). These aberrant axonemal structures are likely a secondary feature of defective remodeling; they may represent cilia in the process of failing.

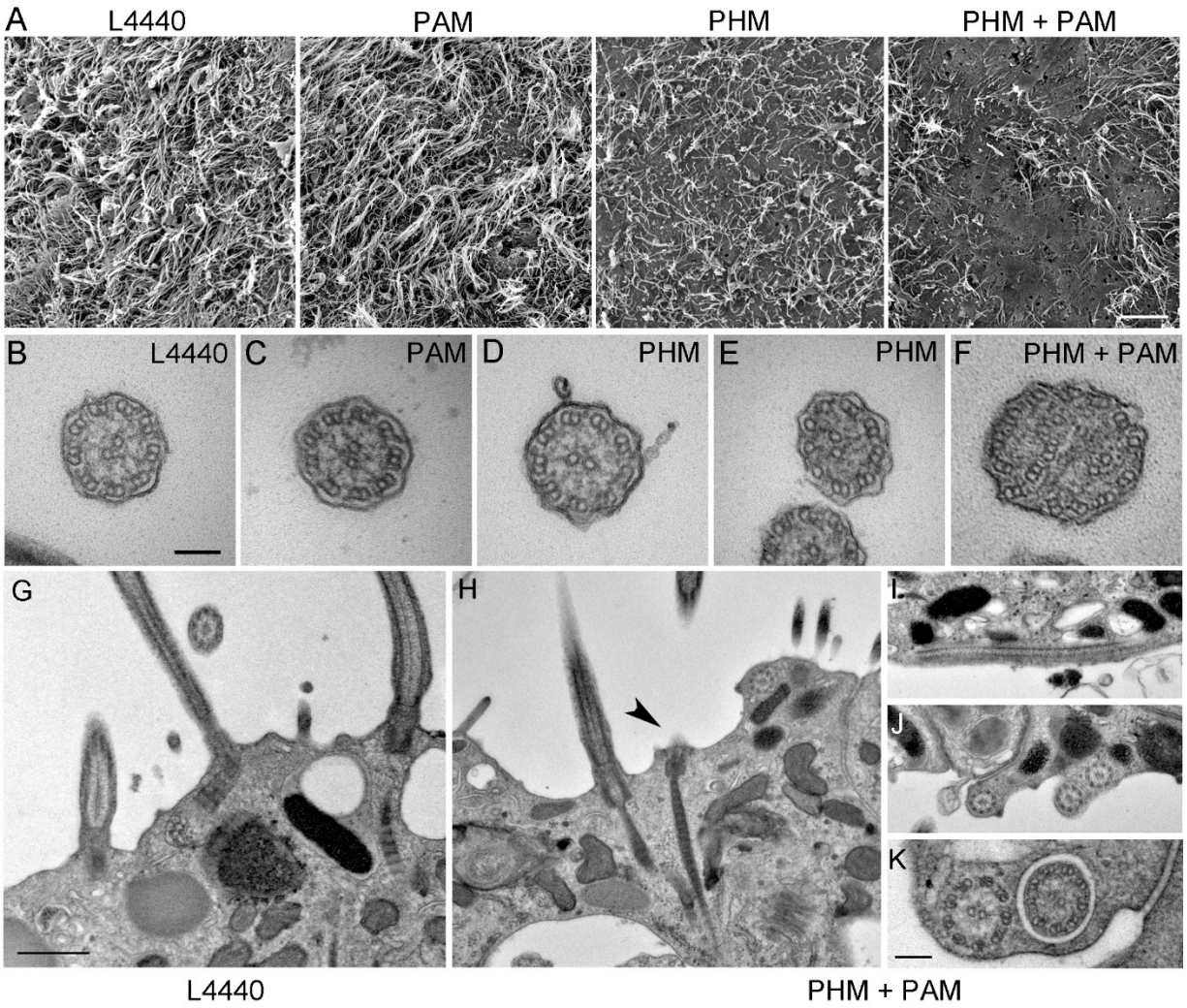

Fig 5. Ciliary morphology is affected in *Smed-phm(RNAi)* and *Smed-pam(RNAi)* planaria (A) Scanning electron micrographs of the ventral surface of an L4440-fed control planarian showed tightly packed cilia, while ciliary density was reduced in *Smed-phm(RNAi)* and *Smed-phm(RNAi)+Smed-pam(RNAi)* planaria; short ciliary stubs were visible on the ventral surface. *Smed-pam(RNAi)* animals displayed a modest, intermediate phenotype. Scale bar, 10 μm. (B-D) Transmission electron micrographs of ciliary cross sections showed normal 9+2 axonemal architecture in L4440, *Smed-pam(RNAi)* and *Smed-phm(RNAi)* planaria. (E-F) Singlet and doublet microtubules visible in the same plane in a *Smed-phm(RNAi)* cilium and abnormal, disorganized doublet microtubules in a *Smed-phm+pam(RNAi)* planarian cilium. Scale bar, 100 nm. (G) Transmission electron micrographs of ciliated ventral epithelium of L4440 and *Smed-phm+pam(RNAi)* (H-K) animals. Normal basal body docking and microtubule extension is visible in L4440; scale bar, 500 nm. In the double knockdowns, ciliary stubs (arrowhead, H) and numerous cytosolic axonemes were visible (H-K). (I) Longitudinal section of a cytosolic axoneme parallel to the plasma membrane. (J) Cytosolic axonemes cut in cross section and all oriented with their distal tips towards the head of the animal. (K) A cytosolic axoneme next to a cilium contained in a ciliary pocket (right). Scale bar, 250 nm. (arrowhead, Fig 5 H).

In *Smed*-L4440 control samples, basal bodies docked at the plasma membrane and cilia extended outward (Fig 5 G). Although similar structures were present in the *Smed-phm+pam(RNAi)* sections, about 50% of docked basal bodies had no cilia emanating from them. Furthermore, we repeatedly noticed the striking occurrence of morphologically normal axonemes in the cytoplasm of the double knockdown animals (n= 57 in *Smed-phm+pam(RNAi)* vs n=0 in control animals); these cytoplasmic axonemes were not surrounded by a membrane and were never observed in any of the other RNAi or L4440 control samples (Fig 5 H-K). Intriguingly, these mislocalized cytosolic axonemes appeared to have a normal 9+2 ultrastructure containing inner and outer dynein arms (Fig 5 K) and were in general oriented along the long axis of the animal with the axonemal distal tip towards the head. The ectopic localization of axonemes in the cytoplasm arising due to PAM deficiency suggests a defect in basal body docking and/or ciliary membrane trafficking.

PAM is required for primary cilia assembly in the developing neuroepithelium of mammals

Deletion of the *Pam* gene in mice results in embryonic lethality; embryos display massive pericardial edema and die by E14.5-E15.5 (Czyzyk et al., 2005). The cause and source of this edema in $PAM^{-/-}$ embryos is unclear, but zebrafish and rodent ciliary mutants display a similar edematous phenotype (Gorivodsky et al., 2009; Lee et al., 2015; Li et al., 2016b; Zhang et al., 2012). To determine if cilia were defective in $PAM^{-/-}$ mice, we analyzed the neuroepithelium of E12.5 wild-type and knockout littermates by scanning electron microscopy, as these cells each possess a singular, primary cilium (Louvi and Grove, 2011; Paridaen et al., 2015). As expected, we observed primary cilia emerging from ciliary pockets in epithelial cells in the lateral ventricular surface of wild type embryos. Cilia were also present in $PAM^{-/-}$ neuroepithelial cells, although their morphology appeared to differ from cilia in wild-type animals (Fig 6 A). Ciliary density was unaffected in the $PAM^{-/-}$ embryos (Fig 6 B). Transmission electron microscopy

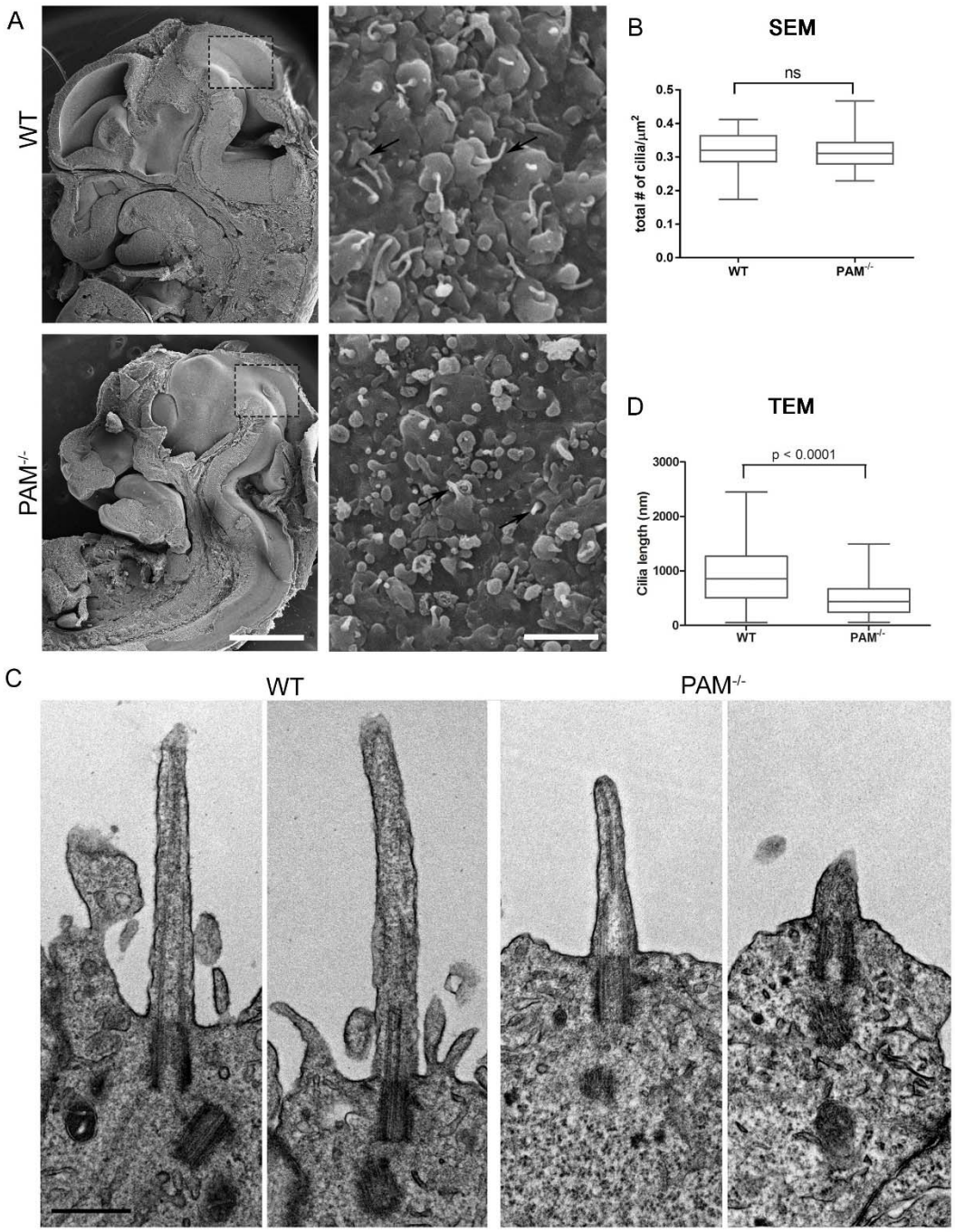

Fig 6. Primary cilia are shorter in PAM$^{-/-}$ neuroepithelial cells (A) Low magnification scanning electron micrographs of longitudinal sections through E12.5 WT and PAM$^{-/-}$ mouse embryos are on the left. Scale bar, 1 mm. The panels on the right show neuroepithelial cell cilia on the ventricular surface of WT and PAM$^{-/-}$ embryos. Scale bar, 2 µm. (B) Ciliary density (number of cilia/µm^2, measured from SEM images) was not significantly different between WT and PAM$^{-/-}$. (C) Representative transmission electron micrographs from E12.5 WT and PAM$^{-/-}$ mouse embryo neuroepithelium. Scale bar, 500 nm. (D) Cilia (measured from TEM images) were significantly shorter ($p<0.0001$, unpaired t-test) in the PAM$^{-/-}$ neuroepithelial cells (0.51±0.04 µm n=69) compared to WT cells (0.90±0.08 µm n=45).

confirmed the presence of stumpy cilia in the PAM$^{-/-}$ animals and allowed measurement of ciliary lengths (Fig 6 C and D) (0.51±0.04 μm n=69 in PAM$^{-/-}$ vs. 0.90±0.08 μm n=45 in WT). These combined data from three very different model organisms clearly reveal that PAM has a key and highly conserved role in ciliogenesis.

PAM deficiency affects trafficking and transition zone proteins in *C. reinhardtii*

We next used *C. reinhardtii* to evaluate the effect of loss of PAM on levels of key ciliary and membrane trafficking proteins. As demonstrated in Fig.1B, lysates prepared from PAM amiRNA lines #3 and #8 had reduced amounts of CrPAM. Although total α-tubulin levels were unaltered in PAM amiRNA cells, levels of acetylated tubulin and poly-glutamylated tubulin, modified forms present in cilia, were both significantly lower compared to control cell lysates (Fig 7 A, B).

To assess the impact of PAM deficiency on membrane trafficking, we assessed levels of Arf1, a Golgi-localized GTPase implicated in vesicular trafficking, and the vesicular coat protein, clathrin. Clathrin and AP1 have been implicated in ciliogenesis and targeting of cargo proteins to the cilium (Kaplan et al., 2010) and the μ1A subunit of AP1 interacts with the cytosolic domain of rat PAM (Bonnemaison et al., 2014). Arf1 levels were unchanged in lysates of PAM knockdown cells, while clathrin levels were increased compared to control lysates (Fig 7 C, D). This result suggested that membrane trafficking processes involving clathrin were affected in PAM amiRNA cells.

Our inability to observe Y linkers and the abnormal accumulation of microtubules and amorphous material in the short ciliary stubs seen in PAM amiRNA cells pointed to a dysfunctional transition zone; this zone regulates protein entry into the cilium and is essential for ciliogenesis (Fig 7 E). Levels of two transition zone components, CEP290 and NPHP4 (Awata et al., 2014) were monitored. Both PAM amiRNA strains contained greatly increased amounts of CEP290 and NPHP4 compared to controls (Fig 7 F, G). CEP290 is a component of the Y linkers

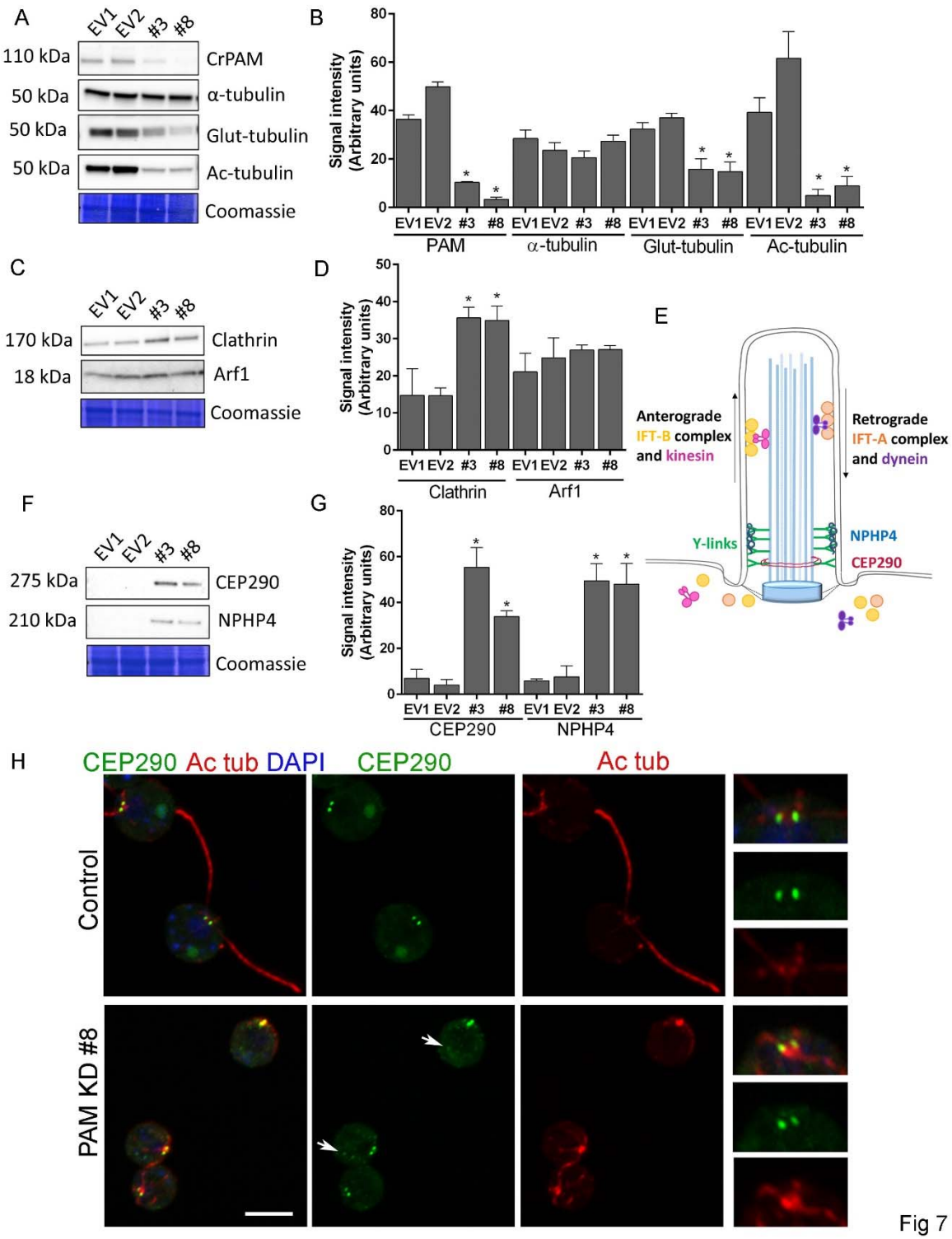

Fig 7

Fig 7. Knockdown of CrPAM alters levels and localization of transition zone proteins At least three lysates of EV1, EV2, #3 and #8 cells were subjected to western blot analysis. Representative blots and Coomassie-stained gels are shown (A, C, F); bar graphs indicate mean normalized intensity from all analyses +/- SEM (B, D, G). Statistical analysis was performed using one-way Anova. * indicates $p < 0.05$ for both EV strains vs both PAM amiRNA

strains. (A, B) Antibodies to CrPAM and modified forms of tubulin were used; acetylated and poly-glutamylated tubulin levels were lower in PAM amiRNA strains, but levels of □-tubulin were unchanged. (C, D) Antisera to clathrin heavy chain and Arf1 were used; PAM amiRNA strains had higher levels of clathrin heavy chain; Arf1 levels were not different. (E) Schematic of IFT and transition zone components in cilia. (F, G) Antisera to transition zone components CEP290 and NPHP4 were used; levels of both transition zone components were increased in PAM amiRNA mutant strains. (H) Maximum projection of optical sections of EV and PAM amiRNA *C. reinhardtii* cells labeled with antibodies to CEP290 (green) and acetylated tubulin (Ac tub, red). Merged images also show DAPI (blue), to locate the nucleus. Arrows point to CEP290 foci in the cell body. Enlargements at right show CEP290 localization at the base of cilia.

and *C. reinhardtii* CEP290 null mutants have short stumpy cilia (Craige et al., 2010) much like those observed in the PAM knockdown cells. NPHP4, a more distal component of the transition zone, is an essential part of the barrier at the ciliary base (Awata et al., 2014). It is possible that cells respond to an assembly defect caused by the reduced levels of CrPAM with a compensatory up-regulation of specific transition zone proteins. Interestingly, RNA-seq analysis revealed that the transcript abundance of these transition zone components was unchanged in PAM amiRNA cells (Table S1), pointing to a post-transcriptional regulatory response that alters CEP290 and NPHP4 protein levels in the absence of PAM.

To evaluate the localization of transition zone components in PAM amiRNA cells, we performed double labeling of cells with antibodies to CEP290 and acetylated tubulin. In control cells, punctate CEP290 staining was apparent at the base of each cilium (Fig 7 H upper panels, enlargements on right). In PAM amiRNA cells, the localization pattern of CEP290 remained unchanged in the basal body region which was identified by using antiserum to acetylated tubulin to locate the anterior portion of the cortical microtubules (Fig 7 H, lower panels). However, additional CEP290 immunoreactive puncta were visible in the cell body (Fig 7 H, arrows). These alterations in the levels of specific transition zone and membrane trafficking proteins, which are critical components of the ciliary assembly machinery, may contribute to the defects observed in PAM amiRNA *C. reinhardtii* cells.

PAM depletion alters levels and localization of IFT proteins in *C. reinhardtii*

Both ultrastructurally and phenotypically, loss of PAM closely paralleled loss of IFT proteins. In *Chlamydomonas*, the anterograde motor kinesin and IFT-B components ferry cargo to the tip of the cilium (Fig 7 E) (Hou et al., 2007; Hsiao et al., 2012; Pazour et al., 2000). Both RNA-seq analysis and immunoblotting showed that the levels of core anterograde IFT-B components such as IFT 46 and IFT 72/74 were unaltered in PAM knockdown cells (Table S1 and Fig 8A, B). Multiple bands observed with the IFT46 antibody may be due to a change in the

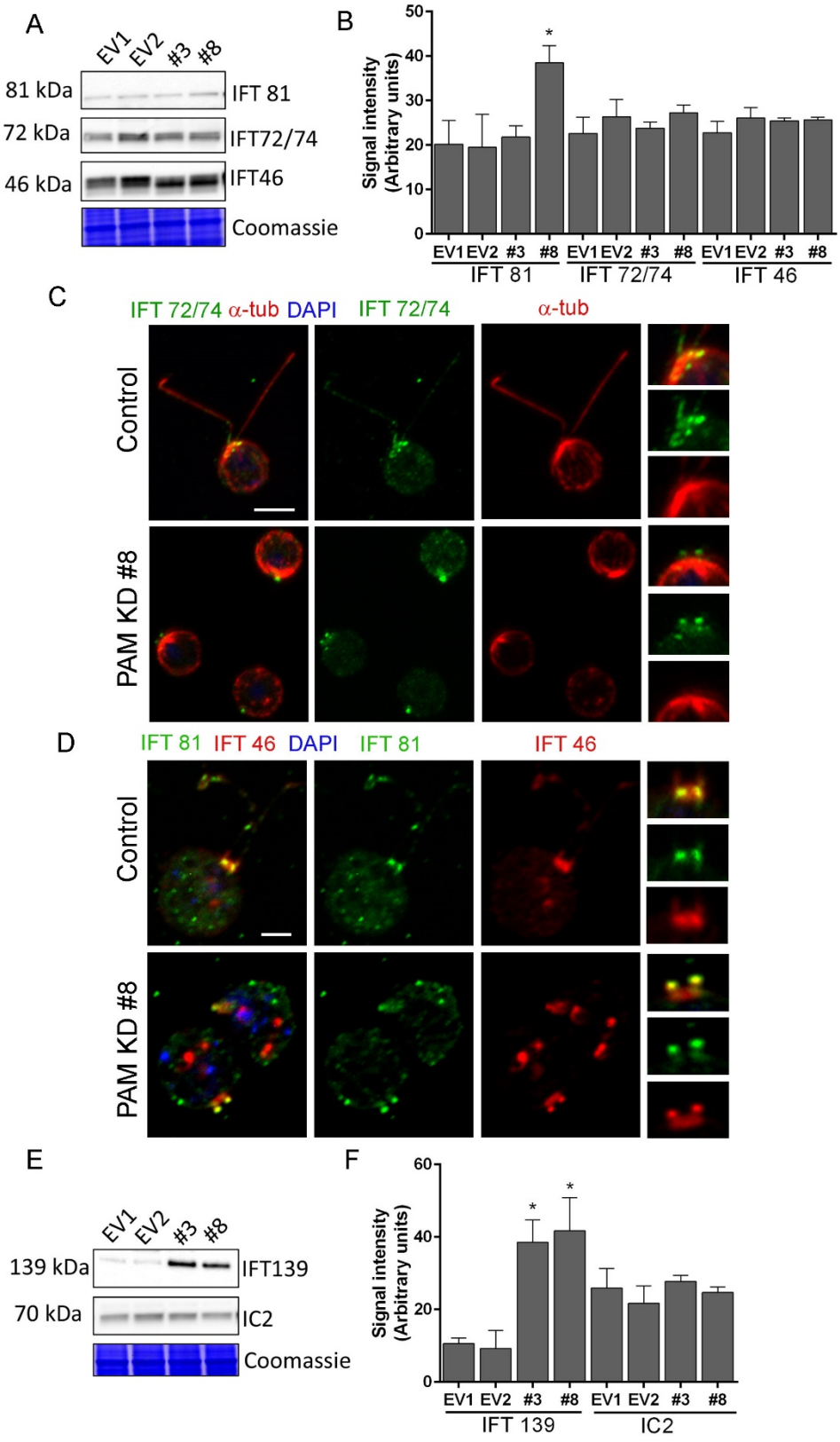

Fig 8. Knockdown of CrPAM alters levels and localization of selected IFT components. (A and B) *C. reinhardtii* EV and PAM amiRNA cell lysates immunoblotted with antibodies to IFT-B

components, IFT 81, IFT 72/74 and IFT 46 and quantified as described for Fig 7; levels of IFT 81 were increased in PAM amiRNA #8 strain compared to EV controls. Representative Coomassie-stained gels show equal loading. (C) In control cells, IFT 72/74 (green) was located at the base of the cilium (enlargement at right) and along its length (marked by antibodies to alpha-tubulin (red)). Images acquired at the same exposure settings showed IFT 72/74 in the ciliary stubs and decreased immunofluorescence in the peri-basal body region (enlargement at right) in PAM amiRNA cells. Scale bar, 5 μm. (D) *C. reinhardtii* control and PAM amiRNA #8 cells co-stained with antibodies to IFT 81 (green) and IFT 46 (red). Images acquired at similar exposure settings showed redistribution of both proteins into ciliary stubs in PAM amiRNA cells (enlargements at right) compared to predominantly peri-basal body localization in controls. (E and F) Representative western blot of a retrograde ciliary transport protein; levels of IFT-A component IFT 139, were higher in cell lysates from PAM amiRNA *C. reinhardtii* cells compared to EV control strains; axonemal outer arm dynein IC2 levels did not differ.

phosphorylation state of the protein as has been observed previously (Hou et al., 2007); phosphatase treatment suggests that its phosphorylation status was altered in PAM amiRNA cells. IFT 81 levels were increased in CrPAM amiRNA strain # 8 but not in strain # 3 (Fig 8 A, B). Since, strain # 8 had lower amounts of CrPAM than strain # 3 (Fig 7A, B), IFT 81 levels may be sensitive only to a severe deficiency in CrPAM.

IFT proteins normally display a punctate localization in the cilium and accumulate at its base, close to the basal body. Using antibodies to α-tubulin to mark the cilium, control cells exhibited the expected localization of IFT 72/74. In PAM amiRNA cells, IFT 72/74 staining was observed in the ciliary stubs (Fig 8 C, insets) and staining in the peri-basal body region was reduced. To determine if these changes in localization were specific to IFT 72/74, we double-labeled control and PAM amiRNA cells with antibodies to IFT 46 and IFT 81. Staining for IFT 46 and IFT 81 showed significant overlap in the basal body region and cilium in control cells. In the PAM amiRNA cells, both IFT components were mostly located in the short ciliary stubs and the amount in the basal body region was reduced (Fig 8 D). The abnormal accumulation of IFT components in the ciliary stubs may contribute to the increase in electron-dense amorphous material observed by electron microscopy (Fig. 3 B-D).

Strikingly, lysates of PAM amiRNA strains contained increased amounts of IFT-A component IFT 139 compared to control cell lysates (Fig 8 E, F). The retrograde IFT dynein motor works with IFT-A components to return proteins from the cilium to the cell body (Fig 7 E) (Hsiao et al., 2012). In *C. elegans,* loss of IFT 139 leads to formation of abnormal, short cilia (Niwa, 2016), and mutations in the human gene encoding IFT 139 (TTC21B) have been linked to nephronophthisis and thoracic dystrophy (Davis et al., 2011; Huynh Cong et al., 2014). Levels of axonemal outer arm dynein intermediate chain (IC2) were unchanged in PAM amiRNA cell lysates (Fig 8 E, F). Thus, changes in PAM levels affect specific components of the IFT

machinery. This compensatory increase occurs post-transcriptionally (Table S1) suggesting that there is no simple connection between the expression of known ciliary proteins and PAM.

PAM depletion affects post-Golgi trafficking in *C. reinhardtii* cells

CrPAM is largely localized to the Golgi region (Kumar et al., 2016a), which supplies the membrane proteins needed by the growing cilium. We next asked if PAM deficiency affected the ultrastructure of this organelle. Transmission electron microscopy revealed alterations in Golgi structure in PAM amiRNA strains #3 and #8 compared to two empty vector control strains (Fig 9 A). Although the area occupied by the Golgi, number of cisternae and Golgi width were not significantly different in PAM amiRNA cells (Fig 9 B, C, D), a significant difference in Golgi curvature was observed (Fig 9 E); Golgi stacks in the knockdown cells were more concave.

Starch grains, which are present in the chloroplast, accumulate when Golgi function is inhibited (Hummel et al., 2010). Since we observed ultrastructural changes in the Golgi complex and changes in clathrin levels, we examined plastid starch grains in PAM amiRNA and control cells by electron microscopy (arrows in Fig 10 A). Quantification revealed that starch grains occupied a larger fraction of the cell area in PAM knockdown cells compared to control cells; cell size did not differ (Fig 10 B, C). To determine whether this morphological change in starch grains correlated with an increase in starch content in the PAM amiRNA cells, we measured starch levels enzymatically and found no significant difference between the knockdown and control cells. Enlarged starch grains without a concomitant increase in starch levels were previously noted in vacuolar membrane protein-1 (VMP1) knockdown strains, which also displayed abnormal Golgi morphology (Tenenboim et al., 2014). These results suggest an impact of PAM knockdown on Golgi function.

To further assess alterations in Golgi function, empty vector and PAM amiRNA cells were cultured under nutrient deficiency conditions known to alter secretion of specific proteins. Iron

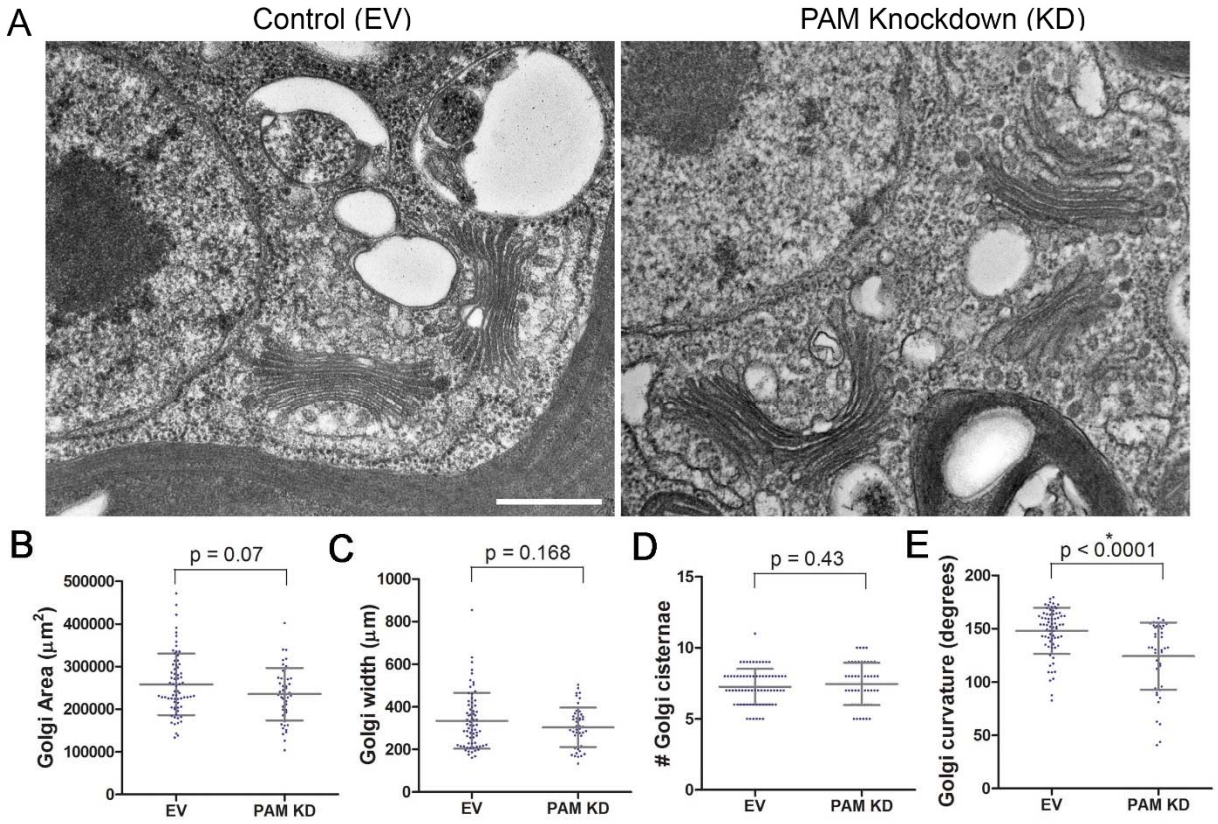

Fig 9. Golgi ultrastructure is altered in PAM amiRNA cells. (A) Transmission electron micrographs showing Golgi morphology in control and PAM amiRNA *C. reinhardtii* cells. Scale bar, 500 nm. Total area occupied by Golgi stacks (B), width of Golgi cisternae at the center of each stack (C) and number of Golgi cisternae (D) did not differ in PAM knockdown vs control cells. The degree of curvature of the Golgi cisternae from the center of the stack to the tip was significantly lower in PAM knockdown cells compared to controls (E). For all graphs, data were plotted as a scatter dot plot with mean ± SD values; unpaired t-test was used for statistical analysis in each case.

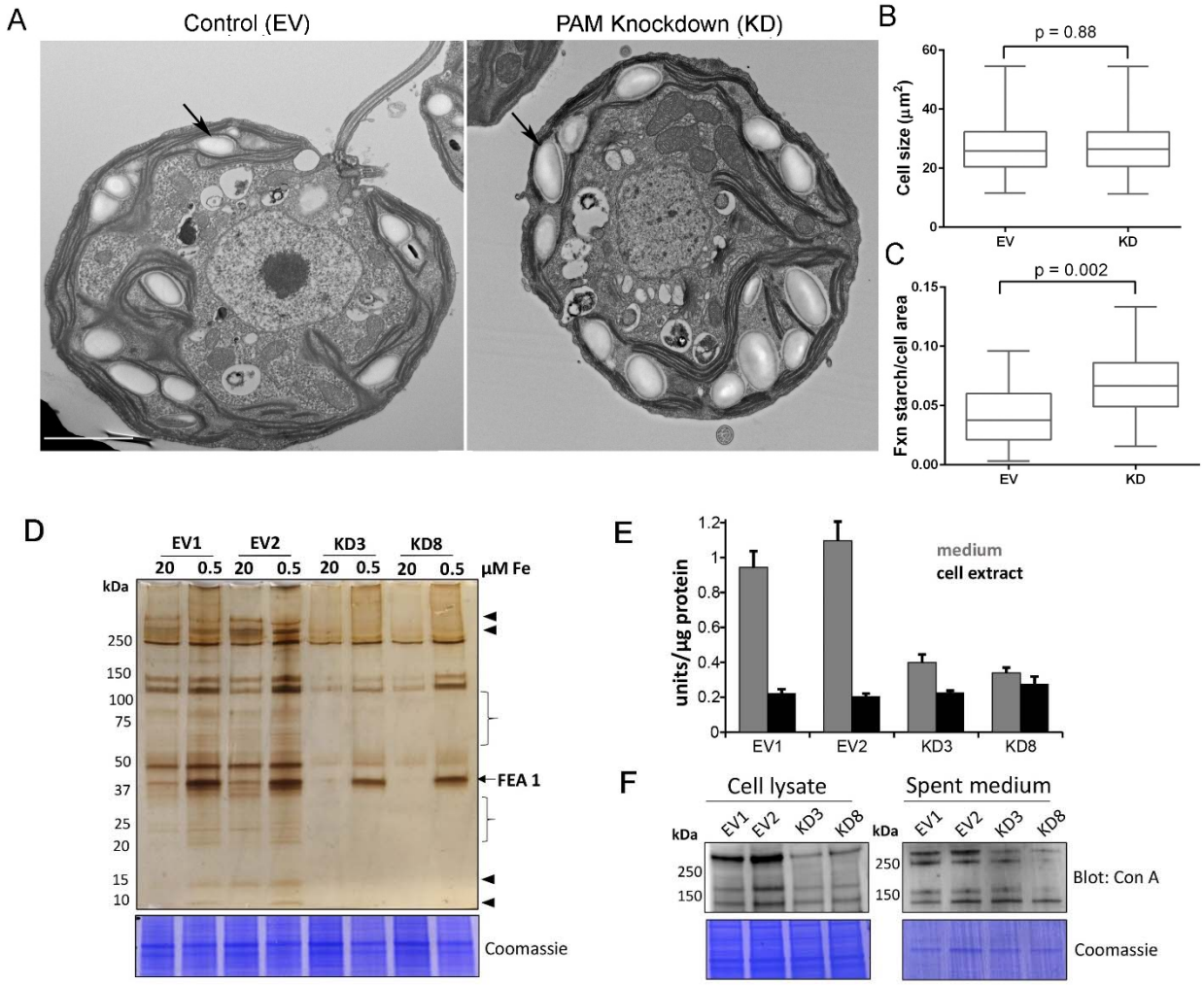

Fig 10. Golgi function is compromised in *C. reinhardtii* PAM knockdown cells. (A) Transmission electron micrographs showing enlarged starch grains in a representative PAM amiRNA cell compared to a control cell. Scale bar, 2 µm. (B) Control and PAM amiRNA cells did not differ in cell size (n>500 measurements from scanning electron micrographs) (C) Starch grains occupied a larger fraction of cell area in PAM amiRNA cells compared to controls (n ~ 20 measurements from TEM images). Unpaired t-test was used to analyze values in box and whisker plots. (D) Control and PAM amiRNA cells cultured in normal (20 µM Fe) and iron deficiency (0.5 µM Fe) conditions showed altered secretion of FEA1 and many other proteins (arrowheads and braces). For each strain, spent medium from an equal amount of total cell protein (verified by Coomassie staining of cell lysates) was analyzed by silver staining. (E) Alkaline phosphatase activity (units/µg cell protein) was assessed in cell lysates and spent media from two different phosphate deprived PAM amiRNA and control strains. 1 unit = 1 nmole/h. (F) Levels of glycosylated proteins detected by biotinylated-Concanavalin A (Con A) differ in cell lysates and concentrated spent media of control and PAM amiRNA cells (Coomassie stain shows equal loading).

deficiency conditions (0.5 μM vs 20 μM Fe) stimulate the secretion of FEA1, an iron concentrating protein (Allen et al., 2007). Spent medium normalized to equal cell protein was analyzed by silver staining. As expected, the 40 kDa FEA1 protein was readily detected in all strains under iron deficiency conditions (Fig 10 D). However, secretion of FEA1 was decreased in the PAM amiRNA strains compared to controls. Furthermore, there were striking differences in the secretome in PAM knockdown cells even under basal conditions (arrowheads and brackets, Fig 10 C). Surprisingly, FEA1 transcript levels were two-fold higher in PAM amiRNA cells than in controls, perhaps reflecting a compensatory measure (Table S1). We also assayed alkaline phosphatase, which is secreted by phosphate-deprived *C. reinhardtii* cells (Quisel et al., 1996). Although cellular alkaline phosphatase activity levels were indistinguishable, alkaline phosphatase secretion was greatly attenuated in both PAM amiRNA strains compared to both controls (Fig 10 E). Taken together, we conclude that the PAM amiRNA cells have a defective secretory pathway. To test whether the Golgi, which is a major site of protein glycosylation, is the affected step, we monitored glycosylation patterns in cell lysates and spent media of control and PAM amiRNA cells using the lectin concanavalin A. Equal amounts of protein from cell lysates of each strain and corresponding aliquots of media were separated by SDS-PAGE and visualized using biotinylated-concanavalin A. Levels of cross-reactive glycoproteins differed in PAM knockdown cells compared to controls (Fig 10 F). Together, our results suggest that altered Golgi function and post-Golgi trafficking contribute to ciliogenesis defects in PAM-deficient *C. reinhardtii* cells.

DISCUSSION

PAM plays a critical role in the assembly of motile and primary cilia

Our work has identified PAM as a crucial, evolutionarily conserved factor that is required for ciliogenesis in multiple cell types. PAM is important for the biogenesis of the motile cilia present in *C. reinhardtii* and on the ventral epithelium of planaria, as well as the normal assembly of the

primary cilia of neuroepithelial cells in mammals. In *C. reinhardtii* and planaria, reduction of PAM led to a dramatic loss of cilia, with assembly failing beyond the transition zone. In *C. reinhardtii*, the ciliary stubs contained amorphous electron dense material thought to consist of IFT particles and short pieces of microtubules at abnormal orientations (Fig 3 B-D). Although basal body docking and cell division were comparable to control cells, extension of the microtubules from the basal body was disrupted in PAM amiRNA cells. The defects observed in these strains phenocopied those reported previously for several IFT mutants, suggesting a role for PAM in protein trafficking to the cilium.

Analyzing the roles of the three PAM genes in planaria revealed additional complexities in the regulation of ciliogenesis (Fig 4). Planarians possessing a ciliated ventral epithelium progressively showed motility defects when PAM genes were silenced. Our RNAi analysis revealed a predominant role for PHM; knockdown of both soluble PHM and membrane PAM resulted in a more robust defect, suggesting roles for both PAM proteins in ciliogenesis (Fig 5 A). Reduction of PHM activity to very low levels by targeting both PHM and PAM led to the striking loss of motile cilia and the ectopic localization of fully assembled axonemes in the cytoplasm of cells in the ventral epithelium (Fig 5 H-K). Thus, along with extension of the microtubules from basal bodies docked at the plasma membrane, PAM activity may be important for proper docking of the ciliary vesicle and orienting the basal body. To our knowledge, this is the first report of ‘exposed’ axonemes in the cytoplasm of multiciliated cells in metazoans. A few studies reported the occurrence of microtubules in the cytoplasm in the absence of ciliary genes, but it is not clear that these microtubules formed an axonemal structure (Boisvieux-Ulrich et al., 1990; Burke et al., 2014; Park et al., 2006). The complete lack of a ciliary membrane around the apparently fully-assembled 9+2 axonemal structure raises the possibility that the supply of membrane to the growing cilium is a key limiting factor in the *Smed-phm+pam(RNAi)* animals.

While reduction of PAM in *C. reinhardtii* and planaria resulted in a dramatic defect in ciliary assembly, complete loss of PAM in mice did not abolish primary cilia formation in neuroepithelial cells, although they were significantly shorter than cilia in wild type animals and in many cases only ciliary stubs were evident (Fig 6). It is unknown if these short cilia are functional, but other mechanisms or factors may partially compensate for the loss of PAM in vertebrates or primary cilia.

Why does loss of PAM lead to closely related, yet pleomorphic defects in ciliogenesis in different organisms? The answer is unclear, but differences in the pathways utilized for assembling cilia in various cell types may contribute to the different phenotypes observed. Indeed, distinct cell- and organism- specific phenotypes have been observed when ciliary genes are mutated (Chaya et al., 2014; Lechtreck et al., 2008; Lechtreck and Witman, 2007). Multiciliated epithelial cells and *C. reinhardtii* cells utilize the extracellular pathway of ciliogenesis, where the basal body first docks at a distinct region of the plasma membrane and ciliary extension into the extracellular environment is a result of axonemal growth. In contrast, fibroblasts and neuroepithelial cells employ the intracellular pathway of ciliogenesis (Molla-Herman et al., 2010), where growth of the axoneme is initiated inside a ciliary vesicle in the cytoplasm. Docking of the ciliary vesicle subsequently leads to emergence of the cilium outward from the cell surface. These are key steps that would be most sensitive to defects in the post-Golgi trafficking of building blocks to the growing cilium.

PAM deficiency alters Golgi ultrastructure, function and post-Golgi trafficking

The Golgi serves as a sorting station for secretory pathway proteins and is the main site of PAM localization in *C. reinhardtii* and mammalian cells (Kumar et al., 2016a). The Golgi supplies membrane proteins required for ciliary expansion; vesicles carrying ciliary cargo must be assembled and trafficked to the growing ciliary base. Loss of PAM in *C. reinhardtii* altered Golgi architecture; Golgi stacks were more curved in PAM amiRNA cells than in control cells (Fig 10

A, E). Golgi morphology is affected by the cytoskeleton, Golgi matrix and mechanical and structural alterations to the Golgi are known to affect the formation of vesicles and tubules (Guet et al., 2014). In agreement with alterations in Golgi function, PAM amiRNA *C. reinhardtii* cells had enlarged starch grains, a response known to reflect defects in the secretory pathway and the trafficking of metabolic enzymes (Hummel et al., 2010). Protein glycosylation, a modification that occurs in the secretory pathway was also affected in the PAM amiRNA cells (Fig 10 F).

The primarily Golgi-localized AP1 complex, known to be important for bi-directional trafficking of proteins between endosomes, secretory granules and the trans-Golgi network, has also been implicated in the ciliary trafficking of proteins (Dwyer et al., 2001; Kaplan et al., 2010). The μ1A subunit of AP1 interacts with the cytosolic domain of PAM; reducing μ1A expression impairs the formation of mature, secretagogue-responsive secretory granules (Bonnemaison et al., 2014). Mature secretory vesicles lack clathrin; clathrin-coated vesicles bud from immature secretory granules, which are localized near the trans-Golgi network. Clathrin levels were almost double that of control cells in *C. reinhardtii* PAM amiRNA strains, again suggesting that vesicular trafficking is abnormal in these cells. Indeed, PAM amiRNA *C. reinhardtii* cells displayed several defects in protein secretion pointing to a dysfunctional Golgi and abnormal post-Golgi trafficking (Fig 10). Furthermore, the transcript abundance of a subset of Bardet Biedl syndrome (BBS) components was altered in the PAM amiRNA cells (Table S1); the BBSome is important for membrane protein trafficking to the cilium (Jin et al., 2010; Lechtreck et al., 2009; Nachury et al., 2007). Thus, alterations in post-Golgi trafficking to the cilium might contribute to defects in ciliogenesis in PAM-deficient cells.

Although the levels of most of the IFT proteins analyzed were unchanged, PAM amiRNA cells displayed a striking increase in the retrograde trafficking IFT-A component, IFT 139. IFT components normally assemble into IFT trains at the base of the cilium, displaying a peri-basal body distribution along with punctate staining in the cilium. In PAM amiRNA cells, several IFT-B

components accumulated in the ciliary stubs and staining at the base of the stubs was decreased, suggesting disrupted transition zone function. The transition zone at the proximal end of the cilium is a site of protein sorting and trafficking that is critical for ciliogenesis. Mutations in transition zone components lead to ciliopathies such as Meckel-Gruber and Joubert syndromes. We were unable to identify distinct Y linkers in our PAM amiRNA *C. reinhardtii* cells. Strikingly, although levels of transcripts encoding CEP290 and NPHP4 were unaltered in PAM amiRNA knockdown cells, levels of CEP290 protein, a component of the Y linkers and NPHP4 protein, a distal transition zone component, were elevated substantially. CEP290 still localized to the base of the cilium in PAM amiRNA cells, but additional foci of CEP290 staining were visible elsewhere in the cell. Together, our biochemical and ultrastructural data suggest that transition zone function is compromised in PAM amiRNA mutant cells. Post-transcriptional control mechanisms appear to play an important role in these responses. These changes in IFT and transition zone protein levels do not occur at the transcriptional level (Table S1), suggesting that there may not be a simple direct connection between the expression of known ciliary proteins and PAM. Post-transcriptional or protein stability changes that contribute to variations in the levels of these proteins in the absence of PAM need further investigation.

Possible mechanisms for the effects of PAM on ciliary assembly

The evolutionarily widespread occurrence of the PAM gene and the results presented here suggest that at least one of the ancestral and conserved roles of PAM is in ciliary assembly. The prevailing theory of ciliary evolution is that polarized trafficking of signaling proteins and receptors from the Golgi complex using coat proteins, such as IFT and COP proteins, gave rise to a plasma membrane sensory patch that ultimately gained a microtubule backbone (Carvalho-Santos et al., 2011; Jekely and Arendt, 2006). It is possible that PAM was included in the set of signaling proteins trafficked to the ciliary compartment from the Golgi in the ancestral eukaryote.

How might PAM regulate cilium biogenesis? Our working model, supported by this report and by previous studies in mammalian systems, is that PAM affects post-Golgi trafficking and controls vesicular transport to the cilium. The cytosolic domain of PAM, which plays an essential role in its trafficking through the secretory and endocytic pathways, is multiply phosphorylated and serves as a scaffold for interacting proteins such as Uhmk1, Kalirin, Trio and Rassf9. Uhmk1, a serine/threonine protein kinase with an RNA binding domain, phosphorylates the C-terminus of PAM. Kalirin and Trio, Rho guanine nucleotide exchange factors, activate Rac1 and RhoA, key regulators of the actin cytoskeleton; Rassf9 has been implicated in epidermal homeostasis (Caldwell et al., 1999; Lee et al., 2011; Steveson et al., 2001). The small pool of PAM located in the cilium may be essential for ciliogenesis. Identifying the domains/regions of PAM necessary for its localization to the cilium will be important to address this issue.

Given the recognized roles of PAM in membrane trafficking mediated by its cytosolic domain, a key question is whether it is PAM protein *per se* or its enzymatic (amidating) activity that is the key factor in ciliogenesis. Currently, two results point to a requirement for active PAM enzyme and an amidated product in ciliary assembly. First, *C. reinhardtii* CrPAM-ΔCD cells, with a PAM protein that lacks most of its C-terminal domain, are capable of assembling a cilium. Second, knockdown of the *Smed-phm* gene, which encodes soluble PHM, alters planarian cilium biogenesis; the bifunctional *Smed-pam* gene is unable to compensate for its loss. How might amidation influence cilium assembly? While a secreted, bioactive peptide product may act as a positive regulator of ciliogenesis, glycine-extended lipids are also PAM substrates (Merkler et al., 2004). The synthesis of oleamide, an amidated lipid, in a mouse neuroblastoma cell line was recently shown to require PAM; siRNA mediated knockdown of PAM resulted in accumulation of the N-acylglycine precursor (Jeffries et al., 2016). Amidated lipids produced by PAM could generate lipid sub-domains in the secretory pathway and serve to enrich secretory pathway

localized proteins into specialized vesicles. Thus, both amidation and membrane trafficking roles of PAM could contribute to ciliogenesis.

METHODS

C. reinhardtii Strains and Culture Conditions

A miRNA targeting *C. reinhardtii CrPAM* was designed according to (Molnar et al., 2009) using the WMD3 tool at http://wmd3.weigelworld.org/. Resulting oligonucleotides

PAMamiFor:

ctagtCCGGTTCTTGTTAGCTGCTCAtctcgctgatcggcaccatgggggtggtggtgatcagcgctaTGAGTGGC

TAACAAGAACCGGg;

PAMamiRev:

ctagcCCGGTTCTTGTTAGCCACTCAtagcgctgatcaccaccacccccatggtgccgatcagcgagaTGAGCA

GCTAACAAGAACCGGa (uppercase letters representing miRNA*/miRNA sequences) were annealed by boiling and slowly cooling-down in a thermocycler and ligated into SpeI-digested pChlamiRNA2 (Molnar et al., 2009), yielding pDS2. pDS2 was linearized by digestion with HindIII and transformed into *C. reinhardtii* strain CC-4351 cw15 mt+ by vortexing with glass beads (Kindle, 1990). The CC-4533 cw15 mt- control and CrPAM-ΔCD (LMJ.RY0402.20428) strains were procured from the indexed *C. reinhardtii* mutant library (Li et al., 2016a). Disruption of the C-terminal domain of CrPAM in CrPAM-ΔCD strain was verified by PCR using protocols described in (Li et al., 2016a). All strains where grown in TAP medium with revised trace elements (Special K) instead of Hutner´s trace elements according to (Kropat et al., 2011). The TAP medium was supplemented with 50 mg L^{-1} of arginine when required.

Planarian Culture Conditions, RNAi and Motility Assays

S. mediterranea were maintained in 1× solution of Montjuïc salts as described previously (Rompolas et al., 2009). Knockdown of PAM mediated by RNAi was accomplished by cloning 300 bp regions of *Smed-phm* (SMU15001346 in the SmedGD Genome database (Robb et al.,

2008)) and *Smed-pam* (SMU15006556) into the L4440 plasmid as described previously (Rompolas et al., 2013; Rompolas et al., 2009). Briefly, the constructs were transformed into HT115 (DE3) *E.coli* cells lacking RNase III to avoid degradation of dsRNA (Newmark et al., 2003). After induction of dsRNA with IPTG, bacterial pellets mixed with calf liver were fed to groups of planarians (~ 20 animals each set) twice a week. For knockdown of *Smed-phm+pam*, the bacterial pellets were mixed in a 1:1 ratio before feeding. Reduction of target gene mRNA expression was monitored 2-3 weeks post feeding by RT-PCR using the same primers used to generate the RNAi vectors.

Planarian gliding motility was monitored during week three by recording their movement over a 60-s period. Subsequent frames were superimposed from decompiled videos using Photoshop CS4 to calculate number of motile animals and their gliding velocity. Ciliary beating was visualized by placing live animals on coverslips with Vaseline/parafilm spacers using an Olympus BX51 microscope with DIC optics. Video segments captured using a high frame rate camera (X-PRI F1) were analyzed using Virtualdub and ImageJ software. Detailed procedures for these assays have been described previously (Rompolas et al., 2013; Rompolas et al., 2009).

Lysate Preparation and PAM Enzyme Assays

C. reinhardtii cells were collected by centrifugation at 2000 rpm for 5 min and resuspended in low ionic strength buffer (20 mM NaTES, 10 mM mannitol, pH 7.4, 1% Triton X-100) with 0.2 M NaCl, Roche protease inhibitor cocktail and PMSF. Cells were homogenized by two rounds of freeze thaw and sonication. Soluble fraction was collected by centrifugation at 9500 ×g for 2 minutes at 4°C. Protein concentration was estimated using the chlorophyll method as described in (Strenkert et al., 2016).

Whole body planarian lysates for enzyme assays were prepared by homogenizing animals in 20 mM NaTES, 10 mM mannitol, pH 7.4, 1% Triton X-100 buffer supplemented with a protease

inhibitor cocktail and PMSF. Lysates were subjected to two rounds of freeze-thaw, sonicated and tumbled at 4°C for 20 minutes. Soluble fractions were collected by centrifuging the samples at 17,000 ×g at 4°C for 20 minutes. BCA protein estimation reagents (Thermo Fisher Scientific) were used for determining protein concentration. PHM and PAL enzyme assays were carried out as previously described (Kolhekar et al., 1997). All enzyme assays were performed in triplicate and mean ± SD were plotted.

Antibodies

The antibodies used are listed in Table S2. Biotin-conjugated concanavalin A (Sigma-Aldrich) followed by avidin HRP (Pierce™, ThermoFisher Scientific) was used to detect glycosylated proteins. The antibody to the luminal enzymatic domains of CrPAM lacking the transmembrane and cytosolic domains was generated by expressing a cDNA corresponding to residues 1-687 followed by a rhodopsin epitope tag at the C-terminus in CHO-DG44 cells. The full length CrPAM construct generated previously (Kumar et al., 2016a) was used as a template for the PCR reaction. Stable cell lines secreting the soluble bifunctional enzyme were generated as described previously (Vishwanatha et al., 2014). Spent medium was collected from cells and the recombinant protein was concentrated by ammonium sulfate precipitation and a tangential crossflow concentrator (Vivaflow, Sartorius) (Chufan et al., 2009). Three rabbits (#314, 317 and 319, Covance) were immunized with CrPHM-PAL-rhod (0.5 mgs) and the resulting sera were affinity purified using NHS-Agarose (Thermo Scientific) conjugated to recombinant CrPHM-PAL protein.

Immunofluorescence

Immunostaining of *C. reinhardtii* cells with CrPAM antibody was performed as described in (Kumar et al., 2016a). For CEP290 and IFT antibodies, cells were allowed to adhere on 0.1% polyethylenimine-coated coverslips and fixed for 5 minutes with methanol at -20°C. Subsequent blocking and antibody incubation steps were done as described in (Craige et al., 2010). All

images were obtained with a Zeiss Axiovert 200M microscope with 63× and 100× oil objectives and AxioVision software. Maximum intensity projections of optical sections collected with the ApoTome module are shown.

Western Blotting and Quantification

Lysates (equal protein) were separated on 4-16% or 10-20% SDS-PAGE gels (BioRad) and transferred to PVDF membranes using standard methods. Samples were heated in Laemmli sample buffer at 55°C for five minutes prior to loading on gels. Immunoblots were visualized using the Syngene Pxi imaging system and band intensities were quantified using GeneTools software.

Scanning Electron Microscopy

C. reinhardtii samples - Cells were fixed in solution by adding equal volume of 5% glutaraldehyde (Electron Microscopy Sciences) in TAP medium for 15 minutes. Cells were collected by centrifugation and placed onto 0.1% polyethylenimine coated coverslips for 5 minutes. After removing non-adherent cells, the coverslips were incubated in 2.5% glutaraldehyde in 0.1M sodium cacaodylate, pH 7.2 for 45 minutes. Samples were dried in an Autosamdri-815 critical point dryer (Tousimis Research) and sputter coated before imaging in a JEOL JSM-5900LV scanning electron microscope. Cell sizes were quantified by manually tracing the outline of cells in Metamorph.

Mice – Tail clips taken from E12.5 embryos obtained after mating $PAM^{+/-}$ mice were used to determine the genotype; embryos were fixed in 2% glutaraldehyde in 1x PBS and tail clips were used to determine the genotype. Embryos were cut in half at the midline using a sharp scalpel in fixative and washed with 0.1M cadodylate buffer. Subsequent steps were performed essentially as described above for *C. reinhardtii* cells. Two pairs of WT and $PAM^{-/-}$ embryos were examined; ciliary density and length were manually measured for both sets using Metamorph. Representative plots from one of two experiments that gave similar results are shown.

Planarian samples - Animals were processed for SEM as described in (Rompolas et al., 2010).

Transmission Electron Microscopy

C. reinhardtii cells - Cells were fixed in suspension by mixing with an equal volume of 5% glutaraldehyde (Electron Microscopy Sciences) in TAP medium for 15 minutes. Cells were pelleted and resuspended in 2.5% glutaraldehyde in 0.1M sodium cacaodylate, pH 7.2 for 45 minutes. Fixed cells were washed in 0.1M sodium cacodylate buffer, osmicated with osmium ferricyanide, dehydrated through an ethanol series and embedded in Epon resin. Thin sections were post-stained with uranyl acetate and lead citrate and visualized in a Hitachi H-7650 transmission electron microscope at 80kV. Two sets of control and PAM amiRNA cells were examined; images were quantified manually using Metamorph. For measurement of Golgi curvature, lines were drawn from the edge of the middle stack to the center of the Golgi and the angle at the point of intersection was measured.

Planaria - Animals were processed for TEM as described in (Rompolas et al., 2010).

Mice - Tail clips were taken from E12.5 embryos obtained after mating $PAM^{+/-}$ mice and used to determine the genotype; embryos were fixed in 1% glutaraldehyde and 2% paraformaldehyde in 1x PBS overnight. The fixative was replaced with 1% glutaraldehyde in 0.1 M cacodylate buffer. Subsequent steps were performed essentially as described above for TEM analysis of *C. reinhardtii* cells. Two pairs of WT and $PAM^{-/-}$ embryos were examined for primary ciliary length measurements.

Starch measurements

Cells were concentrated by centrifugation of 15 ml of culture at 3,600 ×g for 10 min, cells were frozen in liquid nitrogen and stored at -80°C until further use. Starch was obtained from the cell pellet by ethanolic extraction as described in (Garz et al., 2012) with minor modifications. In brief, frozen cell pellet was resuspended twice in in 80% ethanol and heated to 95°C for 30

mins. After an additional washing step with 50% ethanol and 30 minutes at 95°C, starch pellets were incubated in 0.1M NaOH at 95°C for 30 minutes. Hydrolysis of starch was performed by adding HCl 0.5 M + acetate/NaOH 0.1 M pH 4.9 buffer. Cellular glucose levels contained in starch were determined using amyloglucosidase digestion and the Sigma glucose (HK) assay kit (Sigma-Aldrich, St. Louis, MO) according to the manufacturer's instructions.

Secretion experiments

Chlamydomonas cells were cultured under phosphate deficiency conditions for 24 h (Quisel et al., 1996); spent medium was centrifuged to remove cells and debris, followed by filtration using a 0.22 µm filter. A colorimetric substrate, p-nitrophenyl phosphate (PNPP) (Thermo Fisher Scientific), was used as described to determine alkaline phosphatase activity in cell homogenates and spent medium (Quisel et al., 1996). The extinction coefficient of PNPP at 410 nm in alkaline pH was used to determine alkaline phosphatase activity.

Chlamydomonas cells were cultured under iron deficiency conditions for 5 days as described previously (Allen et al., 2007; Glaesener et al., 2013). Spent medium was collected and processed as described above. Cell pellets were harvested for protein determination and medium corresponding to equal amount of cell protein was analyzed by SDS-PAGE followed by silver staining (SilverSNAP kit; Pierce).

RNA extraction, library preparation and RNA sequencing

2-4 x 10^7 cells were collected by centrifugation for 5 min at 1424 x g, 4°C. RNA was extracted using the Trizol reagent as described previously (Strenkert et al., 2011). DNase treatment was performed using Turbo DNAse (Ambion), concentrating and cleaning with the Zymo Research RNA Clean & Concentrator™-5 Kit according to the manufacturer's instructions. For RNA-Sequencing, RNA quality and quantity were determined using a Nanodrop 2000 instrument (Thermo Scientific) and a Bioanalyzer ChiP RNA 7500 series II (Agilent). A stranded Illumina

RNA-Seq library was prepared by the UCLA Clinical Microarray Core with standard Kapa RNAseq library preparation. Library quality control was performed with a Bioanalyzer Chip DNA 1000 series II (Agilent) and the libraries were quantified using Qubit. Libraries were sequenced on a HiSeq 1000 sequencer (Illumina) and single end 50-bp sequences were generated. Sequences were then aligned to the *C. reinhardtii* genome (v5.5) with RNA star. Relative expression estimates were generated using Cuffdiff 2.0.2.

ACKNOWLEDGEMENTS

We thank Maya Yankova (UCHC Electron Microscopy Facility), Andrew Yanik, Taylor LaRese and Ping Wang (UCHC Neuropeptide laboratory) for outstanding technical assistance. We also thank Dr. Branch Craige (UMass Medical School), Dr. Doug Cole (Washington State University) and Dr. Dennis Diener (Yale University) for sharing their antibodies, and Dr Crysten Blaby-Haas (Brookhaven National Laboratories) for helpful discussions. This work was supported by grants DK032949 (to BAE), GM051293 (to SMK) and GM042143 (to SSM) from the National Institutes of Health.

AUTHOR CONTRIBUTIONS

Daniela Strenkert generated the *Chlamydomonas* knockdown strains and performed the biochemical starch measurements in Sabeeha Merchant's laboratory. Ramila Patel-King generated the planaria RNAi lines. Betty Eipper and Richard Mains developed the CrPAM luminal antibody. Dhivya Kumar conducted the remaining experiments under the guidance of Betty Eipper, Richard Mains and Stephen King.

REFERENCES

Allen, M. D., del Campo, J. A., Kropat, J. and Merchant, S. S. (2007). FEA1, FEA2, and FRE1, encoding two homologous secreted proteins and a candidate ferrireductase, are expressed coordinately with FOX1 and FTR1 in iron-deficient *Chlamydomonas reinhardtii*. *Eukaryot Cell* **6**, 1841-1852.

Attenborough, R. M., Hayward, D. C., Kitahara, M. V., Miller, D. J. and Ball, E. E. (2012). A "neural" enzyme in nonbilaterian animals and algae: preneural origins for peptidylglycine alpha-amidating monooxygenase. *Mol Biol Evol* **29**, 3095-3109.

Awata, J., Takada, S., Standley, C., Lechtreck, K. F., Bellve, K. D., Pazour, G. J., Fogarty, K. E. and Witman, G. B. (2014). NPHP4 controls ciliary trafficking of membrane proteins and large soluble proteins at the transition zone. *J Cell Sci* **127**, 4714-4727.

Boisvieux-Ulrich, E., Laine, M. C. and Sandoz, D. (1990). Cytochalasin D inhibits basal body migration and ciliary elongation in quail oviduct epithelium. *Cell Tissue Res* **259**, 443-454.

Bonnemaison, M., Back, N., Lin, Y., Bonifacino, J. S., Mains, R. and Eipper, B. (2014). AP-1A controls secretory granule biogenesis and trafficking of membrane secretory granule proteins. *Traffic* **15**, 1099-1121.

Brown, J. M. and Witman, G. B. (2014). Cilia and Diseases. *Bioscience* **64**, 1126-1137.

Burke, M. C., Li, F. Q., Cyge, B., Arashiro, T., Brechbuhl, H. M., Chen, X., Siller, S. S., Weiss, M. A., O'Connell, C. B., Love, D. et al. (2014). Chibby promotes ciliary vesicle formation and basal body docking during airway cell differentiation. *J Cell Biol* **207**, 123-137.

Caldwell, B. D., Darlington, D. N., Penzes, P., Johnson, R. C., Eipper, B. A. and Mains, R. E. (1999). The novel kinase peptidylglycine alpha-amidating monooxygenase cytosolic interactor protein 2 interacts with the cytosolic routing determinants of the peptide processing enzyme peptidylglycine alpha-amidating monooxygenase. *J Biol Chem* **274**, 34646-34656.

Carvalho-Santos, Z., Azimzadeh, J., Pereira-Leal, J. B. and Bettencourt-Dias, M. (2011). Evolution: Tracing the origins of centrioles, cilia, and flagella. *J Cell Biol* **194**, 165-175.

Chaya, T., Omori, Y., Kuwahara, R. and Furukawa, T. (2014). ICK is essential for cell type-specific ciliogenesis and the regulation of ciliary transport. *EMBO J* **33**, 1227-1242.

Chufan, E. E., De, M., Eipper, B. A., Mains, R. E. and Amzel, L. M. (2009). Amidation of bioactive peptides: the structure of the lyase domain of the amidating enzyme. *Structure* **17**, 965-973.

Craige, B., Tsao, C. C., Diener, D. R., Hou, Y., Lechtreck, K. F., Rosenbaum, J. L. and Witman, G. B. (2010). CEP290 tethers flagellar transition zone microtubules to the membrane and regulates flagellar protein content. *J Cell Biol* **190**, 927-940.

Czyzyk, T. A., Ning, Y., Hsu, M. S., Peng, B., Mains, R. E., Eipper, B. A. and Pintar, J. E. (2005). Deletion of peptide amidation enzymatic activity leads to edema and embryonic lethality in the mouse. *Dev Biol* **287**, 301-313.

Davis, E. E., Zhang, Q., Liu, Q., Diplas, B. H., Davey, L. M., Hartley, J., Stoetzel, C., Szymanska, K., Ramaswami, G., Logan, C. V. et al. (2011). TTC21B contributes both causal and modifying alleles across the ciliopathy spectrum. *Nat Genet* **43**, 189-196.

Dentler, W. (2013). A role for the membrane in regulating *Chlamydomonas* flagellar length. *PLoS One* **8**, e53366.

Dwyer, N. D., Adler, C. E., Crump, J. G., L'Etoile, N. D. and Bargmann, C. I. (2001). Polarized dendritic transport and the AP-1 mu1 clathrin adaptor UNC-101 localize odorant receptors to olfactory cilia. *Neuron* **31**, 277-287.

Fliegauf, M., Benzing, T. and Omran, H. (2007). When cilia go bad: cilia defects and ciliopathies. *Nat Rev Mol Cell Biol* **8**, 880-893.

Garz, A., Sandmann, M., Rading, M., Ramm, S., Menzel, R. and Steup, M. (2012). Cell-to-cell diversity in a synchronized *Chlamydomonas* culture as revealed by single-cell analyses. *Biophys J* **103**, 1078-1086.
Glaesener, A. G., Merchant, S. S. and Blaby-Haas, C. E. (2013). Iron economy in Chlamydomonas reinhardtii. *Front Plant Sci* **4**, 337.
Gorivodsky, M., Mukhopadhyay, M., Wilsch-Braeuninger, M., Phillips, M., Teufel, A., Kim, C., Malik, N., Huttner, W. and Westphal, H. (2009). Intraflagellar transport protein 172 is essential for primary cilia formation and plays a vital role in patterning the mammalian brain. *Dev Biol* **325**, 24-32.
Guet, D., Mandal, K., Pinot, M., Hoffmann, J., Abidine, Y., Sigaut, W., Bardin, S., Schauer, K., Goud, B. and Manneville, J. B. (2014). Mechanical role of actin dynamics in the rheology of the Golgi complex and in Golgi-associated trafficking events. *Curr Biol* **24**, 1700-1711.
Haller, K. and Fabry, S. (1998). Brefeldin A affects synthesis and integrity of a eukaryotic flagellum. *Biochem Biophys Res Commun* **242**, 597-601.
Hou, Y., Qin, H., Follit, J. A., Pazour, G. J., Rosenbaum, J. L. and Witman, G. B. (2007). Functional analysis of an individual IFT protein: IFT46 is required for transport of outer dynein arms into flagella. *J Cell Biol* **176**, 653-665.
Hsiao, Y. C., Tuz, K. and Ferland, R. J. (2012). Trafficking in and to the primary cilium. *Cilia* **1**, 4.
Hummel, E., Osterrieder, A., Robinson, D. G. and Hawes, C. (2010). Inhibition of Golgi function causes plastid starch accumulation. *J Exp Bot* **61**, 2603-2614.
Huynh Cong, E., Bizet, A. A., Boyer, O., Woerner, S., Gribouval, O., Filhol, E., Arrondel, C., Thomas, S., Silbermann, F., Canaud, G. et al. (2014). A homozygous missense mutation in the ciliary gene TTC21B causes familial FSGS. *J Am Soc Nephrol* **25**, 2435-2443.
Jeffries, K. A., Dempsey, D. R., Farrell, E. K., Anderson, R. L., Garbade, G. J., Gurina, T. S., Gruhonjic, I., Gunderson, C. A. and Merkler, D. J. (2016). Glycine N-acyltransferase-like 3 is responsible for long-chain N-acylglycine formation in N18TG2 cells. *J Lipid Res* **57**, 781-790.
Jekely, G. and Arendt, D. (2006). Evolution of intraflagellar transport from coated vesicles and autogenous origin of the eukaryotic cilium. *Bioessays* **28**, 191-198.
Jin, H., White, S. R., Shida, T., Schulz, S., Aguiar, M., Gygi, S. P., Bazan, J. F. and Nachury, M. V. (2010). The conserved Bardet-Biedl syndrome proteins assemble a coat that traffics membrane proteins to cilia. *Cell* **141**, 1208-1219.
Kaplan, O. I., Molla-Herman, A., Cevik, S., Ghossoub, R., Kida, K., Kimura, Y., Jenkins, P., Martens, J. R., Setou, M., Benmerah, A. et al. (2010). The AP-1 clathrin adaptor facilitates cilium formation and functions with RAB-8 in *C. elegans* ciliary membrane transport. *J Cell Sci* **123**, 3966-3977.
Kindle, K. L. (1990). High-frequency nuclear transformation of *Chlamydomonas reinhardtii*. *Proc Natl Acad Sci U S A* **87**, 1228-1232.
Kolhekar, A. S., Mains, R. E. and Eipper, B. A. (1997). Peptidylglycine alpha-amidating monooxygenase: an ascorbate-requiring enzyme. *Methods Enzymol* **279**, 35-43.
Kropat, J., Hong-Hermesdorf, A., Casero, D., Ent, P., Castruita, M., Pellegrini, M., Merchant, S. S. and Malasarn, D. (2011). A revised mineral nutrient supplement increases biomass and growth rate in *Chlamydomonas reinhardtii*. *Plant J* **66**, 770-780.
Kumar, D., Mains, R. E. and Eipper, B. A. (2016). 60 YEARS OF POMC: From POMC and alpha-MSH to PAM, molecular oxygen, copper, and vitamin C. *J Mol Endocrinol* **56**, T63-76.
Kumar, D., Blaby-Haas, C. E., Merchant, S. S., Mains, R. E., King, S. M. and Eipper, B. A. (2016). Early eukaryotic origins for cilia-associated bioactive peptide-amidating activity. *J Cell Sci* **129**, 943-956.
Lechtreck, K. F. and Witman, G. B. (2007). *Chlamydomonas reinhardtii* hydin is a central pair protein required for flagellar motility. *J Cell Biol* **176**, 473-482.
Lechtreck, K. F., Delmotte, P., Robinson, M. L., Sanderson, M. J. and Witman, G. B. (2008). Mutations in Hydin impair ciliary motility in mice. *J Cell Biol* **180**, 633-643.

Lechtreck, K. F., Johnson, E. C., Sakai, T., Cochran, D., Ballif, B. A., Rush, J., Pazour, G. J., Ikebe, M. and Witman, G. B. (2009). The Chlamydomonas reinhardtii BBSome is an IFT cargo required for export of specific signaling proteins from flagella. *J Cell Biol* **187**, 1117-1132.
Lee, C. M., Yang, P., Chen, L. C., Chen, C. C., Wu, S. C., Cheng, H. Y. and Chang, Y. S. (2011). A novel role of RASSF9 in maintaining epidermal homeostasis. *PLoS One* **6**, e17867.
Lee, M. S., Hwang, K. S., Oh, H. W., Ji-Ae, K., Kim, H. T., Cho, H. S., Lee, J. J., Yeong Ko, J., Choi, J. H., Jeong, Y. M. et al. (2015). IFT46 plays an essential role in cilia development. *Dev Biol* **400**, 248-257.
Li, X., Zhang, R., Patena, W., Gang, S. S., Blum, S. R., Ivanova, N., Yue, R., Robertson, J. M., Lefebvre, P. A., Fitz-Gibbon, S. T. et al. (2016). An indexed, mapped mutant library enables reverse genetics studies of biological processes in *Chlamydomonas reinhardtii*. *Plant Cell* **28**, 367-387.
Li, Y., Yagi, H., Onuoha, E. O., Damerla, R. R., Francis, R., Furutani, Y., Tariq, M., King, S. M., Hendricks, G., Cui, C. et al. (2016). DNAH6 and Its Interactions with PCD Genes in Heterotaxy and Primary Ciliary Dyskinesia. *PLoS Genet* **12**, e1005821.
Louvi, A. and Grove, E. A. (2011). Cilia in the CNS: the quiet organelle claims center stage. *Neuron* **69**, 1046-1060.
Merkler, D. J., Chew, G. H., Gee, A. J., Merkler, K. A., Sorondo, J. P. and Johnson, M. E. (2004). Oleic acid derived metabolites in mouse neuroblastoma N18TG2 cells. *Biochemistry* **43**, 12667-12674.
Milgram, S. L., Mains, R. E. and Eipper, B. A. (1993). COOH-terminal signals mediate the trafficking of a peptide processing enzyme in endocrine cells. *J Cell Biol* **121**, 23-36.
Molla-Herman, A., Ghossoub, R., Blisnick, T., Meunier, A., Serres, C., Silbermann, F., Emmerson, C., Romeo, K., Bourdoncle, P., Schmitt, A. et al. (2010). The ciliary pocket: an endocytic membrane domain at the base of primary and motile cilia. *J Cell Sci* **123**, 1785-1795.
Molnar, A., Bassett, A., Thuenemann, E., Schwach, F., Karkare, S., Ossowski, S., Weigel, D. and Baulcombe, D. (2009). Highly specific gene silencing by artificial microRNAs in the unicellular alga Chlamydomonas reinhardtii. *Plant J* **58**, 165-174.
Nachury, M. V., Seeley, E. S. and Jin, H. (2010). Trafficking to the ciliary membrane: how to get across the periciliary diffusion barrier? *Annu Rev Cell Dev Biol* **26**, 59-87.
Nachury, M. V., Loktev, A. V., Zhang, Q., Westlake, C. J., Peranen, J., Merdes, A., Slusarski, D. C., Scheller, R. H., Bazan, J. F., Sheffield, V. C. et al. (2007). A core complex of BBS proteins cooperates with the GTPase Rab8 to promote ciliary membrane biogenesis. *Cell* **129**, 1201-1213.
Newmark, P. A., Reddien, P. W., Cebria, F. and Sanchez Alvarado, A. (2003). Ingestion of bacterially expressed double-stranded RNA inhibits gene expression in planarians. *Proc Natl Acad Sci U S A* **100 Suppl 1**, 11861-11865.
Niwa, S. (2016). The nephronophthisis-related gene ift-139 is required for ciliogenesis in *Caenorhabditis elegans*. *Sci Rep* **6**, 31544.
Paridaen, J. T., Huttner, W. B. and Wilsch-Brauninger, M. (2015). Analysis of primary cilia in the developing mouse brain. *Methods Cell Biol* **127**, 93-129.
Park, T. J., Haigo, S. L. and Wallingford, J. B. (2006). Ciliogenesis defects in embryos lacking inturned or fuzzy function are associated with failure of planar cell polarity and Hedgehog signaling. *Nat Genet* **38**, 303-311.
Pazour, G. J., Dickert, B. L., Vucica, Y., Seeley, E. S., Rosenbaum, J. L., Witman, G. B. and Cole, D. G. (2000). *Chlamydomonas* IFT88 and its mouse homologue, polycystic kidney disease gene tg737, are required for assembly of cilia and flagella. *J Cell Biol* **151**, 709-718.
Prigge, S. T., Kolhekar, A. S., Eipper, B. A., Mains, R. E. and Amzel, L. M. (1997). Amidation of bioactive peptides: the structure of peptidylglycine alpha-hydroxylating monooxygenase. *Science* **278**, 1300-1305.
Quisel, J. D., Wykoff, D. D. and Grossman, A. R. (1996). Biochemical characterization of the extracellular phosphatases produced by phosphorus-deprived *Chlamydomonas reinhardtii*. *Plant Physiol* **111**, 839-848.

Robb, S. M., Ross, E. and Sanchez Alvarado, A. (2008). SmedGD: the *Schmidtea mediterranea* genome database. *Nucleic Acids Res* **36**, D599-606.
Rompolas, P., Patel-King, R. S. and King, S. M. (2009). *Schmidtea mediterranea*: a model system for analysis of motile cilia. *Methods Cell Biol* **93**, 81-98.
Rompolas, P., Patel-King, R. S. and King, S. M. (2010). An outer arm dynein conformational switch is required for metachronal synchrony of motile cilia in planaria. *Mol Biol Cell* **21**, 3669-3679.
Rompolas, P., Azimzadeh, J., Marshall, W. F. and King, S. M. (2013). Analysis of ciliary assembly and function in planaria. *Methods Enzymol* **525**, 245-264.
Schroda, M., Blocker, D. and Beck, C. F. (2000). The HSP70A promoter as a tool for the improved expression of transgenes in *Chlamydomonas*. *Plant J* **21**, 121-131.
Steveson, T. C., Zhao, G. C., Keutmann, H. T., Mains, R. E. and Eipper, B. A. (2001). Access of a membrane protein to secretory granules is facilitated by phosphorylation. *J Biol Chem* **276**, 40326-40337.
Strenkert, D., Schmollinger, S., Sommer, F., Schulz-Raffelt, M. and Schroda, M. (2011). Transcription factor-dependent chromatin remodeling at heat shock and copper-responsive promoters in Chlamydomonas reinhardtii. *Plant Cell* **23**, 2285-2301.
Strenkert, D., Limso, C. A., Fatihi, A., Schmollinger, S., Basset, G. J. and Merchant, S. S. (2016). Genetically programmed changes in photosynthetic cofactor metabolism in copper-deficient *Chlamydomonas*. *J Biol Chem* **291**, 19118-19131.
Tenenboim, H., Smirnova, J., Willmitzer, L., Steup, M. and Brotman, Y. (2014). VMP1-deficient *Chlamydomonas* exhibits severely aberrant cell morphology and disrupted cytokinesis. *BMC Plant Biol* **14**, 121.
Vishwanatha, K., Back, N., Mains, R. E. and Eipper, B. A. (2014). A histidine-rich linker region in peptidylglycine alpha-amidating monooxygenase has the properties of a pH sensor. *J Biol Chem* **289**, 12404-12420.
Waters, A. M. and Beales, P. L. (2011). Ciliopathies: an expanding disease spectrum. *Pediatr Nephrol* **26**, 1039-1056.
Zhang, Q., Liu, Q., Austin, C., Drummond, I. and Pierce, E. A. (2012). Knockdown of ttc26 disrupts ciliogenesis of the photoreceptor cells and the pronephros in zebrafish. *Mol Biol Cell* **23**, 3069-3078.
Zuo, X., Guo, W. and Lipschutz, J. H. (2009). The exocyst protein Sec10 is necessary for primary ciliogenesis and cystogenesis in vitro. *Mol Biol Cell* **20**, 2522-2529.

SUPPLEMENTARY DATA

Table S1. Changes in gene expression of ciliary components in control and PAM-amiRNA cells analyzed by RNA sequencing.

Transcript abundance of genes encoding for intraflagellar transport (IFT), transition zone (TZ), Bardet-Biedl syndrome (BBS) and trafficking components in three control and three PAM amiRNA strains. Mean ± SD RPKM (reads per kilobase per million mapped reads) values from control and PAM amiRNA strains are tabulated.

Table S2. Antibodies used in this study.

The source of each of the antibodies used in this study and the dilution employed for immunofluorescence (IF) and western blot (WB) analysis is tabulated.

Supplementary Video S1. Gliding Motility of Control and RNAi Planaria.

Combined videos showing the movement of control (L4440), *Smed-phm+pam(RNAi)*, *Smed-phm(RNAi)* and *Smed-pam(RNAi)* animals in 9-cm Petri dishes. Videos were captured at 15 fps for 60 secs and play back at 10× real-time.

Supplementary Video S2. Ciliary Motility of Control and *Smed-phm+pam(RNAi)* Planaria

Videos of ventral cilia of control (L4440) and *Smed-phm+pam(RNAi)* planaria were taken at 150 fps and play back at 1/10th real-time.

Table S1

			EV control		PAM KD			
	Protein name	**transcript**	**Mean RPKM**	**Std dev**	**Mean RPKM**	**Std dev**	**Signifi-cantly different?**	**t-test**
	PAM	Cre03.g152850.t1.2	21.24	1.18	6.05	0.14	YES	0.002
IFT-A	IFT144	Cre13.g572700.t1.2	13.68	1.90	11.90	1.63	NO	0.287
	IFT140	Cre08.g362650.t1.1	8.27	1.08	8.01	1.18	NO	0.792
	IFT139	Cre06.g268800.t1.2	12.19	2.24	10.88	0.86	NO	0.425
	IFT121	Cre11.g475000.t1.1	11.83	1.23	11.04	1.50	NO	0.521
	IFT122	Cre01.g065822.t1.1	14.90	1.92	13.10	1.97	NO	0.319
	IFT43	Cre06.g251200.t1.2	10.82	1.74	9.42	1.38	NO	0.338
IFT-B	IFT172	Cre17.g703900.t1.2	10.70	2.90	7.73	1.44	NO	0.212
	IFT88	Cre07.g335750.t1.1	13.14	1.87	11.49	1.50	NO	0.305
	IFT81	Cre17.g723600.t1.2	10.29	3.38	7.89	1.24	NO	0.347
	IFT80	Cre03.g204150.t1.2	13.53	3.49	10.84	1.27	NO	0.314
	IFT72/74	Cre01.g027950.t1.2	16.43	3.63	13.04	1.28	NO	0.243
	IFT25	Cre10.g450350.t1.2	12.46	3.50	10.41	1.30	NO	0.424
	IFT57	Cre10.g467000.t1.2	14.56	3.53	13.57	1.34	NO	0.683
	IFT52	Cre04.g219250.t1.2	18.58	4.20	15.32	1.84	NO	0.313
	IFT46	Cre05.g241637.t1.1	22.88	6.22	20.57	1.99	NO	0.593
	IFT27	Cre01.g047950.t1.1	12.79	2.53	14.21	1.91	NO	0.484
	IFT20	Cre02.g089950.t1.2	18.30	4.60	19.02	1.35	NO	0.816
	IFT22	Cre01.g039200.t1.2	14.35	2.08	12.94	2.07	NO	0.452
TZ	CEP290	Cre03.g167550.t1.1	3.41	1.08	4.21	0.59	NO	0.340
	NPHP4	Cre12.g531400.t1.1	6.08	2.08	8.22	1.31	NO	0.219
BBSome	BBS1	Cre17.g741950.t1.1	10.83	0.34	10.65	0.34	NO	0.545
	BBS2	Cre06.g257250.t1.1	9.18	0.37	8.32	0.11	YES	0.048
	BBS3	Cre16.g664500.t1.2	7.30	1.68	7.99	0.47	NO	0.555
	BBS4	Cre12.g548650.t1.1	4.77	1.16	4.31	0.16	NO	0.568
	BBS5	Cre06.g267550.t1.2	7.11	0.16	7.95	0.61	NO	0.132
	BBS7	Cre01.g043750.t1.1	7.96	0.56	7.94	0.27	NO	0.954
	BBS9	Cre04.g219700.t1.1	5.29	0.13	5.90	0.27	YES	0.038
	BBS8	Cre16.g666500.t1.2	10.28	0.22	10.77	0.35	NO	0.124
Trafficking	Clathrin heavy chain	Cre02.g101400.t1.2	55.03	2.70	57.43	0.66	NO	0.261
	Clathrin light chain	Cre03.g155650.t1.2	58.62	5.96	60.74	3.66	NO	0.634
	Arf1	Cre02.g142687.t1.1	439.62	27.14	450.96	13.84	NO	0.565
Axonemal	RSP1	Cre03.g201900.t1.1	7.67	2.17	5.10	0.93	NO	0.165
	RSP2	Cre10.g427300.t1.2	6.01	1.91	3.80	0.39	NO	0.180
	TUA1 (apha tubulin 1)	Cre03.g190950.t1.2	709.17	76.87	754.24	85.97	NO	0.536
	TUA2 (alpha tubulin 2)	Cre04.g216850.t1.2	568.12	52.71	649.58	33.95	NO	0.099
	TUB1 (beta tubulin 1)	Cre12.g542250.t1.1	343.58	42.58	339.99	23.46	NO	0.906

	TUB2 (beta tubulin 2)	Cre12.g549550.t1.2	544.09	32.45	667.30	64.29	NO	0.060
	Gamma tubulin	Cre06.g299300.t1.2	14.88	2.80	19.72	0.64	NO	0.089
Secreted	FEA1	Cre12.g546550.t1.1	692.21	166.89	1239.12	260.08	YES	0.046
	FEA2	Cre12.g546600.t1.1	5.59	1.52	9.90	7.08	NO	0.403
	Alkaline phosphatase	Cre08.g359300.t1.2	2.80	2.72	5.27	0.49	NO	0.254

TABLE S2: List of antibodies used in this study.

Antibody	Dilution	Source
CrPAM CD	1:500 (IF), 1:1000 (WB)	(Kumar et al., 2016a)
CrPAM lum	1:500 (IF), 1:1000 (WB)	This study
α-tubulin	1:1000 (WB, IF)	Thermo Fisher (B-5-1-2)
Poly-glutamylated tubulin	1:500 (WB)	Adipogen (GT335)
Acetylated α-tubulin	1: 2000 (IF, WB)	Santa Cruz (611-B-1)
IFT 81	1:500 (WB), 1:200 (IF)	Dr. Dennis Diener
IFT 72/74	1:2500 (WB), 1:1000 (IF)	Dr. Dennis Diener
IFT 46	1:1000 (WB), 1:500 (IF)	(Hou et al., 2007)
IFT 139	1:500 (WB)	Dr. Doug Cole
IC2	1:5000 (WB)	(King et al., 1985)
CEP290	1:500 (WB), 1:200 (IF)	(Craige et al., 2010)
NPHP4	1:200 (WB)	(Awata et al., 2014)
Clathrin	1:1000 (WB)	Agrisera (AS10 690)
Arf 1	1:5000 (WB)	Agrisera (AS08 325)

REFERENCES

1. **Kumar D, Blaby-Haas CE, Merchant SS, Mains RE, King SM, Eipper BA.** Early eukaryotic origins for cilia-associated bioactive peptide-amidating activity. *J Cell Sci.* 2016;**129**(5):943-56.
2. **Hou Y, Qin H, Follit JA, Pazour GJ, Rosenbaum JL, Witman GB.** Functional analysis of an individual IFT protein: IFT46 is required for transport of outer dynein arms into flagella. *J Cell Biol.* 2007; **176**(5):653-65.
3. **King SM, Otter T, Witman GB.** Characterization of monoclonal antibodies against *Chlamydomonas* flagellar dyneins by high-resolution protein blotting. *Proc Natl Acad Sci U S A.* 1985;**82**(14):4717-21.
4. **Craige B, Tsao CC, Diener DR, Hou Y, Lechtreck KF, Rosenbaum JL, et al.** CEP290 tethers flagellar transition zone microtubules to the membrane and regulates flagellar protein content. *J Cell Biol.* 2010;**190**(5):927-40.
5. **Awata J, Takada S, Standley C, Lechtreck KF, Bellve KD, Pazour GJ, et al.** NPHP4 controls ciliary trafficking of membrane proteins and large soluble proteins at the transition zone. *J Cell Sci.* 2014;**127**(Pt 21):4714-27.

Chapter 5

A Bioactive Peptide Amidating Enzyme Is Released in Ciliary Ectosomes

Dhivya Kumar, Crysten Blaby-Haas, Maya Bartolotta, Sabeeha Merchant, Richard Mains, Stephen King and Betty Eipper

ABSTRACT

Several studies suggest that cilia not only sense signals from the extracellular environment, but also transmit information in the form of vesicles (Wood et al., 2013; Wang et al., 2014; Cao et al., 2015). The content of extracellular vesicles is regulated and can affect the physiology of the acceptor or donor cells. We recently localized PAM in the cilia of multiple cell types including *Chlamydomonas*, and in this study we demonstrate that PAM is released in extracellular vesicles shed during the sexual life cycle of *Chlamydomonas*. PAM is required for ciliary assembly in *Chlamydomonas*, but the exact mechanism is unclear. Using bioinformatics and mass spectrometric approaches, we identify amidated peptide products in spent medium from *Chlamydomonas* cells, suggesting that this unicellular eukaryote utilizes peptidergic signaling for intercellular communication. Thus, PAM may be involved in the biosynthesis of biologically active peptides required for life transitions in *Chlamydomonas*.

INTRODUCTION

Extracellular vesicles (EVs) are emerging as important mediators of intercellular communication. Previously considered vestiges of apoptotic cells, release of extracellular vesicles is now considered a regulated, evolutionarily conserved process impacting key physiological processes (Lo Cicero et al., 2015). The ability to package a distinct set of lipids, proteins (transmembrane and cytosolic) and nucleic acids in a membrane-bound manner, sets communication with extracellular vesicles apart from classical modes of intercellular signaling using hormones and neurotransmitters. Extracellular vesicles have been called microvesicles, ectosomes, exosomes and microparticles in the literature; these classifications are meant to reflect the source, size and content of a subset of extracellular vesicles. The inability to isolate and characterize a single type of EV, and selectively alter EV cargo has impeded our understanding of the physiological importance of EV release. Extracellular vesicles are derived from two major sources: those generated by pinching off of the plasma membrane are known as ectosomes (100-1000 nm in size), and those released after fusion of multivesicular bodies, which contain intraluminal vesicles, with the plasma membrane are known as exosomes (50-150 nm in size) (Gould and Raposo, 2013; Raposo and Stoorvogel, 2013). Formation of intraluminal vesicles and budding of plasma membrane during ectosome shedding are topologically similar events; the original membrane and protein topology is maintained in both cases (Shifrin et al., 2013).

Cilia are cellular antennae present in almost all eukaryotic cells, specialized to serve sensory or motility related functions. Recent studies show that cilia from *Chlamydomonas reinhardtii*, *Caenorhabditis elegans* and mammals shed extracellular vesicles (ectosomes) (Wood et al., 2013; Wang et al., 2014; Cao et al., 2015). It has been known for many years that *Chlamydomonas* cilia constitutively release membrane vesicles into the medium and that in about 6 hours, the equivalent of an entire ciliary membrane is lost (Snell, 1976; Dentler, 2013). Ectosomes are also released at other phases of the life cycle in *Chlamydomonas*. During

vegetative cell division, ectosomes loaded with a cell wall-degrading lytic enzyme are required for daughter cells to emerge from the mother cell wall (Wood et al., 2013). During the sexual cycle of *Chlamydomonas,* when two gametes of opposite mating type come together, ectosomes containing the agglutinin protein that aids in cell-cell recognition are released into the medium (Cao et al., 2015). Proteomic analysis of ectosomes released by asynchronous vegetative cells indicates that specific proteins are enriched in the ectosomal fraction compared to the ciliary compartment in *Clamydomonas* (Long et al., 2016). Proteins enriched in ectosomes include components of the ubiquitin system, ESCRT pathway proteins and several transmembrane proteins such as FMG1 and polycystin 2. Furthermore, knockdown of ESCRT complex components in *Chlamydomonas* decreases ectosome shedding (Long et al., 2016). These data suggest that there is a sorting machinery that determines the composition of ectosomes in a cell cycle stage dependent manner.

In animals, bioactive peptides are a key method of intercellular communication, and C-terminal amidation is the last step in the biosynthesis of many peptides; examples include oxytocin, neuropeptide Y, and luteinizing hormone-releasing hormone. This step requires molecular oxygen, copper, vitamin C and peptidylglycine alpha-amidating monooxygenase (PAM). PAM is a bifunctional, type I integral membrane protein that functions in the lumen of the secretory pathway. The two enzymatic domains of PAM, peptidylglycine α-hydroxylating monooxygenase (PHM) and peptidyl-α-hydroxyglycine α-amidating lyase (PAL), sequentially process a glycine-extended peptide precursor into an amidated bioactive product and glyoxylate. The unstructured, cytosolic domain of PAM plays a role in the trafficking of PAM through the secretory pathway (Milgram et al., 1993; Milgram et al., 1994). In mammalian cells, PAM that is deposited on the plasma membrane during secretory granule exocytosis is rapidly endocytosed and either returned to the trans-Golgi network or degraded. Signals in the cytosolic domain of PAM govern its entry into the intraluminal vesicles of multivesicular bodies (Back et al., 2010)

and PAM has been identified in proteomic screens of exosomes isolated from prostate cancer cells, squamous cell carcinoma cells and saliva (Gonzalez-Begne et al., 2009; Minciacchi et al., 2015; Sinha et al., 2016).

We recently demonstrated that *Chlamydomonas* PAM is localized in Golgi and cilia (Kumar et al., 2016). This ciliary localization is conserved in mammals, with PAM being present in motile and primary cilia in diverse cell types. PAM is required for ciliary assembly in *Chlamydomonas* and regulates ciliogenesis in metazoans by an unknown mechanism (Chapter 4). While it is possible that an amidated peptide product plays a role in ciliary assembly, no amidated peptides have yet been reported in *Chlamydomonas*. Based on the presence of PAM in multivesicular bodies in mammalian cells, we hypothesized that the cilium-localized PAM in *Chlamydomonas* might be released in ectosomes. Here, we show that PAM is released in extracellular vesicles generated during the mating process in *Chlamydomonas*. We also report the presence of amidated peptides in the medium isolated from mating *Chlamydomonas* cells.

RESULTS

PAM gene expression is upregulated in early zygotes in the sexual life cycle of *Chlamydomonas*

While nutrient-replete, haploid *Chlamydomonas* cells undergo mitotic divisions and reproduce asexually, nutrient-deprived cells (such as under nitrogen starvation conditions) initiate the gametogenesis pathway to generate mating-competent gametes. Differentiated, haploid *plus* and *minus* gametes express sex-specific agglutinins on their ciliary surface and fuse within minutes to form a diploid, quadriflagellated zygote (2n). In the next few hours, the zygote undergoes additional developmental changes, resorbs its cilia, and secretes a thick cell wall that allows it to stay dormant until nutrients become available. The dormant zygote undergoes meiosis under optimal conditions to generate four haploid daughter cells (Fig 1 A).

Chlamydomonas mating is a complex process that involves cell-cell contact mediated by cilia followed by cAMP-based signal transduction and cell fusion. It has been reported that cell-cell contact can trigger the release of ectosomes from the ciliary surface; these ectosomes contain ciliary membrane proteins like SAG1 agglutinin and flagellar membrane glycoprotein 1 (FMG1).

To determine if *PAM* gene expression is altered at specific stages in the life cycle of *Chlamydomonas*, we scanned preexisting RNA-seq data sets (Lopez et al., 2015). We found that *Chlamydomonas reinhardtii* PAM (CrPAM) gene expression varied during the sexual reproductive cycle in two independent RNA sequencing experiments (Fig 1 B and C). In a study performed using high efficiency mating strains of *Chamydomonas* (R3/CC-620 mating type *plus* and CJU10 mating type *minus*), CrPAM transcript levels increased roughly two-fold in zygotic conditions compared to vegetative and gametic stages (Fig 1 B, Lopez et al., 2015). In this experiment, mixed plus and minus gametes were pooled 0.5, 1 and 2 h after mixing and used for RNA-seq analysis (Lopez et al., 2015). These data are in agreement with a second RNA-seq study performed with different sets of strains, where zygotes were collected 45 min and 2 h after mixing gametes of the opposite mating types (Goodenough and Merchant, unpublished) (Fig 1 C). Results from both studies suggest a role for PAM in the early zygote stage during the sexual reproduction cycle in *Chlamydomonas*.

Cellular levels of CrPAM remain unaltered during the sexual cycle of *Chlamydomonas*

To assess whether cellular CrPAM protein levels also varied during zygotic stages, following an increase in transcript levels, we prepared cell lysates from wild type CC124 mating type *minus* and CC125 mating type *plus* strains at different stages of their life cycle. Gametes were collected after a 24 h nitrogen starvation period and zygotic samples were collected at 10 minutes, 1 and 3 hours after mixing mating-competent gametes. We detected CrPAM in total cell lysates prepared from these samples with an antibody against the C-terminal domain

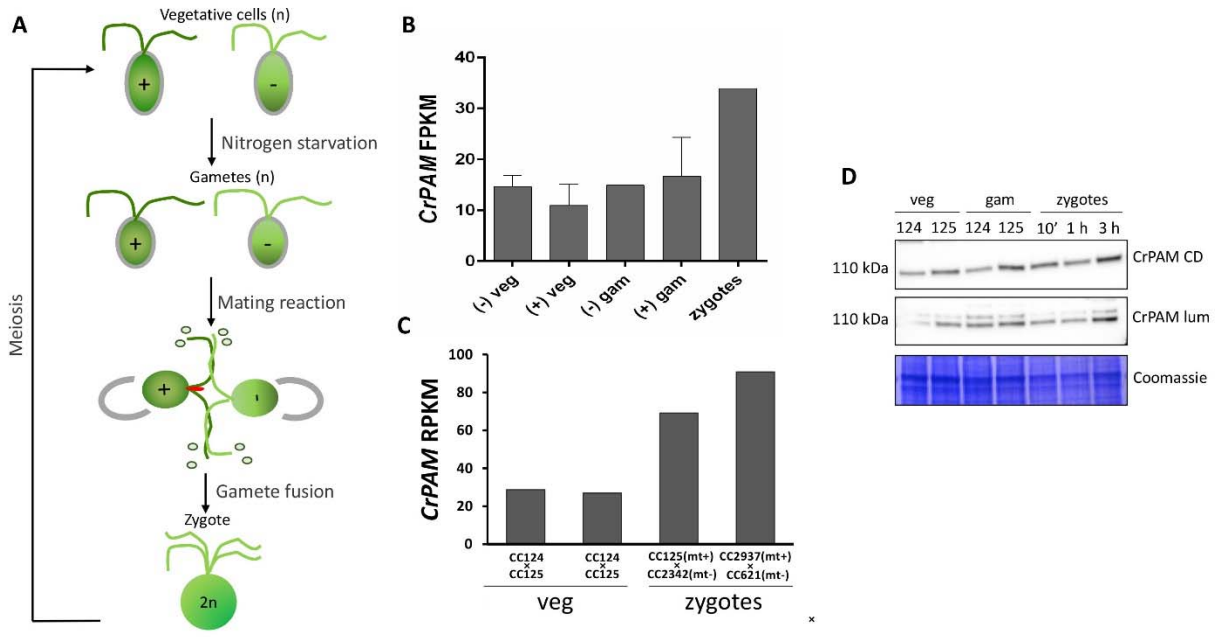

Fig 1. PAM gene expression is differentially regulated during the sexual cycle of *Chlamydomonas* (A) Schematic of the sexual reproductive cycle in *Chlamydomonas*. Under nutrient deprivation conditions, vegetative *Chlamydomonas* cells undergo differentiation to form gametes of plus or minus mating types. Gametes of the opposite mating type interact through agglutinin molecules expressed on their cilia and eventually fuse to form a diploid zygote. The mating reaction involves removal of the cell walls prior to cell fusion and formation of an actin-based mating structure on the plus-mating gamete that depends on cAMP based signaling. Extracellular vesicles shed during the mating process are also shown. **(B)** CrPAM transcript levels (as expressed as fragments per kilobase of transcript per million mapped reads (FPKM)) increase in early zygotic conditions (replotted from a previously published RNA-seq data set) (Lopez et al., 2015). **(C)** CrPAM transcript abundance expressed as median reads per kilobase per million mapped reads (RPKM) from a second independent RNA seq experiment also shows a two-fold increase during zygote stages in *Chlamydomonas*. Duplicate samples from a misture of plus (CC125) and minus (CC124) vegetative cells and zygotes derived from mating of CC125 mt+ and CC2342 mt- or CC2937 mt+ and CC621 mt- gametes were analyzed. **(D)** CrPAM cellular protein levels in vegetative, gametic and zygotic stages immunoblotted with antibodies to the C-terminal domain (CrPAM-CD) or the enzymatic, luminal domain (CrPAM-lum). Coomassie staining shows nearly equal protein loading. The *plus* strain (CC125) contains slightly more CrPAM protein compared to the *minus* strain (CC124).

(CrPAM CD) and an antibody against the luminal, enzymatic domains (CrPAM lum). Mating-type *plus* gametes had slightly higher levels of CrPAM than mating-type *minus* gametes. Furthermore, CrPAM cellular protein levels increased slightly in the 3 h zygote sample, but not in the earlier zygote samples (Fig 1 D).

PAM is present in *Chlamydomonas* ciliary mating ectosomes

We considered the possibility that some CrPAM might be released in ectosomes that are shed into the medium during mating. To test this, we used wild type CC125 mating-type *plus* and fusion-defective HAP2 mating-type *minus* strains to facilitate isolation of extracellular vesicles (Cao et al., 2015). We utilized negative stain transmission electron microscopy to confirm isolation of extracellular vesicles from the medium collected from gametes that were mixed for 1 h, and found numerous vesicles of variable sizes (mean diameter 140 ± 54 nm in diameter from > 50 measurements) (Fig 2 A). This size is consistent with the size of *Chlamydomonas* ectosomes previously reported in the literature.

Next, we immunoblotted total cell lysates and ectosome samples with FMG1 and PAM antibodies. CC125 and HAP2 gametes were collected before and after they had been mixed for 1 h and equal total protein from detergent soluble and insoluble samples were subjected to electrophoresis. In cell lysates, both FMG1 and CrPAM were predominantly present in the detergent soluble fractions and were slightly reduced in the cell lysates prepared from gametes that were mixed for 1 h (Fig 2 B). FMG1 and outer dynein arm intermediate chain 2 (IC2) were used as positive controls since they are both released in ectosomes (Long et al., 2016). CrPAM was also detected in the ectosome sample with both CD and luminal specific antibodies. Note that the cell lysates correspond to three times the total protein analyzed in the ectosome sample. Western blot band intensities were quantified and plotted as OD/µg protein for FMG1 and PAM (using the CD antibody) (Fig 2 C). Based on the initial volumes of cultures used, about

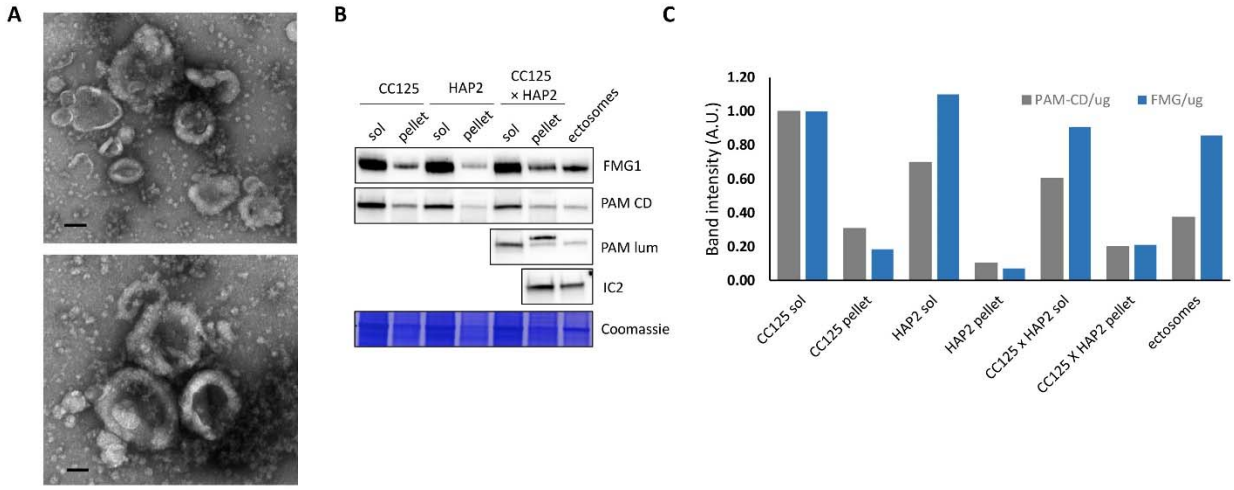

Fig 2. CrPAM is released in ectosomes (A) Negative stain transmission electron micrographs of ciliary ectosomes isolated from spent medium of CC125 *plus* and HAP2 *minus* strains. Scale bars = 100 nm. **(B)** Immunoblots of detergent soluble and insoluble cell lysates and ectosomes. Note that three times as much total cell lysates were loaded compared to the ectosome samples. FMG1and IC2 were used as a marker for ectosomes. CrPAM was detected in ectosomes with both the luminal and CD antibodies. **(C)** Band intensities were quantified and normalized to the highest band intensity. The optical density/μg of protein is plotted for PAM-CD and FMG1.

2% of the total PAM in the cells and 4% of the total FMG1 in the cells is released in ectosomes per hour.

In silico mining identifies potential peptide precursors in the *Chlamydomonas* proteome

Why would CrPAM be released in ectosomes during mating in *Chlamydomonas*? Although plants have been reported to use bioactive peptides for cellular signaling and defense (Salas et al., 2015; Simon and Dresselhaus, 2015), no bioactive peptides have been reported in *Chlamydomonas*. Furthermore, the use of amidated peptides has been considered a feature of metazoans. The presence of active PAM and co-factors that are required for its activity in *Chamydomonas*, suggest PAM could function to synthesize amidated bioactive peptides (Attenborough et al., 2012; Kumar et al., 2016).

In order to identify potential amidated peptide precursors in *Chamydomonas*, we surveyed the *Chlamydomonas reinhardtii* transcriptome for the presence of classic mammalian preproproteins by searching for the presence of an N-terminal signal sequence and dibasic cleavage sites (for prohormone convertase cleavage) preceded by a glycine residue. To narrow the search, we initially imposed restrictions on the size of the putative peptide precursors (less than 250 amino acids) (4832 proteins) and filtered out proteins that included any recognizable structural domains, leaving 3105 proteins. We used NeuroPred (Southey et al., 2008) to determine potential amidation sites in the identified sequences. Since plants lack *PAM*-like genes, we also eliminated any putative preproproteins with homologs in land plants (Fig 3 A). Using this logic, about 800 candidate preproproteins containing at least one potential amidation site were identified in *Chlamydomonas*; 89 of these were predicted to localize in the secretory pathway using PredAlgo, a subcellular localization predictor for green algal sequences (Tardif et al., 2012). The cellular localization could not be predicted with accuracy for the other proteins and it is possible that they do not localize in the secretory pathway.

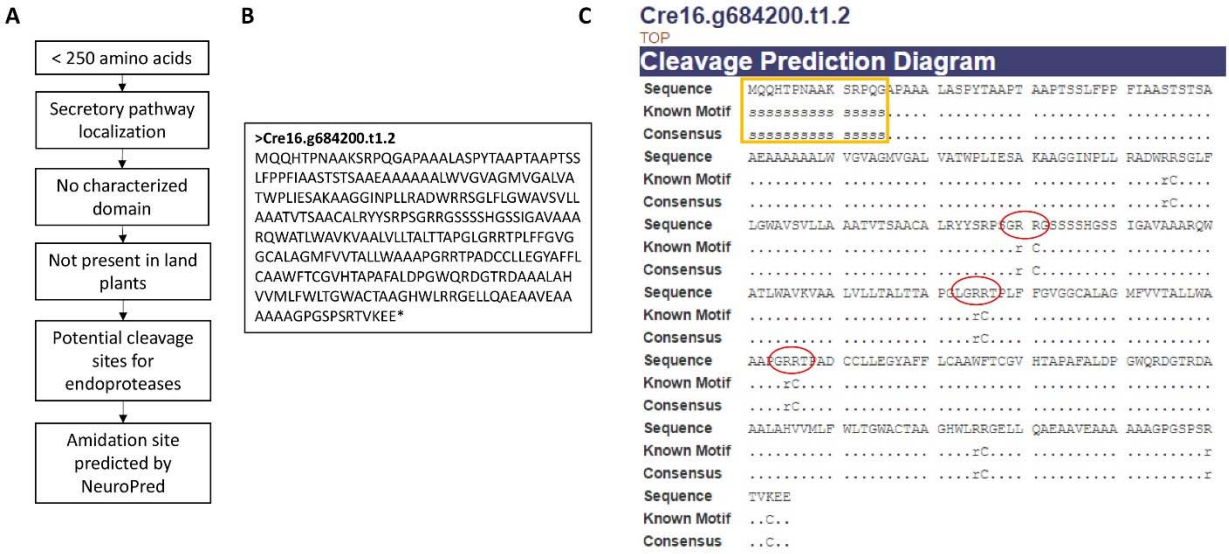

Fig 3. *In silico* data mining identifies potential peptide precursors in the *Chlamydomonas* proteome. (A) Screening strategy used for peptide precursor determination. **(B)** The sequence of one such peptide precursor identified is shown **(C)** NeuroPred predicts a signal sequence (boxed in yellow) and multiple glycine residues followed by dibasic cleavage sites (circled in red) for that particular protein sequence.

The sequence of one potential peptide precursor is shown in Fig 3 B, along with its predicted cleavage and amidation site from NeuroPred (Fig 3 B and C). The predicted signal sequence is boxed in yellow and glycine residues followed by dibasic cleavage sites are outlined in red. For this particular precursor, three amidated products are predicted by NeuroPred (Fig 3 C).

Mass spectrometry identified secreted proteins and potential amidated peptides in the *Chlamydomonas* mating secretome

The most direct method for identification of peptides is mass spectrometry. In order to confirm our *in silico* analysis and identify bioactive peptides secreted by *Chlamydomonas*, we collected the spent medium from mating-competent wild type CC124 and CC125 gametes for the first hour they were mixed. The medium was concentrated seven-fold using a tangential flow filtration system with a 2 kDa molecular weight cut-off filter. We then examined the composition of the spent medium by performing SDS-PAGE and silver staining (Fig 4 A). The two boxed regions in the image were excised for analysis from the silver stained gel .The spent medium concentrated after acidification using a SepPak C18 cartridge was also used for mass spectrometric analysis.

Several extracellular proteins such as cell wall glycoproteins and hydroxyproline rich pherophorins were identified in the mating secretome. By incorporating the amidation mass filter of “Gly-loss + amide”, four high-confidence amidated peptides were identified (Fig 4 B); three were encoded in proteins that include a classic Gly-Basic-Basic sequence (GRR) for proprotein convertase cleavage and one was derived from the C-terminus of an integral membrane protein ending with a –Gly-Arg sequence. A carboxypeptidase B-like cleavage can release the Arg residue, generating the peptidyl-Gly sequence required by PAM. For the two amidated peptides obtained from trypsin-digested gel bands, additional peptides from more N-terminal regions of the same precursors (Cre03.g204500 and Cre12.g487700) were also identified, suggesting that these amidated products might contain much of the coding sequences.

A

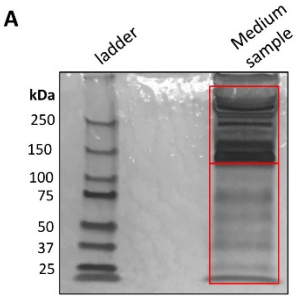

B

Amidated Peptides Secreted by *Chlamydomonas*		
Amidated Product	Parent Gene	Properties of the Full-length Protein Precursor
QALQVLLERE-amide	Cre07.g326650	N-terminal signal sequence + transmembrane domain following the peptide. Expression is down-regulated upon gamete activation, as is PAM.
GENKSLDEDAEGAEGGSIQHG-amide	Cre13.g587350	N-terminal signal sequence. No obvious domains. Highly induced upon gametogenesis.
VLYPNDPAAYAAYAPGTGGGATI-amide	Cre03.g204500	No obvious domains. Highly induced upon gametogenesis.
KPLTSIAVFAKPLVPAAA-amide	Cre12.g487700	N-terminal signal sequence. No obvious domains. Expression is down-regulated upon gamete activation.

C

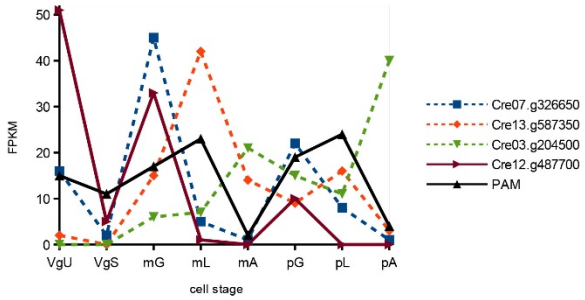

Fig 4. Mass spectrometric identification of amidated peptides in the spent medium of *Chlamydomonas* (A) Silver stained gel of the concentrated spent medium obtained from CC124 minus and CC125 plus gametes undergoing mating. The boxed regions show the two gel pieces used for mass spectrometric analysis. **(B)** Four high confidence amidated peptides identified by mass spectrometry using the "Gly-loss + amide" filter. **(C)** Transcript abundance of CrPAM and the four putative precursors to the amidated peptides identified by mass spectrometry in a previous RNA-seq data set (Ning et al., 2013). VgU = unsynchronized vegetative cells, VgS = synchronized vegetative cells, mG = resting minus gametes, mL = lysin treated minus gametes, mA = db-cAMP activated minus gametes, pG = resting plus gametes, pL = lysin treated plus gametes, pA = db-cAMP activated plus gametes. All four peptides show significant changes in transcript abundance during gametogenesis/gamete activation.

In contrast, no additional peptides derived from the other two amidated peptide precursors (Cre07.g326650 and Cre13.g587350) were identified in the non-digested concentrated medium; thus, these peptides may potentially represent the complete amidated product. This is the first demonstration that *Chlamydomonas* secretes amidated peptide products.

The signaling events that occur during *Chlamydomonas* mating are complex, and molecular details have not been fully elucidated. A previous study has performed a genome-wide transcriptomic analysis of resting and activated gametes; the latter were treated with a cAMP analog to mimic cell-cell contact-based sexual signaling (Ning et al., 2013). The other samples included were gametes treated with a cell-wall degradative enzyme to mimic cell wall removal, which occurs during mating. In this RNA-seq data set, CrPAM transcript levels decrease in response to cAMP gene activation in both *plus* and *minus* gametes (Fig 4 C). Expression of the *Chlamydomonas* peptide precursor genes also changes dramatically during gametogenesis/gamete activation, suggesting that these peptides may play important signaling roles at specific life-cycle stage(s) (Fig 4 C).

DISCUSSION

Role of PAM in life transitions in *Chlamydomonas*

In several species, PAM is essential for life; loss of PAM in mice and *Drosophila* leads to embryonic lethality (Kolhekar et al., 1997; Czyzyk et al., 2005). The most well recognized role of PAM is in the biosynthesis of amidated peptides in the neuroendocrine system. However, several pieces of evidence point to a role of PAM outside the nervous system. Transcriptomic studies and improved enzyme assay protocols have revealed that PAM is ubiquitously expressed in mammals, with the highest levels in the heart where no amidated peptides have been reported. PAM-like genes have been reported in the genomes of several green algae, the placozoan *Trichoplax*, and sponges, all of which lack a nervous system (Attenborough et al.,

2012). We recently demonstrated that the unicellular eukaryote, *Chlamydomonas reinhardtii,* expressed active PAM enzyme, which localizes in the Golgi and cilium (Kumar et al., 2016). Furthermore, we showed that the localization of PAM in cilia is evolutionarily conserved. In mammals, PAM is located in primary cilia (in fibroblasts and epithelial cells) and motile cilia (in ependymal cells, airway epithelial cells and spermatozoa). This work raised several important questions that we have addressed using *Chlamydomonas*, a unicellular organism. First, what is the ancestral role of PAM? Second, what is the function of PAM in cilia?

To address these questions, we scanned preexisting RNA sequencing data sets to determine if PAM gene expression is regulated at any specific stage in the life cycle of *Chlamydomonas*. We found a two-fold change in the levels of PAM transcripts during the sexual life cycle of *Chlamydomonas* in two independent transcriptomic studies (Fig 1 B and C). Mating is a complex process in *Chlamydomonas*, involving a cilium-dependent cAMP-based signal transduction event. A previous study also noted a change in a number of secretory pathway genes at the transcriptome level during the sexual reproductive cycle in *Chamydomonas* (Lopez et al., 2015).

PAM gene expression is also differentially regulated during the light-dark vegetative cycle in *Chlamydomonas*. PAM transcript levels increase continuously until the end of the light cycle and then plummet in the dark phase (Zones et al., 2015). Most major processes including cell division and expression of almost all of the *Chlamydomonas* genome are under circadian control. In the light phase, cells are in the G1 phase and grow in size in preparation for the multiple cell fission events that occur at the light/dark transition or in the dark phase. Based on the pattern of *CrPAM* gene expression, PAM was placed into a cluster that included several vesicular trafficking, protein folding and cell cycle genes (Zones et al., 2015). At the peak of PAM gene expression, a process critical for cell division must take place, ciliary resorption to

allow for repurposing of the basal bodies for mitosis. It is possible that PAM plays a role in this process or other trafficking events that occur at this stage during the vegetative cycle.

A novel enzyme activity in ciliary ectosomes

Recently, the release of extracellular vesicles has been shown to increase during ciliary resorption (Long et al., 2016). Thus, both active transport of ciliary components back to the cell soma by intraflagellar trafficking and shedding of membranous vesicles contribute to resorption of cilia. Coincidentally, mating gametes also shed ciliary ectosomes that contain agglutinin molecules which aid in the initial recognition of opposite mating types (Cao et al., 2015). Based on these observations and the identification of mammalian PAM in multivesicular bodies and exosomes in human samples (Gonzalez-Begne et al., 2009; Back et al., 2010; Minciacchi et al., 2015), we assessed the presence of PAM in ciliary ectosomes shed during the mating process in *Chlamydomonas*. PAM was identified in FMG1-positive vesicles using antibodies directed to its C-terminal domain and luminal domains, suggesting that the full length enzyme is released in ectosomes (Fig 2).

Several questions still need to be addressed regarding the release of PAM in ciliary ectosomes in *Chlamydomonas*. Is PAM only released at specific times during the life cycle of *Chlamydomonas*? Here, we analyzed ectosomes shed during the mating process in *Chlamydomonas*, but it is known that ectosomes are also released during ciliary resorption and during hatching in vegetative cell division. We also find that about 2% of total cellular PAM is released in ciliary ectosomes in one hour. Only a small fraction of PAM resides in the cilium in *Chlamydomonas*; most of the PAM protein is localized in the secretory pathway. Based on previous enzyme assays and the fact that the cilium comprises about 1-2% of total cellular protein, only about 1-2% of total cellular PAM localizes in cilia in vegetative cells (Kumar et al., 2016). Thus, during mating, an entire cilium-equivalent of PAM is released in ciliary ectosomes.

Intercellular communication in a unicellular eukaryote

What are the implications of finding a peptide amidating enzyme in extracellular vesicles? While it is possible that release of PAM in ciliary ectosomes is simply a means of protein turnover, it is also possible that the PAM released in ectosomes plays a role in intercellular communication by regulating gene expression in recipient cells. In mammalian cells, regulated intra-membrane proteolysis releases the C-terminal domain of PAM (called soluble fragment of the PAM cytosolic domain or sf-CD) that localizes in the nucleus and can affect transcription of several genes (Rajagopal et al., 2010; Rajagopal et al., 2012). It is currently unknown if *Chlamydomonas* PAM is subject to a similar intra-membrane proteolysis event to release the soluble cytosolic fragment of PAM that can alter the expression of specific target genes. A third possibility for release of an active enzyme in ectosomes is to act on substrates in the extracellular space. Using bioinformatic approaches we generated a list of putative amidated peptide precursors in the *Chlamydomonas* proteome (Fig 3). Furthermore, we found amidated peptides in the spent medium of *Chlamydomonas* cells using biochemistry/mass-spectrometry approaches (Fig 4). To our knowledge, this is the first report of amidated peptides in *Chlamydomonas*, an organism not reported to communicate using peptidergic signaling. Future studies will focus on determining the role of these putative bioactive peptides in intercellular communication in *Chlamydomonas*.

Extracellular vesicles can be easily isolated from urine, blood and saliva, and therefore they have gained attention as potential biomarkers for pathological conditions. The bottleneck for the use of EVs in diagnostic applications is the difficulty in pinpointing the source of these vesicles. Isolation and characterization of pure ectosomes, such as from *Chlamydomonas* cilia will be useful to characterize and utilize EVs as biomarkers in clinical applications, such as for ciliopathies in the future.

MATERIALS AND METHODS

Cell culture

Chlamydomonas reinhardtii strains CC124 mt-, CC125 mt+ and HAP2 mt- (*Chlamydomonas* resource center) were grown in R medium in a 12 h light/12 h dark cycle at 22°C with aeration. To induce gametogenesis, vegetative cells in log phase were washed and suspended in nitrogen-deficient minimal medium (M-N/5 medium) for 16 h or longer (Iomini et al., 2009). Mating competence of gametes was assessed by mixing the plus and minus gametes and checking for cell agglutination.

Ectosome preparation

Mating ectosomes were prepared as described previously (Cao et al., 2015). Briefly, CC125 mt+ and HAP2 mt- gametes were concentrated (ten-fold) and incubated in autolysin for 30 minutes at 22°C with gentle aeration. Gametes were then washed with nitrogen-free medium, mixed together and incubated for one hour. Cells were collected by centrifugation at 1600 ×g for 10 minutes. The supernatant was centrifuged at 20,000 ×g for 30 minutes to remove cell debris. Ectosomes were pelleted from this supernatant by centrifugation at 200,000 ×g for 1 hour and resuspended in a small volume of nitrogen-free medium supplemented with protease inhibitors.

Cell lysate preparation and western blotting

Total cell lysates were prepared by suspending cells with equal volumes of DTT-sodium bicarbonate buffer (0.1 M DTT, 0.1 M $NaHCO_3$ containing protease inhibitors) and SDS-sucrose buffer (5% SDS and 30% sucrose). For preparation of detergent soluble cell lysates, cells were lysed in a low ionic strength buffer (20 mM Na TES, 10 mM mannitol) containing 1% Triton-X-100 and protease inhibitors followed by two rounds of freeze-thaw and sonication. After tumbling at 4°C for 20 minutes, samples were centrifuged at 18,000 ×g for 10 minutes at 4°C to collect soluble fractions. The pellet was solubilized in SDS lysis buffer (0.5% SDS w/v, 50mM

Tris, pH 8.0 containing protease inhibitors). Samples were loaded onto a SDS-PAGE gel using protein concentration measured determined by a BCA (Pierce) or chlorophyll assay (Strenkert et al., 2016). Equal protein was loaded onto 4-16% SDS-PAGE gels, fractionated, transferred to a PVDF membrane and immunoblotted using standard techniques. The following primary antibodies were used: mouse monoclonal FMG1 (1:1000) (Bloodgood et al., 1986), CT307 affinity-purified rabbit polyclonal to CrPAM-CD (1:1000) (Kumar et al., 2016), CT319 affinity-purified rabbit polyclonal CrPAM-lum (1:1000) (Kumar et al., in preparation) and mouse monoclonal IC2 antibody (1:5000) (King et al., 1985).

Collection of spent medium and mass spectrometry

CC124 and CC125 gametes were checked for high mating efficiency and mixed together for 1 h with gentle aeration at 22°C. Cells were pelleted by centrifugation and the spent medium was filtered through a 0.22 μm filter to remove cell debris. The spent medium was concentrated seven-fold using a tangential flow filtration system with a 2 kDa cutoff (Sartorius Vivaflow 200 Hydrosart, 2K). The concentrated medium was subjected to SDS-PAGE followed by silver staining (Pierce, SilverSnap kit) and partial tryptic digestion; medium was also concentrated after acidification using a Sep-Pak C18 Cartridge (55-105 μm particle size, Waters Corporation, MA, USA) washed with 0.1% trifluoroacetic acid and eluted with 0.1% trifluoroacetic acid, 90% methanol. Tandem mass spectrometric analysis was performed at the Proteomics and Mass Spectrometry Facility, University of Massachusetts Medical School.

ACKNOWLEDGEMENTS

We thank Maya Yankova (UCHC Electron Microscopy Facility) for help with the negative staining TEM and Andrew Yanik (UCHC Neuropeptide laboratory) for outstanding technical assistance. We also thank Dr. Robert Bloodgood (University of Virginia Medical School) for the FMG1 antibody and Dr. Bill Snell (University of Maryland) for sending us the HAP2 strain. This work was supported by grants DK032949 (to BAE), GM051293 (to SMK) and GM042143 (to SSM) from the National Institutes of Health.

AUTHOR CONTRIBUTIONS

Crysten Blaby Hass performed the bioinformatics precursor analysis and some of the RNA-seq analysis in Sabeeha Merchant's laboratory. Maya Bartolotta contributed to ectosome preparations and analysis of cellular PAM levels. Betty Eipper and Dhivya Kumar processed the spent medium for mass spectrometric analysis. Dhivya Kumar conducted the remaining experiments under the guidance of Betty Eipper, Richard Mains and Stephen King.

REFERENCES

Attenborough, R. M., Hayward, D. C., Kitahara, M. V., Miller, D. J. and Ball, E. E. (2012). A "neural" enzyme in nonbilaterian animals and algae: preneural origins for peptidylglycine alpha-amidating monooxygenase. *Mol Biol Evol* **29**, 3095-3109.

Back, N., Rajagopal, C., Mains, R. E. and Eipper, B. A. (2010). Secretory granule membrane protein recycles through multivesicular bodies. *Traffic* **11**, 972-986.

Bloodgood, R. A., Woodward, M. P. and Salomonsky, N. L. (1986). Redistribution and shedding of flagellar membrane glycoproteins visualized using an anti-carbohydrate monoclonal antibody and concanavalin A. *J Cell Biol* **102**, 1797-1812.

Cao, M., Ning, J., Hernandez-Lara, C. I., Belzile, O., Wang, Q., Dutcher, S. K., Liu, Y. and Snell, W. J. (2015). Uni-directional ciliary membrane protein trafficking by a cytoplasmic retrograde IFT motor and ciliary ectosome shedding. *Elife* **4**.

Czyzyk, T. A., Ning, Y., Hsu, M. S., Peng, B., Mains, R. E., Eipper, B. A. and Pintar, J. E. (2005). Deletion of peptide amidation enzymatic activity leads to edema and embryonic lethality in the mouse. *Dev Biol* **287**, 301-313.

Dentler, W. (2013). A role for the membrane in regulating *Chlamydomonas* flagellar length. *PLoS One* **8**, e53366.

Gonzalez-Begne, M., Lu, B., Han, X., Hagen, F. K., Hand, A. R., Melvin, J. E. and Yates, J. R. (2009). Proteomic analysis of human parotid gland exosomes by multidimensional protein identification technology (MudPIT). *J Proteome Res* **8**, 1304-1314.

Gould, S. J. and Raposo, G. (2013). As we wait: coping with an imperfect nomenclature for extracellular vesicles. *J Extracell Vesicles* **2**, doi: 10.3402/jev.v2i0.20389

Iomini, C., Till, J. E. and Dutcher, S. K. (2009). Genetic and phenotypic analysis of flagellar assembly mutants in *Chlamydomonas reinhardtii*. *Methods Cell Biol* **93**, 121-143.

King, S. M., Otter, T. and Witman, G. B. (1985). Characterization of monoclonal antibodies against *Chlamydomonas* flagellar dyneins by high-resolution protein blotting. *Proc Natl Acad Sci U S A* **82**, 4717-4721.

Kolhekar, A. S., Roberts, M. S., Jiang, N., Johnson, R. C., Mains, R. E., Eipper, B. A. and Taghert, P. H. (1997). Neuropeptide amidation in *Drosophila*: separate genes encode the two enzymes catalyzing amidation. *J Neurosci* **17**, 1363-1376.

Kumar, D., Blaby-Haas, C. E., Merchant, S. S., Mains, R. E., King, S. M. and Eipper, B. A. (2016). Early eukaryotic origins for cilia-associated bioactive peptide-amidating activity. *J Cell Sci* **129**, 943-956.

Lo Cicero, A., Stahl, P. D. and Raposo, G. (2015). Extracellular vesicles shuffling intercellular messages: for good or for bad. *Curr Opin Cell Biol* **35**, 69-77.

Long, H., Zhang, F., Xu, N., Liu, G., Diener, D. R., Rosenbaum, J. L. and Huang, K. (2016). Comparative analysis of ciliary membranes and ectosomes. *Curr Biol*. **26**, 3327-3335.

Lopez, D., Hamaji, T., Kropat, J., De Hoff, P., Morselli, M., Rubbi, L., Fitz-Gibbon, S., Gallaher, S. D., Merchant, S. S., Umen, J. et al. (2015). Dynamic changes in the transcriptome and methylome of *Chlamydomonas reinhardtii* throughout its life cycle. *Plant Physiol* **169**, 2730-2743.

Milgram, S. L., Mains, R. E. and Eipper, B. A. (1993). COOH-terminal signals mediate the trafficking of a peptide processing enzyme in endocrine cells. *J Cell Biol* **121**, 23-36.

Milgram, S. L., Eipper, B. A. and Mains, R. E. (1994). Differential trafficking of soluble and integral membrane secretory granule-associated proteins. *J Cell Biol* **124**, 33-41.

Minciacchi, V. R., You, S., Spinelli, C., Morley, S., Zandian, M., Aspuria, P. J., Cavallini, L., Ciardiello, C., Reis Sobreiro, M., Morello, M. et al. (2015). Large oncosomes contain distinct protein cargo and represent a separate functional class of tumor-derived extracellular vesicles. *Oncotarget* **6**, 11327-11341.

Ning, J., Otto, T. D., Pfander, C., Schwach, F., Brochet, M., Bushell, E., Goulding, D., Sanders, M., Lefebvre, P. A., Pei, J. et al. (2013). Comparative genomics in *Chlamydomonas* and *Plasmodium* identifies an ancient nuclear envelope protein family essential for sexual reproduction in protists, fungi, plants, and vertebrates. *Genes Dev* **27**, 1198-1215.
Rajagopal, C., Mains, R. E. and Eipper, B. A. (2012). Signaling from the secretory granule to the nucleus. *Crit Rev Biochem Mol Biol* **47**, 391-406.
Rajagopal, C., Stone, K. L., Mains, R. E. and Eipper, B. A. (2010). Secretion stimulates intramembrane proteolysis of a secretory granule membrane enzyme. *J Biol Chem* **285**, 34632-34642.
Raposo, G. and Stoorvogel, W. (2013). Extracellular vesicles: exosomes, microvesicles, and friends. *J Cell Biol* **200**, 373-383.
Salas, C. E., Badillo-Corona, J. A., Ramirez-Sotelo, G. and Oliver-Salvador, C. (2015). Biologically active and antimicrobial peptides from plants. *Biomed Res Int* **2015**, 102129.
Shifrin, D. A., Jr., Demory Beckler, M., Coffey, R. J. and Tyska, M. J. (2013). Extracellular vesicles: communication, coercion, and conditioning. *Mol Biol Cell* **24**, 1253-1259.
Simon, R. and Dresselhaus, T. (2015). Peptides take centre stage in plant signaling. Preface. *J Exp Bot* **66**, 5135-5138.
Sinha, S., Hoshino, D., Hong, N. H., Kirkbride, K. C., Grega-Larson, N. E., Seiki, M., Tyska, M. J. and Weaver, A. M. (2016). Cortactin promotes exosome secretion by controlling branched actin dynamics. *J Cell Biol* **214**, 197-213.
Snell, W. J. (1976). Mating in *Chlamydomonas*: a system for the study of specific cell adhesion. I. Ultrastructural and electrophoretic analyses of flagellar surface components involved in adhesion. *J Cell Biol* **68**, 48-69.
Southey, B. R., Sweedler, J. V. and Rodriguez-Zas, S. L. (2008). A python analytical pipeline to identify prohormone precursors and predict prohormone cleavage sites. *Front Neuroinform* **2**, 7.
Strenkert, D., Limso, C. A., Fatihi, A., Schmollinger, S., Basset, G. J. and Merchant, S. S. (2016). Genetically programmed changes in photosynthetic cofactor metabolism in copper-deficient *Chlamydomonas*. *J Biol Chem* **291**, 19118-19131.
Tardif, M., Atteia, A., Specht, M., Cogne, G., Rolland, N., Brugiere, S., Hippler, M., Ferro, M., Bruley, C., Peltier, G. et al. (2012). PredAlgo: a new subcellular localization prediction tool dedicated to green algae. *Mol Biol Evol* **29**, 3625-3639.
Wang, J., Silva, M., Haas, L. A., Morsci, N. S., Nguyen, K. C., Hall, D. H. and Barr, M. M. (2014). C. elegans ciliated sensory neurons release extracellular vesicles that function in animal communication. *Curr Biol* **24**, 519-525.
Wood, C. R., Huang, K., Diener, D. R. and Rosenbaum, J. L. (2013). The cilium secretes bioactive ectosomes. *Curr Biol* **23**, 906-911.
Zones, J. M., Blaby, I. K., Merchant, S. S. and Umen, J. G. (2015). High-resolution profiling of a synchronized diurnal transcriptome from *Chlamydomonas reinhardtii* reveals continuous cell and metabolic differentiation. *Plant Cell* **27**, 2743-2769.

Chapter 6

Peptidylglycine-alpha amidating monooxygenase associates with the actin cytoskeleton and is required for both microvillar and ciliary assembly in the zebrafish pronephros

Dhivya Kumar, Rebecca Thomason, Nils Back, Richard Mains, Jonathan Gitlin, Stephen King, Betty Eipper

ABSTRACT

The assembly of membranous extensions such as microvilli and cilia in polarized cells is a tightly regulated, yet poorly understood process. Peptidylglycine alpha-amidating monooxygenase (PAM) is a bifunctional enzyme essential for the biosynthesis of amidated bioactive peptides. Changes in PAM levels can alter secretion and the organization of the actin cytoskeleton in mammalian cells. Here we explore the relationship of PAM with the actin cytoskeleton using *Chlamydomonas*, mammalian cell culture and zebrafish model systems. PAM co-localizes with apical actin in airway epithelial cells. PAM-deficient *Chlamydomonas* cells have an abnormal actin cytoskeleton, and fibroblasts generated from $PAM^{-/-}$ mice have altered Golgi, cell and nuclear morphology. Deletion of PAM in zebrafish recapitulates the edematous phenotype observed in $PAM^{-/-}$ mice, and reveals additional defects in the pronephros. $PAM^{-/-}$ zebrafish embryos display a striking loss of microvilli and subsequently impaired ciliogenesis in the pronephros. Our results point to a critical role for PAM in organizing the actin cytoskeleton during development which could in turn, impact ciliogenesis.

INTRODUCTION

Establishment of cell polarity is a critical process during development. Ciliated epithelia such as those lining the trachea, ventricles and kidney are highly polarized, with apically localized cilia and microvilli (Jimenez et al., 2014; Rostgaard and Thuneberg, 1972). This cellular polarization requires the coordinated actions of the actin cytoskeleton, microtubule network and vesicular trafficking machinery (Bornens, 2008).

Cilia are microtubule-based sensory organelles present in almost all cells in the human body. Multiple, motile cilia in the respiratory epithelium and ventricles propel fluid (such as mucus and cerebrospinal fluid). In other cells, primary, immotile cilia act as sensory and signaling compartments (Fliegauf et al., 2007). For example, primary cilia in the kidneys sense and respond to fluid flow, in part due to the mechanosensory roles of polycystin-1 and -2 (Nauli et al., 2003). Defects in ciliary function lead to a group of heterogeneous, multisystemic disorders collectively termed ciliopathies (Brown and Witman, 2014). Mutations in polycystin-1 and -2 have been linked to polycystic kidney disease, the most common inherited disorder, characterized by kidney cysts and eventual renal failure (Kathem et al., 2014). Dysfunction of motile cilia leads to primary ciliary dyskinesias, where patients exhibit respiratory tract infections due to poor mucociliary clearance (due to abnormal respiratory tract cilia), infertility (due to immotile sperm or oviductal cilia) and *situs inversus* (due to improper functioning of nodal cilia, which are required for left-right patterning). In some cases, hydrocephalus is observed due to dysfunction of ependymal cell cilia (Boon et al., 2013).

Microvilli are actin-rich cellular protrusions that can greatly increase the absorptive, sensory and secretory surface area of epithelial cells (McConnell et al., 2009; Sauvanet et al., 2015). Filamentous actin in microvilli is bundled together by crosslinking proteins such as villin, fimbrin and epsin, while proteins such as ezrin and myosin-1a link the actin bundles to the membrane (Crawley et al., 2014; Sauvanet et al., 2015). Microvilli are robust structures; loss of all three

major actin-bundling proteins (villin, epsin and fimbrin) does not abrogate microvillus formation in mice (Revenu et al., 2012). A lot is known about the structural components of microvilli, yet how cells initiate their assembly, and subsequently regulate and maintain these dynamic structures is unclear.

Peptidylglycine alpha-amidating monooxygenase (PAM) is a bifunctional enzyme required for one of the last steps in the biosynthesis of bioactive peptides such as vasopressin and neuropeptide Y (Kumar et al., 2016b). The enzymatic domains of PAM reside inside the lumen of the secretory pathway, where they sequentially convert an inactive peptide precursor with a C-terminal glycine residue into an amidated, bioactive peptide product (Kumar et al., 2016b). PAM is essential for life; PAM-null mice display severe edema and vasculature defects and do not survive beyond embryonic day E14.5 (Czyzyk et al., 2005). PAM is a type I integral membrane protein containing a cytosolic domain which aids its movement through the secretory and endocytic pathways. This unstructured, cytosolic domain confers additional properties to PAM. The ability of the cytosolic domain to interact with Kalirin and Trio, spectrin-repeat containing Rho GDP/GTP exchange factors (GEFs) for Rac1, RhoG and RhoA and with KIS/Uhmk1, a Ser/Thr protein kinase that interacts with stathmin, correlates with the ability of PAM to affect trafficking through the secretory pathway (Alam et al., 1996). Overexpression of PAM in a neuroendocrine cell line dramatically reorganizes the actin cytoskeleton into a cortical array and inhibits the regulated secretion of peptide products such as ACTH from secretory vesicles (Ciccotosto et al., 1999).

Apart from its well-recognized role in the neuroendocrine system, PAM appears to have an evolutionarily conserved role in ciliogenesis (Chapter 4). This unanticipated discovery was made while characterizing the role of PAM in the unicellular eukaryote, *Chlamydomonas reinhardtii*, where active PAM enzyme is localized in the Golgi and in cilia. In ependymal cells, tracheal epithelial cells and spermatozoa, which have motile cilia, and in fibroblasts, which have primary

cilia, PAM is also present in cilia (Kumar et al., 2016a). PAM-deficient *Chlamydomonas* cells are unable to assemble a cilium beyond the transition zone and have altered levels and localization of several ciliary proteins. RNAi-mediated knockdown of PAM in the planarian *Schmidtea mediterranea* leads to a severe loss of motile cilia on the ventral epithelium, and primary cilia develop abnormally in the neuroepithelium of $PAM^{-/-}$ mice (Chapter 4). How PAM regulates ciliary assembly in these different cell types is not known.

Defects in the actin cytoskeleton are known to impair ciliogenesis (Boisvieux-Ulrich et al., 1990; Kim et al., 2015; Kim et al., 2010). For example, treatment of multiciliated cells with a low dose of cytochalasin D, disrupts the aub-apical actin web and leads to defects in basal body docking and ciliary motility (Werner et al., 2011). Here, we utilize multiple model systems to explore the hypothesis that the connection between PAM and the actin cytoskeleton is both ancient and well conserved and identify a novel requirement for PAM in the formation of actin-based microvilli.

RESULTS

Generation of PAM-null zebrafish

To fully assess the role of PAM during development and its role in the assembly of cilia and actin-based structures, we generated three CRISPR-Cas9 mediated PAM-null zebrafish lines. The zebrafish genome encodes a single PAM gene; the domain structure of the predicted protein is shown in Fig 1 A. Three early truncation mutant lines (*pam*^{mbg5}, *pam*^{mbg9} and *pam*^{mbg10}) that were expected to generate loss of function alleles, were identified; the *pam*^{mbg5} line was used for most of the subsequent phenotypic analyses. Sequencing revealed that frameshift mutations resulted in a premature stop codon and early truncation near the beginning of the PHM domain in all three mutants (Fig 1 B). To confirm loss of PAM enzymatic activity, we performed PHM and PAL enzyme assays with wildtype, heterozygous and PAM-null zebrafish embryo lysates collected at different developmental stages. PHM activity increases steadily in

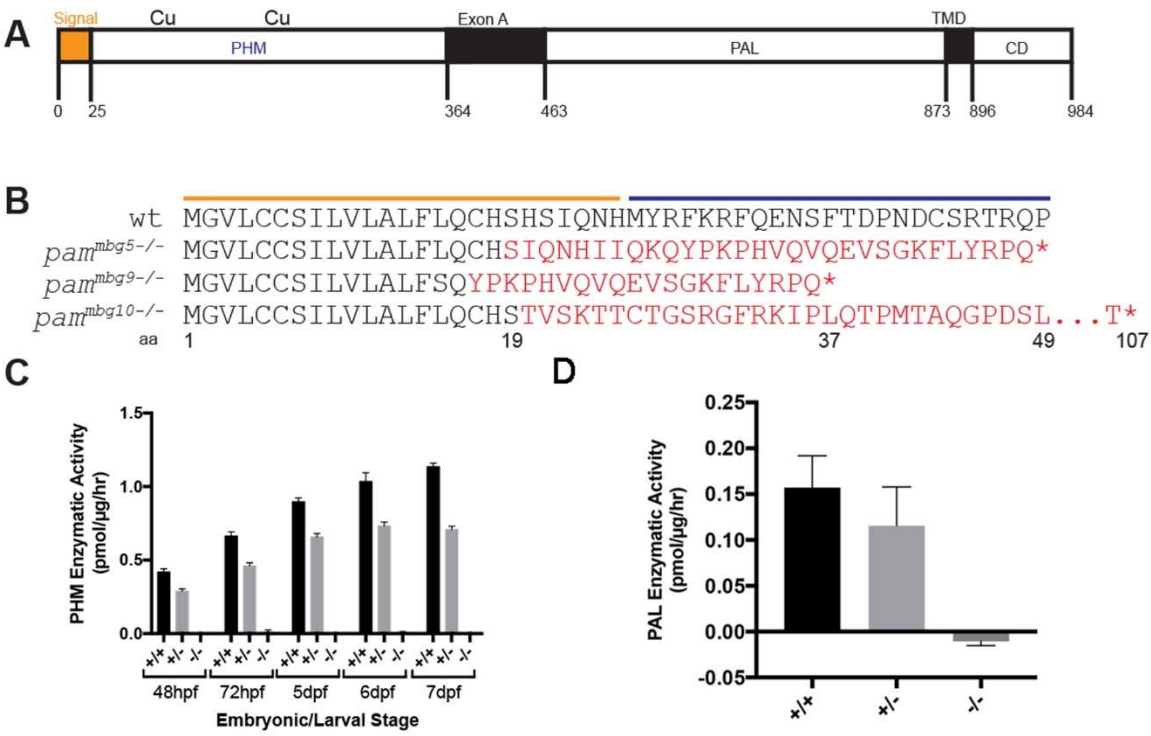

Fig 1. Generation of PAM$^{-/-}$ zebrafish. (A) Schematic depicting the domains in zebrafish PAM protein. Signal sequence (yellow), PHM domain and two copper-binding sites, the linker region (Exon A), the PAL domain, transmembrane domain (TMD) and cytosolic domain (CD) are shown; residue numbers indicate the boundaries corresponding to each domain. **(B)** Expected protein sequences for three PAM mutant lines generated through CRISPR-Cas9 genome editing. Frameshift mutations result in truncation of all three proteins near the beginning of the PHM domain. **(C)** PHM enzyme assays of embryos collected at different developmental stages from wild-type siblings (+/+), heterozygous (+/-) and homozygous (-/-) animals. Homozygous mutants contain no detectable PHM activity. **(D)** PAL enzyme activity in wild-type, PAM$^{+/-}$ and PAM$^{-/-}$ 7dpf zebrafish embryos.

the wild-type zebrafish embryos until 7 days post-fertilization (dpf) (Fig 1 C). A complete lack of PHM and PAL enzyme activity in PAM$^{-/-}$ embryos at all developmental stages indicate that the protein products generated as a result of the frameshifts in the homozygous mutant embryos are non-functional, as expected (Fig 1 C and D). Interestingly, PAM enzyme activity in heterozygous embryos was consistently more than 50% of the activity measured in the wild type animals (Fig 1 C and D).

PAM$^{-/-}$ zebrafish embryos display multiple cilia-related phenotypes

PAM null zebrafish embryos are phenotypically indistinguishable from wild-type siblings until 48hpf (Fig 2 A-D). At 72hpf, cardiac edema is apparent in PAM$^{-/-}$ embryos (asterisks in Fig 2 F compared to 2 E). At 96hpf, the PAM$^{-/-}$ embryos develop cystic kidneys (inset in Fig 2 H) and a smaller eye size (arrowhead in Fig 2 H) compared to wild-type siblings is apparent (Fig 2 G). Dorsal views of control (Fig 2 I) and PAM$^{-/-}$ (Fig 2 J) embryos at 96hpf show the increase in edema around the heart and gut in PAM$^{-/-}$ embryos (arrow in Fig 2 J). At 5dpf, PAM$^{-/-}$ zebrafish (Fig 2 L and N) develop severe edema around the heart (asterisks) and gut (arrow) compared to controls (Fig 2 K and M). Some mild hydrocephalus is also visible at this stage (red arrowhead in Fig 2 L) and the difference in eye size is more obvious (black arrowheads in Fig 2 L and N). PAM$^{-/-}$ zebrafish embryos ultimately die at around 10dpf, presumably due to severe edema that results from pronephric and cardiac dysfunction.

Thus, zebrafish lacking PAM recapitulate the edematous phenotype observed in PAM$^{-/-}$ mouse embryos at E14.5, but show additional defects in the kidney, eyes and brain. Development of fluid-filled cysts in the kidney, hydrocephalus and edema point to a defect in ciliary function; similar phenotypes have been observed in morphants that affect ciliary assembly such as *IFT88/polaris* and *IFT57/hippi*, which have reduced levels of intraflagellar transport proteins (Kramer-Zucker et al., 2005).

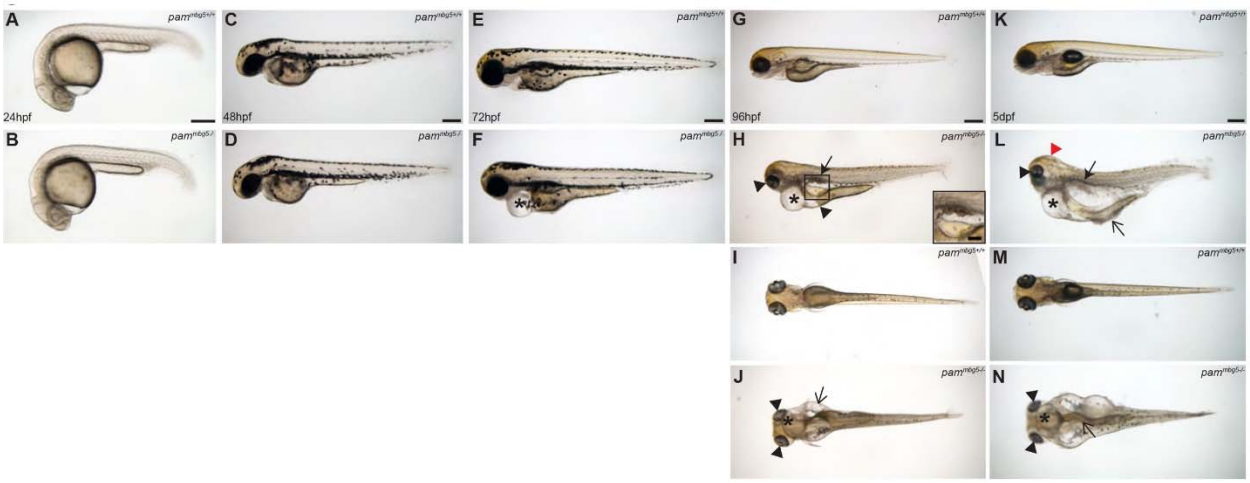

Fig 2. Phenotypic analysis of PAM$^{-/-}$ zebrafish embryos. Comparison of wild-type siblings **(A** and **C)** with PAM$^{-/-}$ mutants **(B, D)** shows no obvious difference at 24 and 48hpf. At 72hpf, PAM$^{-/-}$ embryos develop pericardial edema (asterisks in **F**)**.** Additional edema around the gut (arrow in **H** and **J**)**,** cysts in the kidney (inset in **H**) and smaller eyes (arrowheads in **H** and **J**) can be seen at 96hpf in the PAM$^{-/-}$ embryos **(H** and **J**) compared to controls. Severe edema develops at 5dpf in PAM$^{-/-}$ mutants (**L** and **N**). Additional edema in the brain is also visible (red arrowhead in **L**). Developmentally normal control animals at 5dpf are shown for comparison **(K** and **M**).

PAM$^{-/-}$ zebrafish embryos lack brush border microvilli in the pronephros and subsequently show defects in ciliogenesis.

Based on our phenotypic analysis suggesting ciliary dysfunction, we used transmission electron microscopy to examine the pronephros of 72hpf and 6dpf mutant and wild-type embryos. At 72hpf, we observed a striking loss of brush border microvilli in the PAM$^{-/-}$ zebrafish embryos, compared to the control embryos, where the lumen was occluded with a dense outer array of microvilli surrounding tightly packed cilia (Fig 3). The cilia observed in the PAM$^{-/-}$ mutants appeared to have normal ultrastructure (Fig 3). At 6dpf, the control pronephric lumen was open and contained multiple 9+2 cilia surrounded by apical brush border microvilli. However, the pronephros in the PAM$^{-/-}$ animals lacked microvilli and had very few cilia. Intriguingly, at this stage we also found a few axonemes that had assembled in the cytoplasm of the mutant embryo pronephros cells. These ectopically localized axonemes were not surrounded by a membrane and appeared to have normal morphology (bottom right panel inset in Fig 3); we observed a similar cytosolic axoneme assembly phenotype in planaria following RNAi-mediated reduction of total PAM expression. The occurrence of ectopic cytosolic axonemes lacking a ciliary membrane points to a defect in basal body docking in PAM$^{-/-}$ zebrafish. Thus, loss of brush border microvilli precedes loss of cilia in the pronephros of PAM$^{-/-}$ zebrafish.

PAM co-localizes with apical actin in ciliated airway epithelial cells

We previously showed that PAM localizes in foci along the length of cilia in airway epithelial cells, and at the base of these cilia adjacent to basal bodies stained with gamma-tubulin antibody (Kumar et al., 2016a). Transmission electron micrographs of wild type mouse trachea show a dense array of microvilli at the apical surface of ciliated epithelial cells (Fig 4 A). In order to explore the localization of PAM at the apical surface of these cells, we performed immunoelectron microscopy using a primary antibody to the luminal domain of PAM and a gold-tagged secondary antibody. In wild type mouse tracheal epithelial cells, PAM was present along

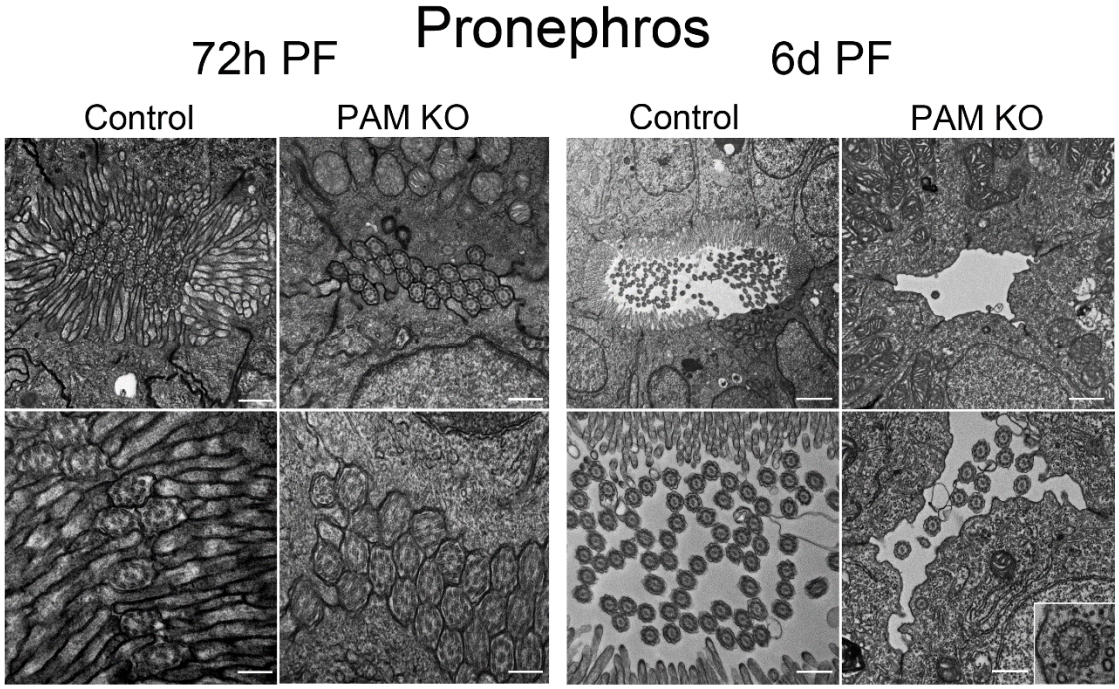

Fig 3. Ultrastructural analysis of control and mutant pronephros. At 72hpf, the kidney lumen of wild-type zebrafish embryos is occluded and numerous cilia surrounded by apical microvilli are visible. Although cilia are visible in the pronephric lumen of PAM$^{-/-}$ zebrafish at this stage, brush border microvilli are entirely absent. At 6dpf, the PAM$^{-/-}$ pronephros shows a severe reduction in the number of cilia along with the absence of a brush border. The kidney lumen of wild-type zebrafish is more open at this stage, yet numerous cilia and microvilli are present. Occasional cytosolic axonemes are also observed in PAM$^{-/-}$ embryos (inset in lower panel).

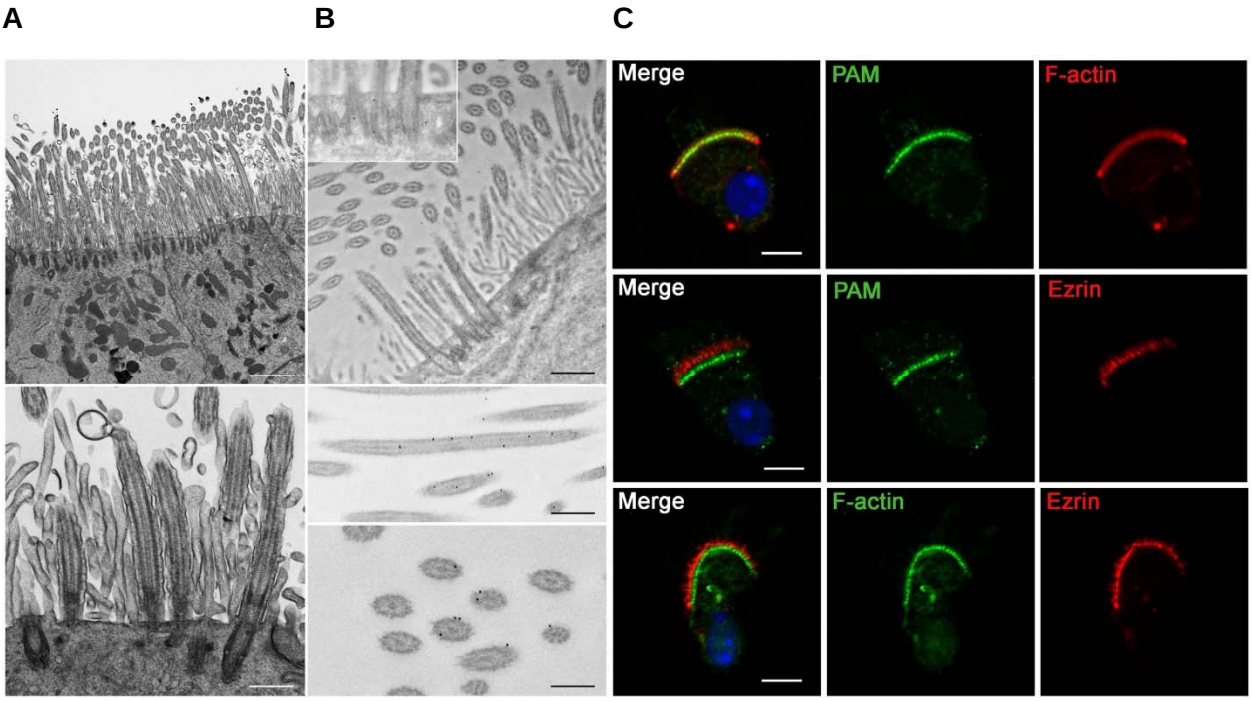

Fig 4. PAM co-localizes with apical F-actin in ciliated airway epithelial cells. (A) Transmission electron micrograph of wild-type mouse trachea shows cilia emanating from a dense array of microvilli at the apical end of the epithelial cells. Scale bar = 2 μm and 500 nm. **(B)** Immunogold labeling of tracheal epithelial cells with an antibody to PAM shows close association of PAM with basal bodies and localization along the length of the cilia. Scale bars = 500, 500 and 250 nm. **(C)** Top panel - Immunostaining of wild type mouse airway epithelial cells with Bodipy-Phalloidin (red) and PAM antibody (green). Scale bar = 5 μm. Center panel - Immunostaining of wild type mouse airway epithelial cells with ezrin (red) and PAM (green) antibodies. Scale bar = 5 μm. Bottom panel - Immunostaining of wild type mouse airway epithelial cells with FITC-Phalloidin (green) and ezrin antibody (red). Scale bar = 5 μm.

the length of cilia (Fig 4 B). In cross sections of cilia, gold particles were detected close to the microtubules (Fig 4 B); PAM was also found to be closely associated with basal bodies in these cells (Fig 4 B and inset).

Since, basal bodies are closely associated with the actin cytoskeleton in polarized tracheal epithelial cells (Pan et al., 2007), we co-labeled airway epithelial cells with fluorescently tagged phalloidin, a fungal toxin that preferentially binds filamentous actin, and antibodies to PAM. PAM co-localized with filamentous actin at the apical surface of the tracheal epithelial cells (Fig 4 C). To test if this staining corresponds to the sub-apical actin web or the cell-proximal region of the microvilli themselves, we immunostained tracheal cells with an antibody to ezrin, a microvillus marker and PAM. Ezrin staining was apical to PAM staining in these cells (Fig 4 C); ezrin was predominantly localized in microvilli which were not detected strongly with phalloidin (Fig 4 C). Collectively, these results suggest a close association of PAM with the apical actin network in polarized tracheal epithelial cells.

Cellular morphology is altered in PAM$^{-/-}$ mouse embryonic fibroblasts

Many aspects of cell morphology depend on the actin cytoskeleton. To explore morphological changes in a tractable mammalian cell culture model, we generated two sets of SV-40 large T antigen-immortalized mouse embryonic fibroblasts (MEFs) from embryonic day 12.5 PAM$^{-/-}$ and wild-type littermate embryos. PAM$^{-/-}$ MEFs were significantly smaller in size than wild-type cells (Fig 5 A). Nuclear size is proportional to cell size (Huber and Gerace, 2007); the nuclei in PAM$^{-/-}$ MEFs were significantly smaller than the nuclei in wild-type MEFs (Fig 5 B).

We next evaluated Golgi morphology using antibody to GM130, a cis-Golgi marker. In wild-type MEFs, GM130 staining showed a perinuclear pattern that surrounded much of the nucleus. In PAM$^{-/-}$ MEFs, GM130 staining surrounded a smaller fraction of the nucleus (Fig 5 C). This difference was quantified by measuring the angle formed by drawing lines from the edges of the

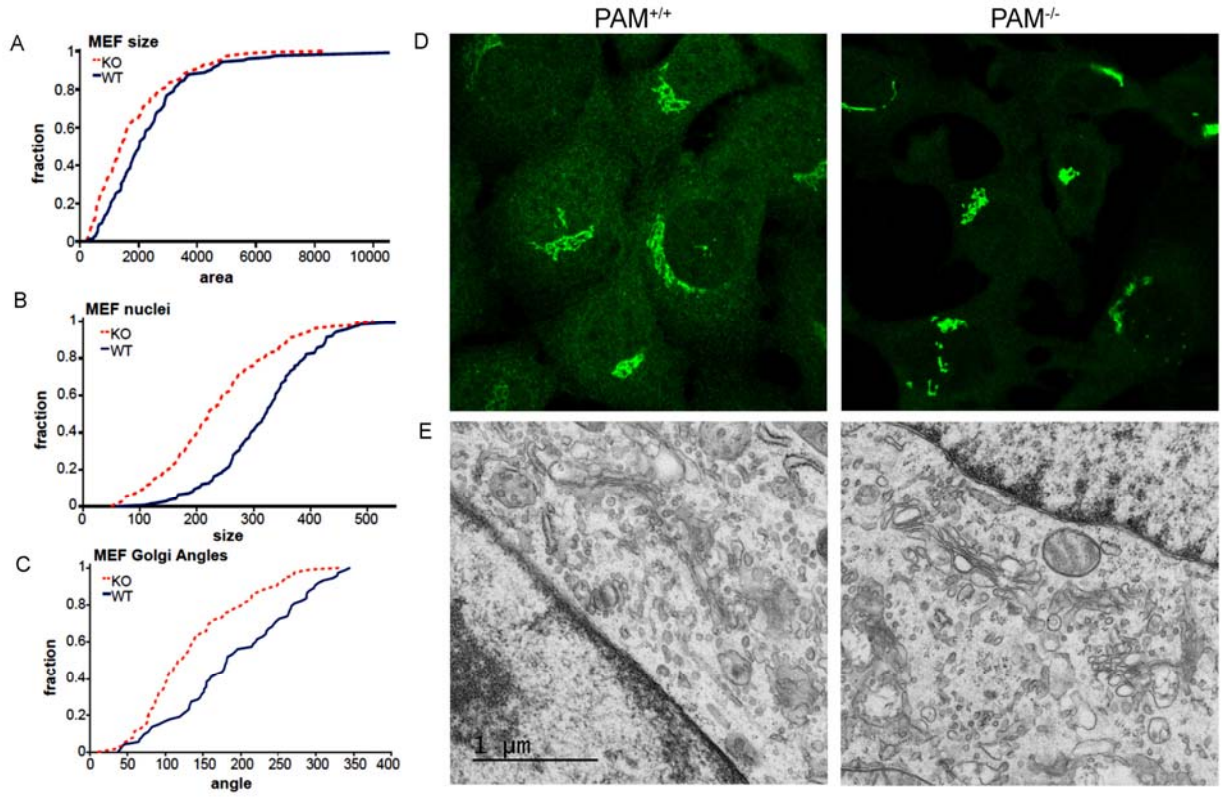

Fig 5. PAM$^{-/-}$ MEFs display altered cell morphology. (A) Kolmogorov-Smirnov plot shows a difference in cell size between wild-type (WT) and PAM$^{-/-}$ (KO) MEFs. PAM$^{-/-}$ MEFs are significantly smaller than wild-type MEFs. **(B)** Nuclei in PAM$^{-/-}$ MEFs are significantly smaller than wild-type MEFs. **(C)** Golgi is more compact in PAM$^{-/-}$ MEFs. The angle formed by drawing lines from the edge of the Golgi cisternae, as observed with GM130 staining, was measured. **(D)** Mannosidase II staining and **(E)** transmission electron microscopy analysis confirms changes in Golgi morphology in PAM-deficient MEFs.

Golgi cisternae to the center of the nuclus. Differences in Golgi morphology were also apparent using an antibody to mannosidase II, a mid-Golgi marker (Fig 5 D), and in transmission electron micrographs, where the Golgi also appeared to be fragmented in the PAM$^{-/-}$ fibroblasts compared to wild type cells (Fig 5 E).

Actin cytoskeleton is altered in PAM deficient *Chlamydomonas* cells

Overexpression of PAM remodels the actin cytoskeleton in mammalian cells (Ciccotosto et al., 1999). We previously showed that knockdown of PAM in *Chlamydomonas* using an artificial microRNA approach resulted in the inability of cells to assemble a cilium. Furthermore, the peri-basal body localization of intraflagellar transport (IFT) proteins required to assemble cilia was disrupted in the knockdown cells (Chapter 4). Using pharmacological actin inhibitors and actin mutants, a previous study showed that actin regulates localization of IFT proteins at the ciliary base and regulates their entry into the cilium in *Chlamydomonas* (Avasthi et al., 2014). To determine if the aberrant localization of IFT components in PAM amiRNA cells was accompanied by alterations in the actin cytoskeleton, we stained *Chlamydomonas* control and amiRNA PAM knockdown cells with fluorescently tagged phalloidin. Control cells displayed a mostly diffuse cytoplasmic staining, with some stronger perinuclear signal (Fig 6 A). However, in the PAM knockdown cells, bright foci of filamentous actin were visible (Fig 6 B and C), often close to the ciliary stubs (arrows in b and c). Thus, the functional association of PAM with actin is evolutionarily conserved.

DISCUSSION

PAM regulates the actin cytoskeleton and cell morphology

Previous studies have pointed to a connection between PAM and the actin cytoskeleton. The ability of the cytosolic domain of PAM to interact with Kalirin and Trio, Rho GEFs for small GTP binding proteins known to regulate actin cytoskeletal organization, is thought to play an

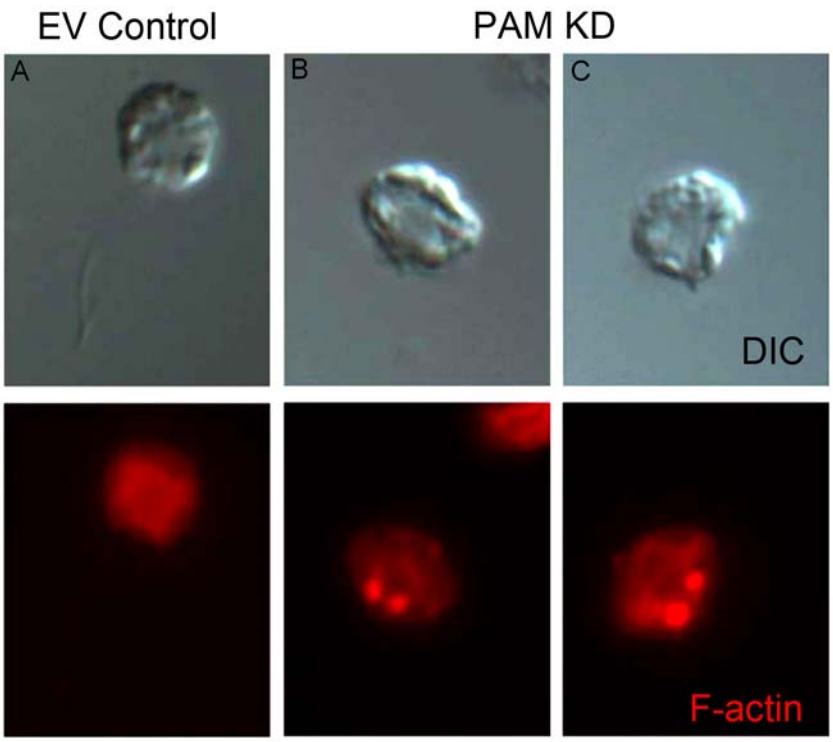

Fig 6. Knockdown of PAM disrupts the actin cytoskeleton in *Chlamydomonas* cells. (A) Control cell with two cilia visible in DIC shows diffuse F-actin staining (red) in the cell body. **(B)** and **(C)** Two examples of PAM amiRNA *Chlamydomonas* cells; these cells only form ciliary stubs (black arrows) and show bright foci of F-actin staining in the cell body.

essential role in the ability of PAM to affect neuroendocrine cell morphology (Alam et al., 1996; Mains et al., 1999). Overexpression of PAM in murine neuroendocrine cells alters the actin cytoskeleton and inhibits the regulated exocytosis of secretory vesicle content (Ciccotosto et al., 1999). In this study, we find that the absence of PAM leads to the loss of actin-based microvilli in zebrafish embryos (Fig 3) and that a reduction in PAM expression affects the actin cytoskeleton in *Chlamydomonas*, thereby revealing an evolutionarily conserved functional association between PAM and actin (Fig 6). The cytosolic domain of PAM is not highly conserved, suggesting that species specific interactions may be used accomplish a similar task in different organisms.

We demonstrate that several features regulated by the actin cytoskeleton - cell size, nuclear size and Golgi architecture - are altered in the $PAM^{-/-}$ MEFs (Fig 5). Nuclear size is proportional to cell size and many factors controlling nuclear size, such as the LINC (linker of nucleoskeleton and cytoskeleton) complex components, including nesprin-2, have been described (Jevtic et al., 2014). Nesprin-2 is thought to regulate nuclear size by linking the outer nuclear membrane to F-actin through its actin-binding domain (Lu et al., 2012; Luke et al., 2008). Furthermore, depolymerization of F-actin results in smaller nuclei, while microtubule depolymerization enlarges nuclear size (Lu et al., 2012; Luke et al., 2008).

The Golgi is also more compact when the actin cytoskeleton is compromised by actin-depolymerizing drugs such as the latrunculins (di Campli et al., 1999; Lazaro-Dieguez et al., 2006; Valderrama et al., 1998). Disruption of actin-binding partners including the Arp2/3 activator WHAMM, cortactin and formin-like 1 (FMNL1) also leads to morphological abnormalities in the Golgi (Campellone et al., 2008; Colon-Franco et al., 2011; Dippold et al., 2009; Kirkbride et al., 2012). Thus, disruption of the actin cytoskeleton may contribute to the altered Golgi organization seen in $PAM^{-/-}$ MEFs.

The actin cytoskeleton has been implicated in the assembly of both primary and motile cilia (Kim et al., 2010; Pan et al., 2007). In primary ciliated cells, actin is thought to regulate ciliogenesis through the transcriptional coactivators YAP/TAZ and vesicular trafficking (Kim et al., 2015). In multicilated cells, the actin cytoskeleton is required for establishment of planar cell polarity and migration of basal bodies formed in the cytoplasm to the apical surface (Boisvieux-Ulrich et al., 1990; Lemullois et al., 1988). The transcriptional regulator Foxj1 that regulates motile ciliogenesis, also affects the formation of a RhoA-mediated apical actin web that aids in basal body docking (Pan et al., 2007). Loss of planar cell polarity pathway components such as Fuzzy and Inturned also affects ciliogenesis and apical actin in *Xenopus* embryos (Park et al., 2006). Furthermore, existence of a ciliary adhesion complex that links basal bodies to the actin cytoskeleton has been postulated based on the presence of focal adhesion proteins (FAK, vinculin and paxillin) in *Xenopus* multiciliated cells (Antoniades et al., 2014).

PAM is closely associated with basal bodies and is present in close proximity to the filamentous actin network detected with phalloidin at the apical surface of tracheal epithelial cells (Fig 4). The actin nucleator cordon-bleu displays a similar, overlapping localization with F-actin at the apical ends of several ciliated cells (in pronephric tubules, nasal pit and neural tube) in zebrafish. Interestingly, loss of cordon-bleu reduces F-actin staining in Kupffer's vesicle and affects ciliary assembly in Kupffer's vesicle and in the pronephros (Ravanelli and Klingensmith, 2011).

Role of PAM in assembly of microvilli and cilia

In mice, deletion of the *PAM* gene results in massive edema and mid-embryonic lethality. However, the source of this edema, first observed in the cardiac region early in development, is unknown (Czyzyk et al., 2005). $PAM^{-/-}$ zebrafish embryos recapitulate the mutant mouse phenotype and additionally, display several striking features, such as hydrocephalus and cystic kidneys, which point to ciliary dysfunction in the brain and pronephros, respectively (Fig 2).

Ultrastructural analysis confirmed a defect in ciliogenesis in the absence of PAM in the pronephros (Fig 3). However, the striking loss of microvilli in the pronephros, which preceded the loss of cilia, suggests that alterations in the actin cytoskeleton contribute to defective ciliogenesis. Furthermore, the connection between PAM, ciliogenesis and the kidney defects observed in zebrafish, suggest that PAM is a novel candidate gene for cystic kidney and ciliary disease.

It is becoming increasingly clear that there is extensive cross-talk between the actin cytoskeleton, ciliogenesis and microvillus assembly. Highly specialized cells, such as those forming the multiciliated epithelia of the ventricles and trachea, must establish apical-basal polarity and subsequently assemble microvilli and cilia on their apical surface. This cell polarization depends heavily on a functionally intact cytoskeleton and polarized membrane trafficking (Rodriguez-Boulan and Macara, 2014). Several polarity factors such as atypical protein kinase C (aPKC), Par3 and Crumbs3 have been implicated in the assembly of cilia (Fan et al., 2004; Rodriguez-Boulan and Macara, 2014). Furthermore, mutations in ciliary axonemal dynein assembly factors, including LRRC50 and DYX1C1, disrupt both cilia and brush border microvilli in the zebrafish pronephros, although the reason is unknown (Chandrasekar et al., 2013; van Rooijen et al., 2008). Collectively, our data suggest a model whereby PAM controls reorganization of the actin cytoskeleton to regulate both ciliogenesis and microvillar assembly.

MATERIAL AND METHODS

Chlamydomonas Cell Culture

Chlamydomonas cells transformed with plasmids containing artificial micro RNA sequences directed against PAM were generated as described previously (Chapter 3). Cells were grown in TAP medium (Kropat et al., 2011) under constant light in a shaking incubator at 22°C.

Mouse embryonic fibroblasts

Male and female PAM$^{+/-}$ C57BL/6 mice were mated for one night and embryos were harvested at 12 days gestational age. After removal of the tail for RT-PCR genotyping, individual whole embryos were cleaned of placenta and internal red organs, diced, and dissociated with 0.25% Trypsin-0.53 mM EDTA (Life Science or Gemini [both were used]), triturated, and filtered through a 40 µm filter. Cells were grown in a T75 flasks or 6-well dishes, using DMEM-F12 (Lonza) with Pen-Strep (Mediatech), HEPES (Mediatech), and 10% fetal bovine serum (Hyclone). The genotype of each line was verified by RT-PCR and by quantitative real-time PCR on the cultured cells after more than 20 passages, and by PHM enzyme assay of cell extracts. Cells were typically passaged twice a week with Trypsin-EDTA using a 3- or 4-fold dilution. Cell lines were immortalized using the vector Ef1a_Large_T-antigen_Ires_Puro (Addgene 318922). A 50% confluent T75 flask was transfected with 20 µg vector and 30 µl Lipofectamine-2000 (Life Science), followed by selection with 0.4 µg/ml puromycin. After cells died off and colonies grew up, cells were passaged every other day with a 1:4 split, and after a month a 1:10 split was used every second day.

Immunofluorescence

Chamydomonas cells and tracheal epithelial cells (isolated from wild-type mice) were immunostained as described previously (Kumar et al., 2016a; Pedersen et al., 2007). The following antibodies/stains were used: affinity-purified rabbit polyclonal PAM JH629 antibody (1:3000), Bodipy-phalloidin (1:1000) (ThermoFisher Scientific), mouse monoclonal GM130 antibody (1:1000) (BD Transduction Laboratories). Hoechst 33342 (ThermoFisher Scientific) was used to stain the nucleus.

Zebrafish protocols

Zebrafish were maintained according to Marine Biology Laboratory institutional guidelines. CRISPR-Cas9 mediated mutagenesis was carried out as described (Hwang et al., 2013).

Electron microscopy was performed as described (Malicki et al., 2011). Sections were visualized in a Hitachi H-7650 transmission electron microscope at 80kV.

For preparation of zebrafish embryo lysates for enzyme assays, embryos were homogenized in low ionic strength buffer (20 mM Na TES, 10 mM mannitol) containing 1% Triton X-100 and protease inhibitors. Following two rounds of freeze thaw, samples were incubated at 4°C for 20 minutes and then centrifuged at 18,000 × g for 15 minutes at 4°C to collect soluble fractions. PHM and PAL enzyme assays were performed as described (Kolhekar et al., 1997).

ACKNOWLEDGEMENTS

We thank Maya Yankova (UCHC Electron Microscopy Facility) for help with the zebrafish samples and Andrew Yanik (UCHC Neuropeptide laboratory) for outstanding technical assistance. This work was supported by grants DK032949 (to BAE) and GM051293 (to SMK) from the National Institutes of Health.

AUTHOR CONTRIBUTIONS

Rebecca Thomason performed most of the zebrafish experiments in Jonathan Gitlin's laboratory at the Marine Biological Laboratory, Woods Hole, MA. Nils Back did the mannosidase staining and the electron microscopy analysis on the MEFs. Richard Mains generated large T antigen immortalized MEF cell lines. Dhivya Kumar performed the enzyme assays on the zebrafish samples and conducted the remaining experiments under the guidance of Betty Eipper, Richard Mains and Stephen King.

REFERENCES

Alam, M. R., Caldwell, B. D., Johnson, R. C., Darlington, D. N., Mains, R. E. and Eipper, B. A. (1996). Novel proteins that interact with the COOH-terminal cytosolic routing determinants of an integral membrane peptide-processing enzyme. *J Biol Chem* **271**, 28636-40.

Antoniades, I., Stylianou, P. and Skourides, P. A. (2014). Making the connection: ciliary adhesion complexes anchor basal bodies to the actin cytoskeleton. *Dev Cell* **28**, 70-80.

Avasthi, P., Onishi, M., Karpiak, J., Yamamoto, R., Mackinder, L., Jonikas, M. C., Sale, W. S., Shoichet, B., Pringle, J. R. and Marshall, W. F. (2014). Actin is required for IFT regulation in *Chlamydomonas* reinhardtii. *Curr Biol* **24**, 2025-32.

Boisvieux-Ulrich, E., Laine, M. C. and Sandoz, D. (1990). Cytochalasin D inhibits basal body migration and ciliary elongation in quail oviduct epithelium. *Cell Tissue Res* **259**, 443-54.

Boon, M., Jorissen, M., Proesmans, M. and De Boeck, K. (2013). Primary ciliary dyskinesia, an orphan disease. *Eur J Pediatr* **172**, 151-62.

Bornens, M. (2008). Organelle positioning and cell polarity. *Nat Rev Mol Cell Biol* **9**, 874-86.

Brown, J. M. and Witman, G. B. (2014). Cilia and diseases. *Bioscience* **64**, 1126-1137.

Campellone, K. G., Webb, N. J., Znameroski, E. A. and Welch, M. D. (2008). WHAMM is an Arp2/3 complex activator that binds microtubules and functions in ER to Golgi transport. *Cell* **134**, 148-61.

Chandrasekar, G., Vesterlund, L., Hultenby, K., Tapia-Paez, I. and Kere, J. (2013). The zebrafish orthologue of the dyslexia candidate gene DYX1C1 is essential for cilia growth and function. *PLoS One* **8**, e63123.

Ciccotosto, G. D., Schiller, M. R., Eipper, B. A. and Mains, R. E. (1999). Induction of integral membrane PAM expression in AtT-20 cells alters the storage and trafficking of POMC and PC1. *J Cell Biol* **144**, 459-71.

Colon-Franco, J. M., Gomez, T. S. and Billadeau, D. D. (2011). Dynamic remodeling of the actin cytoskeleton by FMNL1gamma is required for structural maintenance of the Golgi complex. *J Cell Sci* **124**, 3118-26.

Crawley, S. W., Mooseker, M. S. and Tyska, M. J. (2014). Shaping the intestinal brush border. *J Cell Biol* **207**, 441-51.

Czyzyk, T. A., Ning, Y., Hsu, M. S., Peng, B., Mains, R. E., Eipper, B. A. and Pintar, J. E. (2005). Deletion of peptide amidation enzymatic activity leads to edema and embryonic lethality in the mouse. *Dev Biol* **287**, 301-13.

di Campli, A., Valderrama, F., Babia, T., De Matteis, M. A., Luini, A. and Egea, G. (1999). Morphological changes in the Golgi complex correlate with actin cytoskeleton rearrangements. *Cell Motil Cytoskeleton* **43**, 334-48.

Dippold, H. C., Ng, M. M., Farber-Katz, S. E., Lee, S. K., Kerr, M. L., Peterman, M. C., Sim, R., Wiharto, P. A., Galbraith, K. A., Madhavarapu, S. et al. (2009). GOLPH3 bridges phosphatidylinositol-4- phosphate and actomyosin to stretch and shape the Golgi to promote budding. *Cell* **139**, 337-51.

Fan, S., Hurd, T. W., Liu, C. J., Straight, S. W., Weimbs, T., Hurd, E. A., Domino, S. E. and Margolis, B. (2004). Polarity proteins control ciliogenesis via kinesin motor interactions. *Curr Biol* **14**, 1451-61.

Fliegauf, M., Benzing, T. and Omran, H. (2007). When cilia go bad: cilia defects and ciliopathies. *Nat Rev Mol Cell Biol* **8**, 880-93.

Huber, M. D. and Gerace, L. (2007). The size-wise nucleus: nuclear volume control in eukaryotes. *J Cell Biol* **179**, 583-4.

Hwang, W. Y., Fu, Y., Reyon, D., Maeder, M. L., Tsai, S. Q., Sander, J. D., Peterson, R. T., Yeh, J. R. and Joung, J. K. (2013). Efficient genome editing in zebrafish using a CRISPR-Cas system. *Nat Biotechnol* **31**, 227-9.

Jevtic, P., Edens, L. J., Vukovic, L. D. and Levy, D. L. (2014). Sizing and shaping the nucleus: mechanisms and significance. *Curr Opin Cell Biol* **28**, 16-27.
Jimenez, A. J., Dominguez-Pinos, M. D., Guerra, M. M., Fernandez-Llebrez, P. and Perez-Figares, J. M. (2014). Structure and function of the ependymal barrier and diseases associated with ependyma disruption. *Tissue Barriers* **2**, e28426.
Kathem, S. H., Mohieldin, A. M. and Nauli, S. M. (2014). The roles of primary cilia in polycystic kidney disease. *AIMS Mol Sci* **1**, 27-46.
Kim, J., Jo, H., Hong, H., Kim, M. H., Kim, J. M., Lee, J. K., Heo, W. D. and Kim, J. (2015). Actin remodelling factors control ciliogenesis by regulating YAP/TAZ activity and vesicle trafficking. *Nat Commun* **6**, 6781.
Kim, J., Lee, J. E., Heynen-Genel, S., Suyama, E., Ono, K., Lee, K., Ideker, T., Aza-Blanc, P. and Gleeson, J. G. (2010). Functional genomic screen for modulators of ciliogenesis and cilium length. *Nature* **464**, 1048-51.
Kirkbride, K. C., Hong, N. H., French, C. L., Clark, E. S., Jerome, W. G. and Weaver, A. M. (2012). Regulation of late endosomal/lysosomal maturation and trafficking by cortactin affects Golgi morphology. *Cytoskeleton (Hoboken)* **69**, 625-43.
Kolhekar, A. S., Mains, R. E. and Eipper, B. A. (1997). Peptidylglycine alpha-amidating monooxygenase: an ascorbate-requiring enzyme. *Methods Enzymol* **279**, 35-43.
Kramer-Zucker, A. G., Olale, F., Haycraft, C. J., Yoder, B. K., Schier, A. F. and Drummond, I. A. (2005). Cilia-driven fluid flow in the zebrafish pronephros, brain and Kupffer's vesicle is required for normal organogenesis. *Development* **132**, 1907-21.
Kropat, J., Hong-Hermesdorf, A., Casero, D., Ent, P., Castruita, M., Pellegrini, M., Merchant, S. S. and Malasarn, D. (2011). A revised mineral nutrient supplement increases biomass and growth rate in *Chlamydomonas reinhardtii*. *Plant J* **66**, 770-80.
Kumar, D., Blaby-Haas, C. E., Merchant, S. S., Mains, R. E., King, S. M. and Eipper, B. A. (2016a). Early eukaryotic origins for cilia-associated bioactive peptide-amidating activity. *J Cell Sci* **129**, 943-956.
Kumar, D., Mains, R. E. and Eipper, B. A. (2016b). 60 YEARS OF POMC: From POMC and alpha-MSH to PAM, molecular oxygen, copper, and vitamin C. *J Mol Endocrinol* **56**, T63-76.
Lazaro-Dieguez, F., Jimenez, N., Barth, H., Koster, A. J., Renau-Piqueras, J., Llopis, J. L., Burger, K. N. and Egea, G. (2006). Actin filaments are involved in the maintenance of Golgi cisternae morphology and intra-Golgi pH. *Cell Motil Cytoskeleton* **63**, 778-91.
Lemullois, M., Boisvieux-Ulrich, E., Laine, M. C., Chailley, B. and Sandoz, D. (1988). Development and functions of the cytoskeleton during ciliogenesis in metazoa. *Biol Cell* **63**, 195-208.
Lu, W., Schneider, M., Neumann, S., Jaeger, V. M., Taranum, S., Munck, M., Cartwright, S., Richardson, C., Carthew, J., Noh, K. et al. (2012). Nesprin interchain associations control nuclear size. *Cell Mol Life Sci* **69**, 3493-509.
Luke, Y., Zaim, H., Karakesisoglou, I., Jaeger, V. M., Sellin, L., Lu, W., Schneider, M., Neumann, S., Beijer, A., Munck, M. et al. (2008). Nesprin-2 Giant (NUANCE) maintains nuclear envelope architecture and composition in skin. *J Cell Sci* **121**, 1887-98.
Mains, R. E., Alam, M. R., Johnson, R. C., Darlington, D. N., Back, N., Hand, T. A. and Eipper, B. A. (1999). Kalirin, a multifunctional PAM COOH-terminal domain interactor protein, affects cytoskeletal organization and ACTH secretion from AtT-20 cells. *J Biol Chem* **274**, 2929-37.
Malicki, J., Avanesov, A., Li, J., Yuan, S. and Sun, Z. (2011). Analysis of cilia structure and function in zebrafish. *Methods Cell Biol* **101**, 39-74.
McConnell, R. E., Higginbotham, J. N., Shifrin, D. A., Jr., Tabb, D. L., Coffey, R. J. and Tyska, M. J. (2009). The enterocyte microvillus is a vesicle-generating organelle. *J Cell Biol* **185**, 1285-98.

Nauli, S. M., Alenghat, F. J., Luo, Y., Williams, E., Vassilev, P., Li, X., Elia, A. E., Lu, W., Brown, E. M., Quinn, S. J. et al. (2003). Polycystins 1 and 2 mediate mechanosensation in the primary cilium of kidney cells. *Nat Genet* **33**, 129-37.
Pan, J., You, Y., Huang, T. and Brody, S. L. (2007). RhoA-mediated apical actin enrichment is required for ciliogenesis and promoted by Foxj1. *J Cell Sci* **120**, 1868-76.
Park, T. J., Haigo, S. L. and Wallingford, J. B. (2006). Ciliogenesis defects in embryos lacking inturned or fuzzy function are associated with failure of planar cell polarity and Hedgehog signaling. *Nat Genet* **38**, 303-11.
Pedersen, L. B., Rompolas, P., Christensen, S. T., Rosenbaum, J. L. and King, S. M. (2007). The lissencephaly protein Lis1 is present in motile mammalian cilia and requires outer arm dynein for targeting to *Chlamydomonas* flagella. *J Cell Sci* **120**, 858-67.
Ravanelli, A. M. and Klingensmith, J. (2011). The actin nucleator Cordon-bleu is required for development of motile cilia in zebrafish. *Dev Biol* **350**, 101-11.
Revenu, C., Ubelmann, F., Hurbain, I., El-Marjou, F., Dingli, F., Loew, D., Delacour, D., Gilet, J., Brot-Laroche, E., Rivero, F. et al. (2012). A new role for the architecture of microvillar actin bundles in apical retention of membrane proteins. *Mol Biol Cell* **23**, 324-36.
Rodriguez-Boulan, E. and Macara, I. G. (2014). Organization and execution of the epithelial polarity programme. *Nat Rev Mol Cell Biol* **15**, 225-42.
Rostgaard, J. and Thuneberg, L. (1972). Electron microscopical observations on the brush border of proximal tubule cells of mammalian kidney. *Z Zellforsch Mikrosk Anat* **132**, 473-96.
Sauvanet, C., Wayt, J., Pelaseyed, T. and Bretscher, A. (2015). Structure, regulation, and functional diversity of microvilli on the apical domain of epithelial cells. *Annu Rev Cell Dev Biol* **31**, 593-621.
Valderrama, F., Babia, T., Ayala, I., Kok, J. W., Renau-Piqueras, J. and Egea, G. (1998). Actin microfilaments are essential for the cytological positioning and morphology of the Golgi complex. *Eur J Cell Biol* **76**, 9-17.
van Rooijen, E., Giles, R. H., Voest, E. E., van Rooijen, C., Schulte-Merker, S. and van Eeden, F. J. (2008). LRRC50, a conserved ciliary protein implicated in polycystic kidney disease. *J Am Soc Nephrol* **19**, 1128-38.
Werner, M. E., Hwang, P., Huisman, F., Taborek, P., Yu, C. C. and Mitchell, B. J. (2011). Actin and microtubules drive differential aspects of planar cell polarity in multiciliated cells. *J Cell Biol* **195**, 19-26.

Chapter 7

Significance and Future Directions

Over the years, several cell biological, molecular and developmental aspects of PAM biology have been investigated in great detail in mammalian systems. These studies have unearthed a vast amount of information on its enzymatic activity, processing, structure and the critical roles played by this enzyme in the neuroendocrine system (Chapter 2). Along the way, multiple studies have pointed to additional non-neural roles for PAM, yet, this possibility was not explored in any systematic manner. In 2012, a phylogenetic study surveyed several eukaryotic genomes and made the surprising discovery that *PAM*-like genes were present in the genomes of green algae and sponges, both of which lack anything resembling a neuroendocrine system (Attenborough et al., 2012).

Building on this intriguing finding, we found that the genome of the unicellular, green alga, *Chlamydomonas reinhardtii*, encoded active PAM enzyme (Chapter 3). More unexpected was our finding that the enzyme localized to the Golgi and the cilium in *Chlamydomonas* cells and in mammalian cells (Chapter 3). The presence of PAM in mammalian motile and sensory cilia suggested to us that this enzyme has an evolutionarily conserved, critical signaling or sensory role requiring its presence in this compartment.

A new role for an old enzyme

The obvious next step was to determine the role of this enzyme in *Chlamydomonas* and in cilia. Recognizing that these roles might be disparate, we utilized additional ciliary model systems including the planarian, *Schmidtea mediterranea,* zebrafish and a previously generated mouse mutant (Czyzyk et al., 2005). Interestingly, disruption of PAM in each of these model systems greatly impaired the assembly of cilia (Chapter 4). In *Chlamydomonas*, ciliary assembly is halted at very early stages when CrPAM expression is reduced and results in stubs filled with electron

dense material and fragmented microtubules. In planaria, the phenotype is that of severe ciliary loss from the ventral epithelium, with the unusual appearance of 'naked' axonemes (lacking a membrane) neatly arranged in the cytoplasm, just below the apical plasma membrane. Primary cilia in the neuroepithelium of PAM-deficient mouse embryos are stunted, while in zebrafish, ciliogenesis is impacted in the pronephros (kidney), leading to the development of renal cysts and edema (Chapter 6).

While these results underscore the evolutionarily conserved requirement of PAM for ciliogenesis, they also highlight the great diversity observed in ciliary assembly and function. Not all cilia are built in the same way, and they certainly do not all perform the same functions (Chapter 1). Moving forward, special attention must be paid to cell- and tissue- specific ciliogenesis pathways along with genetic modifiers that lead to these phenotypic variations.

How might a bioactive peptide amidating enzyme influence ciliogenesis? Currently it is unknown whether the enzymatic activity of PAM is required for this process. Answering this question is absolutely key to understanding the mechanism and will guide the discovery of either novel amidated products (peptides or lipids) or functional interactors that regulate ciliogenesis along with PAM (Fig 1). A complementary approach will be to utilize comparative genomics and phylogenetic tools to identify the ciliogenesis machinery 'functional module' to which PAM belongs (Sung and Leroux, 2013). Although the distribution of the *PAM* gene largely correlates with the presence of cilia, there are notable exceptions to this rule; for example, PAM has been lost in excavates (such as *Trypanosoma*) and Chromalveolates (such as *Tetrahymena*) (Chapter 3). Thus, identifying genes that are expressed in organisms that have PAM but have been lost in organisms lacking PAM may reveal a unique sub-set of genes that affect ciliogenesis. Recently, we performed RNA sequencing to identify global gene expression changes that occur in *Chlamydomonas* cells in the absence of PAM (preliminary results, unpublished). Transcription of a subset of uncharacterized ciliary genes (flagellar associated

proteins or FAPs) were differentially regulated in PAM-deficient cells. It will be interesting to determine if these FAPs are part of the PAM functional module and how they affect ciliogenesis.

Actin(g) up

So far, a myriad of functions ranging from the biosynthesis of peptides to membrane trafficking and the assembly of cilia and microvilli have been associated with PAM. How does PAM participate in all of these diverse cellular processes? In order to fully address this question, the common underlying process/factor amongst all these activities must be identified. We found that loss of PAM alters cell morphology in fibroblasts, and that PAM$^{-/-}$ zebrafish are unable to assemble actin-based microvilli in their pronephros (Chapter 6). Based on these results, we hypothesize that a functional interaction between PAM and the actin cytoskeleton may tie PAM to these diverse cellular processes (Fig 1).

Actin is known to regulate multiple cellular activities, including cell polarity, ciliogenesis and membrane trafficking. The actin-based cytoskeleton is also an evolutionarily conserved feature of eukaryotic cells, similar to membrane trafficking and ciliogenesis (Bornens, 2008; Sung and Leroux, 2013). Thus, the dependence of processes such as ciliogenesis and membrane trafficking on the conserved interaction between PAM and actin could have arisen early in the history of eukaryotes.

Ancestral peptidergic signaling

In trying to determine the ancestral role of PAM in *Chlamydomonas*, we considered whether they might utilize peptidergic signaling for intercellular communication. *In silico* approaches identified several precursors that could generate amidated products and mass spectrometric analysis of spent mating medium identified several amidated peptides (Chapter 5). Exploring the roles of these putative bioactive peptides will undoubtedly be important, especially for a green alga where peptidergic signaling has never been reported. Also intriguing is the release of active

PAM in extracellular vesicles from *Chlamydomonas* cilia (Chapter 5). With several reports demonstrating the tight regulation of extracellular vesicle content (Wood et al., 2013; Cao et al., 2015; Long et al., 2016), the physiological significance of releasing PAM in this manner must be investigated. If this process is evolutionarily conserved, this finding could have implications for the development of biomarkers for copper- and endocrine- related disorders.

Several G-protein coupled receptors (GPCRs) such as neuropeptide Y receptors (NPY2R, NPY5R), somatostatin receptor 3 (SSTR3) and melanin concentrating hormone receptor (MCHR1) have been reported to localize to cilia (Schou et al., 2015). Furthermore, a chemical screen in *Chlamydomonas* identified several GRCRs as regulators of ciliary length and motility (Avasthi et al., 2012). The consequence of ciliary localization of these GPCR on G-protein signaling is still unclear, but these findings establish the importance of cilia in several aspects of peptidergic signaling pathways.

The other monooxygenases

PAM belongs to a small family of copper-dependent monooxygenases that includes dopamine β-hydroxylase and monooxygenase-X. Dopamine β-hydroxylase has well recognized roles in the neuroendocrine system, where it converts dopamine into norepinephrine (Senard and Rouet, 2006). The function of monooxygenase-X is unknown, although it is predicted to act on an endoplasmic reticulum-localized hydrophobic substrate (Xin et al., 2004). Recently, monooxygenase-X has been implicated in olfaction based on its expression in the olfactory epithelium (Kim et al., 2014). Interestingly, dopamine β-hydroxylase and monooxygenase-X like genes are encoded in the *Chlamydomonas* genome (preliminary, unpublished results). Determining if these genes encode active enzymes and defining their roles in *Chlamydomonas* could be very informative.

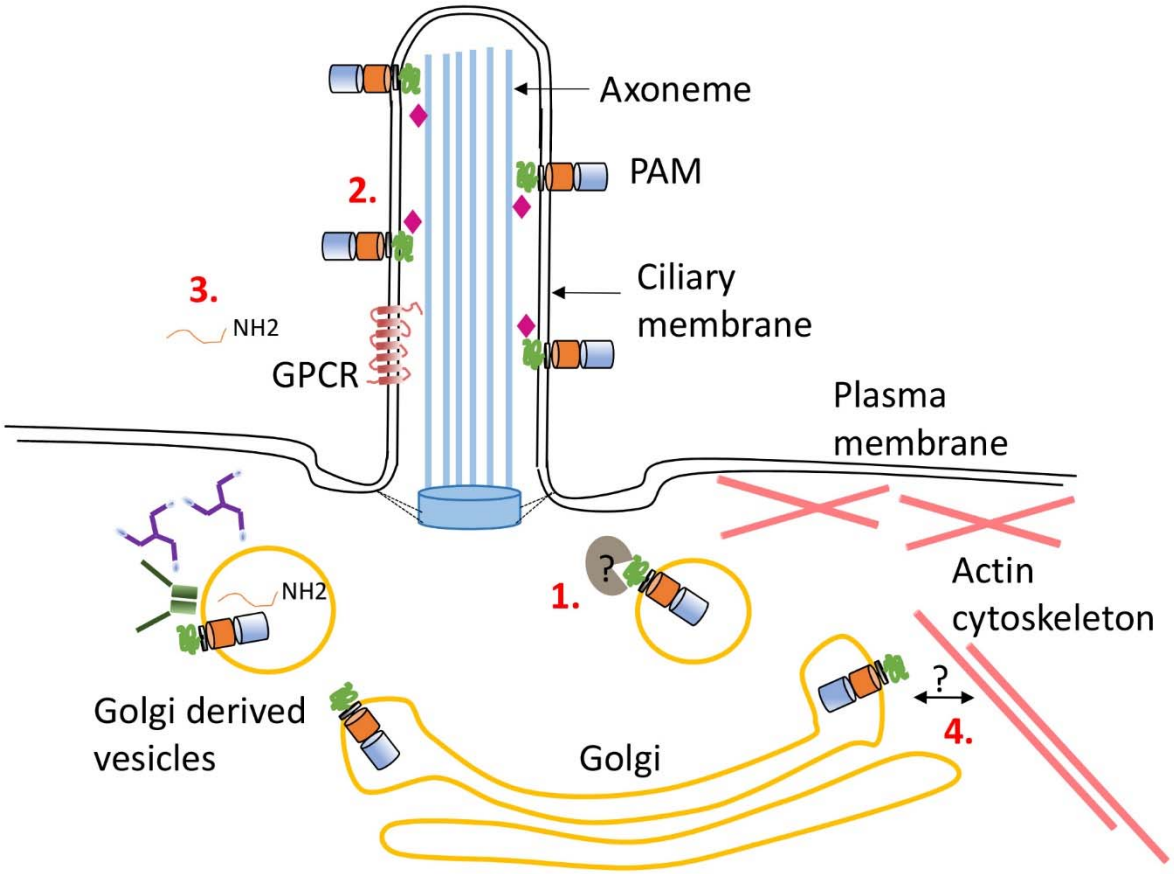

Fig 1. Model of PAM functions in cilia and ciliogenesis. Our data reveal a novel localization of PAM in cilia and a PAM requirement for ciliogenesis. Many questions still remain to be answered, some of which are highlighted here. (1) How is PAM trafficked into the cilium? Does this trafficking require the intraflagellar transport system or the Bardet-Biedl (BBSome) complex? (2) How is PAM retained in the cilium? Our data show that PAM is tethered to the axoneme in *Chlamydomonas*, presumably *via* its C-terminal domain. Does PAM interact directly or indirectly with the ciliary microtubules? (3) Is a bioactive amidated product required for ciliogenesis and does PAM perform an enzymatic role in the cilium? (4) Does PAM interact with the actin cytoskeleton to regulate ciliogenesis? Is this mediated through its effects on polarized membrane trafficking?

Final conclusions

The studies presented here have identified several novel aspects of PAM biology, and as a consequence also presented us with more questions (Fig 1). Determining the mechanism by which PAM regulates ciliary assembly is a top priority. However, the consequences of PAM localization in cilia (if any) once the cilium is assembled are not yet known. Does PAM play an enzymatic role in the ciliary compartment, and if so, on what substrate(s)? How is PAM trafficked and retained in the cilium? To this end identifying its interacting partners in the cilium and domains required for ciliary trafficking are key.

Finally, our work has raised the possibility that PAM is a novel candidate gene for ciliary diseases. Currently, ciliopathy disease panels include a defined set of about 200 genes. We propose that PAM should be added to the gene panel currently used to interrogate samples from human ciliopathy patients with unknown etiology. Based on the function of PAM, we predict that special emphasis must be paid to ciliopathies such as Bardet-Biedl syndrome, where endocrine abnormalities and kidney cysts are part of the disease pathology.

REFERENCES

Attenborough, R. M., Hayward, D. C., Kitahara, M. V., Miller, D. J. and Ball, E. E. (2012). A "neural" enzyme in nonbilaterian animals and algae: preneural origins for peptidylglycine alpha-amidating monooxygenase. *Mol Biol Evol* **29**, 3095-3109.

Avasthi, P., Marley, A., Lin, H., Gregori-Puigjane, E., Shoichet, B. K., von Zastrow, M. and Marshall, W. F. (2012). A chemical screen identifies class a G-protein coupled receptors as regulators of cilia. *ACS Chem Biol* **7**, 911-919.

Bornens, M. (2008). Organelle positioning and cell polarity. *Nat Rev Mol Cell Biol* **9**, 874-886.

Cao, M., Ning, J., Hernandez-Lara, C. I., Belzile, O., Wang, Q., Dutcher, S. K., Liu, Y. and Snell, W. J. (2015). Uni-directional ciliary membrane protein trafficking by a cytoplasmic retrograde IFT motor and ciliary ectosome shedding. *Elife* **4**:e05242.

Czyzyk, T. A., Ning, Y., Hsu, M. S., Peng, B., Mains, R. E., Eipper, B. A. and Pintar, J. E. (2005). Deletion of peptide amidation enzymatic activity leads to edema and embryonic lethality in the mouse. *Dev Biol* **287**, 301-313.

Kim, D. S., Wang, Y., Oh, H. J., Lee, K. and Hahn, Y. (2014). Frequent loss and alteration of the MOXD2 gene in catarrhines and whales: a possible connection with the evolution of olfaction. *PLoS One* **9**, e104085.

Long, H., Zhang, F., Xu, N., Liu, G., Diener, D. R., Rosenbaum, J. L. and Huang, K. (2016). Comparative analysis of ciliary membranes and ectosomes. *Curr Biol*. **26**, 3327-3335.

Schou, K. B., Pedersen, L. B. and Christensen, S. T. (2015). Ins and outs of GPCR signaling in primary cilia. *EMBO Rep* **16**, 1099-1113.

Senard, J. M. and Rouet, P. (2006). Dopamine beta-hydroxylase deficiency. *Orphanet J Rare Dis* **1**, 7.

Sung, C. H. and Leroux, M. R. (2013). The roles of evolutionarily conserved functional modules in cilia-related trafficking. *Nat Cell Biol* **15**, 1387-1397.

Wood, C. R., Huang, K., Diener, D. R. and Rosenbaum, J. L. (2013). The cilium secretes bioactive ectosomes. *Curr Biol* **23**, 906-911.

Xin, X., Mains, R. E. and Eipper, B. A. (2004). Monooxygenase X, a member of the copper-dependent monooxygenase family localized to the endoplasmic reticulum. *J Biol Chem* **279**, 48159-48167.